भाभा परमाणु अनुसंधान केंद्र का आधिकारिक द्विमासिक प्रकाशन
The official bi-monthly publication of Bhabha Atomic Research Centre

भा.प.अ.कें. न्यूज़लेटर
BARC Newsletter

मई-जून 2025 May-June 2025 Issue No. 2025:3 ISSN: 0976-2108

- BARC-TIFR Pelletron LINAC Facility
- Weak Binding & Clustering
- Hot Rotating Nuclei

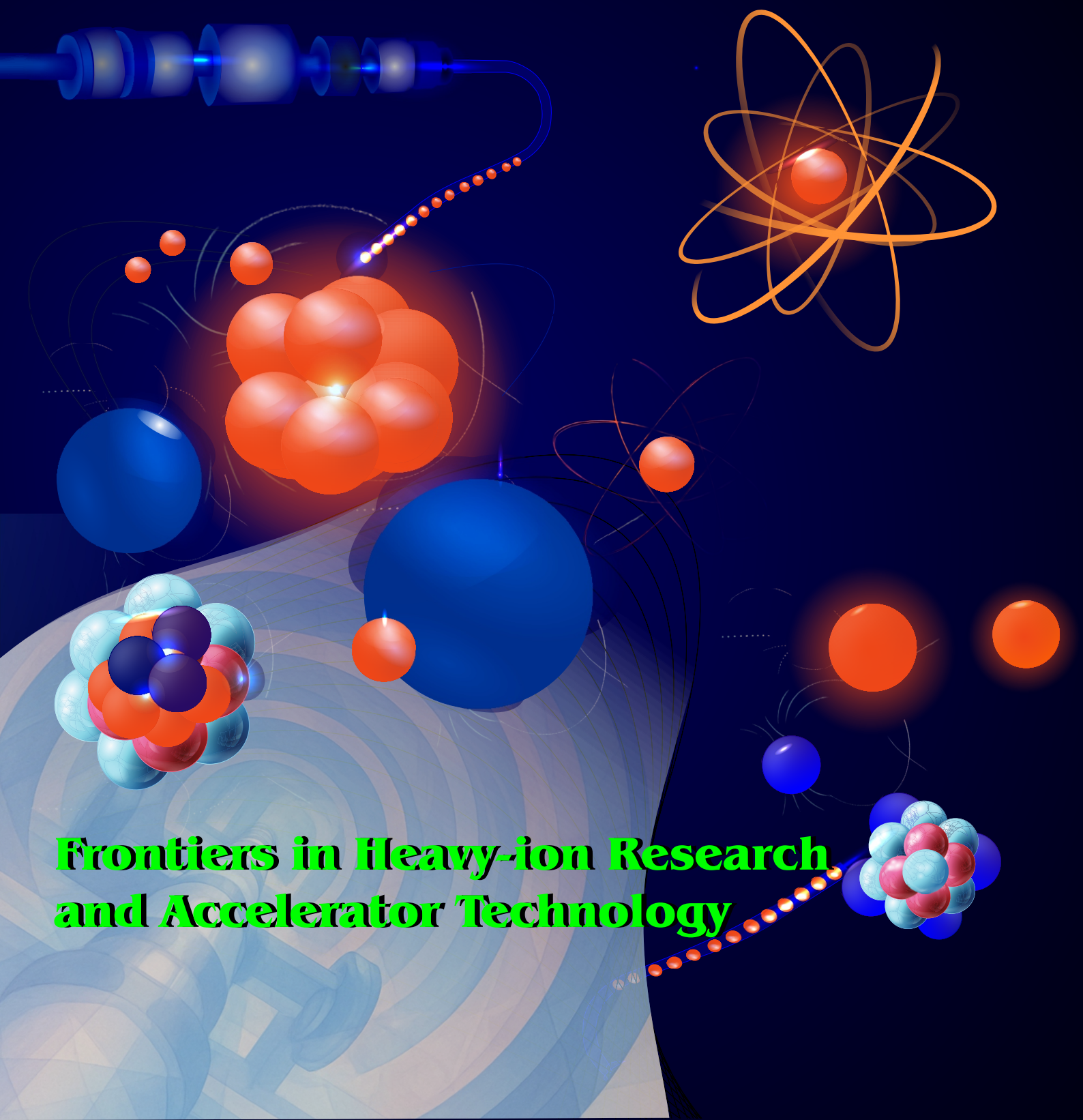

Frontiers in Heavy-ion Research and Accelerator Technology

BARC Newsletter
May-June 2025
ISSN: 0976-2108

About the Illustration on the Front Cover

The front cover illustration depicts the diverse range of advanced research and development activities in BARC in nuclear physics and nuclear astronomy domains. Additionally, it captures the essence of important outcomes contributed by the efforts of broader scientific community at the BARC-TIFR Pelletron Facility.

foreword

Towards Aatmanirbhar Bharat Through Heavy-Ion Accelerator Development and Utilization program

A major leap for the R&D activities related to accelerator based nuclear physics and allied areas happened with the installation of the 14UD Pelletron Accelerator in December 1988 as a collaborative project between the Bhabha Atomic Research Centre (BARC) and the Tata Institute of Fundamental Research (TIFR). This accelerator is nearing more than three-and-a-half decades of successful operations, catering to a large community of scientists in the country. The commissioning of the indigenously developed superconducting linear accelerator in November 2007 to boost the energy of the heavy ion beam delivered from the Pelletron accelerator has further enhanced the capability of this facility. Several notable contributions in the area of structure and reaction dynamics of hot rotating nuclei and allied areas have emanated using this facility, culminating in an exceptionally large number of theses and peer reviewed journal publications of international repute.

To cater to the growing demand and to explore the expanding horizon of heavy-ion research, the community has embarked on development of an accelerator facility with capability beyond the PLF in terms of energy, intensity and variety. This project involves collaboration of multiple divisions across various BARC groups to design, develop, install and construct accelerator systems & facilities such as cryogenic system for SRF cavities, RF supply and control system, radiation safety and protection system, civil infrastructure for accelerator and experimental beam halls and architectural landscaping, etc. Under “Aatmanirbhar Bharat” impetus, the project envisages the development of Niobium Quarter Wave Resonators (QWRs) from raw material available within the country to the final product, with the help of existing expertise within BARC and through setting up of Niobium processing facilities and associated laboratories. This facility is envisaged to deliver stable isotope beams of proton to uranium as well as neutron rich radioactive beams (RIBs) of energy up to 10 MeV per nucleon. This will open up new avenues of fundamental research and enhance radioisotope applications.

The present thematic issue of the BARC Newsletter is an attempt to showcase the achievements in the past decades and chalk out future courses of heavy ion accelerator development as well as heavy-ion research activities in India.

I commend the contributing authors, associate editor, and SIRD editorial team for their exceptional efforts and camaraderie in creating this thematic issue in a time-bound manner.

We are grateful to Scientific Information Resource Division (SIRD) and the Newsletter Editorial Committee for offering us the opportunity to bring out this thematic issue on developments in BARC-TIFR Pelletron LINAC facility and future accelerators for nuclear physics research. We hope that the readers will enjoy reading the articles published in this issue and it will also serve as an important reference for the future as we are passing through an important juncture of development of experimental facilities for nuclear physics research.

Dr. T. Sakuntala
Associate Director
Physics Group
Bhabha Atomic Research Centre

This page intentionally left blank

ASSOCIATE EDITORS' *message*

Driving Fundamental and Allied Research through Heavy Ion Accelerator Program

We are extremely delighted to get this opportunity to bring out this thematic issue of the BARC newsletter on Frontiers in Heavy-ion Research and Accelerator Technology. The Pelletron LINAC facility (PLF), a joint venture between BARC and TIFR, has completed more than three-and-a-half decades of successful operation, catering to a large community of scientists in the country. The laboratory is equipped with several state-of-the-art experimental facilities to pursue cutting edge research in nuclear, atomic, condensed matter and interdisciplinary areas. A number of application-based research activities have also been established over the years. While most of the research activities are led by the researchers from BARC and TIFR, scientists and students from universities and other research centres within and outside the country have also been the active users of this accelerator. About 170 PhD theses and over 750 publications in peer reviewed journals, including 37 publications in Physical Review Letters and other letter papers, have resulted from the research activities of this laboratory.

As the Pelletron LINAC facility (PLF) continues to be a centre of excellence in heavy ion research, it is planned to augment this accelerator with new generation high gradient accelerating tubes and Superconducting Radio Frequency (SCRF) Niobium cavities. Further to cater the growing demand of the vibrant research community, a versatile ECR (Electron Cyclotron Resonance) Ion Source (IS) based heavy ion accelerator facility capable of accelerating stable and unstable nuclei with higher beam currents to energies beyond the capability of BARC-TIFR Pelletron-LINAC Facility, is planned as a greenfield facility at the BARC-Vizag accelerator complex.

This thematic issue of BARC Newsletter contains articles encompassing the full spectrum of research activities carried out by the research groups in BARC and TIFR in the past along with our future endeavours. We take this opportunity to acknowledge all the authors for their valuable contributions in this thematic issue. We are thankful to Dr. S. M. Yusuf, Former Director, Physics Group and Dr. Anit Kumar Gupta, Former Head, Nuclear Physics Division (NPD) for their keen interest, guidance and encouragement in bringing out this issue. We earnestly acknowledge the guidance of Shri Manoj Singh (Head, SIRD and Editor, Newsletter), the sincere and hardworking role of the newsletter editorial team of SIRD for the compilation of the articles, the creative work by the editorial team in designing the front cover and their dedicated efforts in bringing out BARC Newsletter in a time-bound manner. We also take this opportunity to express our deepest gratitude to all our past and present colleagues, who have played a very vital role in establishing, operating, and maintaining PLF as a world-class facility. The constant support from NPD (BARC), Department of Nuclear and Atomic Physics (TIFR), Electronic Division (BARC), Central Workshop (BARC & TIFR) and Technical Services (TIFR) towards this facility is greatly appreciated.

Dr. S. Santra
Outstanding Scientist &
Head, Nuclear Astrophysics Section

Dr. K. Mahata
Scientific Officer/H
Nuclear Physics Division

FRONTIERS IN HEAVY-ION RESEARCH AND ACCELERATOR TECHNOLOGY

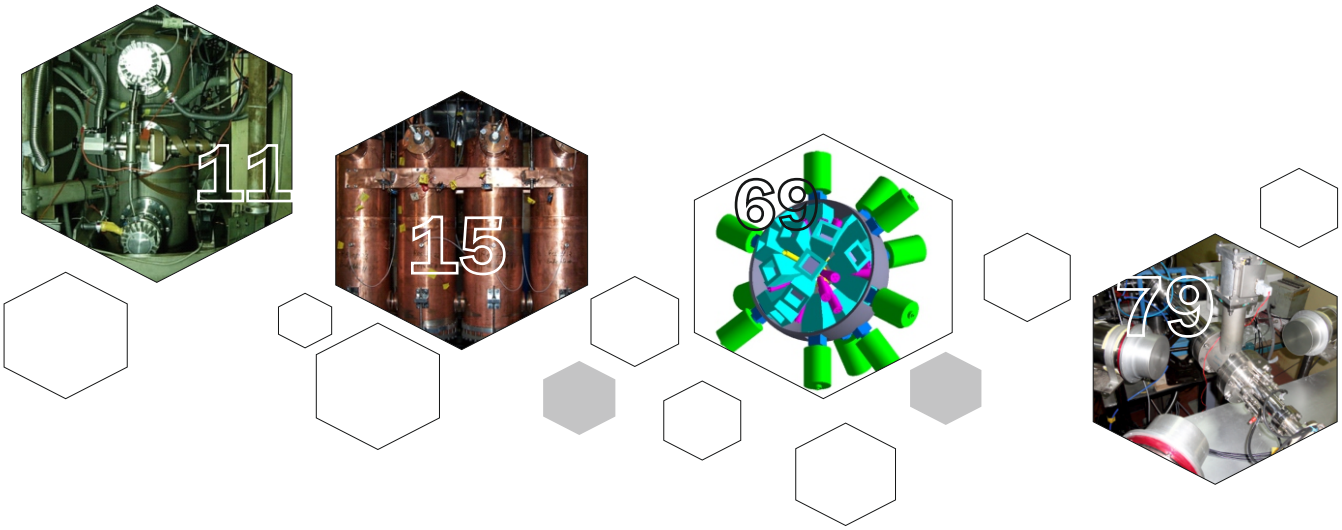

CONTENTS

ARTICLES OF FORTHCOMING ISSUE

- Training School Graduation Function (OCES 2024 program): Principal Secretary to the Prime Minister of India, Dr. P.K. Mishra, attends.
- Trombay Colloquium : DST Secretary Prof. Abhay Karandikar and Molecular Genetist Dr. T. Mohapatra deliver captivating talks.
- Women Scientific Officers of BARC lead outreach program in the national capital.
- Latest developments in industry Technology Transfer and Collaboration in nuclear spin-offs by BARC.
- Research Highlights.

This page is intentionally left blank

सुविधा विकास, प्रचालन एवं अनुरक्षण

1

भापअ केंद्र-टीआईएफआर पेलेट्रॉन त्वरक

जे. ए. गोरे[1,*], एन. मेहरोत्रा[1], एस. सी. शर्मा[1], जे. पी. नायर[1], आर. पालित[3], वी. नानल[3] और ए. श्रीवास्तव[1,2]

[1]नाभिकीय भौतिकी प्रभाग, भाभा परमाणु अनुसंधान केंद्र (भापअ केंद्र), ट्रांबे, मुंबई – 400085, भारत

[2]होमी भाभा राष्ट्रीय संस्थान, अणुशक्तिनगर, मुंबई – 400094, भारत

[3]डीएनएपी, टाटा इंस्टीट्यूट ऑफ फंडामेंटल रिसर्च, मुंबई-400005, भारत

भापअ केंद्र-टीआईएफआर पेलेट्रॉन लीनॉक (एलआईएनएसी) सुविधा की त्वरण नली

सारांश

भापअ केंद्र-टीआईएफआर पेलेट्रॉन लीनॉक (एलआईएनएसी) सुविधा देश के त्वरक-आधारित अनुसंधान कार्य हेतु नाभिकीय भौतिकी, परमाणु एवं संघनित पदार्थ भौतिकी तथा बहु-विषयक क्षेत्रों के लिए एक कार्यस्थल (गतिशक्ति/प्रगतिकारक) रही है। त्वरक आधारित मूलभूत एवं अनुप्रयुक्त अनुसंधान समुदाय की बढ़ती अपेक्षाओं को पूरा करते हुए, इसने भविष्य में देश के हरित-क्षेत्र त्वरक हेतु विकास कार्यक्रमों को भी सुविधाजनक बनाया है। यह आलेख, भारी द्रव्यमान के उच्च ऊर्जा कणपुंजों के साथ त्वरक के लिए भविष्य के विकास कार्यक्रमों के साथ-साथ देश में त्वरक-आधारित गतिविधियों के ऐतिहासिक परिप्रेक्ष्य को संक्षेप में प्रस्तुत करता है।

Facility Development, Operation & Up-keep

1

BARC-TIFR Pelletron Accelerator

J. A. Gore[1,*], N. Mehrotra[1], S. C. Sharma[1], J. P. Nair[1], R. Palit[3], V. Nanal[3] and A. Shrivastava[1,2]

[1]Nuclear Physics Division, Bhabha Atomic Research Centre (BARC), Trombay, Mumbai-400085, INDIA

[2]Homi Bhabha National Institute, Anushakti Nagar, Mumbai – 400094, India

[3]DNAP, Tata Institute of Fundamental Research, Mumbai-400005, INDIA

Accelerating tube of Pelletron.

ABSTRACT

The BARC-TIFR Pelletron LINAC facility has been a workhorse for accelerator-based research in the country in the domains of nuclear physics, atomic and condensed matter physics and multidisciplinary areas. While catering to the expanding horizons of the accelerator based basic and applied research community, it has also facilitated developmental programmes for futuristic green-field accelerator in the country. This article would briefly present a historical perspective of accelerator-based activities in the country along with the future developmental programmes for accelerator with higher energy beams of heavier masses.

KEYWORDS: *Pelletron, LINAC, Heavy-ion, Radiation applications*

**Author for Correspondence: J. A. Gore*
E-mail: jagore@barc.gov.in

Introduction

The Pelletron accelerator has been operational on a round the clock basis since 1988, serving diverse users from within and outside DAE. The Pelletron accelerator has been consistently working with very high efficiency, delivering a wide variety of ion beams ranging from proton to Iodine. A number of developmental activities have been carried out in-house to improve the performance of the accelerator. While a majority of the researchers at this facility are scientists from BARC and TIFR, the experimental community includes researchers and students from VECC, SINP and universities within India and abroad. About 150 Ph.D. theses and about 750 publications in international refereed journals have resulted from the research activities at the PLF. These include a large number of publications in high impact international scientific journals.

The accelerator has been a workhorse for accelerator-based research in the country in the domains of nuclear physics, atomic and condensed matter physics and multidisciplinary areas. This article briefly presents a historical perspective of accelerator-based activities in the country. The accelerator developmental and associated activities which have increased the scope of accelerator utilization shall be described later. The accelerator continues to serve the diverse physics communities in fundamental and applied research. The accelerator while catering to the expanding horizons of the accelerator based basic and applied research community has also facilitated developmental programmes for futuristic green-field accelerator in the country. This article would also present the future developmental programmes for accelerator with higher energy beams of heavier masses.

Historical Perspective

The accelerator development in the Department of Atomic Energy set out in the fifties. One MeV Cockroft–Walton accelerator was commissioned at Tata Institute of Fundamental Research (TIFR), Mumbai in 1953. In early sixties a 5.5 MV Van de Graaff accelerator manufactured by High Voltage Engineering Corporation (HVEC), was installed at the Bhabha Atomic Research Centre (BARC), Mumbai that provided much-needed boost to accelerator-based research in the country. In the late seventies, the only accelerator facility in medium energy range available in the country was indigenously developed Variable Energy Cyclotron at Kolkata. In order to meet the diverse requirements of nuclear physics community, a Medium Energy Heavy Ion Accelerator (MEHIA) project was conceived to accelerate ions right from proton to highest possible mass at intermediate energies. In 1982, the project MEHIA started, where a 14 UD Pelletron Accelerator was purchased from M/s NEC, USA and installed at Tata Institute of Fundamental Research campus, Mumbai. This accelerator was commissioned on 30th December 1988 [1] and since then it has been serving as a major facility for heavy ion accelerator based research in India.

Developmental Activities & associated applications at BARC-TIFR Pelletron Accelerator over last 35 years

Since its inception, the accelerator has been continuously working with progressively increased efficiency. The accelerator upgradation was done by implementing

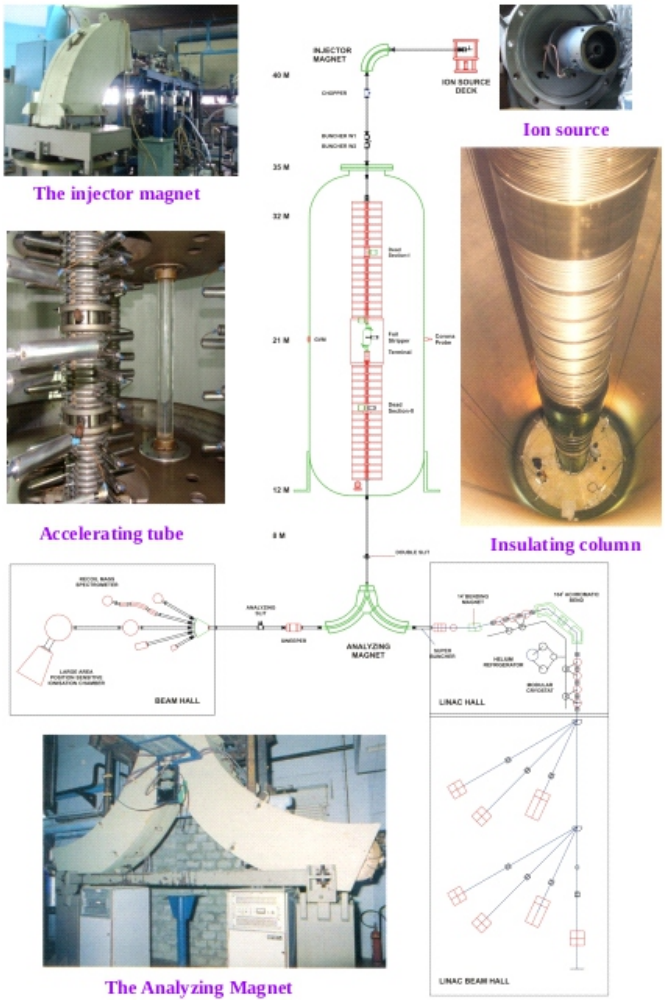

Fig.1: Schematic layout of the BARC-TIFR Pelletron LINAC facility.

following features; the original NEC accelerator has voltage grading based on corona needles that were replaced by resistances, a new terminal potential stabilizer was installed, two turbomolecular pumps were introduced in the terminal to improve performance of gas stripper, development of negative ion beams for a wide range of species [2].

At BARC-TIFR Pelletron Linac Facility (PLF), various application-oriented programmes such as radioisotopes production, radiation damage studies (space bound devices, yield improvement in wheat and rice seeds), secondary neutron production for cross-section measurements, radiation dosimetry studies, ion irradiation in semiconductor crystals for photoconductive Tera Hz emitters, Accelerator Mass Spectrometry, and production of track-etch membranes, are also pursued. Experimental facilities are attached to dedicated beamlines installed in the Cascade beam hall for Pelletron energies and two new LINAC beam halls I and II for both Pelletron and LINAC boosted energies.

The accelerator based developmental activities and the application-oriented programs have resulted in enhanced uptime and utilization of the accelerator.

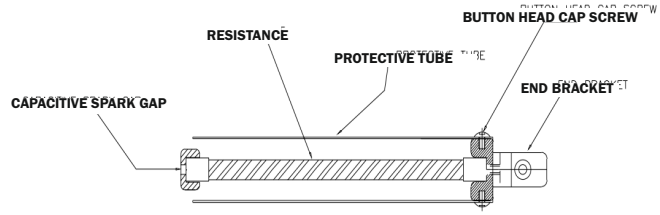

Fig.2: Details of resistance mount assembly.

Resistor Grading

An important consideration in high voltage design of an electrostatic accelerator is the potential grading system used to divide the terminal potential equitably (or as required) across the column or tube electrode gaps. Development of very high values ceramic metal resistor technology has been found to be most suitable for use in high voltage grading chains. Corona needles in high-energy column were replaced by these resistances. A resistance chain consisting of 2 GΩ per gap in the column and 1 GΩ per gap in the accelerating tube (1 GΩ resistors; 1008 in columns and 924 in accelerating tubes) was installed. As a result a voltage stability of 0.01% has been achieved and the operation of accelerator has become very stable even at lower terminal voltages, and it is now possible to deliver beam even at as low voltage as 4 MV.

Accelerator Based Spectrometry

Due to the enhanced stability and high voltage control achieved with the resistor grading system, Accelerator Mass Spectrometry based experiments with ^{36}Cl based measurements could be performed, successfully. As the interfering isobar in the ^{36}Cl detection is ^{36}S, a segmented gas detector was developed in-house to circumvent the rather intense isobaric interference. The ratio obtained for standard sample is in agreement with the value specified by the Prime Lab within a statistical error of 12%. Such a good agreement obtained for direct measurement of ratio indicates that transmission for Cl isotopes through the accelerator is well optimized. Estimated detection limit is ~ 7 x 10^{-14} [3]. These experiments were subsequently extended to ^{129}I.

Recirculating Terminal Gas-Stripper

Gas pressure has a major role in getting intense and highly stripped ions, but at the same time bad vacuum conditions in accelerator tube causes loss of beam transmission due to charge exchange and scattering. The gas stripper system was originally installed with Titanium Sublimation pumps in high voltage terminal section. These pumps require periodic replacement of cartridges and pumping speed of these pumps used to come down with time. A new recirculation gas stripper system has been installed, consisting of two Turbo Pumps in place of sublimation pumps. The gas stripper system is utilized during accelerating beryllium beam through Pelletron [4] and also while accelerating beams through Linac. The installation of turbo pump in the accelerator tank is based on an existing stripper housing (see Fig.3).

Linux based Control System

The Pelletron accelerator parameters are controlled and monitored through a Linux based software and associated graphical User Interface (GUI). The operator interacts through the GUI to control and monitor the accelerator. The GUI incorporates features like software assignable meters and slider controls. This has obviated the need for shaft encoders and assignable meters that were in use for the past twenty years. The control system software consisting of client-server architecture utilizing ethernet connectivity is relatively more reliable and user friendly compared to the old system that was DOS based and was in use for twenty years.

Pelletron control system hardware

The Pelletron control system hardware is CAMAC based. The CAMAC interface modules are more than twenty years old. To ensure continuity of the CAMAC platform, general purpose FPGA based CAMAC modules like DAC [5], ADC and digital input/output modules have been designed and developed at the Pelletron accelerator (see Fig.4). All the modules have been tested. Of these, a 16 channel, 12 bit CAMAC ADC module has been installed and is currently in continuous use.

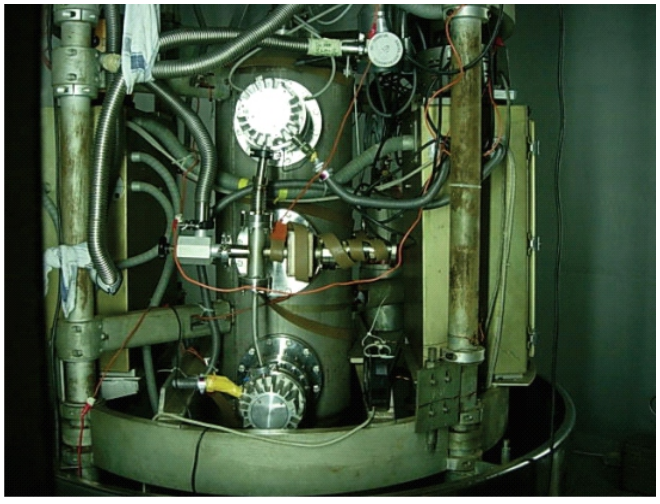

Fig.3: Terminal Gas Stripper System.

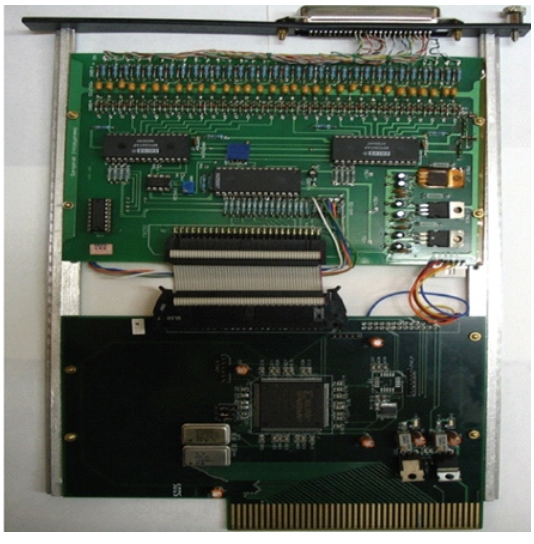

Fig.4: FPGA based CAMAC ADC module.

Ion Source and Beam Development

To produce a wide range of negative ions, sources such as SNICS (Source of Negative Ions by Cesium Sputtering) and Alphatross are commonly used in tandem accelerator facilities. An ion source test bench was set up to meet the increasing demand of intensity and quality of beams at Pelletron Accelerator Facility. The sputter characteristics of the cathodes are optimized using the 'cooking systematics' generated in the ion source laboratory. Different types of composite-sputter cathodes, gas feed-sputter cathodes and disc covered-gas feed-sputter cathodes have been developed and tested at our test bench, with particular emphasis given to the elements of user's interest [6,7]. Composite-sputter cathodes development has led to a significant reduction in the down time of the accelerator by eliminating the beam changeover delays and enhanced ion source lifetime. Gas feed-sputter cathodes provide molecular negative ions of low electron affinity elements. Disc covered-gas feed-sputter cathodes are developed to generate negative ions of the rare earth elements without impairing the ionization efficiency of ionizer. Over the years, various versions of high intensity negative ion sources based on cesium sputtering i. e. SNICS, Gas feed-SNICS, MC-SNICS (Multi Cathode Source of Negative Ions by Cesium Sputtering) have been developed, in house [8, 9]. Recently, ^{9}Be beam has been accelerated through Pelletron Accelerator Facility, successfully. Given to the toxicity of beryllium, a dedicated ion source was used and stringent safety requirements were followed as recommended by the BARC Safety Committee (BSC), BARC, at different levels of production, acceleration, and utilization [10].

Track Etch Membrane Set Up

Microporous membranes with well-defined and uniform pore size and pore density, uniform thickness, high tensile strength and inertness to toxic environments are in good demand for growing number of scientific and technological applications. Heavy ion accelerators provide greater flexibility to produce Track Etch Membrane (TEM) of a wide range as they can provide various heavy ions of different atomic number (Z), kinetic energy (E) and particle flux. Pore densities of the order of 106 to 108 pores/cm^2 and pore size of the order of 0.2 to 1.0 micron are required for many applications. A magnet was used to scan the heavy ions from the accelerator in horizontal direction and the polymer film was moved in vertical direction using a roller mechanism. The scanner magnet gives a peak magnetic field of 1.35 Kgauss [11]. To get larger deflection higher charge states of the desired ions are produced using post stripper. The deflection, at the exit of the scanner is few centimeters, which is then widened using a horn chamber of one metre length. At the end of the scanner deflection up to 25 cm is achieved. The film is wound on a perspex shaft of 19 mm diameter and is continuously unwound on to another roller that is driven by a D.C. motor from outside the chamber.

Coupling is done using a vacuum rotary feedthrough. The linear speed of the film is kept at 60 cm/min. The beam is defocused in vertical direction to get almost uniform particle distribution. These membranes are being used by Radiation Medicine Centre, Mumbai to immobilize antibodies against specific analyte and are also used for purification of gases, in separating various Actinides and metals.

Fig.5: Proton Beam Irradiation Setup.

High Current Irradiation Set Up

Drift space above analyzing magnet has been modified to accommodate a Proton Beam Irradiation Setup at 6 meter level at this facility (see Fig.5). This setup is capable of delivering proton beam in the energy range of 2 MeV to 26 MeV and current in μA range. The shielding at this level is such that radiation is within permissible limit when proton beam with high energy and high current is accelerated. In order to study radiation effects on metals at a higher temperature a hot target assembly is developed which can go up to 500^{0} C. Radionuclides such as ^{52}Mn, ^{67}Ga, ^{96}Tc, and ^{236}Pu have been produced for radiopharmaceutical applications.

Radiation Biology Set Up

A thin window (20μm) of Titanium is placed at 30^{0} N beam line to bring out ion beam in air. Various users have used this facility. A large area proton beam of size 25 mm to 40 mm diameter in air was made available to Indian Space Research Organization for testing their on-line electronic devices.

Future Programmes

The experimental nuclear physics (NP) research has progressed rapidly with the advancement in accelerator technology. Currently, in India, Pelletron-LINAC accelerator facilities at Mumbai and Delhi and the cyclotron accelerators at Kolkata are driving the NP research. Most of the interesting NP results have come from experiments performed at and around a beam energy region called Coulomb energy where the projectile has just enough energy to overcome the mutual electrostatic repulsion between projectile and target which varies roughly as a product of projectile and target atomic number. There is a need to have higher energy beams of heavier masses with higher beam current compared to the current accelerators in India, which can bring in not only higher

nuclear temperature but also higher angular momentum thus expanding the horizons of NP research in the country.

To cater to the demands of the NP community, a versatile ECR (Electron Cyclotron Resonance) Ion Source (IS) based heavy ion accelerator facility capable of accelerating wider species of beams at higher beam currents to energies beyond the capability of BARC-TIFR Pelletron-LINAC Facility, is planned as a greenfield facility at BARC-Vizag accelerator complex. This accelerator facility consisting of an ECR-IS, a room temperature radiofrequency quadrupole (RT-RFQ) and low & high beta superconducting radio frequency (SRF) niobium cavities would be developed to produce, accelerate and transport the highly charged high current stable ion beams to experimental facilities in beam halls for experimental studies.

Acknowledgement

The authors thank their colleagues of Pelletron Accelerator Facility for their contribution. We are also thankful to all past members of the division for their constant support and encouragement.

References

[1] S. S. Kapoor, V.A. Hattangari and M.S. Bhatia,Indian J. Pure and App.Phys. 27 (1989) 623.

[2] A. K. Gupta, P. V. Bhagwat and R. K. Choudhury, Proceedings of Heavy Ion Accelerator Technology (HIAT09), June 08-12, 2009, Venice (Italy)

[3] P. Surendran, A. Shrivastava, A. K. Gupta, R. M. Kale, J. P. Nair, M. Hemalatha, K. Mahata, M. L. Yadav, H. Sparrow, R. G. Thomas, P. V. Bhagwat, S. Kailas, Nucl. Inst. & Meth. Phys. Res. B 267 (2009) 1171.

[4] S. C. Sharma, N.G. Ninawe, M.L. Yadav, M. Ekambaram, Ramjilal, U.V. Matkar, Q. N. Ansari, R. L. Lokare, Ramlal, A. K. Gupta, R. G. Pillay and P. V. Bhagwat, Indian Particle Accelerator conference (Inpac-2009), Feb. 10-13, 2009, RRCAT, Indore.

[5] S. G. Kulkarni, J. A. Gore, A. K. Gupta, P. V. Bhagwat,R. K. Choudhury, Indian Particle Accelerator conference (Inpac-2009), Feb. 10-13, 2009, RRCAT, Indore, India.

[6] A. K. Gupta, N. Mehrotra, R. M. Kale, D. Alamelu, and S. K. Aggarwal, DAE Symposium on Nuclear Physics, Dec. 2003.

[7] A. K. Gupta, N. Mehrotra, R. M. Kale, D. Alamelu, and S. K. Aggarwal , DAE-BRNS 50th Symposium on Nuclear Physics, BARC, Mumbai, Dec. 12-16 (2005).

[8] A. K. Gupta, P. Ayyub, European Physical Journal D 17 (2001) 221.

[9] S. C. Sharma, R. M. Kale and A. K. Gupta, DAE symposium on Nuclear Physics, Dec. 21-25, (1998).

[10] A. K. Gupta, R. M. Kale, N. Mehrotra, P. N. Bhat, S. Soundararajan, A. Shanbag, D. D. Thorat, P. V. Bhagwat, R. K. Choudhury, Indian Particle Accelerator conference (Inpac-2009), Feb. 10-13, 2009, RRCAT, Indore, India.

[11] J. P. Nair et al. J Radioanal Nucl Chem (2014) 302:947–950.

भापअ केंद्र –टीआईएफआर पेलेट्रॉन सुविधा

2

अतिचालक लीनॉक एवं संबंद्ध विकास

वी.नानल[1,*], ए.श्रीवास्तव[2,3], आर.पलित[1] और जे.ए.गोरे[2]

[1]डीएनएपी, टाटा मूलभूत अनुसंधान संस्थान,मुंबई-४००००५,भारत
[2]नाभिकीय भौतिकी प्रभाग,भाभा परमाणु अनुसंधान केंद्र, ट्रांबे,मुंबई-४०००८५,भारत
[3]होमी भाभा राष्ट्रीय संस्थान, अनुशक्ति नगर, मुंबई-400094, भारत

एक क्रायोस्टेट के अंदर चार चौथाई तरंग अनुनादकों का संयोजन।

सारांश

भाभा परमाणु अनुसंधान केंद्र और टाटा मूलभूत अनुसंधान संस्थान के बीच एक सहयोगी परियोजना के रूप में स्थापित पेलेट्रॉन लीनॉक सुविधा, भारत में भारी-आयन त्वरक-आधारित अनुसंधान के लिए एक मुख्य केंद्र रहा है। 14 MV पेलेट्रॉन त्वरक का दिसंबर 1988 में कमीशनन किया गया और त्वरित किरणपुंजों की संवृद्धि हेतु स्वदेशी रूप से विकसित अतिचालक लीनॉक अभिवर्धक के साथ संवर्धन किया गया। लीनॉक अभिवर्धक की प्रावस्था I को 2002 में शुरू किया गया और दूसरी प्रावस्था II पूरी होने के बाद, यह सुविधा नवंबर 2007 में उपयोगकर्ताओं को समर्पित की गई । यह देश का प्रथम अतिचालक त्वरक है और अतिचालक लीनॉक का विकास भारत में त्वरक प्रौद्योगिकी में एक प्रमुख मील का पत्थर है। लीनॉक अभिवर्धक के अधिकांश महत्वपूर्ण घटकों को स्वदेशी रूप से अभिकल्पित और विकसित किया गया है। नाभिकीय, परमाणु, संघनित पदार्थ, जैव-पर्यावरणीय भौतिकी एवं अनुप्रयोगों में सीमांत अनुसंधान को आगे बढ़ाने के लिए इस केंद्र में विभिन्न प्रकार की अत्याधुनिक प्रयोगात्मक सुविधाएं विकसित की गई हैं। यह सुविधा वैज्ञानिक रूप से उपयोगी है और इसके महत्वपूर्ण रोचक परिणाम सामने आए हैं। यह लेख लीनॉक के विकास, संबंधित उपकरण और कुछ अनुप्रयोग-अभिविन्यासित कार्यक्रमों की एक झलक प्रदान करता है।

BARC-TIFR Pelletron Facility

2

Superconducting LINAC and Associated Developments

V. Nanal[1,*], A. Shrivastava[2,3], R. Palit[1] and J. A. Gore[2]

[1]DNAP, Tata Institute of Fundamental Research, Mumbai-400005, INDIA
[2]Nuclear Physics Division, Bhabha Atomic Research Centre, Trombay, Mumbai-400085, INDIA
[3]Homi Bhabha National Institute, Anushakti Nagar, Mumbai – 400094, India

Assembly of four quarter wave resonators inside a cryostat.

ABSTRACT

The Pelletron Linac Facility, set up as a collaborative project between the Bhabha Atomic Research Centre and the Tata Institute of Fundamental Research, has been a major centre for heavy-ion accelerator-based research in India. The 14 MV Pelletron accelerator was commissioned in December 1988 and was augmented with the indigenously developed superconducting Linac booster to enhance the energy of the accelerated beams. The phase I of linac booster was commissioned in 2002, and after the completion of phase II, the facility was dedicated to users in November 2007. This is the first superconducting accelerator in the country, and the development of the superconducting Linac is a major milestone in the accelerator technology in India. Most of the critical components of the Linac booster have been designed and developed indigenously. A variety of state-of-the-art experimental facilities have been developed at this centre to pursue frontier research in nuclear, atomic, condensed matter, bio-environmental physics and applications. The facility is scientifically productive and has led to significant interesting results. This article gives a glimpse of the developments of the Linac, associated instrumentation and some application-oriented programmes.

KEYWORDS: *Superconducting LINAC, Pelletron accelerator, Pelletron*

**Author for Correspondence: V. Nanal*
E-mail: nanal@tifr.res.in

Introduction

The Pelletron Linac Facility (PLF), set up as a collaborative project between the Bhabha Atomic Research Centre (BARC) and the Tata Institute of Fundamental Research (TIFR), has been a major centre for heavy ion accelerator-based research in India [1]. The Pelletron accelerator (procured from NEC, USA) was formally inaugurated on 30th December 1988 and marked an important milestone in nuclear physics research in India. The facility was augmented with the indigenously developed superconducting linac booster to enhance the energy of the accelerated beams [2].The phase I (Superbuncher +3 Modules) of the Linac booster was commissioned in 2002 and after the completion of phase II (4 Modules), the facility was dedicated to users on 28th November 2007. This is the first superconducting accelerator in the country. *Development of the superconducting Linac is a significant milestone in the accelerator technology in India. Most of the critical components of the Linac booster have been designed and developed indigenously.*

A variety of state-of-the-art experimental facilities have been developed at this centre to pursue frontier research in nuclear, atomic, condensed matter, bio-environmental physics and applications. The facility is scientifically productive, with ~75% uptime, and serves the experimental community comprising scientists and students from BARC, TIFR, research centres, and universities within India and abroad. Till date more than 350 users from about 50 institutions (including Universities, IITs) have carried out the research at this facility. About 165 Ph.D. theses and about 825 publications (including 40 Letters) in international refereed journals have resulted from the research activities at the PLF. More details about the facility, programs and publications can be found at the PLF webpage https://www.tifr.res.in/pell/

The linac booster consists of seven liquid helium cryostat modules, each housing four lead-coated (2 μm) copper quarter wave resonators (See Figure 1). The cavities are designed to operate at 150 MHz with an optimum acceptance at a velocity corresponding to β=0.1. In order to maintain a stable phase and amplitude of the electric field in the cavity, the RF controller cards based on a self-excited loop (SEL) with phase and amplitude feedback have been developed indigenously. The cryogenic system for the LINAC has been designed for a typical power dissipation of 6 W in each resonator. The LINAC Phase I (superbuncher + 3 modules) and Phase II (4 modules) are connected by an achromatic, isochronous mid-bend magnet system (QD-MD-QD-QDMD-QD). A compact longitudinal phase space is essential for acceptance in Phase II after the mid-bend and for optimization of the beam quality at target position.

The heart of the cryogenic system for the heavy-ion superconducting linac booster is a custom-built liquid helium refrigerator, the Linde TCF50S. The refrigerator is designed with a dual JT (Joule-Thomson valve) at the final cooling stage, which allows simultaneous connections to the module cryostats and to a liquid helium storage dewar (1000 Litre). The two-phase helium at 4.5 K produced at the JT stage in the refrigerator is delivered to the cryostats through a cryogenic distribution system. The phase separation is achieved in the individual cryostats and the cold (4.5 K) helium gas is returned,

Fig.1: Assembly of four quarter wave resonators inside a cryostat.

by the distribution system, back to the helium refrigerator. The cryogenic distribution system is designed to deliver both liquid helium and liquid nitrogen to the cryostats.

The performance of QWR is found to be excellent with an average energy gain of 0.4 MV/q per cavity corresponding to 80% of the design value (Q~1-2 x 10^8, an average accelerating field of 2-2.5 MV/m). Beam transmission from the entry to the exit of the LINAC is found to be 80% and the beam timing (FWHM) of ~ 600 ps is measured at the target position. For acceleration of different beams, an algorithm for RF power and phase settings of the individual resonators has been devised. The Linac is routinely operated for experiments using beams of ^{12}C to ^{35}Cl. Due to growing interest in studying light ion induced reactions at higher energies, we have also accelerated ^{7}Li (E < 10 MeV/A) and ^{10,11}B (E < 8 MeV/A) beams through Linac. The terminal gas stripper is routinely used for Silicon and heavier beam operations with LINAC.

Recent Developments at Linac

Various sub-systems of the LINAC are continuously being improved to facilitate ease of operations and improve the reliability.

The refrigeration plant has been upgraded to enhance the refrigeration capacity to ~450 Watts at 4.5K without LN2 pre-cool, from the original capacity of ~300 Watts. This completely eliminates the use of liquid Nitrogen for plant pre-cooling, which helps to reduce operational costs and more importantly improves the stability of operations. The entire plant upgrade was successfully completed at site. A 400 KVA UPS has been installed for the main Helium Compressor to minimize failures due to power fluctuations. Improvements have been made to the helium recovery system for minimizing helium losses.

While setting the beam acceleration through Linac, the phases of cavities are independently set for appropriate acceleration of the bunched beams injected from the Pelletron. In order to improve the reliability and accuracy of the RF phase settings, a high-precision phase measurement unit has been developed based on the AD8302 phase detector chip. In order to obtain a complete range of 360°, two chips are required to

generate the phase angle along with the quadrant information. The phase difference between the master oscillator and the cavity pickup is processed in two detector chips operating 90^0 out of phase. The outputs are processed to obtain the absolute phase angle and the quadrant information. This is then displayed in the range $\pm180^0$ or $0\text{-}360^0$.

Detailed phase stability measurements of the RF subsystem consisting of various RF devices, which operate at different sub-harmonic of the Linac clock, have been carried out. It was observed that temperature instabilities, ground loops and poor RF/EMI shielding due to aging effects were responsible for the phase jitter and drifts. The long-term drifts and phase noise in the RF control of the LE buncher system have been minimized to a level better than 50 ps.

The control systems for cryogenic distribution, coupler, tuners, and beam line slits have been indigenously developed and installed. Most of the instrumentation systems are controlled/monitored through silicon lab-based microcontrollers and are designed with a user friendly interface. The status of vacuum and beam line valves (open/close) can be viewed from the control room via LabView interface. A simple scintillator detector system, consisting of CsI crystal developed at BARC, coupled to a commercial PMT, is being set up to monitor the radiation levels around the cryostat and to enable the requisite access restriction for safety of personnel. A PIC18F4520 microcontroller based remote display unit for neutron area monitors is developed. The search & secure system has been upgraded to sequential mode to comply with safety requirements.

EPICS (Experimental Physics and Industrial Control System), an open-source toolset widely used for accelerator control, is being implemented to upgrade the Java-based distributed control system of the Linac. The EPICS-based control system has been developed and installed for the beam transport modules, including dipole, quadrupole, steerer magnets, and beam diagnostic devices (Faraday cup and Beam Profile Monitor controllers). The Input/Output Controller (IOC) for the beam control system is built on the EPICS Base 7 platform, running on Linux with the Asyn module and stream device protocol over IP. The front-end GUI is developed using Phoebus CSS. Additionally, we have developed a standalone slit control system and a remote-controlled stepper motor controller for the tuner and coupler system. The integration of these systems, along with the Beam Transport control system, into a unified GUI is currently in progress.

The Target lab, which is extensively used to prepare specialised self supporting targets for in-beam experiments, with natural and isotopically enriched materials, and stripper carbon foils for the accelerator. A new 4-pocket electron gun setup and a new rolling machine have been installed. Resistive evaporation setup has been refurbished. A dedicated thickness monitor setup to measure alpha energy-loss using standard alpha source has been set up.

For heat treatment of low-beta Nb cavities, a custom-designed, bottom loading, high-vacuum-high-temperature furnace to operate at a maximum of 1200^0C has been installed at TIFR. The design was optimized to provide a vertical hot zone of 600 mm diameter and 1000 mm high with a load capacity of 100 kg. The heat shields were optimized to achieve the maximum operating temperature at a modest power of less than 20kW.

ELOG, a web based application, is set up for operation and maintenance record keeping. This also includes inventory, major fault log and is completely shareable.

Beam Scanner and Variable Pulse Width Chopper

We have developed a simple method of beam scanning using an X-Y magnetic steerer in the beamline. A triangular waveform is applied to control the excitation current in the steerer for scanning the beam simultaneously in both horizontal (X) and vertical (Y) planes. A programme generates a raster pattern governed by a presettable number of X sweeps for each Y sweep. The scan area, step size and scanning speed are adjustable parameters. The dwell time at each of X-Y position was adjusted considering the time constant arising due to the inductance of the steerer. Typically, a beam scan on a ~10 x 10 mm^2 is achieved in ~5 sec. The scanner has been successfully employed for uniform irradiation of GaAs substrate for photoconductive THz applications using ^{12}C beam

Lifetime measurements in gamma spectroscopy are a crucial tool in nuclear physics. To measure the lifetimes in the intermediate range of milliseconds to minutes, a novel beam chopper based on beamline steerer magnet is developed. The beam is swept away on a nearby Tantalum slit, in the desired time window by controlling the high-current power supply of the steerer magnet using a square wave. The system is powered by an ARM Cortex-M3 32-bit RISC processor, part of the ARM® Cortex™-M3 family. It features a graphic touch-screen LCD and is fully programmable through a user-friendly menu. Both the voltage levels (to control the degree of beam deflection) and the timing at each voltage level (to control the beam on/off duration) can be programmed. The beam deflection can occur either horizontally or vertically using the X or Y steerer power supply. The beam chopper was successfully tested with a 45 MeV ^{12}C beam decay spectroscopy of ^{139}Ce (halflife ~ ms).

Experimental Programmes

There are a total of seven beam lines housed in two separate caves-hall 1 and 2 (See Figures 2 and 3). Experiments are performed in both halls with beams from Linac as well as from Pelletron. In addition, beams from Pelletron are available in the cascade hall (5 beam lines) and proton/neutron irradiation setup at 6 m. The research activities at the facility span a variety of problems in nuclear, atomic, condensed matter physics and interdisciplinary areas. The research work in nuclear physics, which is the main thrust of this facility, covers areas of nuclear structure studies at high angular momentum and excitation energies; and the heavy ion reaction dynamics-elastic, inelastic, transfer, fusion and fission reactions. In addition, studies pertaining to nuclear data generation relevant to nuclear reactors as well as IAEA coordinated research programs on advanced nuclear reactors, nuclear astrophysics, and elemental analysis using PIGE (Particle Induced Gamma Emission) are carried out. Application-oriented programs like radioisotopes production, radiation damage studies (space-bound devices, yield improvement in wheat & rice seeds), secondary neutron

Fig.2: Experimental area User Hall 1 where both Pelletron and LINAC beams are located.

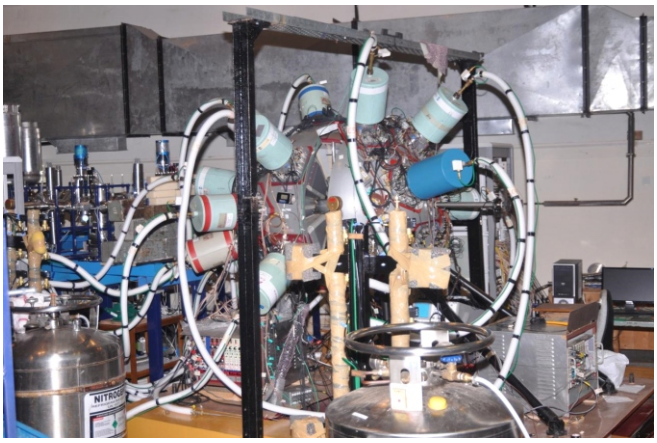

Fig.3: Picture of the Indian National Gamma Array with the Compton suppressed clover detectors in user Hall 2 at PLF.

production for cross section measurements, radiation dosimetry studies, ion irradiation in semiconductor crystals for photoconductive THz emitters, Accelerator Mass Spectrometry, production of track-etch membranes etc., are also pursued. Many new experimental activities have been initiated in the recent past by different user groups.

Major experimental facilities include:

- Clover Detector Array for discrete gamma ray spectroscopy with auxiliary detectors
- 150 cm diameter Scattering Chamber, with two independently rotatable arms permitting detector rotation and target ladder adjustment from remote without beam interruption using Programmable Logic Controller, for charged particle spectroscopy and fission studies
- BaF_2/$LaBr_3$ array for high energy gamma ray studies with BGO/NaI(Tl) multiplicity filter
- Charged Particle Array based on Si pad (ΔE) and CsI(E) detectors
- Neutron Detectors Array of 18 Liquid Scintillation detectors and Annular parallel plate avalanche counter having 12 segments with angular coverage from 5^0 to 11^0, for Time of Flight Technique based compound nucleus residue tagging
- MWPC and Si-strip detectors for angular distribution measurements of particles
- 7.0 Tesla superconducting magnet for hyperfine interaction studies
- Irradiation setup and Low background offline counting facility
- Electron spectrometer, X-ray detector setups, recoil-ion spectrometer, atomic-hydrogen source and a multiple target holder assembly for atomic physics studies with gas and foil targets
- High current proton (upto 24 MeV, ~200 nA) and neutron irradiation (through (p,n) reaction on Li, Be targets) facility

A Momentum Achromat for light Rare Ion Experiments (MARIE) is under development. A VME based DAQ and advanced digital DAQ with analysis programs are developed in-house. In addition, Indian National Gamma Array (INGA) was installed at PLF [3], a new readout scheme based on the Digital Signal Processing (DSP) technique. The INGA, consisting of a 24 Clover HPGe detector array with a total photo-peak detection efficiency of ~5%, is a powerful "femtoscope" for the study of the structure of atomic nuclei at high spins (see Fig. 3). More than 50 experiments have been successfully completed. A versatile low-temperature high-magnetic-field setup is used for an on-line time differential perturbed angular distribution (TDPAD) technique to study different problems in solid state physics [4] as well as for measurements of nuclear g-factors, an essential ingredient for understanding nuclear structure at high excitation energies. The R&D efforts in instrumentation in the laboratory have also led to various international collaborations, including those with major upcoming RIB facilities such as FAIR and SPIRAL2.

Interdisciplinary Research Programmes

Demand for production and separation of clinically important radionuclides from non-reactor source has grown in recent years. The research work at PLF has resulted in development of innovative techniques on methods for separation of no-carrier-added radionuclides using benign chemicals and chemical pathways following the mandate of Green Chemistry [5].

Prof. Prabhu's group have demonstrated continuous wave (CW) terahertz generation from antennas fabricated on ^{12}C-irradiated semi-insulating (SI) GaAs substrates [6]. The dark current drawn by the antennas fabricated on irradiated substrates is up to 4 orders of magnitude lower compared to antennas fabricated on un-irradiated substrates, while the photocurrents decrease by only orders of magnitude. This can be attributed to the strong reduction of the carrier lifetime by about 2.5 orders of magnitude. Reduced thermal heating allows for higher bias voltages to the irradiated antenna devices resulting in higher CW terahertz power, just slightly lower than that of low-temperature grown GaAs (LT GaAs) at similar excitation conditions.

The radiation damage studies for space devices/components are also routinely performed at PLF, TIFR.

Shanmugam *et al.* [7] had studied the Silicon Drift Detector (SDD), intended to be used in Chandrayaan-2 instruments, with an aim to understand and quantify spectroscopic performance degradation due to irradiation. The expected end-of-life (EOL) 10MeV equivalent proton fluence was modeled using SPENVIS simulation software. The Silicon Drift Detector was irradiated with 10 MeV protons for the doses up to 24 krad in logarithmic steps and measured the energy resolution and the leakage current at each dose and it was shown that the energy resolution degradation was acceptable for the cumulative proton dose of ~11 krad, which was within acceptable limits.

Future Plans

To increase the mass acceptance of the heavy-ion superconducting Linac, it was decided to replace the lead plated Cu cavities (β=0.1) by low beta (β=0.07) bulk-Niobium (Nb) cavities, in the first linac module. This together with high-voltage upgrade of the Pelletron will lead to significant increase in overall performance.

The Nb QWR design has been finalised and two SS prototypes (one at CDM-BARC and one at CWK-TIFR) have been fabricated. For the design qualification, resonant frequency measurement and field mapping using the bead-pull method was done. A precision bead-pull test setup has been developed at TIFR, employing a 6 mm diameter teflon bead for this purpose. Changes in electric field and resonant frequency were measured in two ways - i) frequency modulation technique with a high-precision signal generator and a 500 MHz digital oscilloscope, and ii) measurement of the electric field from the phase shifts using a Vector Network Analyzer. The comparison with simulations is then used to optimize and finalise the Nb QWR dimensions. Efforts are underway for the development of digital LLRF control for the superconducting cavities and solid state amplifiers.

Upgradation of the various experimental facilities is an ongoing process. The development of heavier ion beams, such as ^{40}Ca, ^{48}Ti, ^{56}Fe, and ^{58}Ni, has been initiated. Additionally, efforts to develop special beams of isotopes like ^{3}He, ^{10}Be, and ^{14}C due to their significant scientific interest are underway.

Acknowledgments

The BARC-TIFR Pelletron Linac Facility is an unique and exceptional facility. Right from the inception to continued productive operations, it has been a great teamwork of generations of scientists, technicians, and support staff. We are thankful to all those who have been instrumental in shaping the facility. We gratefully acknowledge the PLF staff, users, DNAP (TIFR), NPD(BARC) and various other sections of TIFR and BARC, for their constant support.

References

[1] S.S. Kapoor et al., Indian Journal of Pure and Appl. Phys. 27, 623 (1989)

[2] R.G. Pillay et al., Nuclear India 49, no.3, 24 (2012)

[3] R. Palit et al., Nucl. Inst. Meth. Phys. Res. A 680, 90 (2012)

[4] S.K. Mohanta et al., Phys. Rev. B87, 125125 (2013)

[5] M. Maiti and S. Lahiri, Radiochim. Acta 97, 663 (2009)

[6] Prathmesh Deshmukh, et al., Optics Letters 40, 4540 (2015)

[7] M. Shanmugam et al., Journal of Instrumentation 15, P01002 (2020)

नाभिकीय अभिक्रिया

3

^{6,7}Li एवं ^{9}Be जैसे दुर्बल-बंध प्रक्षेपास्त्रों से जुड़ी अभिक्रियाएँ

एस.संत्रा
नाभिकीय खगोल भौतिकी अनुभाग, भाभा परमाणु अनुसंधान केंद्र (भापअ केंद्र), ट्रांबे, मुंबई – 400085, भारत
होमी भाभा राष्ट्रीय संस्थान, अणुशक्तिनगर, मुंबई – 400094, भारत

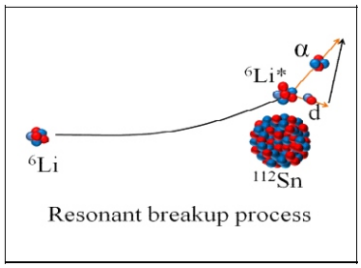

अनुनादी विभंजन प्रक्रम

सारांश

भापअ केंद्र-टीआईएफआर पेलेट्रॉन लीनॉक (एलआईएनएसी) सुविधा, मुंबई में मध्यम से भारी द्रव्यमान के कई लक्षित नाभिकों पर दुर्बल-बंध ^{6,7}Li और ^{9}Be प्रक्षेप्यों को शामिल करते हुए विशिष्ट एवं समावेशी मापन किए गए श्रृंखला के कई अनोखे परिणाम दृष्टिगत हुए हैं। इन प्रक्षेपकों के कई नए प्रक्षेप्य विभंजन मोड एवं नए समूह संरचनाओं की खोज की गई । प्रक्षेप्य के अनुनाद एवं गैर-अनुनाद विभंजन के तरीकों, संलयन अभिक्रियाओं, प्रत्यास्थ प्रकीर्णन, पूर्ण एवं अपूर्ण संलयन अनुप्रस्थ काट पर समूह संरचना के भूमिका की जांच की गई। प्रक्षेप्य को विभंजन की ओर ले जाने वाली अल्प-विभंजन सीमा ने प्रत्यास्थ प्रकीर्णन के साथ-साथ सभी अभिक्रिया चैनलों पर भारी प्रभाव दर्शाया है।

Nuclear Reactions

3

Reactions involving Weakly-bound Projectiles like ^{6,7}Li and ^{9}Be

S. Santra
Nuclear Astrophysics Section, Bhabha Atomic Research Centre (BARC), Trombay, Mumbai-400085, INDIA
Homi Bhabha National Institute, Anushakti Nagar, Mumbai-400094, INDIA

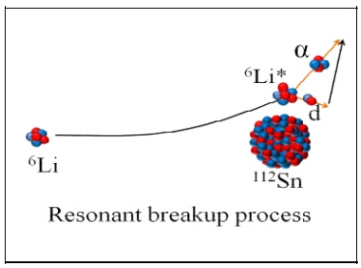

Resonant Break-up Process

ABSTRACT

A series of exclusive & inclusive measurements involving weakly bound ^{6,7}Li, and ^{9}Be projectiles on several target nuclei of medium to heavy masses have been carried out at BARC-TIFR Pelletron LINAC facility, Mumbai leading to many interesting results. Several new projectile breakup modes and new cluster structures of these projectiles were discovered. The role of cluster structure of the projectile on its resonant and non-resonant breakup modes, fusion reactions, elastic scattering, complete and incomplete fusion cross sections were investigated. The low breakup threshold leading to the breakup of the projectile showed a huge impact on elastic scattering as well as all the reaction channels.

KEYWORDS: *Weakly bound projectiles, resonant & non-resonant breakup, cluster structure, complete & incomplete fusion, transfer reaction, coupling effect*

**Author for Correspondence: S. Santra*
E-mail: ssantra@barc.gov.in

Introduction

The study of reactions involving weakly bound stable projectiles such as ^{6,7}Li and ^{9}Be provides an opportunity to study nuclear reactions very similar to radioactive ion beams because of their similarities in low breakup threshold energies of the valence nucleons and cluster structures. Hence, compared to the reactions involving tightly bound projectiles, these reactions are accompanied additionally with projectile breakup channels. The identification of various breakup channels in a reaction and their possible effects on reaction dynamics make the study very interesting and challenging.

Understanding the reaction mechanisms of weakly bound projectiles and the coupling of their breakup on various reaction channels is very important, especially in the context of the increasing number of the radioactive ion beam facilities and the quest for super heavy elements by the fusion of nuclei near the drip line.

In recent years extensive studies have been carried out for the reactions involving the above weakly bound projectiles with different target nuclei. Results of some of these studies are highlighted below.

Resonant and Non-resonant Breakup of ^{6,7}Li

A series of measurements involving all the three projectiles on several target nuclei of medium to heavy masses have been carried out at Pelletron-LINAC facility, Mumbai. Majority of these work during last 10 years focused on the exclusive measurements of two breakup fragments in coincidence to investigate the possible dominant breakup modes. During the process, many new breakup channels have been identified and their cross sections have been measured, particularly in the reactions ^{6}Li+^{112}Sn and ^{7}Li+^{112}Sn.

For exclusive measurements, where the coincidence yield is expected to be very low, two large area Si-Strip-Detector Arrays with a maximum angular coverage of ~100 degree has been setup as shown in Fig.1. The strip detector arrays consist of ten to fourteen strip detectors, each of which has 16 horizontal and 16 vertical strips. This leads to a total of 1280 and 1792 pixels of the two detector arrays respectively for sensing the position of the detected particles. Number of electronic signals collected from each strip telescope is 48 that lead to a total of 240-336 signals from the full strip detector arrays. Both the projectiles (^{6,7}Li) can breakup into two fragments by any of the following processes: (i) Direct breakup (ii) Resonant breakup or (iii) Transfer-breakup. Several resonant breakup channels have been observed for the first time. For example, the breakup of ^{6}Li into α+d through its 3rd resonance state 1^{+}(5.65 MeV) (see Fig.2, left panel) [1], the breakup of ^{7}Li into α+t through its 2nd resonance state 5/2^{-} (6.67 MeV) (see Fig.2, right panel) [2] and breakup of ^{8}Be into 2 alpha through the 3rd resonance state 4^{+}(11.31 MeV) in the reaction (^{7}Li,^{8}Be ->2α) [3]; all of them have been observed for the first time. In addition, the observation of ^{6}He+p breakup suggests of a new possible cluster structure ^{7}Li as ^{6}He+p [2] other than that of the well-known ^{4}He+^{3}H and ^{6}Li+n structures. Cross sections for direct and resonant breakup of radioactive ^{7}Be nuclei produced in a transfer reaction ^{112}Sn(^{6}Li,^{7}Be→α+^{3}He)^{111}In have been measured. Breakup of ^{7}Be into α and ^{3}He cluster fragments via its resonant states of 7/2^{-}(4.57 MeV) and 5/2^{-}(6.73 MeV) in the continuum have been identified for the first time using the measured distribution of α–^{3}He relative energy and the reaction *Q* value obtained from the α–^{3}He coincident events. Significant cross sections for breakup of ^{7}Be into its cluster fragments directly or through resonant states highlight the importance of the

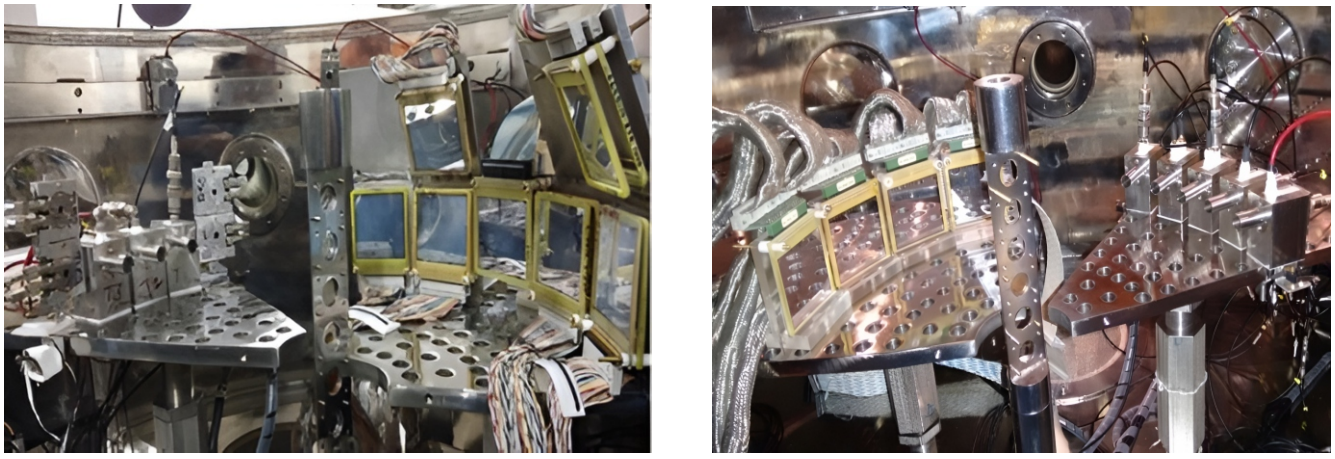

Fig.1: Typical detector setups inside the scattering chamber consisting of 5 sets of single telescopes and 7 (5) sets of strip telescopes, shown in left (right) panel, used for the breakup cross section measurements.

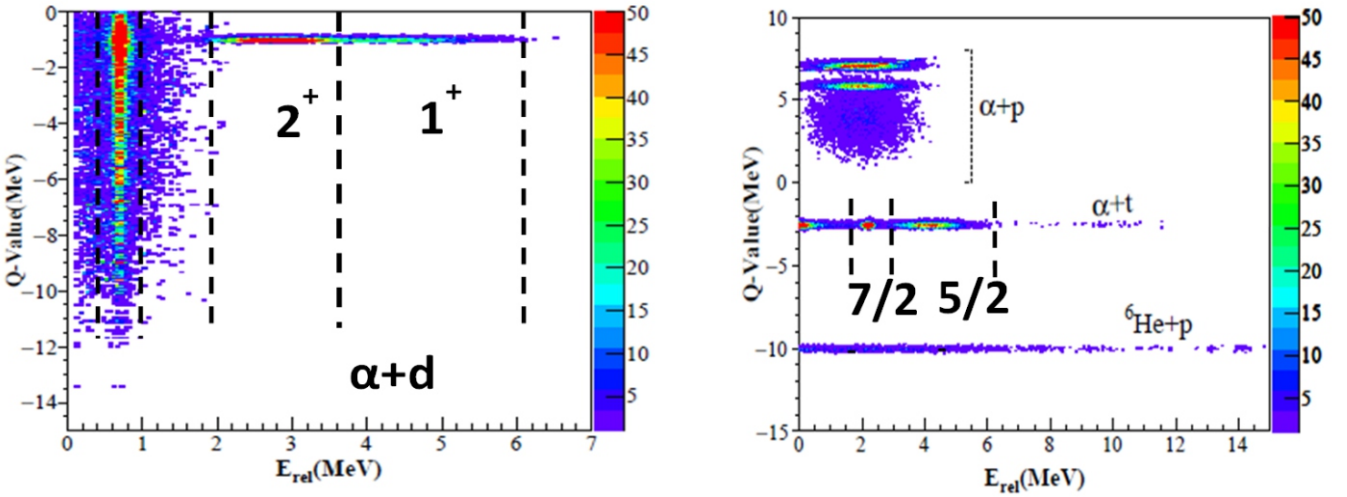

Fig.1: Q-value versus relative energy plots corresponding to breakup of ^{6}Li alpha+d via 3^{+}, 2^{+} and 1^{+} resonances (left panel) and ^{7}Li→alpha+t via 7/2- and 5/2- resonances (right panel).

ground-state structure of ^{7}Be as a cluster of α and He [4]. All the above observations of breakup through higher resonances have been possible due to the use of the large area Si Strip Detector Arrays. Another interesting observation is that, in all of the breakup modes, one of the breakup fragments is an alpha particle. By measuring as many such channels as possible and estimating the cross sections of the remaining non-measurable alpha producing channels together we have tried to understand the reaction mechanism of large inclusive alpha cross sections for each of the reactions.

Breakup Capture Cross sections

Role of various cluster structures of ^{7}Li in the dynamics of fragment capture was studied for the first time from the particle gamma coincidence measurement. A detailed analysis of the measured yields of the evaporation residues for different excitation energies (E*) of the composite system based on a new dynamical classical trajectory model were performed. These calculations, constrained by the measured fusion, ^{4}He and ^{3}H capture cross-sections, unambiguously illustrate a two-step process - breakup followed by fusion in the case of the capture of ^{3}H and ^{4}He, while in the case of ^{6}He+p and ^{5}He+d configurations massive transfer arising from bound states is inferred to be the dominant mechanism. This work clearly demonstrated the role played by the cluster structure of ^{7}Li in understanding the reaction dynamics at energies around the Coulomb barrier [5].

Non-capture versus Capture Cross sections

Reaction dynamics involving weakly bound nucleus ^{7}Li, populating the continuum states, was studied by performing particle-particle (using Si-Strip detector array) and particle – gamma (using Si-detector telescope + INGA array) coincidence measurements. For the first time simultaneous investigation of all the major reaction processes, breakup, nucleon transfer followed by breakup, and fragment capture reaction channels along with elastic scattering and fusion reaction. The rather complete nature of the data set combined with state of the art theoretical calculations has improved the understanding of the reaction dynamics involving weakly bound stable nuclei and provided an important benchmark for future experiments with radio-active ion beams that are available in low intensities [6,7].

Cluster Transfer versus Breakup Fusion

The origin of the large α particle production and incomplete fusion in reactions involving weakly-bound α+x cluster nuclei still remains unresolved. While the (two-step) process of breakup followed by capture of the "free" complementary fragment (x) is widely believed to be responsible, a few recent studies suggest the dominant role of (direct) cluster stripping. To achieve an unambiguous experimental discrimination between these two processes, a coincidence measurement between the outgoing α particles and γ rays from the heavy residues has been performed for the ^{7}Li (α+triton)+^{93}Nb system. Proper choice of kinematical conditions allowed for the first time a significant population of the region accessible only to the direct triton stripping process and not to breakup followed by the capture of the "free" triton (from the three-body continuum). This result, also supported by a cluster-transfer calculation, clearly establishes the dominance of the direct cluster-stripping mechanism in the large alpha production [8].

Complete and Incomplete Fusion

The complete and incomplete fusion cross sections for the ^{7}Li + ^{124}Sn,^{205}Tl reactions [9-11] were measured using online and offline characteristic γ-ray detection techniques. A simultaneous explanation of complete, incomplete, and total fusion (TF) data was also obtained from the calculations based on the continuum discretized coupled channel method. Similar measurements performed with ^{6}Li having lower breakup threshold gave higher incomplete fusion cross-section. The total fusion cross section ratio between ^{6}Li and ^{7}Li induced reactions shows an increasing trend as the energy decreases below the barrier while it remains unity at above-barrier energies.

Summary

The exclusive and inclusive measurements involving weakly bound ^{6,7}Li, and ^{9}Be projectiles on series of target nuclei of medium to heavy masses have been carried out at Pelletron-LINAC facility, Mumbai leading to many interesting results. Several new projectile breakup modes and new cluster configurations of these projectiles were discovered. The role of the cluster structures of the projectiles on the resonant and non-resonant breakup modes, fusion reactions, elastic scattering, complete and incomplete fusion cross sections were investigated. The low breakup threshold leading to the breakup of the weakly bound projectiles showed a huge impact on elastic scattering, fusion and several other reaction channels.

References

[1] D. Chattopadhyay et al., Phys. Rev. C 94, 061602 (Rapid Comm.) (2016).

[2] D. Chattopadhyay et al., Phys. Rev. C 97, 051601 (Rapid Comm.) (2018).

[3] D. Chattopadhyay et al., Phys. Rev. C 98, 014609 (2018).

[4] D. Chattopadhyay et al., Phys. Rev. C 102, 021601(R) (2020).

[5] A. Shrivastava et al., Phys Letts B 718,931(2013).

[6] S. K. Pandit et al., Phys Rev C 93, 061602 (Rapid Comm.) (2016)

[7] S. K. Pandit et al., Phys. Rev. C 96, 044616 (2017).

[8] S. K. Pandit et al., Physics Letters B, 820, 136570 (2021).

[9] V. V. Parkar et al., Phys. Rev. C 97, 014607 (2018).

[10] V. V. Parkar et al., Phys. Rev. C 109, 014610 (2024).

[11] V. V. Parkar et al., Phys. Rev. C 98, 014601 (2018).

नाभिकीय अभिक्रिया

4

दुर्बल-बंध स्थिर नाभिक से जुड़े अभिक्रिया तंत्र को उजागर करना

एस.के. पंडित[1,2,*], ए.के. श्रीवास्तव[1,2], के. माहात[1,2], के. रामचंद्रन[1] और पी.सी. राउत[1,2]
[1]नाभिकीय भौतिकी प्रभाग, भाभा परमाणु अनुसंधान केंद्र (भापअ केंद्र), ट्रांबे, मुंबई – 400085, भारत
[2]होमी भाभा राष्ट्रीय संस्थान, अणुशक्तिनगर, मुंबई – 400094, भारत

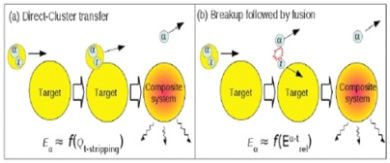

^{7}Li (α+ t) + लक्षित अभिक्रिया हेतु समूह के विभंजन में से एक के संलयन के बाद (a) प्रत्यक्ष-समूह हस्तांतरण और (b) विभाजन को दर्शाने वाला चित्रण।

सारांश

कण-कण और कण-γ-किरण संयोग माप का उपयोग करके ^{7}Li (α+ t) + ^{93}Nb प्रणाली के लिए दुर्बल-बंध में स्थिर नाभिक से जुड़े अभिक्रिया तंत्र की जांच की गई। विभिन्न विघटन अभिक्रिया चैनलों को समझने के लिए कण-कण संयोग माप किया गया, जबकि कण-γ-किरण संयोग माप का उपयोग बड़े α कण उत्पादन और अपूर्ण संलयन अभिक्रिया चैनलों की उत्पत्ति को समझने के लिए किया जाता है। टी-कैप्चर तंत्र को ~ 70% प्रभावित करता पाया गया। गतिज स्थितियों के उचित चयन ने पहली बार क्षेत्र की एक महत्वपूर्ण आबादी को केवल प्रत्यक्ष ट्राइटन स्ट्रिपिंग प्रक्रिया के लिए सुलभ होने की अनुमति दी और इसके बाद "मुक्त" ट्राइटन (त्रि-निकाय निरंतरता से) पर नियंत्रण के बाद विभंजन की अनुमति नहीं दी। यह परिणाम, स्पष्ट रूप से बड़े अल्फा उत्पादन में प्रत्यक्ष क्लस्टर-स्ट्रिपिंग तंत्र के प्रभुत्व को स्थापित करता है।

Nuclear Reactions

4

Unravelling the Reaction Mechanisms involving Weakly-bound Stable Nuclei

S. K. Pandit[1,2,*], A. K. Shrivastava[1,2], K. Mahata[1,2], V. V. Parkar[1,2], K. Ramachandran[1] and P. C. Rout[1,2]
[1]Nuclear Physics Division, Bhabha Atomic Research Centre (BARC), Trombay, Mumbai-400085, INDIA
[2]Homi Bhabha National Institute, Anushakti Nagar, Mumbai-400094, INDIA

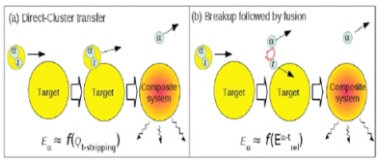

Illustration depicting (a) direct-cluster transfer and (b) breakup followed by fusion of one of the cluster fragments for ^{7}Li(α+t)+target reaction.

ABSTRACT

The reaction mechanisms involving weakly bound stable nuclei has been investigated using particle-particle and particle-γ-ray coincidence measurements for ^{7}Li(α+t)+^{93}Nb system. Particle-particle coincidence measurements were carried out to understand various breakup reaction channels, while particle-γ-ray coincidence measurements is utilised to understand the origin of the large α particle production and incomplete fusion reactions channels. The t-capture mechanism is found to be dominant ~70%. Proper choice of kinematical conditions allowed for the first time a significant population of the region accessible only to the direct triton stripping process and not to breakup followed by the capture of the "free" triton (from the three-body continuum). This result, clearly establishes the dominance of the direct cluster-stripping mechanism in the large alpha production.

KEYWORDS: *Direct nuclear reaction, weakly bound nuclei, fusion, cluster in nuclei*

**Author for Correspondence: S. K. Pandit*
E-mail: sanat@barc.gov.in

Introduction

Exploring the properties of weakly bound stable and unstable nuclei with α+x cluster structure, e.g., ^{6,8}He, ^{6,7}Li, and ^{7,9}Be, is a topic of current interest [1,2] and also a focus of the next generation of high intensity isotope-separation online (ISOL) radioactive ion beam facilities. Apart from elastic scattering and fusion, due to the low breakup threshold of such nuclei, the population of the continuum is probable and consequently a large coupling effect is expected at energies around the Coulomb barrier. This may take place directly through inelastic excitation of the projectile (prompt or resonant breakup) or by nucleon transfer leaving the ejectile in an unbound state (transfer breakup) [1–15]. Another reaction channel, breakup followed by capture of fragments (only part of the projectile fuses) known as incomplete fusion is an important reaction and interestingly it is dominant over fusion at energies below the Coulomb barrier.

The origin of the observed large inclusive α-particle production cross sections compared to that of the complementary fragments is also important to understand. Different reaction mechanisms, e.g., breakup (direct and sequential), nucleon transfer followed by breakup, cluster transfer, incomplete fusion and compound nuclear (CN) evaporation, contribute to the α-yield.

It is difficult to separate the contributions of these individual reaction mechanisms from an inclusive measurement. Exclusive measurements are therefore needed to disentangle the different reaction processes, discussed above. In this investigation, we aimed to disentangle different reaction channels utilising exclusive measurements and quantum mechanical coupled channels calculations.

Experimental Details

All the measurements were carried out at the Pelletron-Linac facility, Mumbai, with ^{7}Li beams of 24, 26, 28, and 30 MeV. A self-supporting ^{93}Nb foil of thickness ~1.75 mg/cm^2 was used as a target. For the measurements of breakup reaction channels, the requirements of high granularity to detect low-lying resonant states and large solid angle to measure low cross-section events were achieved using segmented large area Si telescopes of active area 5 × 5 cm^2. The ΔE-detectors (50 μm thick) were single-sided and the E-detectors (1.5 mm thick) were double-sided with 16 strips allowing a maximum of 256 pixels. Two such telescopes, set 30◦ apart, were mounted at a distance of 16 cm from the target on a movable arm in a scattering chamber. In this geometry, the cone angle between the two detected fragments ranged from 1^0 to 24^0. The angular range 30^0–130^0 (around the grazing angle) was covered by measurements at different angle settings. Three Si surface barrier detector telescopes (thicknesses: ΔE ~ (20-50 μm, E ~ 450–1000 μm) were used to obtain the elastic scattering angular distribution at forward angles (25^0–40^0) where the count rate is too high for the strip detectors to cope with. Two Si surface-barrier detectors (thickness ~300 μm) were kept at ±20^0 for absolute normalization. The detectors were calibrated using the known α energies from a ^{239}Pu-^{241}Am source and the ^{7}Li+^{12}C reaction at 24 MeV. Breakup fragments in coincidence were measured at beam energies of 24, 28, and 30 MeV.

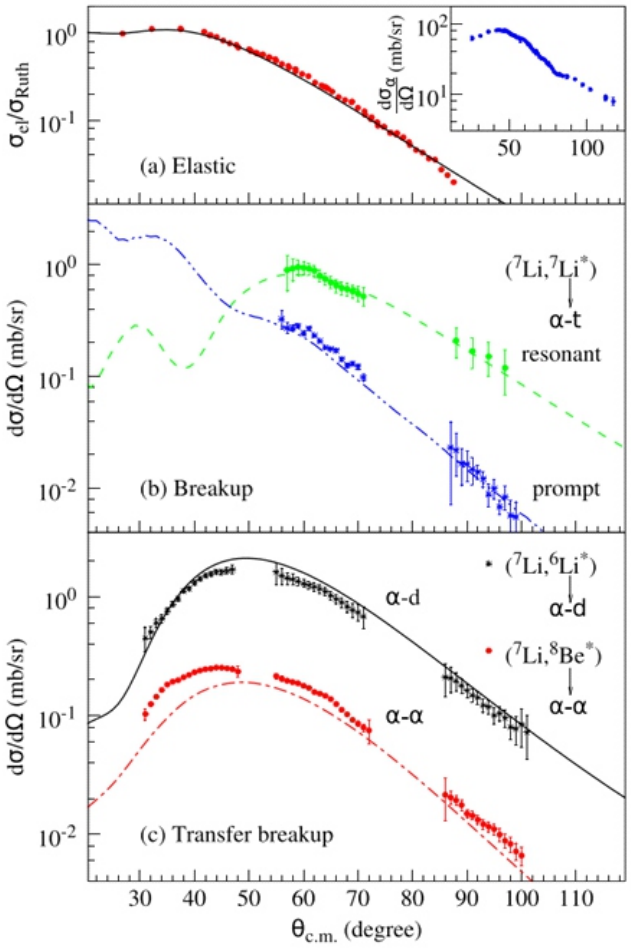

Fig.1: Measured inclusive and exclusive cross sections for the ^{7}Li+^{93}Nb system at 28 MeV. (a) Elastic scattering data and the CDCC calculation. The inclusive cross section for α production is shown in the inset. (b) Prompt and resonant (from the 7/2$^-$ state) breakup of ^{7}Li, shown as asterisks and filled circles, respectively.

Two independent experiments were carried out for in-beam and off-beam γ-ray counting. Both the measurements were performed at beam energies of 24, 26, 28, and 30 MeV, some of which are common to the exclusive measurement of breakup fragments.

Prompt γ-ray transitions were detected using the Indian National Gamma Array (INGA) [16], consisting of 18 Compton suppressed high purity germanium (HPGe) clover detectors. In this particular array configuration, the detectors were arranged at six different angles with three detectors each at ±40^0, −65^0, and −23^0, two detectors at +65^0 and four detectors at 90^0. Three Si surface barrier telescopes (thicknesses: ΔE ~15–30 μm, E ~ 300–5000μm), were placed inside the scattering chamber at 35^0, 45^0, and 70^0 for the detection of charged particles around the grazing angle. One Si surface barrier detector (thickness ~300 μm) was fixed at 20^0 to monitor Rutherford scattering for absolute normalization purposes. The time stamped data were collected using a digital data acquisition system with a sampling rate of 100 MHz [16]. Efficiency and energy calibration of the clover detectors were carried out using standard calibrated ^{152}Eu and ^{133}Ba γ-ray sources.

The off-line γ-ray counting was carried out using an efficiency calibrated high-purity germanium (HPGe) detector. Low background was achieved by using graded shielding (Cu, Cd sheets of thickness ~2 mm each followed by 5 cm of Pb). Aluminum catcher foils of thickness ~1 mg/cm^2 were used together with each target foil to stop the recoiling residues. The target and catcher foil assemblies were irradiated for ~6 h (beam current ~50 nA) at each bombarding energy and counted together at a distance of 10 cm from the detector. A CAMAC scaler which recorded the integrated current in intervals of 1 min duration was used to monitor beam current.

Data Analysis and Results (A)

Detected particles were identified from energy loss information and tagged by kinetic energy (E), identity (A, Z), and scattering angle (θ, φ) with respect to the beam axis. The relative angles (θ_{rel}) between the fragments were calculated from the measured scattering angles (θ_1, φ_1; θ_2, φ_2). The fragments' mass, kinetic energy (E_1, E_2), and θ_{rel} were used to calculate their relative energy (E_{rel}). The excitation energy of the ejectile prior to breakup was obtained by adding the breakup threshold to the measured E_{rel}. The E_{rel} spectra for α+α, α+d, and α+t exhibit peaks at 0.092, 0.71, and 2.16 MeV that correspond to the breakup of ^{8}Be (g.s.), ^{6}Li (2.18 MeV, 3$^+$), and ^{7}Li (4.63 MeV, 7/2$^-$), respectively.

The excitation energy of the target-like nuclei was determined using the missing energy technique. For the transfer reactions, this was found to peak around the energy $E^*=Q_{gg}-Q_{opt}$, as expected from the semi classical theory of trajectory matching [17]. Here Q_{gg} and Q_{opt} are the ground state and optimum Q values, respectively.

The efficiency for the detection of fragments in coincidence was estimated using the Monte Carlo technique, taking into account the excitation of the target as well as the ejectile, the Q value of the reaction, the energy resolution, and detection threshold. The efficiency depends on the velocity of the ejectile prior to breakup as well as the relative velocity of the fragments [18,19]. The scattering angle of the ejectile prior to breakup was assumed to be isotropic. The scattered energy of the ejectile was calculated using kinematics. The breakup fragment emission in the rest frame of the ejectile was also considered to be isotropic. The velocities of each fragment in the rest frame of the ejectile were calculated using energy and momentum conservation laws. These velocities were added to the velocity of the ejectile prior to breakup to get their velocities in the laboratory frame. It was checked whether both fragments hit two different vertical and horizontal strips. Events satisfying this condition were considered as detectable events for estimation of the efficiency. The conversion of the energy and scattering angle from the laboratory frame to the c.m. frame of the target-projectile in event-by-event mode automatically takes care of the Jacobian of the transformation.

The angular distributions of elastic scattering, projectile breakup, and transfer followed by breakup for the ^{7}Li+^{93}Nb system at 28 MeV are shown in Fig.1. The elastic scattering data are presented in Fig.1(a). The errors on the data points are due to statistics. The ^{7}Li*⟶ α + t breakup via the 7/2$^-$ state and the continuum below this resonance are shown in Fig.1(b). The cross sections for 1p pickup leading to the ^{8}Be(g.s.) are shown in Fig.2(c). These data are restricted to ^{92}Zr excitation energies up to 3.0 MeV, as information on the spectroscopic factors is available only in this energy range. For 1n stripping, the cross sections for α + d breakup events from the ^{6}Li 3$^+$ (2.18 MeV) state are shown in Fig.2(c). Excited states of 94Nb up to 1.0 MeV were considered. The differential cross sections for α+d events from the breakup of ^{6}Li formed after 1n stripping are larger than those for α+t events from the resonant breakup of ^{7}Li, while those for α+α events due to 1p pickup forming ^{8}Be are smaller [20, 21].

Data Analysis and Results (B)

The residues populated by t-capture, complete fusion (CF), and nucleon(s)-transfer identified by detecting their characteristic γ-rays. The α-particle gated γ-ray spectrum, were obtained, which shows the major reaction processes contributing to the α-particle yield. The relative yields of γ-ray transitions from the residues of t- capture (^{94,95}Mo) are found to be greater than the others. The other reaction mechanisms contributing to the α yields, namely, 1p pickup (^{7}Li,^{8}Be ⟶ α + α)^{92}Zr, inelastic excitation (^{7}Li,^{7}Li* ⟶ α + t)^{93}Nb, 1n stripping (^{7}Li,^{6}Li* ⟶ α + d)^{94}Nb, and 2n-stripping (^{7}Li,^{5}Li ⟶ α+p)^{95}Nb were also identified.

The cross sections for the residues from the t-capture mechanism, ^{94,95}Mo, were extracted. For ^{94}Mo, the yrast γ-ray transitions built on the ground state up to the $J^\pi = 10^+$ excited state was considered. The cross sections for 95Mo were obtained by adding the γ-ray transitions feeding directly to the ground state. The ^{93}Mo nucleus has a 21/2$^+$ isomeric state at E_{ex} =2.425 MeV with half-life $T_{1/2}$ = 6.85 h. The cross section for ^{93m}Mo was obtained by following the radioactive decay of the isomeric state. The uncertainty in the measured cross sections were estimated considering (1) statistics, (2) γ-ray detection efficiency, and (3) available spectroscopic information of the residues. For off-beam measurements uncertainty in the target thickness was also included.

The α-capture and 2n-stripping mechanisms lead to ^{95,96}Tc and ^{95}Nb. These nuclei are radioactive with reasonable half-

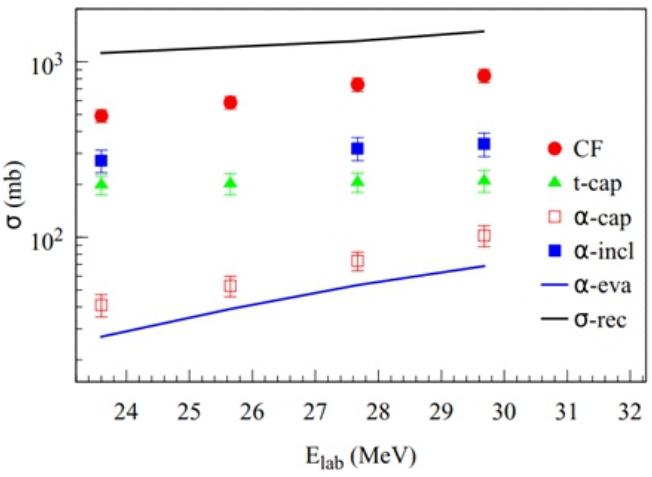

Fig.2: The measured cross sections for t-capture, α-capture, CF, inclusive-α are denoted by filled triangles, open squares, filled circles, and filled squares, respectively. The blue line is the estimated α-evaporation cross section from the statistical model calculations. The calculated reaction cross sections are also shown by the black line.

lives for decay from their ground states [$T_{1/2}$(^{95}Tc) = 20.0 h, $T_{1/2}$(^{96}Tc) = 4.28 d, $T_{1/2}$(^{95}Nb) = 34.99 d] as well as from metastable states [$T_{1/2}$(^{95}Tc) = 61 d, $T_{1/2}$(^{96}Tc) = 51.5 m, $T_{1/2}$(^{95}Nb) = 3.61 d]. The *γ*-ray transitions corresponding to decay of ^{95,96}Tc and ^{95}Nb were identified. The cross sections were extracted following the half-lives of each transition. The complete fusion of ^{7}Li with ^{93}Nb forms the compound nucleus (CN) ^{100}Ru, which decays predominantly by neutron and proton emission. The characteristic prompt γ-ray transitions of the evaporation residues (ERs) $^{96-98}$Ru and ^{97}Tc were also identified. The cross sections of $^{96-98}$Ru and ^{97}Tc were obtained using the in-beam method. The cross sections for ^{97}Ru were also extracted using the off-beam *γ*-ray counting method and found to be consistent with the in-beam measurements and with the values reported in Ref. [22].

The cross sections of individual residues from α and t-capture were corrected for the contribution from the compound nucleus. The t-capture, α-capture, and complete fusion cross sections were obtained by taking the sum of individual residue cross sections and are presented in Fig.2 [23]. The cross sections for t-capture are found to be larger than those for α-capture at all energies, in agreement with the results reported in earlier studies with ^{7}Li projectiles [24-26]. The estimated α-particle evaporation and the extracted reaction cross sections are also plotted in Fig.3.

The t-capture reaction can arise due to either direct stripping of a cluster from a bound state of the projectile or fusion of one of the "free" fragments after breakup of the projectile, i.e., so called breakup-fusion [23]. These two mechanisms were disentangled by proper kinematic conditions. The α-particle energy spectrum at 35^{0} gated with the characteristic γ-rays of ^{94,95}Mo shows a substantial

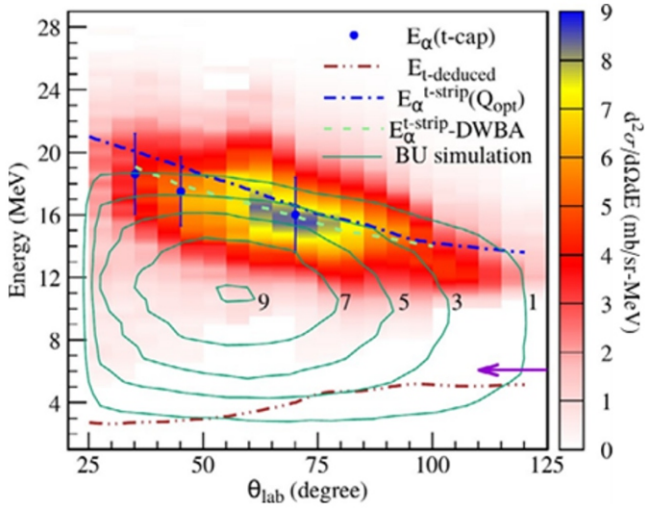

Fig.3: Measured energy-angle correlation spectrum of inclusive α particles in the ^{7}Li+^{93}Nb reaction compared with the kinematical line for Q_{opt} (dot-dashed line) and the DWBA calculations (dashed line) for t stripping. Mean values of the measured α-energy at three different laboratory angles in coincidence with prompt γ rays are shown as filled circles along with the width (FWHM). The results of a breakup simulation are shown as contours (see text for details). The energy of the triton calculated from the mean energy of the inclusive α spectra assuming breakup followed by capture of a triton by the target is shown by the dot-dot-dashed line. The arrow indicates the position of the Coulomb barrier between the triton and ^{93}Nb.

population of $E_α$ >20.5 MeV. From Q-value arguments of free-t-fusion, the α-particles ($E_α$ >20.5) must be exclusively due to direct t-cluster stripping from bound states of ^{7}Li to bound states (with respect to triton emission) of 96Mo, allowing us to put a lower limit of ~30% on this contribution [27].

The energy-angle correlations of the α-particles were analyzed for further investigation. The experimental correlations obtained from the inclusive and exclusive measurements are compared with those estimated as due to direct stripping and breakup in Fig.3. The measured inclusive and exclusive correlations exhibit similar characteristics. While the experimental correlations are in good agreement with both the kinematical curve using the optimum Q-value and DWBA calculations for t-stripping over a wide angular range (25^{0}-125^{0}), the result of the breakup simulation has very different characteristics. This further demonstrates that breakup does not make a significant contribution to the α-particle production and ICF. The energy of the triton (E_t) deduced from the measured mean values of $E_α$ assuming the α-t breakup mechanism is found to be less than the Coulomb barrier between the t-fragment and ^{93}Nb (indicated by the arrow) over the whole angular range. This also indicates that, due to the fusion barrier, breakup followed by fusion of the triton is very unlikely. This systematic investigation establishes the dominance of cluster stripping over breakup-fusion as the main source for the large α-yields and ICF.

Summary and Conclusion

In summary, the present work reports for the first time a detailed study of the various breakup mechanisms, 1p pickup and 1n stripping to unbound states of the ejectile and direct breakup, for the same system at energies close to the Coulomb barrier. The absolute cross sections for t-capture, α-capture, and 2n stripping along with the complete fusion were also measured using the in-beam and off-beam *γ*-ray counting methods. The present study shows that the t-capture mechanism is the dominant reaction channel for the production of α particles and accounts for 62−73% of the measured inclusive α cross sections. The 2n stripping (^{5}Li → α + p) cross sections together with earlier data on the 1p pickup (^{8}Be → α + α), inelastic excitation (^{7}Li* → α + t), and 1n stripping (^{6}Li* → α + d) explain ~ 15% of the inclusive α cross sections. The statistical model predictions of the compound nuclear contributions from α-evaporation account for 10−20% of the inclusive α cross sections. With proper choice of kinematical conditions, it has been possible for the first time to populate with significant strength the part of the spectrum accessible to triton cluster stripping only and not to breakup. This provides direct experimental evidence for the dominant role of the stripping process and also allows a meaningful comparison with theoretical models. CDCC, DWBA and CCBA calculations were performed to analyze a comprehensive data set comprising elastic scattering, direct breakup, transfer breakup and t-stripping reaction channels.

This unique comprehensive dataset offers a test-bench for further development of state-of-the-art theoretical formalisms (e.g. [28-30]) for reactions involving weakly bound stable/radioactive nuclei, which are also used to simulate nucleosynthesis.

Acknowledgment

We acknowledge the accelerator staff for ensuring smooth running of the machine. The help extended by P. Patale during the experiment is also acknowledged.

References

[1] N. Keeley, N. Alamanos, K. W. Kemper, and K. Rusek, Prog. Part. Nucl. Phys. 63, 396 (2009).

[2] L. F. Canto, P. R. S. Gomes, R. Donangelo, J. Lubian, and M. S. Hussein, Phys. Rep. 596, 1 (2015).

[3] J. L. Quebert, B. Frois, L. Marquez, G. Sousbie, R. Ost, K.´ Bethge, and G. Gruber, Phys. Rev. Lett. 32, 1136 (1974).

[4] C. Signorini et al., Phys. Rev. C 67, 044607 (2003).

[5] A. Shrivastava, A. Navin, N. Keeley, K. Mahata, K. Ramachandran, V. Nanal, V. V. Parkar, A. Chatterjee, and S. Kailas, Phys. Lett. B 633, 463 (2006).

[6] A. Pakou et al., Phys. Lett. B 633, 691 (2006).

[7] S. Santra, V. V. Parkar, K. Ramachandran, U. K. Pal, A. Shrivastava, B. J. Roy, B. K. Nayak, A. Chatterjee, R. K. Choudhury, and S. Kailas, Phys. Lett. B 677, 139 (2009).

[8] F. A. Souza et al., Nucl. Phys. A 821, 36 (2009).

[9] D. H. Luong, M. Dasgupta, D. J. Hinde, R. du Rietz, R. Rafiei, C. J. Lin, M. Evers, and A. Diaz-Torres, Phys. Lett. B 695, 105 (2011).

[10] E. C. Simpson, K. J. Cook, D. H. Luong, S. Kalkal, I. P. Carter, M. Dasgupta, D. J. Hinde, and E. Williams, Phys. Rev. C 93, 024605 (2016).

[11] R. Rafiei, R. du Rietz, D. H. Luong, D. J. Hinde, M. Dasgupta, M. Evers, and A. Diaz-Torres, Phys. Rev. C 81, 024601 (2010).

[12] D. H. Luong, M. Dasgupta, D. J. Hinde, R. du Rietz, R. Rafiei, C. J. Lin, M. Evers, and A. Diaz-Torres, Phys. Rev. C 88, 034609 (2013).

[13] D. Martinez Heimann et al., Phys. Rev. C 89, 014615 (2014).

[14] S. P. Hu et al., Phys. Rev. C 93, 014621 (2016).

[15] O. A. Capurro, A. J. Pacheco, A. Arazi, P. F. F. Carnelli, J. O. Fernandez Niello, and D. Martinez Heimann, Nuc. Phys. A 945, 186 (2016).

[16] R. Palit, S. Saha, J. Sethi, T. Trivedi, S. Sharma, B. Naidu, S. Jadhav, R. Donthi, P. Chavan, H. Tan, and W. Hennig, Nucl. Instrum. Methods Phys. Res. A 680, 90 (2012).

[17] D. M. Brink, Phys. Lett. B 40, 37 (1972).

[18] J. E. Mason, S. B. Gazes, R. B. Roberts, and S. G. Teichmann, Phys. Rev. C 45, 2870 (1992).

[19] S. K. Pandit, K. Mahata, A. Shrivastava, V. V. Parkar, K. Ramachandran, J. Instrum. 14 (01) (2019) T01005.

[20] S. K. Pandit, A. Shrivastava, K. Mahata, N. Keeley, V. V. Parkar, P. C. Rout, K. Ramachandran, I. Martel, C. S. Palshetkar, A. Kumar, A. Chatterjee, and S. Kailas, Phys. Rev. C 93,061602(R) (2016).

[21] S. K. Pandit, A. Shrivastava, K. Mahata, V. V. Parkar, N. Keeley, P. C. Rout, K. Ramachandran, C. S. Palshetkar, I. Martel, A. Kumar, A. Chatterjee, S. Kailas, Phys. Rev. C 100, 014618 (2019).

[22] D. Kumar, M. Maiti, and S. Lahiri, Phys. Rev. C 94, 044603 (2016).

[23] S. K. Pandit, A. Shrivastava, K. Mahata, V. V. Parkar, R. Palit, N. Keeley, P.C. Rout, A. Kumar, K. Ramachandran, S. Bhattacharyya, V. Nanal, C. S. Palshetkar, T.N. Nag, S. Gupta, S. Biswas, S. Saha, J. Sethi, P. Singh, A. Chatterjee, S. Kailas, Phys.

Rev. C 96, 044616 (2017).

[24] A. Shrivastava, A. Navin, A. Diaz-Torres, V. Nanal, K. Ramachandran, M. Rejmund, S. Bhattacharyya, A. Chatterjee, S. Kailas, A. Lemasson, R. Palit, V. V. Parkar, R. Pillay, P. C. Rout, and Y. Sawant, Phys. Lett. B 718, 931 (2013).

[25] M. Dasgupta, P. R. S. Gomes, D. J. Hinde, S. B. Moraes, R. M. Anjos, A. C. Berriman, R. D. Butt, N. Carlin, J. Lubian, C. R. Morton, J. O. Newton, and A. Szanto de Toledo, Phys. Rev. C 70, 024606 (2004). [26] V. V. Parkar, V. Jha, and S. Kailas, Phys. Rev. C 94, 024609 (2016).

[27] S. K. Pandit, A. Shrivastavaa, K. Mahata, N. Keeley, V. V. Parkar, R. Palit, P. C. Rout, K. Ramachandran, A. Kumar, S. Bhattacharyyae, V. Nanal, S. Biswas, S. Saha, J. Sethi, P. Singh, S. Kailas, Phys. Lett. B 820, 136570 (2021).

[28] J. Lei, A.M. Moro, Phys. Rev. Lett. 122, 042503 (2019).

[29] J. Rangel, M. Cortes, J. Lubian, L. Canto, Phys. Lett. B 803, 135337 (2020).

[30] A. Diaz-Torres, D. J. Hinde, J. A. Tostevin, M. Dasgupta, and L. R. Gasques, Phys. Rev. Lett. 98, 152701 (2007).

नाभिकीय अभिक्रिया

5

दुर्बल-बंध नाभिक के साथ विविध अभिक्रिया चैनलों का व्यवस्थित अध्ययन

वी. वी. पार्कर[1,2,*], वी. झा[1,2] और एस. कैलाश[3]
[*]नाभिकीय भौतिकी प्रभाग, भाभा परमाणु अनुसंधान केंद्र (भापअ केंद्र), ट्रांबे, मुंबई – 400085, भारत
[2]होमी भाभा राष्ट्रीय संस्थान, अणुशक्तिनगर, मुंबई – 400094, भारत
[3]मुंबई विश्वविद्यालय-पऊवि मौलिक विज्ञान उत्कृष्ट केंद्र, मुंबई-400098, भारत

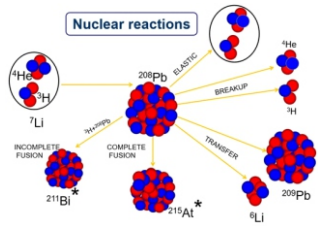

दुर्बल-बंध नाभिक के साथ नाभिकीय अभिक्रिया ।

सारांश

पिछले तीन दशकों में भापअ केंद्र-टीआईएफआर पेलेट्रॉन लीनॉक (एलआईएनएसी) त्वरक सुविधा, मुंबई का उपयोग करके दुर्बल-बंध प्रक्षेपकों (^{6,7}Li, ^{9}Be आदि) के साथ प्रत्यास्थ प्रकीर्णन, संलयन, विघटन एवं हस्तांतरण जैसी विभिन्न नाभिकीय अभिक्रियाओं का अध्ययन किया गया। हमने सभी अभिक्रिया चैनलों हेतु उपलब्ध आकड़ों के समुच्चय के साथ व्यवस्थित अध्ययन किया है। मापों एवं अध्ययनों के विवरण रिपोर्ट में दर्शाये गए हैं।

Nuclear Reactions

5

Systematic Study of various Reaction Channels with Weakly-bound Nuclei

V. V. Parkar[1,2,*], V. Jha[1,2] and S. Kailas[3]
[1]Nuclear Physics Division, Bhabha Atomic Research Centre (BARC), Trombay, Mumbai-400085, INDIA
[2]Homi Bhabha National Institute, Anushakti Nagar, Mumbai-400094, INDIA
[3]UM-DAE Centre for Excellence in Basic Sciences, Mumbai-400098, INDIA

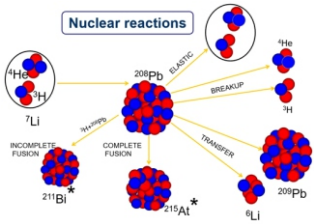

Nuclear Reactions with weakly-bound nuclei.

ABSTRACT

Various nuclear reactions like elastic scattering, fusion, breakup and transfer have been studied with weakly bound projectiles (^{6,7}Li ^{9}Be etc.) using the BARC-TIFR Pelletron LINAC accelerator facility, Mumbai over the last three decades. We have performed systematic studies with the available set of data for all the reaction channels. The details of the measurements and systematic studies are given in this report.

KEYWORDS: *Complete and Incomplete fusion, breakup, alpha production, neutron transfer, systematic study*

**Author for Correspondence: V.V. Parkar*
E-mail: vparkar@barc.gov.in

Introduction

Weakly bound nuclei are characterized by predominant cluster structures and low separation energies; *viz*; ^{6}Li→α+d, $S_{\alpha d}$ = 1.46 MeV, ^{7}Li→α+t, $S_{\alpha t}$ = 2.46 MeV, ^{9}Be→α+ α+n, $S_{\alpha\alpha n}$ = 1.57 MeV. These small separation energies suggest that these nuclei can easily break in the nuclear or Coulomb field, which in turn can influence the scattering and/or reaction cross-sections [1,2]. A schematic diagram of different possibilities for the breakup in the reaction of a typical two-cluster projectile ^{7}Li interacting with target A is shown in Fig.1. Study of nuclear reactions involving weakly bound projectiles is very interesting because of the observation of several unusual features compared to the case of strongly bound projectiles. With this in view, we have carried out several investigations using BARC-TIFR Pelletron Linac facility over last three decades to understand the reaction mechanisms involving these stable weakly bound projectiles on a range of target nuclei. Energy and angular distributions as well as integrated cross sections were measured for various reaction observables like elastic scattering, transfer, breakup and fusion around Coulomb barrier energies. A suppression in complete fusion cross section at above Coulomb barrier energies [1-13], a drastic change in the energy dependence of the optical potential [1,2], and a large production of α particles [1,2,6,14-16] are some of the important features associated with the above reactions. These observations are known to be largely due to the effect of projectile breakup on other channels. Recently, we have also done a compilation of available experimental data for complete and incomplete fusion, α particle production, neutron transfer and reaction cross sections which was utilised to understand the systematic behaviour with strongly and weakly bound projectiles. These studies help in building the foundation for similar studies with unstable weakly bound nuclei to be available with upcoming radioactive ion beam (RIB) facilities. Some of the results from the systematic study are highlighted in this report.

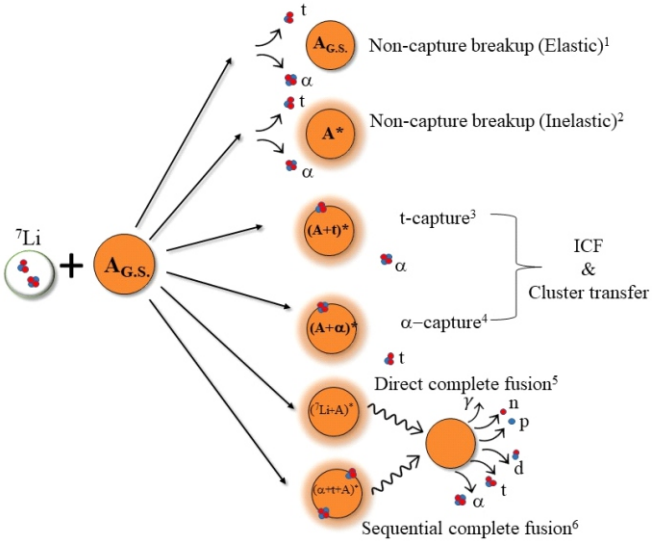

Fig.1: Pictorial representation of various reaction processes involving two-cluster ^{7}Li (α+t) projectile interacting with target A.

Results and Discussion

Fusion cross sections

Fusion cross section is defined as the probability of formation of compound nucleus. The fusion cross sections are mostly estimated by direct detection of evaporation residues or online and/or offline γ-ray de-excitations from the evaporation residues. Fusion can be divided into two parts: Complete and Incomplete fusion. When the entire projectile or all its fragments are captured, then the process is known as Complete Fusion (CF). If only a part of the projectile fuses with the target, then the process is known as incomplete fusion (ICF). In the case of weakly bound nuclei, both CF and ICF processes are important. It is seen in many systems that there is an enhancement of CF cross sections over the one dimensional barrier penetration model calculation. It is also found that CF cross sections are suppressed when compared to predictions based on a coupled channel model at energies above the Coulomb barrier. In addition, reduced fusion cross sections with weakly bound projectiles at energies normalized to the Coulomb barrier were also found to be systematically lower than those with strongly bound projectiles forming a similar compound nucleus (Fig.2(a)). In particular, experiments with ^{6,7}Li and ^{9}Be projectiles on medium and heavy mass targets have led to interesting conclusions on the systematics

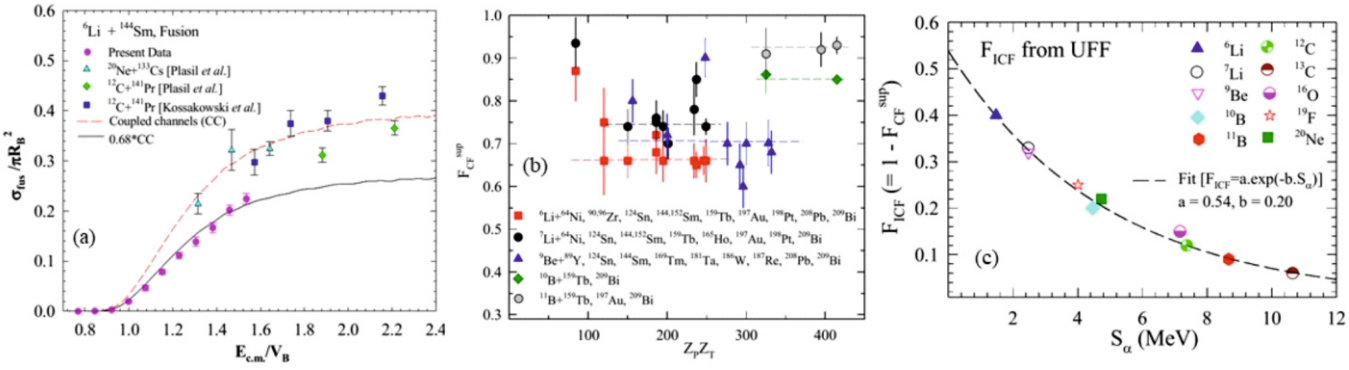

Fig.2: (a) Comparison of reduced fusion cross sections as a function of reduced energy for different systems involving SBP and WBP forming the same CN, (b) Systematics of F^{sup}_{CF} as a function of Z_pZ_T for different systems involving ^{6,7}Li, ^{9}Be, and ^{10,11}B projectiles, (c) ICF fraction (F_{ICF}) obtained for various projectiles as a function of α-separation energy, S_α. Figure taken from Ref. [6].

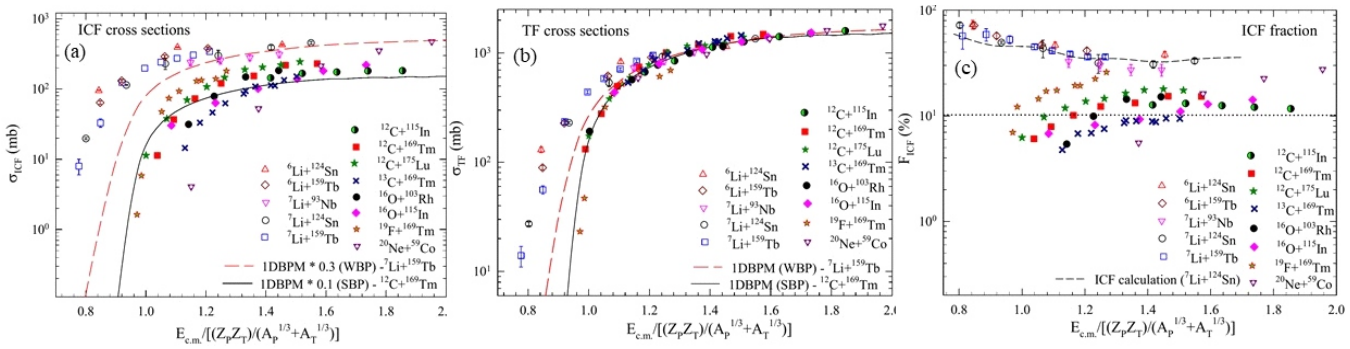

Fig.3: (a) ICF and (b) TF cross sections and (c) ICF fraction as a function of reduced energy for systems involving WBP and SBP. Figure taken from Ref. [6].

of the CF suppression factor. The suppression in CF involving these projectiles is found to be independent of target mass in many studies (Fig.2(b)). Further the suppression factor shows an increasing trend with decrease in the breakup threshold of the projectile (Fig.2(c).

We have also compiled ICF data available for both strongly (^{12,13}C, ^{14}N, ^{16}O, ^{19}F, ^{20}Ne) and weakly bound (^{6,7}Li, ^{9}Be, ^{6,8}He) projectiles. A systematic behaviour of ICF cross sections (σ_{ICF}) is observed for various projectile–target systems as a function of reduced energy (E_{red}) as shown in Fig.3(a). In general, σ_{ICF} for the WBP systems is higher than that for the SBP systems. A comparison of the total fusion (TF) cross sections (σ_{TF}) as a function of reduced energy (E_{red}) for different WBP and SBP systems is shown in Fig.3(b). The TF cross sections are enhanced for ^{6,7}Li WBP systems as compared to the SBP systems at below barrier energies. This can be mainly attributed to larger contribution of ICF for WBP systems at these energies. At above barrier energies, TF cross sections for both WBP and SBP systems are similar and these can explained well by calculations. A quantitative assessment of the relative contribution of ICF to TF cross sections was also made using the percentage ICF fraction ($F_{ICF}(\%) = (\sigma_{ICF}/\sigma_{TF}).100$) as shown in Fig.3(c). The increase of $F_{ICF}(\%)$ at sub-barrier energies in case of WBP may be attributed to the increased importance of ICF driven by breakup and transfer processes as compared to the CF processes. The $F_{ICF}(\%)$ is smaller in case of SBP and it shows a larger variation among values for different systems.

A systematic analysis of the fusion cross sections around the Coulomb barrier energies with stable weakly bound (^{6}Li, ^{7}Li, ^{9}Be) and strongly bound ^{12}C projectiles on various targets was also performed by using the neutron flow model and coupled channels approach. The analysis shows that both models are successful in explaining the near barrier fusion data. Further, it is also observed that the collective degrees of freedom as well as the neutron flow influence the near barrier fusion process involving weakly bound projectiles [12,13].

Inclusive α production

As the weakly bound nuclei have the α+x cluster structure with very low separation energy, the α production cross sections are found to be very large compared to their counterpart. The angular distribution of these α-particles were measured using silicon detector array and the integrated production cross sections were extracted. The yield of evaporation a particles due to the CF contribution can be separated out using the statistical model predictions. The CF part has been estimated from the statistical model calculations using code PACE2 and non-CF inclusive α production cross sections have been determined. The plot of non-CF inclusive α production cross sections with reduced energy for various projectile types (WBP, SBP, RIB) is shown in Fig.4. An increase in cross section with incident energy and a reasonable similarity in the behaviour involving different systems for the same type of projectile nuclei (WBP and SBP) is observed [6,15]. In WBP, two lines corresponding to ^{6}Li,^{9}Be and ^{7}Li are shown with dotted and dashed lines respectively. The line for RIB is shown by dashed dot dot line while SBP region is shown in hashed region because of slight variation. Overall, three distinct regions *viz*; RIB, WBP and SBP are clearly distinguished from the plot. The significant contribution of breakup of projectile like nucleus after neutron transfer apart

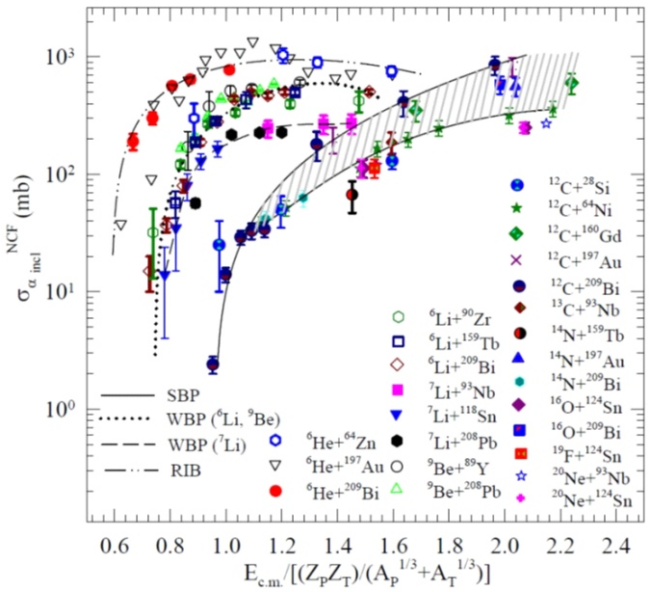

Fig.4: Systematic comparison of inclusive α production cross sections due to non-CF processes for different nuclear systems in three categories: (I) SBP, (ii) stable WBP, and (iii) RIB. Lines are guide to an eye.

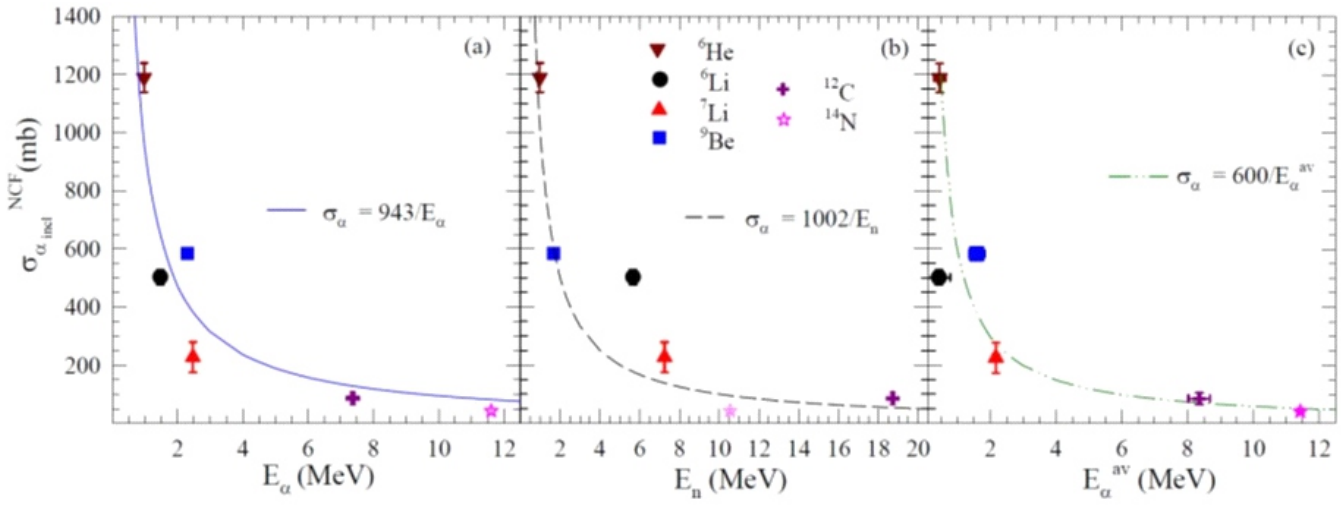

Fig.6: (a) Value of non-CF inclusive α cross section for various projectiles at 1.2Vb as a function of binding energies of (a) α (E_α), (b) neutron (E_n), and (c) average of α binding energies of the projectile and projectile like nucleus after neutron transfer ($E_{av}\alpha$) is shown. The lines are fit to the data.

from processes like direct breakup of the projectile, capture of a fragment of the projectile by the target leaving α as a spectator suggest that both α and neutron binding energies play a vital role in α production [15]. In view of this, it is suggested that $E_{av}\alpha$, average of α binding energies of the projectile and projectile like nucleus after neutron transfer is a suitable variable to describe the α production data for variety of projectiles [15].

The non-CF a cross section with heavy target at ≈ 1.2Vb is plotted for all the projectiles and shown as a function of E_α and E_n in Fig.5(a) and (b) respectively. $1/E_\alpha$ and $1/E_n$ behaviour was found to describe the α data of all the systems very well. the α binding energy values of the projectile like nuclei after neutron transfer (from projectile or to projectile from the target) are very similar to the α binding energies of the projectile. Hence a new variable $E_{av}\alpha$ which is equal to $0.7E_\alpha$(of projectile) + $0.3E_\alpha$(n−tr) (of projectile like nucleus after neutron transfer) which is used in Fig.5(c). This procedure takes into account the dependence on α binding energies of the projectiles and also on neutron binding energies through the process of neutron transfer and the resultant α binding energies of the projectile like nuclei. This procedure gives the best fit to the data.

Neutron transfer

Neutron transfer (stripping and pickup) cross sections were also extracted from offline γ-ray measurements and are plotted in Fig.6 [A-C] for ^{7}Li[17], ^{6}Li[18] and ^{9}Be[19] respectively. As can be seen from the figures [A-C], universal behavior in the cross sections is observed in all the plots. The data was then fitted with modified Wong formula with introduction of neutron separation energies (and transfer probabilities) of the projectile and fitted (shown as lines). From the fit, early onset of these transfer processes as compared to the nominal barrier as observed in data [17-19]. In the case of ^{9}Be, neutron transfer is found to be dominant at below barrier energies [20].

Summary

The systematic study of fusion, α production and neutron transfer with weakly bound projectiles is performed. In the fusion studies, it is observed that the CF cross sections are suppressed above barrier energies with respect to model calculations for total fusion and this amount of suppression is commensurate with ICF cross sections. Also, the suppression factor is found to remain constant for a particular projectile and it increases with decreasing the separation energy of the projectile. Study of ICF cross sections with systems involving strongly and weakly bound projectiles has been performed. The ICF cross sections with WBP systems are higher than that with SBP systems at all the energies. ICF cross sections with WBP increases at below barrier energies, showing the importance of breakup channel. A systematic study of the α-particle production in reactions involving both the weakly and strongly bound projectiles at energies around the Coulomb barrier has been performed and a distinction based on projectile type is obtained. The neutron transfer study suggests early onset of transfer processes as compared to the nominal barrier. Similar studies with upcoming RIBs will be vital in extending these systematics.

Acknowledgments

We are grateful to all the collaborators for help and support at various stages during this research work. We also acknowledge the Pelletron-LINAC accelerator staff at TIFR, Mumbai for giving excellent quality of beam during this research.

References

[1] Vivek Vijay Parkar, Reaction Dynamics Around Coulomb barrier with Weakly Bound Nuclei, BARC Newsletter (Founders day special Issue October 2016) 126-130.

https://www.barc.gov.in/barc_nl/2016/spl2016.pdf

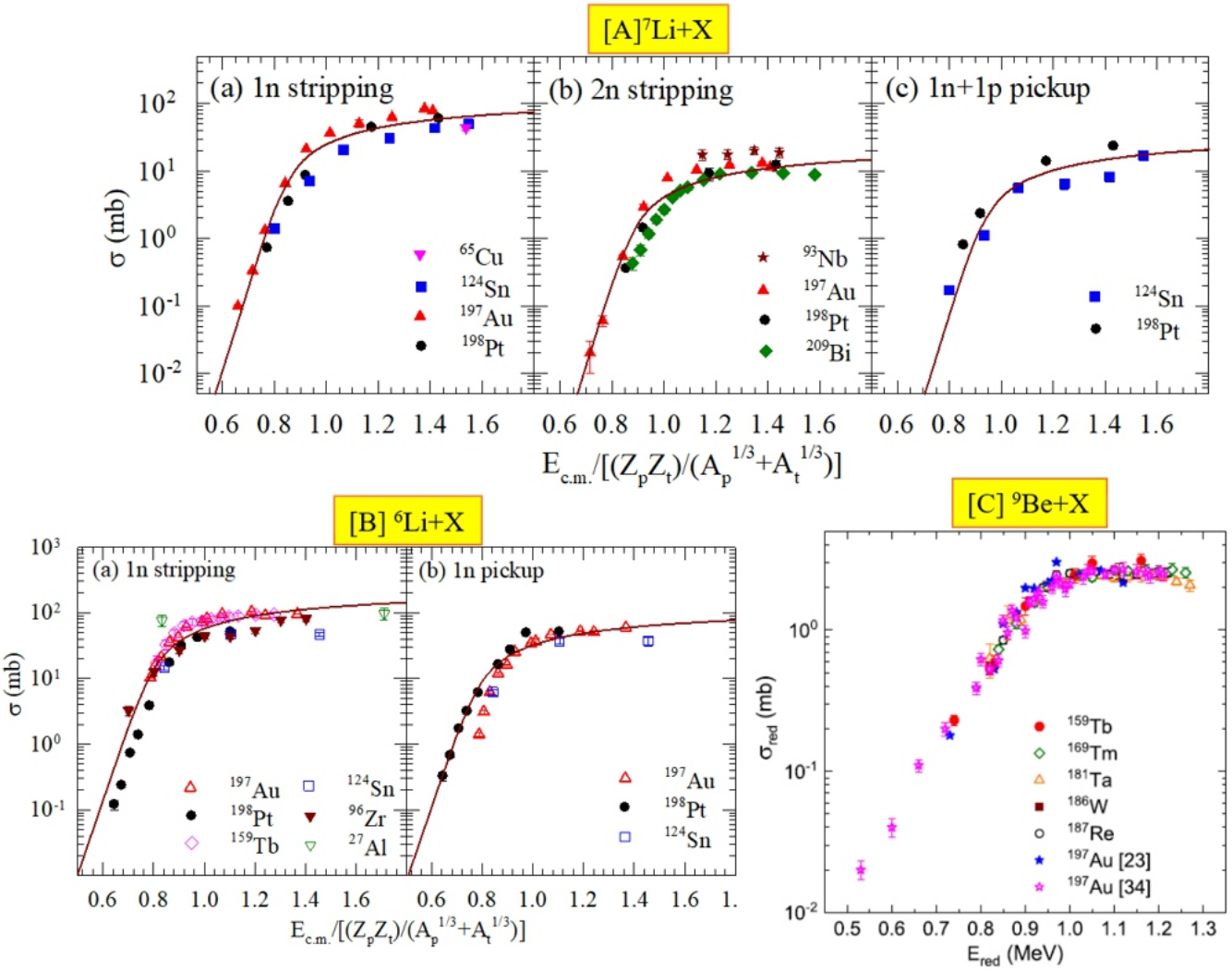

Fig.6: Systematic behaviour of neutron transfer cross sections in [A] ^{7}Li [17], [B] ^{6}Li [18] and [c] ^{9}Be [19] induced reactions.

[2] Vivek Vijay Parkar, Understanding Features of Weakly Bound Nuclei, Physics News - Bulletin of the Indian Physics Association 50(3) (2020) 31-36. https://www.tifr.res.in/~ipa1970/news/2020/JulySept/A6PN_VP.pdf

[3] L. F. Canto, P.R.S. Gomes, R. Donangelo, J. Lubian, M.S. Hussein, Recent developments in fusion and direct reactions with weakly bound nuclei, Physics Reports 596 (2015) 1-86. http://dx.doi.org/10.1016/j.physrep.2015.08.001. [4] B. B. Back, H. Esbensen, C. L. Jiang, K. E. Rehm, Recent developments in heavy-ion fusion reactions, Reviews of Modern Physics 86 (2014) 317-360. https://doi.org/10.1103/RevModPhys.86.317.

[5] V. V. Parkar, Systematic of Incomplete fusion with strongly and weakly bound projectiles, Proceedings DAE Symposium on Nuclear Physics 64 (2019) 19-20. https://sympnp.org/proceedings/.

[6] V. Jha, V. V. Parkar, S. Kailas, Incomplete fusion reactions using strongly and weakly bound projectiles, Physics Reports 845 (2020) 1-58. https://doi.org/10.1016/j.physrep.2019.12.003.

[7] V. V. Parkar, V. Jha, S. Kailas, Exploring incomplete fusion fraction in ^{6,7}Li induced nuclear reactions, EPJ Web of Conferences 163 (2017) 00044(1-4). https://doi.org/10.1051/epjconf/201716300044.

[8] V. V. Parkar, V. Jha, S. Kailas, Exploring contributions from incomplete fusion in ^{6,7}Li+^{209}Bi and ^{6,7}Li+^{198}Pt reactions, Physical Review C 94 (2016) 024609(1-6). http://dx.doi.org/10.1103/PhysRevC.94.024609.

[9] V. V. Parkar, Prasanna M., Ruchi Rathod, V. Jha, S. K. Pandit, A. Shrivastava, K. Mahata, K. Ramachandran, R. Palit, Md. S. R. Laskar, B. J. Roy, Bhushan Kanagalekar, B. G. Hegde, Fusion of ^{7}Li with ^{205}Tl at near-barrier energies, Physical Review C 109 (2024) 014610(1-8). https://doi.org/10.1103/PhysRevC.109.014610.

[10] V. V. Parkar, S. K. Pandit, A. Shrivastava, R. Palit, K. Mahata, V. Jha, K. Ramachandran, Shilpi Gupta, S. Santra, Sushil K. Sharma, S. Upadhyaya, T. N. Nag, Sutanu Bhattacharya, T. Trivedi, S. Kailas, Fusion reaction studies for the ^{6}Li+^{124}Sn system at near-barrier energies, Physical Review C 98 (2018) 014601(1-10). https://doi.org/10.1103/PhysRevC.98.014601.

[11] V. V. Parkar, Sushil K. Sharma, R. Palit, S. Upadhyaya, A. Shrivastava, S. K. Pandit, K. Mahata, V. Jha, S. Santra, K. Ramachandran, T. N. Nag, P. K. Rath, Bhushan Kanagalekar, T. Trivedi, Investigation of complete and incomplete fusion in the 7Li+124Sn reaction near Coulomb barrier energies, Physical Review C 97 (2018) 014607(1-9). https://doi.org/10.1103/PhysRevC.97.014607.

[12] S. Appannababu, V. V. Parkar, V. Jha, S. Kailas, Fusion systematics for weakly bound nuclei using neutron flow and collective degrees of freedom, Physical Review C 106 (2022) 054612(1-6). https://doi.org/10.1103/PhysRevC.106.054612.

[13] S. Appannababu, V. V. Parkar, V. Jha, S. Kailas, Stelson model for fusion reactions of ^{9}Be on ^{169}Tm, ^{181}Ta, ^{187}Re and ^{197}Au, European Physical Journal A 60 (2024) 145(1-6). https://doi.org/10.1140/epja/s10050-024-01364-w.

[14] V. V. Parkar, V. Jha, S. Kailas, Interesting features in systematics of alpha production for ^{6,7}Li induced reactions, Proceedings DAE Symposium on Nuclear Physics 64 (2019) 523-524. https://sympnp.org/proceedings/.

[15] V. V. Parkar, V. Jha, S. Kailas, Systematics and mechanisms of alpha production with weakly and strongly bound projectiles, European Physical Journal (Letters) A 59 (2023) 88(1-5). https://doi.org/10.1140/epja/s10050-023-01011-w.

[16] Satbir Kaur, V. V. Parkar, S. K. Pandit, A. Shrivastava, K. Mahata, K. Ramachandran, Sangeeta Dhuri, P. C. Rout, A. Kumar, Shilpi Gupta, Investigation of reaction and alpha production cross sections with ^{9}Be projectile, Nuclear Physics A 1046 (2024) 122864(1-12). https://doi.org/10.1016/j.nuclphysa.2024.122864.

[17] V. V. Parkar, A. Parmar, Prasanna M., V. Jha, S. Kailas, Investigation of neutron transfer in ^{7}Li+^{124}Sn system, Physical Review C 104, (2021) 054603(1-7). https://doi.org/10.1103/PhysRevC.104.054603. [18] V. V. Parkar, A. Parmar, Prasanna M., V. Jha, S. Kailas, Investigating neutron transfer in the ^{6}Li+^{124}Sn system, Physical Review C 107 (2023) 024602(1-6). https://doi.org/10.1103/PhysRevC.107.024602.

[19] Malika Kaushik, S. K. Pandit, V. V. Parkar, G. Gupta, Swati Thakur, V. Nanal, H. Krishnamoorthy, A. Shrivastava, C. S. Palshetkar, K. Mahata, K. Ramachandran, S. Pal, R. G. Pillay, Pushpendra P. Singh, Investigating neutron transfer in the ^{9}Be+^{197}Au system, Physical Review C 104 (2021) 024615(1-8). https://doi.org/10.1103/PhysRevC.104.024615.

[20] Prasanna M., V. V. Parkar, V. Jha, A. Parmar, Bhushan. A. Kanagalekar, B. G. Hegde, Role of neutron transfer in the reaction mechanism of ^{9}Be+^{169}Tm, ^{181}Ta, ^{187}Re and ^{197}Au systems, Nuclear Physics A 1029 (2023) 122570(1-12). https://doi.org/10.1016/j.nuclphysa.2022.122570.

नाभिकीय अभिक्रिया

6

अप्रत्यास्थ प्रकीर्णन अभिक्रियाओं के माध्यम से न्यूक्लिऑन-नाभिक अंतःक्रिया की जांच

आई. मजुमदार

नाभिकीय एवं परमाणु विज्ञान विभाग, टाटा मूलभूत अन्वेषण संस्थान, होमी भाभा मार्ग, मुंबई-400005, भारत

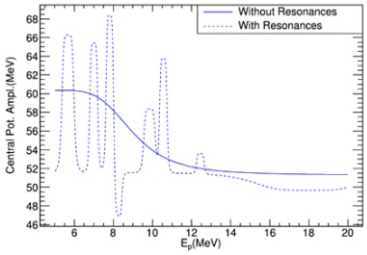

अनुनाद सहित एवं रहित आपतित प्रोटॉन ऊर्जा के साथ केंद्रीय-संभावित अवधि के आयाम में अंतर

सारांश

इस आलेख में, हम 8-16 MeV की प्रोटॉन ऊर्जा हेतु $^{16}O(p,p'\gamma)^{16}O$ अभिक्रिया से 6.13, 6.92 एवं 7.12 MeV γ-किरणों के पूर्ण उत्पादन अनुप्रस्थ काट की रिपोर्ट करते हैं। तीन γ-किरणों के कोणीय वितरण को 9 MeV पर सात कोणों से मापा गया। अनुप्रस्थ काट आकड़ों का विश्लेषण करने के लिए एक विस्तृत फेनोमेनोलॉजिकल ऑप्टिकल मॉडल पोटेंशियल (ओ. एम. पी.) स्थापित किया गया। ^{16}O की निचली स्थितियों को जोड़ा गया और विरूपण मापदंडों का उपयोग करके ऑप्टिकल क्षमता को विकृत किया गया। नाभिकीय संरचना प्रभावों की गणना के लिए अनेक अनुनाद शामिल किए गए। आंकड़े के साथ गणनाओं की तुलना चैनल युग्मन, $p+^{16}O$ प्रणाली में अनुनाद एवं प्रक्षेप्य ऊर्जा के साथ अनुदैर्ध्य-काट की भिन्नता में लक्ष्य विरूपण की जटिल भूमिकाओं को प्रकट करती है।

Nuclear Reactions

6

Probing Nucleon-Nucleus Interaction through Inelastic Scattering Reactions

I. Mazumdar

[1]Department of Nuclear and Atomic Physics, Tata Institute of Fundamental Research, Homi Bhabha Road, Mumbai-400005, INDIA

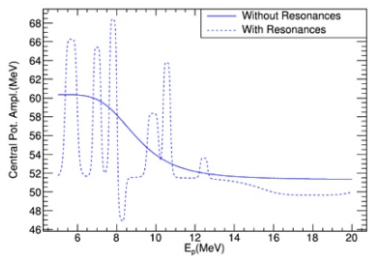

Variation of the amplitude of central-potential term with incident proton energy, with and without resonances.

ABSTRACT

In this article, we report the absolute production cross-section of 6.13, 6.92 and 7.12 MeV γ-rays from the $^{16}O(p, p'\gamma)^{16}O$ reaction for proton energy of 8-16 MeV. Angular distributions of the three γ-rays have been measured for seven angles at 9 MeV. A detailed phenomenological optical model potential (OMP) was set up to analyze the cross-section data. Low-lying states of ^{16}O were coupled and the optical potential was deformed using deformation parameters. Several resonances were included in the calculations to account for the nuclear structure effects. The comparisons of the calculations with the data bring forth the rather complex roles of channel couplings, resonances in the $p+^{16}O$ system and target deformation in the variation of the cross sections with projectile energy.

KEYWORDS: *Optical model potential, Nuclear reactions, γ-ray cross-section*

**Author for Correspondence: I. Mazumdar*
E-mail: indra@tifr.res.in

Introduction

Notwithstanding the overarching role of heavy-ion-induced reactions in nuclear physics, light-ion-induced reactions continue to have their own importance. A variety of light-ion-induced reactions, namely, elastic and inelastic scattering, capture, charge exchange, knock-out etc, are essential to probe the quantum structure of low-lying states, reaction dynamics and nucleon-nucleus interactions. Nucleon–nucleus (NA) scattering plays a significant role in studying how nucleon-nucleon (NN) interaction dynamics and the structure of the target nucleus can give rise to complicated many-body NA scattering. Furthermore, the knowledge of NA scattering can be used to understand nucleus–nucleus (AA) scattering as a superposition of corresponding NA interactions [1]. Apart from the nuclear structure point of view, NA scattering measurements for light nuclei are also valuable for γ-ray astronomy [2]. Guided by these objectives, our group has completed a series of measurements to study the low-lying states of light nuclei such as ^{12}C, ^{16}O, ^{10,11}B for insights into the nuclear structure and to contribute towards γ-ray astronomy [3,4]. It is worth mentioning that we have also measured alpha particle-induced scattering cross sections for comparative studies of isospin dependence of nucleon-nucleus interaction. In this brief report we discuss our measurements and theoretical analysis of 160(p,p'γ)^{16}O reaction as a representative case of the larger body of work [5].

The primary aim of this work is to measure the angular distributions and absolute production cross-sections of the three low-lying transitions, namely, 6.13, 6.92 and 7.12 MeV. Fig.1 shows the partial level scheme of these low-lying transitions of ^{16}O [6]. In the energy range of 8–16 MeV, only three groups (Dyer *et al.* [7], Boromiza *et al.* [8], Kiener *et al.* [9]) have reported production cross-sections of these transitions. However, owing to the thick target used by Boromiza *et al*, the uncertainty in proton beam interaction energy was quite large. This becomes problematic in low-energy regions where there are several resonances. Moreover, the cross-section for 6.92 MeV γ-ray was not reported. The cross sections reported in [9] were normalised to previous measurements of Dyer *et al* [7] instead of absolute measurements. The absolute cross sections of 6.92 MeV have not been reported so far.

We have attempted to measure the angular distributions and absolute cross sections of all these three transitions. The measured cross sections have been compared with our calculations using optical model potentials (OMPs) within the framework of coupled channel analysis and including several resonances for the p+^{16}O system. We have generated the OMPs from global fits to a large body of experimental data available in the literature. The potentials so generated, have been used to calculate the total and differential angular distribution cross sections for both ^{16}O(p,p')^{16}O and ^{16}O(p,p'γ)^{16}O reactions. The comparisons of the calculations with the data bring forth the rather complex roles of target deformation, channel couplings and resonances in the p+^{16}O system.

Experimental Details

The experiment was performed at the TIFR-BARC Pelletron facility at TIFR, Mumbai. Self-supporting Mylar target of thickness 2.22 mg cm^{-2} was bombarded with protons at 15 beam energies from 8 to 16 MeV. The γ-rays were detected by a large volume 3.5"×6" cylindrical Lanthanum Bromide detector. This large volume detector has been thoroughly characterised for γ-rays of energy ranging from a few hundred keV to 22.5 MeV [10]. The detector was placed at angles of 45^{o}, 60^{o}, 75^{o}, 90^{o}, 105^{o}, 120^{o}, and 135^{o} with respect to the beam direction for angular distribution measurements. Fig.2 presents a typical gamma-ray spectrum measured by the large volume detector at proton beam energy of 10 MeV. One of the crucial aspects of the data reduction and extraction of the absolute cross section is the accurate estimation of the background. The background is created by the tails of the multiple gamma rays and ambient radioactivity. We have tried to generate the background by rigorous Monte Carlo calculations using the GEANT4 package. The spectral shapes for a host of gamma rays produced from the reaction have been generated by the GEANT4. The GEANT4 generated background is shown in Fig.2. The absolute production cross sections of the three transitions were extracted from the efficiency corrected yields for all the beam energies. A fuller description of the theoretical analysis and reproduction of the measured cross sections are provided in the following section.

Theoretical Analysis

Optical model analysis has played a central role in nuclear reaction studies. The OMP can successfully explain the scattering of the nucleon from medium to heavy mass (A > 40) target nuclei and at high incident projectile energy (> 40 MeV). However, this formalism has only been reasonably successful for low mass nuclei bombarded by low energy projectiles [11, 12]. There have been instances when the conventional parameterisation of OMP has been found inadequate in describing the elastic scattering data for light target nuclei. The cause of these inadequacies has been assigned to resonances in the compound nucleus, limitations of Woods Saxon form factor, coupling of various channels, giant resonances, etc [13]. The ^{16}O(p,p'γ)^{16}O scattering can be modelled as a two-step process; first, the excitation, followed by the de-excitation of the oxygen nucleus. The formal development of the theoretical optical potential allows for a clean separation between the elastic and inelastic channels and the relation between the two [14].

In essence, it is assumed in an optical model that if the elastic and the total reaction channels are well understood (Optical Theorem), then the other channels are mere details. The interaction of a nucleus with a proton projectile of energy in the 5–20MeV range poses challenges to theorists, even if only to describe the elastic scattering channel. To circumvent much

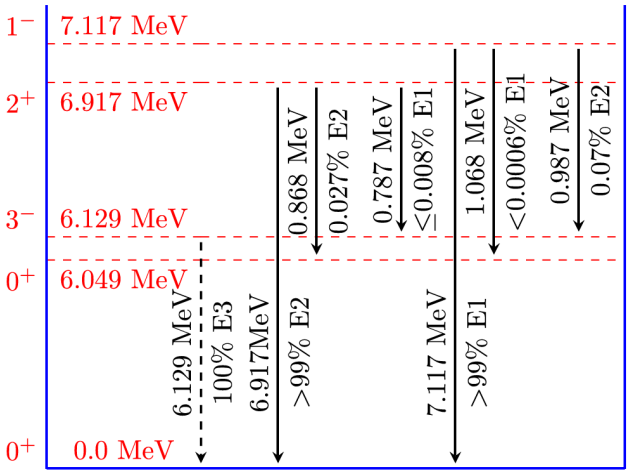

Fig.1: Partial level scheme of ^{16}O.

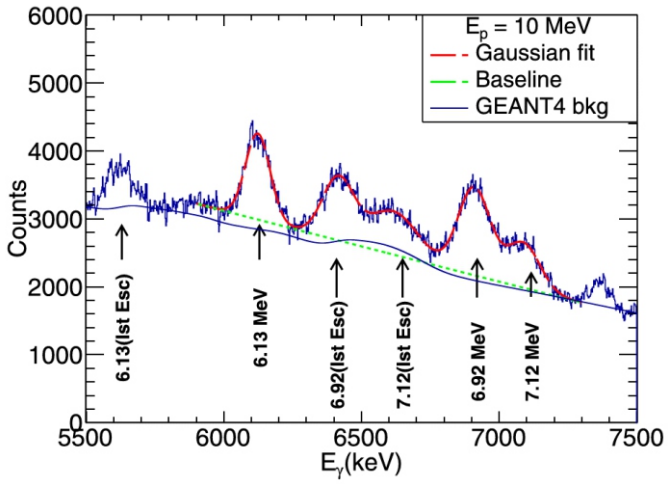

Fig.2: A typical measured γ-ray spectrum. Different full energy peaks from de-excitation of ^{16}O nuclei and the corresponding 1st escape peaks are labelled. The overall smooth Compton background under the peaks used in the multi-peak fittings is shown by the dotted green line. The GEANT4 simulated background is shown by the solid blue line.

of the theoretical challenge of this energy region, one can use phenomenological optical potentials, which are blatantly fit to the elastic scattering data. The trade-off for a good quality fit to the elastic channel data is a lack of physical insight. Microscopic notions of anti-symmetry, Pauli blocking, nucleon degrees of freedom, resonances, and nuclear matter properties all get absorbed into this macroscopic 'cloudy ball'. The quality of the fits improves with increase in the number of parameters. Several intertwined steps are involved in calculating the cross-section, such as setting up the OMP, optimizing parameters, inclusion of resonances and deformations, coupling of channels, etc. These steps work simultaneously, rather than sequentially, to provide final cross-section values.

As mentioned in the introductory part we have generated the OMP for the reaction by fitting a large body of global data of elastic scattering, angular distributions, analysing powers etc.

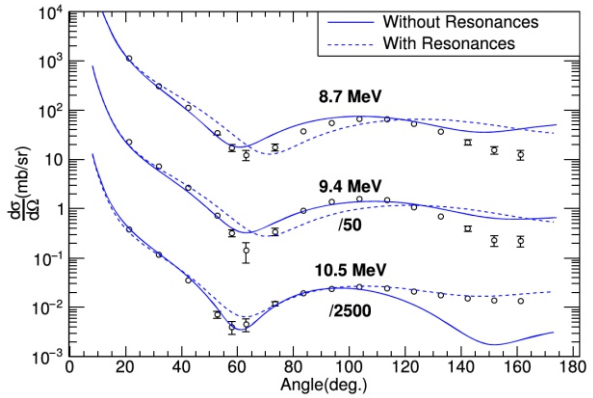

Fig.3: Optical Model fits to the elastic scattering data available in literature.

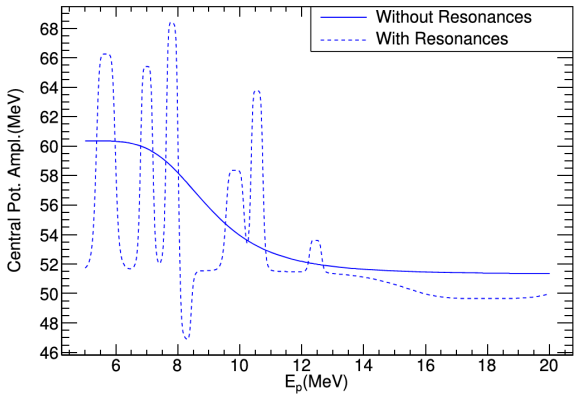

Fig.4: Variation of the amplitude of central-potential term with incident proton energy with and without resonances.

Fig.3 shows the fits to the elastic scattering angular distributions for $^{16}O(p, p)^{16}O$ reaction. The effect of nuclear structure on the scattering process manifest through nuclear deformation, coupling of states and inclusion of resonances in the p+^{16}O system. The macroscopic, phenomenological optical model is a good doorway to describe inelastic scattering considering collective nuclear excitation, namely, vibration and rotation. These vibration and rotation models have successfully described excitation bands in heavier nuclei. It assumes that the nucleus is non-spherical and has multi-pole deformations that are either causing an excited rotation and/or vibrational mode. It starts by expanding the radius, assuming a series of deformations.

$$R(\theta) = R_0[1 + \beta_2 Y_2^0(\theta) + \beta_4 Y_4^0(\theta) + \beta_6 2Y_6^0(\theta) + \dots]$$

Where βi's are deformation parameters. In a rotational model, these are corresponding to quadrupole, octupole, and hexadecapole rotational modes, whereby symmetry, of only even modes are allowed [15, 1]. There is a partial wave-dependent asymmetry in the polar angle separating $\vec{r}$ and $\vec{r}\,'$ in coordinate space. The same common multi-pole expansion can be performed on the optical potential, with, $x=\cos(\theta)$

$$V_\lambda(|\vec{r}|, |\vec{r}'|) = \frac{1}{2}\int_{-1}^{+1} V(\vec{r}, \vec{r}', x) P_\lambda(x) dx$$

where R=r⃗'- r⃗. The rotational bands are very common in heavy nuclei but are rarely used by themselves in the oxygen nucleus, they are usually combined with vibrations. The vibrational mode looks similar:

$$R(\theta) = R_0\left[1 + \sum_{\lambda,\mu} \alpha_\lambda^\mu\right]$$

where

$$\alpha_\lambda^\mu = \frac{\beta_\lambda^\mu}{\sqrt{2\lambda+1}}\{b_{\lambda,\mu} + (-1)^\mu b^+_{\lambda,-\mu}\}$$

As can be seen the α_λ^μ contain deformation parameters (β_λ^μ) and phonon creation ($b^+_{\lambda,-\mu}$) and destruction ($b_{\lambda,\mu}$) operators. With a vibrational mode the phonons can follow all allowed electric and magnetic transitions. One can then expand the potential in a Taylor series to first order as:

$$V(r,R) = V(r,R_0) + \frac{d}{dR_0}V(r,R_0)R_0\sum_{\lambda,\mu}\alpha_\lambda^\mu Y_\lambda^\mu(\theta,\phi)$$

So these phonon excitations are also derived from the non-spherical nature of the nucleus. The vibrational, rotational, and a combination of both models can be calculated by common distorted born approximation codes [16, 17, 18]. These codes take as input an elastic channel optical potential and then place it into the chosen vibrational/rotational mode, as the potential into the Schrödinger equation. In our calculations we have assumed a first order vibrator model and have considered the ground state and six excited states.

Next to the nuclear deformation, other critical features of such calculations are coupling of the channels and inclusion of resonances that emanate from the ^{17}F compound nucleus. As mentioned earlier, the OMP parameters, extracted from our global fits to existing data, have been used within a coupled channel formalism to calculate the cross sections. The importance and power of coupled channel calculations are, by now, very well established. The specific structures in the cross-section plots appear only with the inclusion of channel couplings. In addition to channel couplings, another important necessity is to consider the role of virtual resonance states in the compound nucleus ^{17}F. The ^{16}O nucleus has a significant chance of entering a compound resonance with the projectile, which accentuates the interaction strength, thus raising or lowering the cross-sections of every channel in this energy region. Thus, the optical potential, in the energy range from 5 to 20 MeV, did not always achieve great fits with a smooth function but was augmented with a series of seven resonances consistently. Many of these elastic data resonances are caused by virtual states in ^{17}F. We provide below the equations for the final optical potential, including these narrow energy resonances. Fig.4 presents variation of the amplitude of central-potential term with incident proton energy with and without resonances.

Fig.5 and 6 present our data along with the output of our OM calculations for the angular distributions of the gamma

$$V_0 = -111.533 - \frac{1.9125(E-18.000)^4}{(E-18.000)^4+3.000^4} + \sum_i^{res.}\frac{A_{0i}(E-E_i)^6}{(E-E_i)^6+W_i^6}$$

$$W_0 = -0.416 + \frac{0.2965(E-18.934)^4}{(E-18.934)^4+3.1487^4}$$

$$V_S = 6.4697 + \frac{4.6311(E-8.4178)^4}{(E-8.4178)^4+4.1768^4}$$

$$W = 2.3981 - \frac{5.8619(E-22.00)^4}{(E-22.00)^4+10.3884^4} + \sum_i^{res.}\frac{A_{0i}(E-E_i)^6}{(E-E_i)^6+W_i^6}$$

$$r_0 = 0.6748 - \frac{0.055231(E-17.7335)^4}{(E-17.7335)^4+3.6787^4} + \sum_i^{res.}\frac{R_{0i}(E-E_i)^6}{(E-E_i)^6+W_i^6}$$

$$a_0 = 0.5431 + \frac{0.196843(E-5.000)^4}{(E-5.000)^4+16.1121^4}$$

$$r_s = 1.7125 - \frac{0.083141(E-16.17)^4}{(E-16.17)^4+3.000^4} + \sum_i^{res.}\frac{R_{si}(E-E_i)^6}{(E-E_i)^6+W_i^6}$$

$$a_s = 0.38018 - \frac{0.04292(E-21.692)^4}{(E-21.692)^4+3.038^4}$$

$$V_{so} = 8.67746 - \frac{1.95582(E-17.777)^4}{(E-17.777)^4+3.000^4} + \sum_i^{res.}\frac{R_{soi}(E-E_i)^6}{(E-E_i)^6+W_i^6}$$

$$W_{so} = -0.01782 - \frac{1.3537(E-10.381)^4}{(E-10.381)^4+4.707^4}$$

$$r_{so} = 0.5538 + \frac{0.31743(E-20.442)^4}{(E-20.442)^4+3.00^4} + \sum_i^{res.}\frac{R_{soi}(E-E_i)^6}{(E-E_i)^6+W_i^6}$$

$$a_{so} = 0.3440 + \frac{0.11343(E-6.8494)^4}{(E-6.8494)^4+4.344^4}$$

$$r_c = 1.3830 + \frac{0.2713(E-5.000)^4}{(E-5.000)^4+4.308^4}$$

rays and total production cross sections, respectively [5]. Our calculations of the total cross-sections for the three γ-rays agree fairly well with the measured values. However, there still exist differences between theory and experiments regarding finer structures in the cross sections. It is observed that the value of the target deformation has a considerable effect on the total cross-sections. In the spirit of our phenomenological calculation, we acknowledge that the sensitivity upon deformation merits further study. The discrepancies that persist in terms of finer structure are very likely due to complex and connected structural effects which are yet to be fully understood. There are subtle roles played by both coupling of the channels and resonances, and what may surmise is that the calculation at these low energies loses much of its predictive power. The conclusion carries the unmistakable stamp of the complexity of the problem. It leaves much scope for further improvement in the calculation.

Summary

Proton induced inelastic scattering reactions are of great importance in probing the quantum structure of low-lying

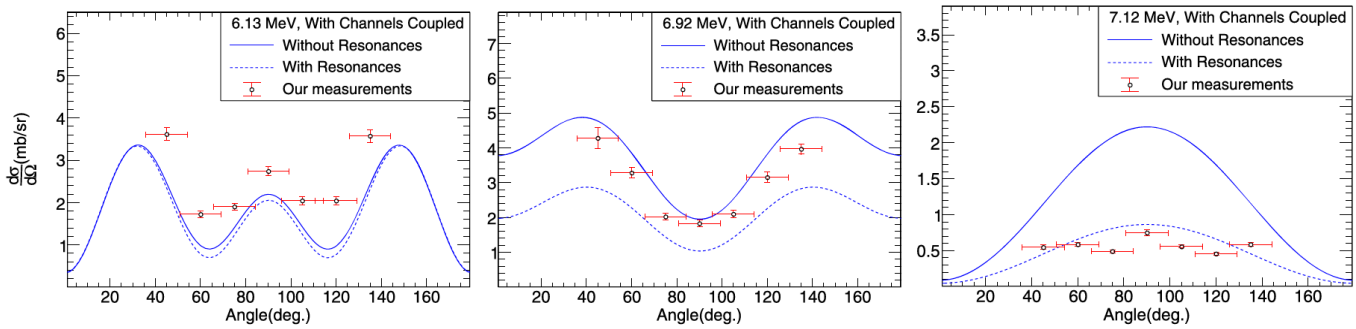

Fig.5: Measured and calculated differential cross-sections for angular distribution of 6.13, 6.92 and 7.12 MeV γ-rays for 9 MeV proton. The coupled channel calculations have been performed with and without resonances.

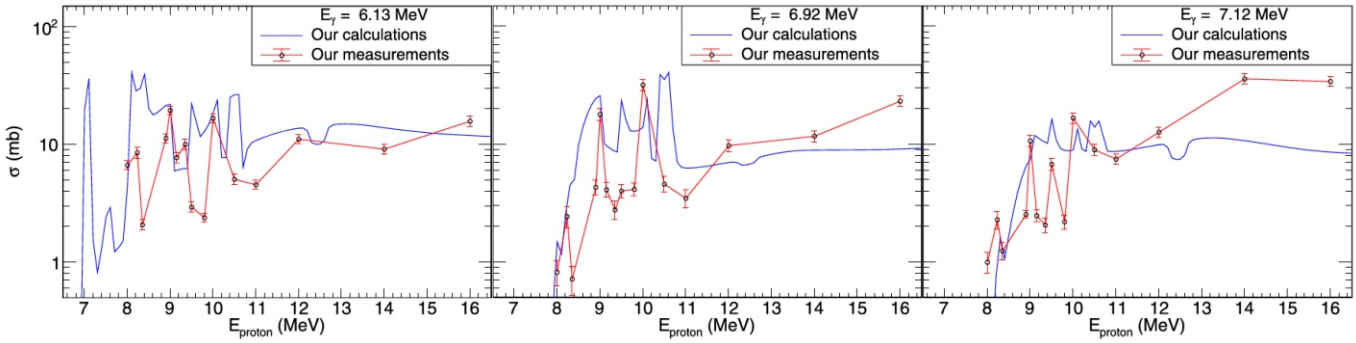

Fig.6: Measured and calculated total cross-sections for production of 6.13, 6.92 and7.12 MeV γ-rays.

excited states in light nuclei. We have initiated a systematic study of the angular distribution and absolute cross sections of (p, p'γ) reaction on different light nuclei. It is worth noting that unlike (p, p') reaction there are dearth of data for (p, p'γ) reactions from nuclei, like, ^{12}C, ^{16}O, ^{10,11}B etc. On the theoretical side, the reproduction of absolute cross sections from inelastic scattering experiments continues to be a formidable challenge due to the myriad complexities of nuclear structure and reaction mechanisms at low energy and low mass regions. In this report we have presented absolute production cross sections of three transitions in ^{16}O. The absolute cross section of the 6.92 MeV has been reported for the first time [5]. We have made serious efforts to develop a detailed theoretical analysis package within the framework of Optical Model formalism. The OM potentials have been generated from fits to a large body of global data. The analysis clearly reveals the complexity of the problem and the importance of channel couplings, resonances and nuclear deformations.

Acknowledgment

Indranil Mazumdar wishes to thank his collaborators, V. Ranga, S. P. Weppner, R. Sariyal, S. Panwar, A. K. R. Kumar, A. K. Gourishetty, S. M. Patel and P. B. Chavan. He would also like to thank the staff members of the TIFR Pelletron facility for providing the beam for the entire duration of the experiment. DAE is acknowledged for supporting this research work.

References

[1] Ray L, Hoffmann G W and Coker WR 1992 Nonrelativistic and relativistic descriptions of proton nucleus scattering Phys. Rep. 212, 223–328

[2] Ramaty R, Kozlovsky B and Lingenfelter R E 1979 Nuclear g-rays from energetic particle interactions Astrophys. J. Suppl. 40, 487–526

[3] Mazumdar I, Dhibar M, Weppner S P, Anil Kumar G, Rhine Kumar A K, Patel S M, Chavan P B, Bagdia C D and Tribedi L C 2019 Studies in nuclear structure and big bang nucleosynthesis using proton beams Acta Phys. Polon. B 50, 377

[4] Dhibar M, Mazumdar I, Anil Kumar G, Weppner S P, Rhine Kumar A K, Patel S M and Chavan P B 2018 Study of 12C(p,p'g)12C reaction arXiv:1806.02126

[5] V. Ranga, I. Mazumdar, S P Weppner, S. Panwar, R. Sariyal, S. M. Patel, P.B. Chavan, A. K. Rhine Kumar and G. Anil Kumar, Measurement of proton induced absolute production cross section of 6.12, 6.92 and 7.12 MeV g-rays from 160(p, p'g)160 reaction, Journal of Physics G: Nucl. Part. Phys. 51 (2024) 045101

[6] Tilley D R, Weller H R and Cheves C M 1993 Energy levels of light nuclei A = 16–17 Nucl. Phys. A 564 1–183

[7] Dyer P, Bodansky D, Seamster A G, Norman E B and Maxson D R 1981 Cross sections relevant to g-ray astronomy: proton induced reactions Phys. Rev. C 23, 1865

[8] Boromiza M et al 2020 Nucleon inelastic scattering cross sections on 160 and 28Si Phys. Rev. C 101, 024604

[9] Kiener J, Berheide M, Achouri N L, Boughrara A, Coc A, Lefebvre A, de Oliveira Santos F and Vieu C 1998 g-ray production

by inelastic proton scattering on 160 and 12C Phys. Rev. C 58, 2174–9

[10] Mazumdar I, Gothe D A, Anil Kumar G, Yadav N, Chavan P B and Patel S M 2013 Studying the properties and response of a large volume (946 cm3) LaBr3:Ce detector with g-rays up to 22.5 MeV Nucl. Instrum. Methods Phys. Res., Sect.A 705, 85–92

[11] Amos K, Dortmans P J, von Geramb H V, Karataglidis S and Raynnal J 2000 Nucleon–Nucleus Scattering: A Microscopic Nonrelativistic Approach (Boston: Springer) pp 276–536

[12] Weppner S P, Penney R B, Diffendale G W and Vittorini G 2009 Isospin dependent global nucleon–nucleus optical model at intermediate energies Phys. Rev. C 80 034608

[13] Petler J S, Islam M S, Finlay R W and Dietrich F S 1985 Microscopic optical model analysis of nucleon scattering from light nuclei Phys. Rev. C 32, 673–84

[14] Watson K M 1953 Multiple scattering and the many-body problem–applications to photomeson production in complex nuclei Phys. Rev. 89, 575–87

[15] Jelley N A 1990 Fundamentals of Nuclear Physics (Cambridge: Cambridge University Press) chapter 8

[16] Raynal J 1994 Notes on ECIS94 Technical Report CEA-N-2772, Commisariat 'a l'Energie Atomique, Saclay, France pp 1–145

[17] Raynal J 2006 ECIS-06.

http://www.oecd-nea.org/tools/abstract/detail/nea-0850

[18] Thompson I J 2006 FRESCO. http://www.fresco.org.uk20] S. K. Pandit, A. Shrivastava, K. Mahata, N. Keeley, V. V. Parkar, P. C. Rout, K. Ramachandran, I. Martel, C. S. Palshetkar, A. Kumar, A. Chatterjee, and S. Kailas, Phys. Rev. C 93,061602® (2016).

नाभिकीय अभिक्रिया

7

नाभिकीय खगोल-भौतिकी से संबंधित अध्ययन

एस. संत्रा[1,2,*] और ए. बैश्य[1,2]

[1]नाभिकीय खगोल भौतिकी अनुभाग, भाभा परमाणु अनुसंधान केंद्र (भापअ केंद्र), ट्रांबे, मुंबई – 400085, भारत
[2]होमी भाभा राष्ट्रीय संस्थान, अणुशक्तिनगर, मुंबई – 400094, भारत

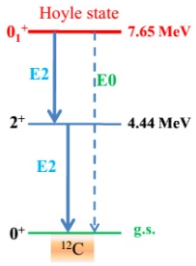

^{12}C की वास्तविक स्थिति में हॉयल अवस्था का रेडियोसक्रिय क्षय

सारांश

^{12}C की एक अनुनाद अवस्था को हॉयल अवस्था के नाम से जाना जाता है, जिसके माध्यम से 3α अभिक्रिया ^{12}C की आंकी गई प्रचुरता को दर्शाने के लिए ^{12}C के उत्पादन को ~ 10^8 गुना बढ़ा देती है और सितारों में कार्बन एवं ऑक्सीजन का अनुपात भारी तत्वों के संश्लेषण के लिए प्रासंगिक है। इस अध्ययन से पता चलता है कि ^{12}C की हॉयल अवस्था के 3 में प्रत्यक्ष क्षय के विभिन्न तरीकों की शाखन को विभाजित करना हॉयल अवस्था की प्रारंभिक संरचना से अत्यधिक प्रभावित है। एक बहुत ही गर्म ($T_9 = 0.1$ से 10) और सघन (10^6 gm/cm^3) तारकीय वातावरण में ^{12}C के हॉयल अवस्था के कण-प्रेरित व्युत्तेजन और उच्च अनुनाद (9.64 MeV, 3_1^- और 9.87 MeV, 2_2^+) ^{12}C उत्पादन दर हेतु वृद्धिकारक पाए गए हैं। संयोग से टूटने वाले कणों की सापेक्ष ऊर्जाओं के प्रयोगात्मक वितरण के विभिन्न संयोजनों की तुलना हॉयल अवस्था की विभिन्न क्षय प्रक्रियाओं को अलग करने के लिए अनुकरणीय माना जाता है।

Nuclear Reactions

7

Studies related to Nuclear Astrophysics

S. Santra[1,2,*] and A. Baishya[1,2]

[1]Nuclear Astrophysics Section, Bhabha Atomic Research Centre, Trombay, Mumbai-400085, INDIA and
[2]Homi Bhabha National Institute, Training School Complex, Anushaktinagar, Mumbai-400094, INDIA

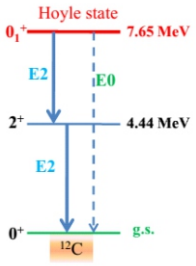

Radiative decay of the Hoyle state to the ground state of ^{12}C

ABSTRACT

A resonant state of ^{12}C, named Hoyle state, through which the 3α reaction increases the production of ^{12}C by ~10^8 times to explain the observed abundance of ^{12}C and the ratio of carbon to oxygen in stars relevant for synthesizing heavier elements. The study shows that the branching of different modes of direct decay of Hoyle state of ^{12}C into 3α is highly influenced by the initial structure of the Hoyle state. In a very hot($T_9 = 0.1$ to 10) and dense (10^6 g/cm^3) stellar environment the particle-induced de-excitations of the Hoyle state and higher resonances (9.64 MeV, 3_1^- and 9.87 MeV, 2_2^+) of ^{12}C are found to enhance the ^{12}C production rate. Different combinations of experimental distribution of relative energies of the coincident breakup α particles are compared with simulations to disentangle different decay processes of the Hoyle state.

KEYWORDS: *Hoyle state,3α cluster structure, relative energy distribution, direct decay processes, nuclear astrophysics, ^{12}C abundance, up-scattering*

**Author for Correspondence: Satyaranjan Santra*
E-mail: ssantra@barc.gov.in

Introduction

In recent years a lot of attention is drawn worldwide towards the study of the Hoyle state as well as ^{12}C production. Work on this area has been initiated recently in our laboratory. The BARC-TIFR Pelletron-Linac facility has been used for the related experiments. The results of some of the theoretical and experimental investigations are highlighted below.

Effect of Initial 3α Cluster Configurations in ^{12}C on the Direct Decay of its Hoyle State

We investigate the implications of initial 3α configurations in ^{12}C corresponding to different decay modes of its Hoyle state on the penetrability ratios. Considering the second 2^+ (10.03 MeV) state to be a collective excitation of the Hoyle state, the direct 3α decay width for the Hoyle state has been calculated using the ratio of the barrier penetration probability of the Hoyle state to the 2^+ state. The semi-classical Wentzel–Kramers–Brillouin (WKB) approximation has been employed to determine the penetrability ratio, resulting in an upper limit on the branching ratio of the direct decay of the Hoyle state in "equal phase-space" (DDφ) mode as $\Gamma_{3\alpha}/\Gamma < 3.1 \times 10^{-6}$. However, this limit for "linear chain" (DDL) decay is $\Gamma_{3\alpha}/\Gamma < 2.6 \times 10^{-7}$, which is one order of magnitude smaller than the DDφ decay and the limit for "equal energy" (DDE) decay is $\Gamma_{3\alpha}/\Gamma < 1.5 \times 10^{-5}$, which is greater than both DDφ and DDL decays. It implies that the limit on direct decay probability is strongly dependent on the initial configuration of the 3α cluster. A further probe using a bent-arm-like 3α initial configuration shows that the direct decay probability is maximum when the angle of the bent arm is ≈120^0, an important ingredient for understanding the Hoyle-state structure [1]

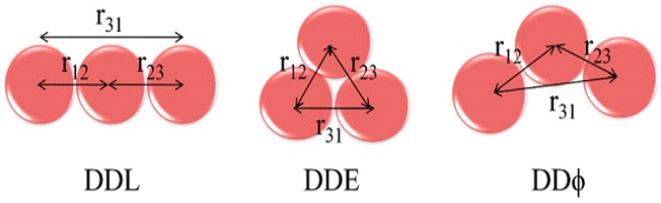

Fig.3: Initial 3α cluster configurations for direct decay modes in linear chain (DDL), equal energy (DDE), and equal phase space (DDφ).

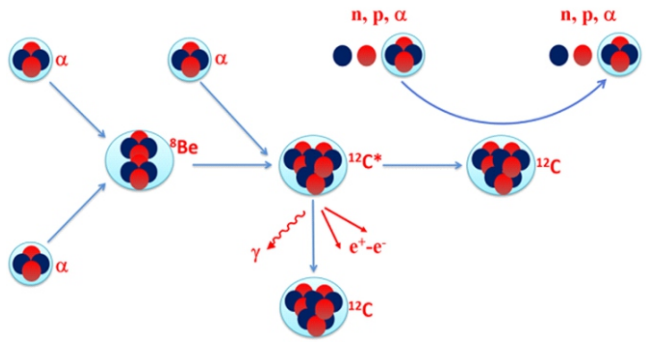

Fig.3: A cartoon of the particle-induced de-excitation process, that competes with the spontaneous radiative deexcitation (γ or e^+-e^- pair emission).

Light-particle-induced De-excitations of 3_1^- and 2_2^+ Resonances of ^{12}C in Extreme Stellar Conditions

The particle-induced de-excitations of the 9.64 MeV, 3_1^- and 9.87 MeV, 2_2^+ resonances of ^{12}C increase the ^{12}C production rate in a very hot and dense stellar environment. The enhancements in ^{12}C production in such environments were estimated for a particle (n, p, and α) density of 10^6 g/cm^3 in the temperature range of T_9 = 0.1 to 10. Enhancement due to neutron-induced de-excitation was found to be the maximum.

The net ^{12}C production rate due to the combined contributions from 7.65 (Hoyle state), 9.64, and 9.87 MeV states is much higher compared to the rate adopted by NACRE compilation. In case of a typical collapsing massive star with temperature dependent densities, for any of the 3_1^- or 2_2^+ resonances, the enhancement factor due to n, p, and α-induced de-excitations together can be as high as 600 [2].

Measurement of the Direct Decay Modes of the Hoyle State

We have carried out two experiments to measure the direct 3α decay branching ratio of the Hoyle state of ^{12}C to investigate recent theoretical prediction [1] which is considerably lower than the presently measured upper limit. Data analysis of the pilot measurement shows that using different analysis techniques such as, Dalitz plot technique, relative energy of ^{8}Be like α pair spectrum and RMS energy deviation spectrum together, contributions from different decay modes can be extracted with better precision. An improved experiment has been carried out using a larger beam time, bigger detector setup consisting of eight large area double sided silicon strip detectors (DSSD) and a beam energy closer to a different resonance in ^{12}C+^{12}C reaction. In addition to precision direct decay branching measurement we planned to confirm the observation of a state at 7.458 MeV, named as Effimov state, which lies very close to the Hoyle state [3].

Over the last decade, numerous experiments have been performed to quantify the direct decay component of the Hoyle-state which is supposed to throw new light on the structure. An upper limit of 0.019% was put by T. Rana et al. [4] which is

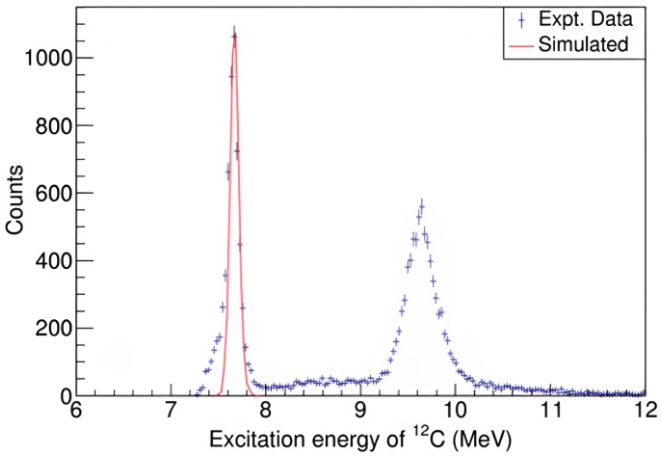

Fig.3: Excitation energy spectrum by reconstructing 3 simultaneous α particle momenta.

actually the upper limit of DDφ decay, for DDL decay they put an upper limit of 0.004% and for DDE decay the same is 0.012%. a comparison of the results obtained in some of the major experiments shows a clear trend that with increasing statistics, the upper limit of direct decay is decreasing. Recent calculations for the upper limit of direct decay [1,5] show the upper limit is even two orders of magnitude smaller than what has been found in the highest statistics experiment so far [4]. This indicates that we need even higher statistics to go further down the upper limit. It has been shown [1] that the resolution plays a major role while extracting the contributions from different decay modes. This was the motivation behind performing an even higher statistics experiment than Rana *et al.* [4] with even better angular resolution.

Here we report a new high-precision measurement of the DD branching ratio utilizing an optimized array of eight double-sided silicon strip detectors and advanced kinematic reconstruction techniques, yielding over 2.2 × 10^5 fully reconstructed Hoyle state events.

As can be seen from Fig.3, the Hoyle state at 7.65 MeV as well as 9.65 MeV 3^- state has been populated. For further analysis of the Hoyle state, the events under the 7.65 MeV peak are chosen. These events are a mixture of both the sequential and direct decay events. In order to disentangle these two kinds of events, we have used three sophisticated techniques: i) Dalitz plot analysis ii) Relative energy of ^{8}Be like α pair and iii) RMS energy deviation spectrum.

A comparison between simulated and experimental Dalitz plots reveals that sequential decay is dominant as expected. However, in order to quantify the individual direct decay components, we have to resort to other techniques.

The distribution of the lowest relative energy between any two α-particles in each 3α decay event of the Hoyle state is called "relative energy of ^{8}Be like α pair spectrum". So, all sequential decay (SD) events decaying through the ^{8}Be ground state will contribute to the peak at a relative energy of ~ 92 keV, the breakup energy of $^8Be_{g.s.}$, whereas for DDL it should peak around 95 keV and for DDE mode of decay, it should peak at E_{rel}≈ 188 keV. So, this technique can differentiate between SD and DDE but not between SD and DDL. The relative energy distribution of the ^{8}Be like pairs in the experimental data is displayed in Fig.6 along with those obtained from simulation events for SD, DDE, DDL and DDφ processes in the same figure to show the nature of distribution for different types of decays. It is seen that the experimental distribution is dominated by the peak at around 92 keV signifying strong dominance of the SD process. The results of the simultaneous fit are shown in Fig.4.

The root mean square energy deviation, E_{rms} can be defined as, $E_{rms} = \sqrt{[<E_{rel}(ij)^2> - <E_{rel}(ij)>^2]}$, where, $E_{rel}(ij)$ are the relative energy between the α particles from the decay of the Hoyle state, and the average is over all possible pairs of the 3α events. Fig.5 displays the distribution of E_{rms} for the fully detected events along with the simulated spectra for different modes. It is clear from the relation for E_{rms} that DDE should contribute prominently in the neighbourhood of $E_{rms} \approx 0$ in the distribution, subject to finite broadening due to the total instrumental resolution. The results of the simultaneous fits show that the sequential decay constitutes the major contribution.

A new method of data analysis was employed including both the "folded Dalitz plot projections" and "normalized energy difference" methods, supplemented by Bayesian soft-assignment classification, to disentangle DD events from the overwhelming sequential decay background. We determined an upper limit of 0.018% for the DDϕ mode (and 0.002% for the DDE mode) at the 2σ confidence level, and a realistic branching ratio of approximately 0.0018% for Ddϕ using Bayesian inference. These results provide the most stringent experimental limits to date, closer to the recent theoretical predictions, and reinforce the dominance of sequential decay. This work has significant implications for nuclear structure models and the astrophysical rate of carbon production in stars.

Summary

Systematic measurements related to the famous Hoyle state of ^{12}C have been carried out to understand the structure

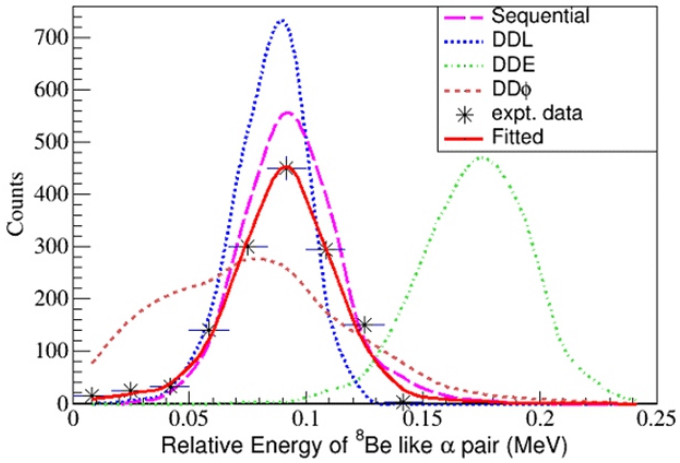

Fig.4: Simultaneous fit of different decay modes with experimental data for relative energy analysis to delineate individual direct decay contributions.

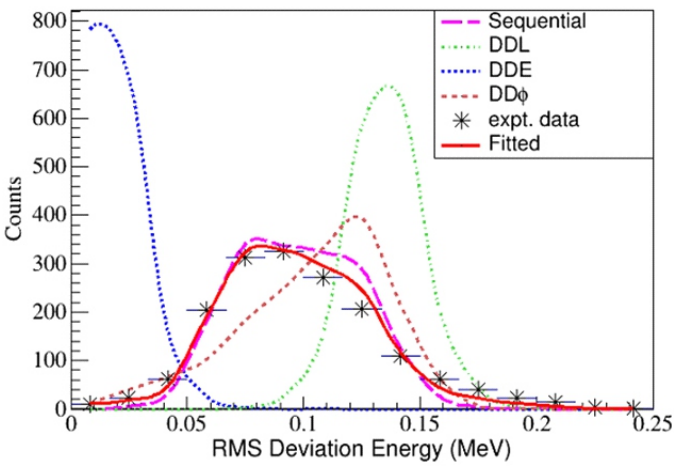

Fig.5: Simultaneous fit of different decay modes with experimental data for rms energy deviation analysis to determine individual contributions.

of this resonance state as well as the effect on the three alpha reaction rate due to the variation in the environmental condition. It was observed that the initial three-alpha cluster structure has a huge impact on the probability of different direct decay modes. In a highly dense and hot star, the production of ^{12}C was found to be enhanced due to the upscattering of protons, neutrons and alpha particles off ^{12}C proceeding through its different resonance states. A new upper limit on the existence of another resonance state called Effimov state, very close to the Hoyle state, has been obtained from a high precision 3-alpha breakup measurement. In the investigation of direct decay branching of the Hoyle state, an upper limit of about 0.0018% was obtained for the most dominant DDϕ mode using Bayesian inference. These results provide the most stringent experimental limits to date.

References

[1] A. Baishya *et al.*, Phys. Rev. C 104, 024601 (2021).

[2] A. Baishya *et al.*, Phys. Rev. C 108, 065807 (2023).

[3] A. Baishya, *et al.*, arXiv:2507.03514 [nucl-ex] (2025).

https://doi.org/10.48550/arXiv.2507.03514

[4] T. K. Rana *et al.*, Phys. Lett. B 793, 130 (2019); https://doi.org/10.1016/j.physletb.2019.04.028

[5] R. Smith, M. Gai, M. W. Ahmed, M. Freer, H. O. U. Fynbo, D. Schweitzer, and S. R. Stern, Phys. Rev. C 101, 021302(R) (2020); https://doi.org/10.1103/PhysRevC.101.021302

नाभिकीय अभिक्रिया

8

नाभिकीय-स्तर घनत्व का अध्ययन

एस. संत्रा[1,2,*] और पी. सी. राउत[1,2]
[*]नाभिकीय खगोल भौतिकी अनुभाग, भाभा परमाणु अनुसंधान केंद्र (भापअ केंद्र), ट्रांबे, मुंबई – 400085, भारत
[2]होमी भाभा राष्ट्रीय संस्थान, अणुशक्तिनगर, मुंबई – 400094, भारत

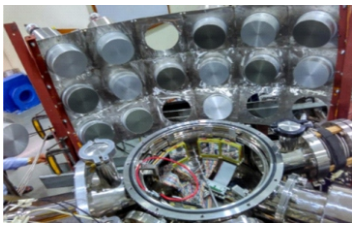

Si पट्टिका संसूचक सरणी द्वारा आवेशित कण का पता लगाने के साथ-साथ तरल सिंटिलेटर संसूचक सरणी का उपयोग करके न्यूट्रॉन स्पेक्ट्रा के विशेष माप हेतु प्रयोगात्मक व्यवस्था।

सारांश

न्यूट्रॉन वाष्पीकरण स्पेक्ट्रा के एक विशेष माप के माध्यम से नाभिकीय स्तर घनत्व की सामूहिक वृद्धि और विकृत ^{171}Yb, ^{161}Dy में उत्तेजन ऊर्जा के साथ इसके धूमिल होने की स्थिति का पता लगाया गया। ^{169}Tm और ^{159}Tb पर ^{7}Li-प्रेरित अभिक्रिया में एक ट्राइटन के स्थानांतरण के माध्यम से ^{172}Yb एवं ^{162}Dy नाभिक की बहुसंख्यता प्राप्त की गई। न्यूट्रॉन स्पेक्ट्रा के सांख्यिकीय मॉडल विश्लेषण ने सूक्ष्म गणनाओं के अनुरूप 42±2 के एक बड़े सामूहिक वृद्धि कारक को उजागर किया। मैक्सवेलियन औसत न्यूट्रॉन प्रग्रहण अनुप्रस्थ काट को समझने में मापित परमाणु स्तर घनत्व का एक बड़ा प्रभाव पाया गया।

Nuclear Reactions

8

Study of Nuclear-level Density

S. Santra[1,2,*] and P. C. Rout[1,2]
[1]Nuclear Astrophysics Section, Bhabha Atomic Research Centre (BARC), Trombay, Mumbai-400085, INDIA
[2]Homi Bhabha National Institute, Anushakti Nagar, Mumbai-400094, INDIA

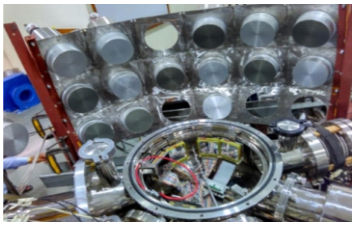

The experimental set-up for exclusive measurement of neutron spectra using liquid scintillator detector array along with charged particle detection by Si strip detector array.

ABSTRACT

The collective enhancement of nuclear level density and its fade-out with excitation energy in the deformed ^{171}Yb, ^{161}Dy, obtained through an exclusive measurement of neutron evaporation spectra. The ^{172}Yb and ^{162}Dy nuclei were populated via the transfer of a triton in a ^{7}Li-induced reaction on ^{169}Tm and ^{159}Tb. Statistical model analysis of the neutron spectra revealed a large collective enhancement factor of 42±2, consistent with microscopic calculations. The measured nuclear level densities were found to have a huge implication in the understanding of the Maxwellian Averaged Neutron Capture cross section.

KEYWORDS: *Nuclear-level density, Radiative neutron capture, Neutron evaporation spectra, Shell effect, Shell damping factor*

**Author for Correspondence: S. Santra*
E-mail: ssantra@barc.gov.in

Introduction

The nuclear level density (NLD) is a fundamental property of the nuclei. It is defined as the number of nuclear energy levels per unit excitation energy (E*), and increases rapidly with E*. The NLD is a crucial input in statistical model calculations of compound nuclear decay. It is also required in the study of fission hindrance in heavy nuclei, the giant dipole resonance built on excited states, the yields of evaporation residues in fusion evaporation reactions, production of heavy elements in stellar processes etc. Due to the liquid drop like properties of the nucleus, the NLD is expected to have a smooth behavior with respect to the mass (A) and atomic number (Z). However, this behavior is modified by the excitation energy dependent nuclear shell effects. Deformed nuclei are found to have a larger NLD compared to their spherical counterparts. In our lab we have studied various aspects of the NLD.

Shell Effect on Nuclear Level Density and its Damping with Excitation Energy near Pb Region

The nuclear level density makes a transition from the shell-dominated regime at low excitation energy to that of a classical liquid drop at high excitation. The shell effect is disappeared at high excitation energy (~40 MeV) and its implication to fission fragment anisotropy has been predicted by Ramamurthy, Kapoor and Kataria in 1970 [1]. The damping of the nuclear shell effect with excitation energy has been measured, using the experimental setup as shown in Fig.1, through an analysis of the neutron spectra following the triton transfer in the ^{7}Li induced reaction on ^{205}Tl. The measured neutron spectra demonstrate the expected large shell correction energy for the nuclei in the vicinity of doubly magic ^{208}Pb and a small value around ^{184}W. A quantitative extraction of the allowed values of the damping parameter (γ), along with those for the asymptotic nuclear level density parameter (a=A/δa), has been made for the first time [2]. The measured damping factor was extracted from the data and found to be $\gamma=0.06^{+0.01}/_{-0.02}$ MeV^{-1}. (see Fig. 2).

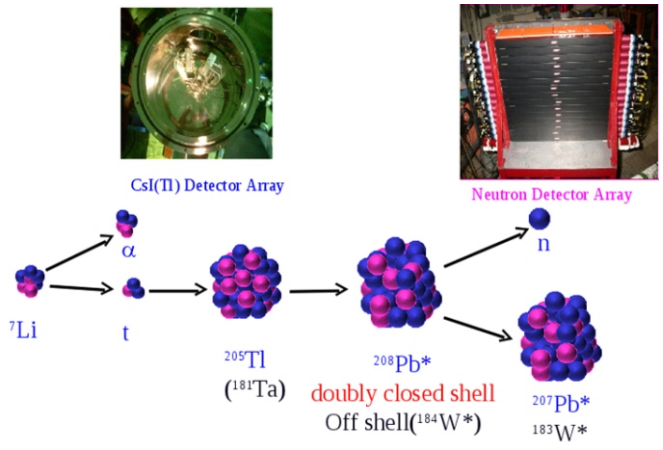

Fig.1: Experimental set-up for exclusive measurement of neutron spectra using~1 m^2 plastic scintillator array.

Collective Enhancement of Nuclear Level Density

The occurrence of collective rotational motion implies an increase in the degrees of freedom available for low E* and thus a significant increase in the NLD. The collective enhancement of the nuclear level density is predicted to be damped out with excitation energy. The exclusive measurements of neutron spectra following alpha particle emission in ^{11}B+^{181}Ta, ^{197}Au systems [3] forming compound nuclei ^{192}Pt and ^{208}Po respectively have been carried out at the PLF, Mumbai. An array of 15 liquid scintillators (two inch thick and 5 inch diameter) was used for fast neutron measurement and two telescope consisting of Si-strip detectors were used for the measurement of alpha particle by energy loss technique. The inverse level density parameter k (=δa) as a function of excitation energy of the residual nucleus has been extracted by fitting the neutron spectra with statistical model calculation (see Fig.3). Statistical model calculations were performed considering an enhancement level density $\rho_{int}K_{coll}$ where ρ_{int} is intrinsic level density and K_{coll} is the enhancement factor. K_{coll} as a function of excitation energy (or temperature) was obtained and extracted value of critical temperature where collective enhancement vanishes agrees well with the theoretically predicted value.

Experimental Evidence of Large Collective Enhancement of Level Density and its Significance in Radiative Neutron Capture

In the continuation of the NLD program, two more measurements on nuclear level density have been carried out for nuclei with mass A ~170. The collective enhancement of nuclear level density and its fade out with excitation energy in

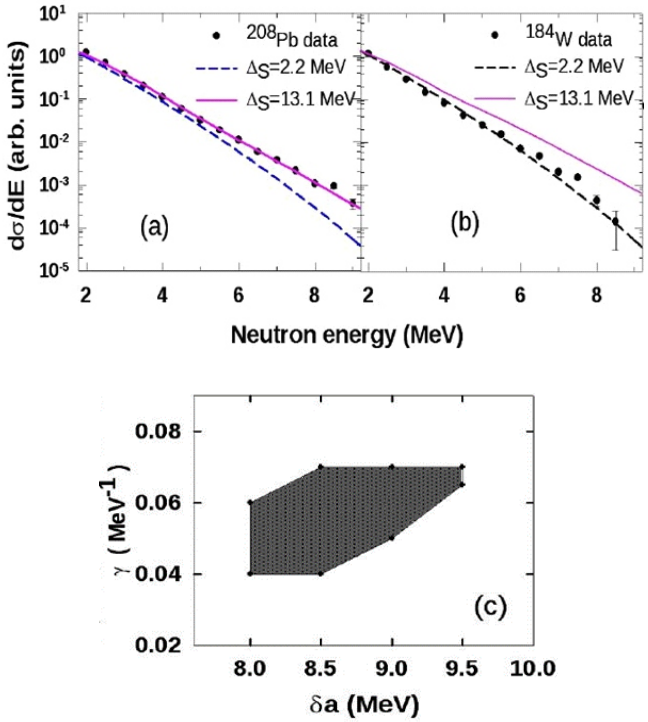

Fig.2: (a, b) Effect of shell correction on neutron spectra from ^{208}Pb and ^{184}W, (c) Exclusion plot between level density parameter and shell damping factor [2].

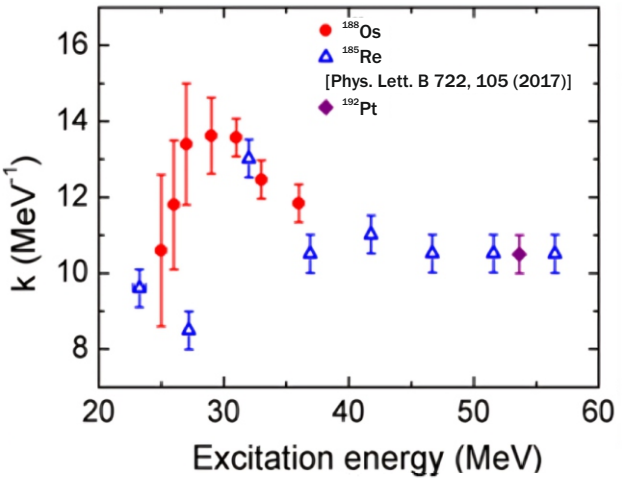

Fig.3: Inverse level density parameter as a function of the excitation energy of the nuclei.

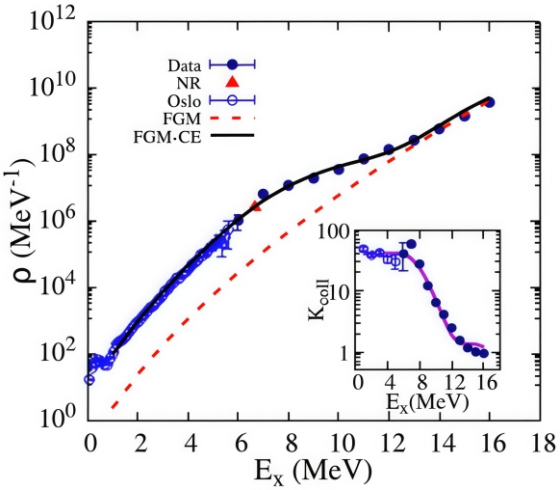

Fig.4: The NLD obtained as a function of excitation energy using Oslo data (open circles) [34] and present experiment (filled circles), normalized to the level density at the neutron resonance point (NR) (triangle). The dashed red line shows intrinsic level density from fermi gas model (FGM) and black solid line shows fermi gas level density with collective enhancement (FGM-CE), both obtained using CASCADE with the level density formulae described in the text. The inset shows collective enhancement with excitation energy obtained from the combined data sets.

the deformed ^{171}Yb and ^{161}Dy nuclei have been inferred through exclusive measurements of neutron spectra. These two nuclei were populated via the stripping transfer of a triton in a ^{7}Li-induced reaction on ^{169}Tm and ^{159}Tb respectively. The statistical model analysis of neutron spectra demonstrated large collective enhancement factors of 40±3 and 42±2 respectively [4,5], consistent with recent microscopic model predictions but very different from the existing measurements for the nearby deformed nuclei. This is the largest collective enhancement factor obtained from the measurements and reported in any system to date. A fade-out in the enhancement has been observed at the energy of 14±1 MeV. The complete form of energy dependent collective enhancement was experimentally deduced for the first time by combining the measured NLD with the Oslo data as shown in Fig. 4.

The neutron-capture process is responsible for the formation of the heavy nuclei between iron and the actinides [6]. In order to find the implication of large collective enhancement, we have calculated the Maxwellian average neutron capture cross section (MACS) at 30 KeV for ^{171}Yb and ^{170}Yb. The MACS at 30 KeV were calculated using our measured NLD given as input in the TALYS code. This is achieved by incorporating our collective enhancement form into the TALYS-1.96 reaction code [7].

The level density of the Fermi gas model with the measured collective enhancement was used to calculate the MACS and then compared to KADoNIS-v1 [8] and estimation of Bao et al. [9] for both ^{171}Yb and ^{170}Yb, as shown in Fig.5(a) and (b), respectively. To see the effect of collective enhancement on MACS, various TALYS calculations with different collective enhancement factors have been performed. Fig.5 shows the MACS calculated using TALYS with the enhancement factor 40 and the reported enhancement factor 10 in nearby mass region. The default gamma-ray strength function (gSF), the Simplified Modified Lorentzian (SMLO, strength 9) and default optical model potential parameters [10] were used in the calculation. It's important to note that even with different

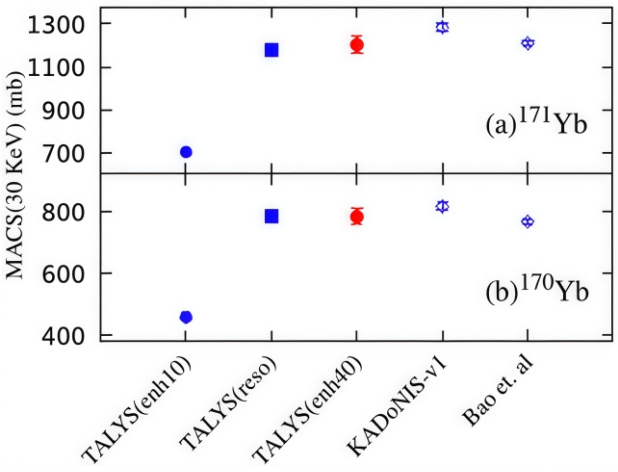

Fig.5: (a) Calculated MACS at 30 KeV for ^{171}Yb using the Talys-1.96 and its comparison with KADoNIS-v1 compilation, well-established Bao et al. estimation, (b) Same as (a) for ^{170}Yb. Here, TALYS(enh10) and TALYS(enh40) were using the present level density prescription with enhancement factor 10 and 40, respectively. TALYS(reso) was the calculated MACS using the measured level density at neutron resonance energy.

combinations of gSF and a collective enhancement factor of 40, the calculated values of MACS are similar to experimental values. However, using an enhancement factor of 10 showed significant differences from the experimental values. The predicted MACS using the present level density prescription, including the measured enhancement factor (TALYS(enh40)), agrees with the experimental MACS values, while the collective

enhancement factor 10 (TALYS(enh10)) could not be reproduced well. Therefore, in a statistical model, it is necessary to include the proper NLD prescription with collective enhancement, which significantly improves the predicted capture cross sections relevant for the astrophysical s-process.

References

[1] V. S. Ramamurthy, S. S. Kapoor, S. K. Kataria, Phys. Rev. Lett. 25, 386 (1970).

[2] P. C. Rout et al., Phys. Rev. Lett. 110, 062501 (2013).

[3] G. Mohanto et al., Phys Rev. C 100, 011602 (2019)

[4] T. Santhosh et al., Phys. Lett. B 841, 137934 (2023).

[5] T. Santhosh et al., Phys Rev. C 108, 044317 (2023).

[6] F. Käppeler, R. Gallino, S. Bisterzo, W. Aoki, Rev. Mod. Phys. 83, 157 (2011).

[7] A. Koning, S. Hilaire, S. Goriely, TALYS-1.9 A Nuclear Reaction Program. User Manual; Nuclear Research and Consultancy Group (NRG), Petten, The Netherlands, 2015.

[8] KADoNiS-The Karlsruhe Astrophysical Database of Nucleosynthesis in Stars, online at https://exp-astro.de/kadonis1.0.

[9] Z.Y. Bao, H. Beer, F. Käppeler, F. Voss, K. Wisshak, T. Rauscher, At. Data Nucl. Data Tables, 76, 70 (2000).

[10] A.J. Koning, J.P. Delaroche, Nucl. Phys. A 713, 231 (2003).

भारी-आयन प्रेरित नाभिकीय विखंडन

9

एक नए प्रकार का विखंडनः भापअकें-टीआईएफआर पेलेट्रॉन लीनॉक सुविधा द्वारा योगदान

के. माहात[1,2,*], वी. कुमार[1,2], के. रामचंद्रन[1], ए. श्रीवास्तव[1,2], एस.के. पंडित[1,2], वी.वी. पार्कर[1,2]

[1]नाभिकीय भौतिकी प्रभाग, भाभा परमाणु अनुसंधान केंद्र (भापअ केंद्र), ट्रांबे, मुंबई – 400085, भारत

[2]होमी भाभा राष्ट्रीय संस्थान, अणुशक्तिनगर, मुंबई – 400094, भारत

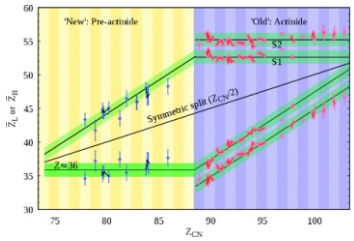

असममित विखंडन में हल्के एवं भारी खंडों की माध्य प्रोटॉन संख्या प्री-एक्टिनाइड्स और एक्टिनाइड्स के बीच एक विस्मयकारी संबंध दर्शाती है।

सारांश

परमाणु विखंडन की व्यापक समझ, जिसमें नाभिकीय ऊर्जा से लेकर रेडियोआइसोटोप के उत्पादन तक के विस्मयकारी अनुप्रयोग हैं और जो आधुनिक भौतिकी की कई अवधारणाओं के लिए एक परीक्षण वस्तु है, इसे अब तक समझा नहीं जा सका है। क्वांटम बहु-निकाय प्रणाली की बड़े पैमाने पर सामूहिक गति इतनी जटिल है कि आठ दशकों से अधिक समय बीत जाने के बाद भी इस क्षेत्र में प्रयोगात्मक अवलोकनों द्वारा विकास संचालित होता रहा है। ^{180}Hg के बीटा-विलंबित विखंडन में असममित द्रव्यमान वितरण के अप्रत्याशित अवलोकन ने प्री-ऐक्टिनाइड नाभिक के विखंडन में बड़े पैमाने पर सैद्धांतिक एवं प्रयोगात्मक कार्यों हेतु आकर्षित किया है। यह आलेख, भापअ केंद्र-टीआईएफआर पेलेट्रॉन लीनॉक सुविधा का उपयोग करके असममित विखंडन अन्वेषण का वर्णन किया गया है।

Heavy-ion Induced Nuclear Fission

9

A New type of Fission: Contributions from the BARC-TIFR Pelletron LINAC Facility

K. Mahata[1,2,*], V. Kumar[1,2], K. Ramachandran[1], A. Shrivastava[1,2], S. K. Pandit[1,2] and V. V.Parkar[1,2]

[1]Nuclear Physics Division, Bhabha Atomic Research Centre (BARC), Trombay, Mumbai-400085, INDIA

[2]Homi Bhabha National Institute, Anushakti Nagar, Mumbai-400094, INDIA

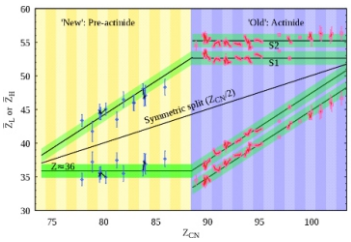

Mean proton number of the light and heavy fragments in asymmetric fission render a striking connection between pre-actinides and actinides.

ABSTRACT

Comprehensive understanding of nuclear fission, which has tremendous applications ranging from nuclear energy to production of radioisotopes and is a testing ground for many concepts of the modern physics, remains elusive. This large-scale collective motion of the quantum many-body system is so complex that even after more than eight decades the developments in this field are steered by the experimental observation. Unexpected observation of asymmetric mass distribution in beta-delayed fission of ^{180}Hg garnered tremendous theoretical and experimental interest in fission of pre-actinde nuclei. This article describes the investigations of asymmetric fission using the BARC-TIFR Pelletron LINAC facility.

KEYWORDS: *Asymmetric fission, Shell corrections, Heavy-ion induced fusion-fission, Entrance channel dependence*

**Author for Correspondence: K. Mahata*
E-mail: kmahata@barc.gov.in

Introduction

Nuclear fission is an example of large-scale collective motion of nuclei, where a single nearly spherical nuclei undergoes deformation and finally splits into two or more fragments. Drastic rearrangements of nucleons take place during this process. The macroscopic Liquid Drop Model (LDM), which explains the gross properties of fission, predicts symmetric fission to be most probable. However, the low energy fission of actinides was observed to be dominantly asymmetric. This was attributed to the preferential fragment formation near magic nuclei that have large shell (microscopic) corrections. The incorporation of oscillating quantum shell corrections, which moulded many hills and valleys in the smooth LDM potential energy surface, also explained the observations of fission isomers and near constancy of fission barrier of the actinides. This also led to the predictions of existence of island of stability beyond actinides, which gave a huge impetus for heavy-ion induced nuclear reaction studies. The elements in this island are called super heavy elements (SHE) and are completely stabilized by the shell corrections as there is no liquid drop barrier for them.

Attempts to form SHE in fusion of two heavy nuclei by overcoming their Coulomb repulsion opened a new dimension to the nuclear physics research. The composite system, produced when two heavy-ion come in contact, possess high excitation energy and angular momentum. Evolution of such systems needed detailed investigations. As shell corrections weakens with the increase in excitation energy, it is paramount to consider the gradual damping of shell correction in order to have reliable prediction of the fission survivability of such hot and rotating compound nucleus. At high excitation energies, the effect of dissipation is also observed. The presence of dissipation slows down the dynamical evolution, enhancing the neutron emission probability and fission survivability. It was also realized that when the charge product (Z_1Z_2) of the colliding partners is larger than 1000, the composite system may reseparate before forming fully equilibrated compound nucleus. This phenomenon is called quasi-fission and has drawn tremendous attention as it severely impedes formation of the SHE. Apart from the charge product, deformation, difference in N/Z ratio and magicity of the colliding partners are found to influence the dynamical evolution in heavy-ion induced reactions.

Reliable predictions of fission properties are very crucial not only for harnessing nuclear energy and production of radioisotopes in a more safe and efficient way, but also for understanding synthesis of heavy elements and neutrino physics research. Even though, lots of progress have taken place, a comprehensive understanding of the heavy-ion induced fission process has not been achieved so far and experimental surprises still steer the progress in this field. Particularly, fission in the pre-actinde region remained less explored as the fission probability is low. Fission studies in this region, having large ground state shell corrections and a balanced fission-neutron evaporation competition, might help to understand the two key factors, namely the damping of shell correction and dissipative dynamics of nuclear medium.

Asymmetric fission in pre-actinides

Mass asymmetric split, which dominates in low-energy fission of actinides, was found to recede while moving towards lighter nuclei. Though the experimental mass distributions around A = 200 displayed slight dip around symmetric split, mass distributions for A<200 were characterized by single peak as expected form the LDM behaviour. A recent experimental observation at ISOLDE, CERN in beta-delayed fission of ^{180}Hg [1] has generated lots of excitements in this area as it has challenged the understanding of fission developed through the study in the actinide region. In case of ^{180}Hg, the liquid drop model favoured symmetric fragment, ^{90}Zr, has magic numbers of neutrons (N = 50) and semi-magic numbers (Z = 40) protons. Thus, from liquid drop model as well as fragment magicity point of view, symmetric fission was expected to be preferred. However, the experimental mass distribution of ^{180}Hg in beta-delayed fission was found to be dominantly asymmetric. This observation garnered tremendous theoretical and experimental interest in this field. Though most of the theoretical model studies were limited to a few cases, the predictions of Brownian Shape Motion (BSM) model are available for a large number of nuclei [2].

Beta-delayed fission studies are limited to a few nuclei and have limited statistics. Experimentally, heavy-ion fusion-fission route was also explored to study the same phenomena systematically. Several studies were carried out using the BARC-TIFR Pelletron LINAC facility. Due to the Coulomb barrier, it is not possible to keep the excitation energy of the fissioning system very low. In case of beta-delayed fission, the excitation energy is just above the fission barrier. While the light particle (p, α) induced fission studied have been carried out down to excitation energy 10 MeV above the barrier, heavy-ion induced studies are limited to even higher excitation energies. At higher excitation energies shell effects diminish considerably, reducing the preference for the shell driven fission mode(s). However, it allows the study of damping of shell correction with excitation energy, which has implication in fission survivability of heavy and super-heavy compound nuclei. Observation of asymmetric fission in ^{35}Cl+^{144,154}Sm [3] was one of the first few studies, which showed the sensitivity of heavy-ion fusion-fission to the newly observed asymmetric fission mode in the

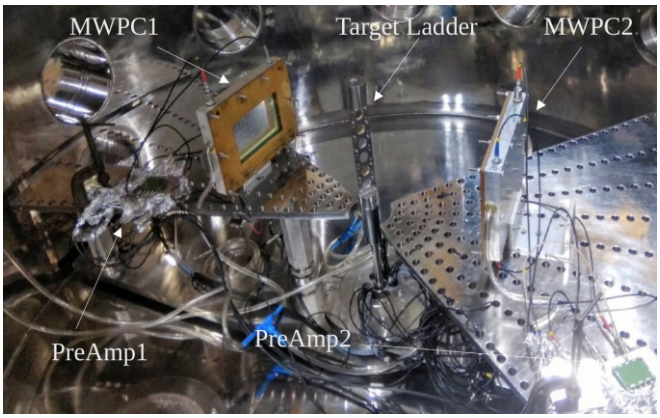

Fig.1: A photograph of the experimental setup used for fission fragment mass distribution measurement at the BARC-TIFR Pelletron LINAC facility.

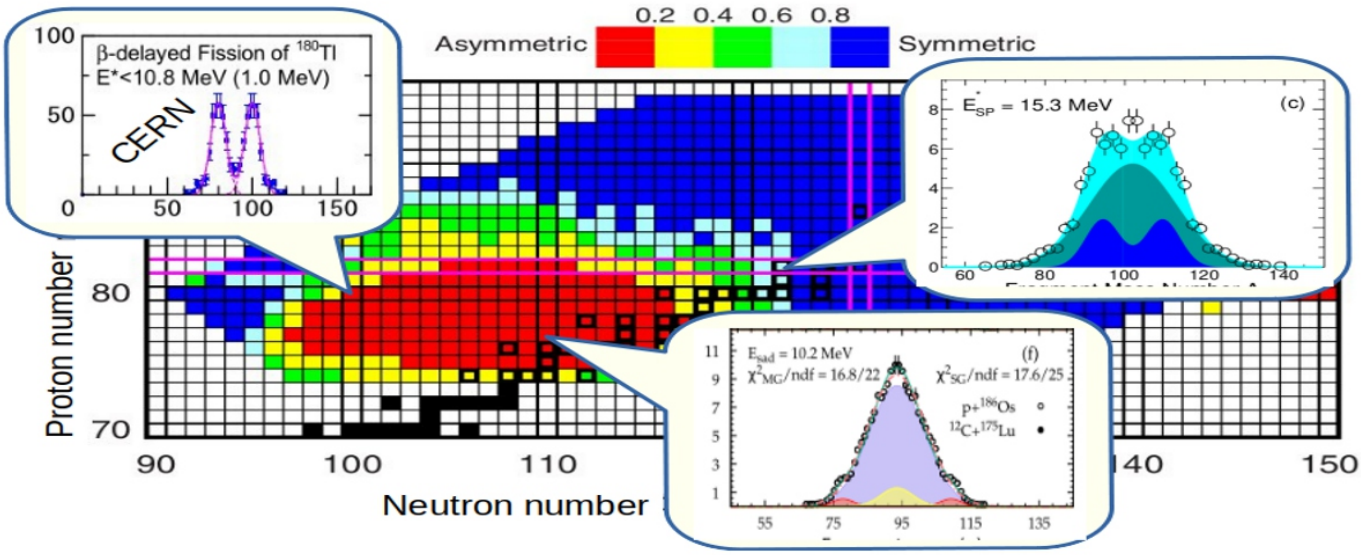

Fig.2: Brownian Shape Model (BSM) predicted ratio of the symmetric-yield to peak-yield for pre-actinide nuclei are shown in colored pixel. A few experimental mass distributions (mass number vs yields) in callouts show the experimental trend.

pre-actinide region. Several other studies [4-6] were performed using the BARC-TIFR Pelletron LINAC facility, which have improved our understanding of mass asymmetric fission in the pre-actinides and the fission process in general. A photograph of the experimental setup for the measurement of fission fragment mass distributions is shown in Fig.1. The setup consists of two large area Multi-Wire Proportional Chambers (MWPC) to measure the velocities and emission angles of the fission fragments in coincidence. Fragment masses are determined by applying momentum conservation.

Microscopic origin of asymmetry in fission of pre-actinides

Different theoretical models have proposed different mechanisms to explain the observed asymmetry in this region. The BSM model ascribe this to the neutron shell at 110 of the fissioning nuclei around the saddle deformation, which makes the outer saddle asymmetric. In a microscopic energy density functional (EDF) calculation, Scamps and Simenel have concluded the dominance of octupole effects, in most cases driven by neutron configurations. Another interpretation relates the asymmetric splits to prescission configurations involving molecular structures.

In Fig.2 the experimental trend is compared with the BSM model predictions. The BSM model predicts a large island of asymmetry (marked red) in the pre-actinide region. However, the experimental studies differ significantly with the predictions. It should be mentioned here the BSM predictions corresponds to excitation energy just above the fission barrier. The experimental data for ^{180}Hg also corresponds similar excitation energy. Other two data set pertaining particle induced fission has excitation energy around 10-15 MeV above the fission barrier. Though the contribution of the asymmetric component gradually diminishes with increase in excitation energy, the peak position associated with neutron or proton shell is expected to remain same. The experimental results for ^{180}Hg (in the left edge of the island) and ^{204}Pb (right edge of the island) agree well with the BSM model predictions in terms of magnitude and position of the asymmetric peak. However, the experimental results for ^{187}Ir (at the heart of the predicted island) differ significantly from the BSM model expectation. BSM model not only predicts large asymmetry, it also predicts very asymmetric fragments in low energy fission of ^{187}Ir. The experimental mass distributions of ^{187}Ir, shows an additional narrow symmetric contribution, which is in agreement with the $Z \approx 36$ stabilization in the light fragment.

While the presence of asymmetric mode in low energy fission of pre-actinide is confirmed by many experiments. Its origin is still debated and more experimental studies are required to chart the boundary and shape of the predicted island of asymmetry in the pre-actinide region. Our systematic study of the available experimental mass distributions, it was revealed that the mean value of Z of the light fragment, evaluated assuming unchanged charge density (UCD), varies

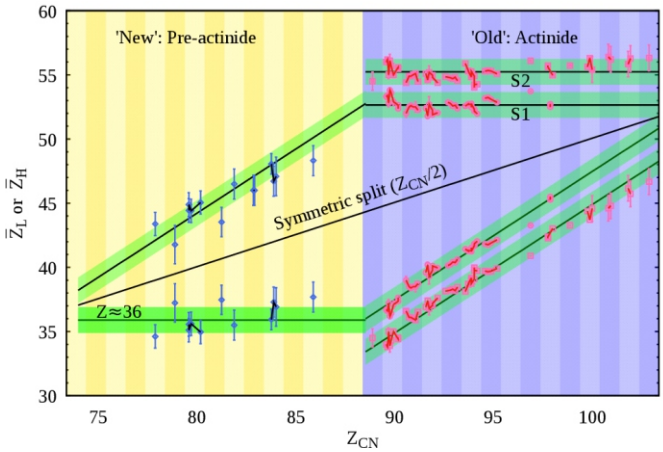

Fig.3: Evaluation of the peak position of the light and heavy fragment peaks corresponding to different asymmetric fission modes across the nuclear chart.

less as compared to that of the heavy fragment with Z the fissioning nuclei. No preferential population of neutron number was observed. Thus, it was concluded that the light fragment proton shells with Z ≈ 36 provide the stabilization in asymmetric fission of pre-actinide nuclei [7]. The dominance of Z ≈ 36 has been further reaffirmed in a recent GSI experiment through direct charge distribution measurement [8]. This is in contrast with the observations in the actinide region, where the proton shell stabilization in the heavy fragment was found to drive the asymmetry. The observed proton shell stabilization in the light fragment in low-energy fission of pre-actinide was also substantiated by the EDF calculation, which showed that the shell correction associated with the proton configuration in the pre-fragments dominates over that of the neutron configurations.

The evolution of the peak position of the light and the heavy asymmetric peaks is shown in Fig.3. It has rendered a striking connection between the pre-actinide and the actinide region, establishing the general dominance of proton shell in low-energy fission. It rises a fundamental question as why the proton configuration dominates in sharing of nucleons during fission process. Is the Coulomb repulsion between the protons keep the away from the neck, allowing specific shell configuring to manifest, while the neutron sub-systems are disturbed due to the presence of the neutron-rich neck. As discussed earlier, the position of the light fragment peak remains stable at Z ≈ 36 and the mean Z of the heavy fragment increase monotonically taking them away from the position of the symmetric split as the Z of the fissioning nucleus increases. At the boundary of the pre-actinide and actinide a role reversal takes place, where the proton shell stabilization in the heavy fragment starts to dominate, forcing the light fragment to take the excess protons.

Role of Entrance Channel Dynamics in Fission of Pre-actinides

Dynamics also plays a very vital role in nuclear reaction in general and in heavy-ion induced fusion-fission reaction in particular. Dynamics in the entrance channel in heavy-ion fusion fission reaction might delay the equilibration of some of the degrees of freedoms, preventing formation of compound nucleus and altering the outcomes substantially. Fission fragment mass distribution is a sensitive probe to study the entrance channel dynamics, particularly the mass flow dynamics Quasifission, a non-compound (non-equilibrated) nuclear process, is being studied experimentally as well as theoretically with great vigor as it hinders formation of super-heavy elements. It strongly depends on the entrance channel parameters like charge product (or mass asymmetry), deformation of the colliding nuclei, shell closure and neutron excess in addition to the compound nucleus (CN) fissility. There are extensive experimental evidence of entrance dependence in fission of systems with higher fissility and entrance channel charge product. However, its extent in the sub-Pb region remained unexplored and largely neglected. Investigation of this aspect is essential for an accurate modeling of the excitation energy dependence of the microscopic effects discussed earlier. Particularly, ignoring quasifission might lead to ambiguity in the inferred multimodal fission recently observed in the pre-actinide region.

In order to address this issue, experiments were carried out to measure the fission fragment mass and total kinetic energy distribution for ^{191}Au, populated in i) ^{16}O+^{175}Lu and ii) ^{37}Cl+^{154}Sm reactions utilizing the BARC-TIFR Pelletron facility. Beam energies was so chosen that the excitation energy and the angular momentum populated are similar for both the reactions. Details of the measurements can be found in Ref. [4].

In Fig.4 the measured fragment mass distributions for both the systems are compared. As can be seen from the figure, the measured mass distribution for heavier projectile (^{37}Cl) is much wider as compared to the lighter projectile (^{16}O) induced reaction. The observed difference is much larger than that expected due to the small change in excitation energy and angular momentum. The statistical dependence of the mass distribution widths on excitation energy and angular momentum is also determined in the same experiment. Thus, it provided compelling evidence of presence of quasi-fission in the sub-lead region. The characteristic of the quasi-fission contribution is obtained by subtracting the distribution for ^{16}O+^{175}Lu reaction form that for ^{37}Cl+^{154}Sm reaction. The quasi-fission contribution, which has dynamic origin, is also found to overlap with microscopic asymmetric component. The Di-Nuclear System (DNS) model calculation, which reproduces the observed quasi-fission probability and its distribution, has revealed the persistence of shell effects in the emerging light fragments of the di-nuclear system. Thus, the study demonstrated for the first time that not only the microscopic shell effects, but the dynamics in the entrance channel also has a significant role in influencing the fission of nuclei in the newly identified island of mass asymmetry.

Comparison of the experimental mass ratio widths of neutron deficient nuclei near Pb is shown in Fig.5. The mass ratio is defined as the ratio of the fragment mass to the mass of the fissioning nucleus. The fitted mass ratio widths for most of the heavier projectile (^{35,37}Cl, ^{40,48}Ca and ^{48}Ti) induced and lighter projectile (^{13}C, ^{16}O and ^{24}Mg) Ca and Ti induced reactions involving both spherical as well as deformed targets exhibit significantly larger widths as compared to C - Mg induced reactions. Further, all the systems involving ^{154}Sm (deformed) target with heavy beams show an increase in the width with

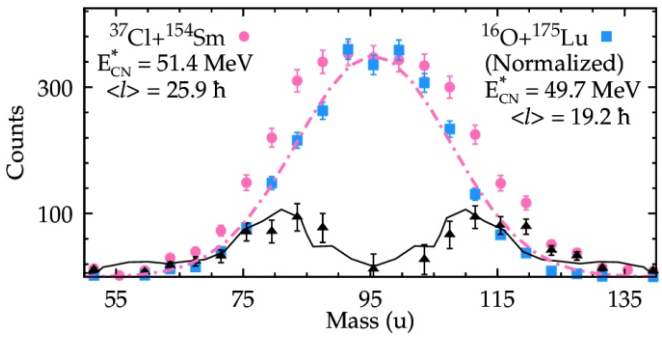

Fig.4: Experimentally measured fission fragment mass distributions for ^{16}O+^{175}Lu and ^{37}Cl+^{154}Sm reactions with similar excitation energy and angular momentum are compared. The difference between the two distributions is shown in black triangle. The continuous black line is the Di-Nuclear system (DNS) model prediction of quasi-fission contribution for the heavier system.

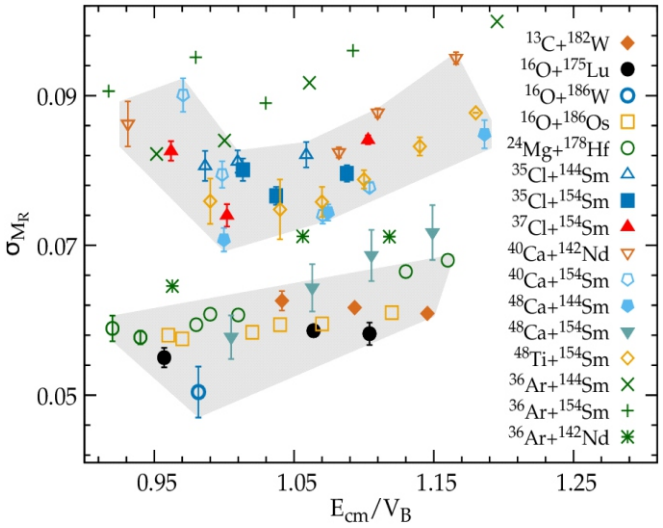

Fig.5: Width of the mass ratio distributions as a function of energy in centre-of-mass (E_{cm}) relative to the Coulomb barrier energy (V_B) are compared. The region of C, O, Mg and Cl, Ca (except $^{48}Ca+^{154}Sm$) are shaded separately to highlight the difference among them.

decreasing energy below the Coulomb barrier. In case of neutron rich $^{48}Ca+^{154}Sm$ system, the quasifission exhibits signature of fast time scale, i.e., observation of mass-angle correlation in asymmetric splits, which are clearly separated from the fusion-fission (symmetric) products. The widths of the symmetric distributions are found to be comparable to those of lighter ion induced reactions, thus having no significant contribution from quasifission in the symmetric region. While no such distinctly separate quasifission contribution is observed for $^{48}Ca+^{144}Sm$ and $^{40}Ca+^{154}Sm$, widths of the symmetric distribution for these systems are found to be larger as compared to those for $^{48}Ca+^{154}Sm$ system and other lighter ion induced reactions. The above induced reactions show distinctly different behavior as shown by the shaded regions. In general, Cl, comparison indicates that most of the systems involving heavier projectile are having contribution from the quasi-fission process.

Summary and outlook

Rapid progress was witnessed in last few years in low-energy fission of pre-actinides. Observation of mass asymmetric fission has provided an opportunity to test the fission models beyond the actinide region to improve their reliability. Different theoretical models have suggested different mechanism as the underlying driving force for the asymmetry. Our study suggests, proton shell stabilization in the light fragment mainly govern the asymmetric split.

Acknowledgments

We acknowledge the accelerator staff for the smooth operation of the machine. Technical help from P. Patale and A. Kumar during experiments are also acknowledged.

References

[1] A. Andreyev *et al.*, Phys. Rev. Lett. 105 252502 (2010).

[2] P. Möller *et al.*, Phys. Rev. C 91, 044316 (2015).

[3] R. Tripathi *et al.*, Phys. Rev. C 92 024610 (2015).

[4] S. Gupta *et al.*, Phys. Lett. B 803, 135297 (2020).

[5] S. Dhuri *et al.*, Phys. Rev. C 106, 014616 (2022).

[6] V. Kumar *et al.*, Phys. Rev. C 109, 014613 (2024).

[7] K. Mahata *et al.* Phys. Lett. B 825, 136859 (2022)

[8] Morfouace *et al.*, Nature 641, 339 (2025).

नाभिकीय अभिक्रिया

10

विखंडन की असामान्य विधि

एस. संत्रा[1,2,*] और ए. पाल[1,2]
[1]नाभिकीय खगोल भौतिकी अनुभाग, भाभा परमाणु अनुसंधान केंद्र (भापअ केंद्र), ट्रांबे, मुंबई – 400085, भारत
[2]होमी भाभा राष्ट्रीय संस्थान, अणुशक्तिनगर, मुंबई – 400094, भारत

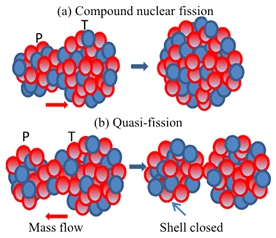

आंशिक-विखंडन में अवलोकित कोश प्रभाव का चित्रण।

सारांश

इस आलेख में, भापअ केंद्र-टीआईएफआर पेलेट्रॉन लीनॉक (एलआईएनएसी) सुविधा का उपयोग करके विखंडन माप में हाल ही में देखे गए विखंडन के असामान्य विधियों के कुछ उदाहरण दिए गए हैं। इन अवलोकनों में निम्नवत शामिल हैं : (क) ^{257}Md नाभिक के विखंडन के लिए सबसे दुर्लभ विखंडन क्षय विधि में से एक, जिसे सुपरशॉर्ट विधि के रूप में जाना जाता है। (ख) 70 MeV तक की उच्च उत्तेजना ऊर्जा पर विखंडन खंड द्रव्यमान वितरण पर कोश प्रभाव, और; (ग) धीमे आंशिक-विखंडन में कोश प्रभाव का प्रमाण ।

Nuclear Reactions

10

Exotic Modes of Fission

S. Santra[1,2,*] and A. Pal[1,2]
[1]Nuclear Astrophysics Section, Bhabha Atomic Research Centre, Trombay, Mumbai-400085, INDIA
[2]Homi Bhabha National Institute, Anushakti Nagar, Mumbai-400094, INDIA

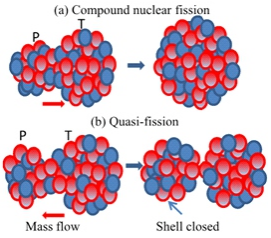

Depiction of observed shell effect in quasi-fission.

ABSTRACT

A few examples on exotic modes of fission observed recently in the fission measurements using the BARC-TIFR Pelletron Linac facility are briefed in this article. These observations include: (a) One of the rarest fission decay modes, known as Supershort mode, for the fission of ^{257}Md nucleus (b) Shell effect on the fission fragment mass distribution at excitation energy as high as 70 MeV and (c) Evidence of shell effect in slow quasi-fission.

KEYWORDS: *Super-short mode of fission, multi-chance fission, slow quasi-fission*

**Author for Correspondence: S. Santra*
E-mail: ssantra@barc.gov.in

Introduction

Nuclear fission continues to be a very fascinating topic due to its ever impressive varieties in its reaction mechanism. With the observation of several new modes of fission at specific compound nucleus mass region these studies have become even more attractive. A few examples on exotic modes of fission observed recently in the fission measurements using the BARC-TIFR Pelletron-Linac facility are: (a) Observation of one of the rarest fission decay modes, known as Super-short mode, for the fission of ^{257}Md nucleus, (b) Shell effect on the fission fragment mass distribution at excitation energy as high as 70 MeV and (c) Evidence of shell effect in slow quasi-fission.

Observation of Super-short Mode of Fission from Heavy Actinide (^{257}Md)

Super-short mode of fission is generally observed when both the nascent fission fragments have the atomic and neutron numbers close to that of the doubly magic ^{132}Sn. This is a very rare mode of fission which is generally observed from the neutron rich fissioning nuclei with A>257 [1-5]. In order to search for the presence of such mode in ^{257}Md nucleus, it was populated using ^{19}F+^{238}U fusion reaction and the mass and TKE (total kinetic energy) distributions of fission fragments produced from the ^{257}Md compound nuclei for E_{beam} = 87.1, 93 and 98 MeV were measured [6]. As shown by open circles in Figs. 1(a-c), it can be observed that, for all the beam energies, the TKE distributions peak at energies close to 198 MeV, as expected from the Viola systematic- the empirical relationship developed by V.E. Viola and colleagues to predict the total kinetic energy (TKE) of fission fragments based on the Coulomb parameter of the fissioning nuclei. Due to the skewness in the shape of the TKE distributions, particularly for the first two beam energies (87.1 and 93.0 MeV) with equivalent compound nuclear excitation energies E*=37.5 and 42.9 MeV respectively, the best fit could only be achieved with two Gaussian distributions: one around 193 MeV and the other around 230 MeV, as shown by filled gray and cyan regions, respectively, in Figs. 1(a-c). It may be observed that in these two plots the peak corresponding to low TKE is much closer to the value obtained from the Viola systematics, whereas the peak corresponding to high TKE is possibly due to the super-short mode of fission, where large Coulomb repulsion between the two compact fragments is expected to generate higher TKE. At E_{beam} = 98 MeV with E*=57.6 MeV as shown in [Fig.1(c)], the TKE distribution shows a very small contribution from super-short mode, indicating the weakening of the super-short mode at higher beam energies. To confirm that the above super-short mode observed in ^{257}Md, populated in the ^{19}F+^{238}U reaction, is not due to some structure of the delivered pulsed beam or any target related issues, the results have been compared with different reactions measured using same beam (^{19}F) but a different target (^{232}Th) and then using the same target (^{232}Th) but different beam (^{18}O) in the same experimental setup [6]. From the ^{19}F+^{232}Th reaction at E_{beam} = 93 and 98 MeV, corresponding to E* = 47.6 and 52.4 MeV, the TKE distributions were found to be perfectly Gaussian in shape, as expected [see Figs.1(e) and 1(f)]. Similarly, the results were compared with the other compound nucleus ^{256}Fm, populated in the ^{18}O+^{238}U reaction, at E_{beam} = 80.9 MeV, corresponding to E* = 36.3 MeV, the excitation energy region where the super-short mode has been observed for the ^{257}Md nucleus. It was found that the TKE distributions for ^{256}Fm could also be fit by using a single-Gaussian function [see Fig.1(d)], thereby confirming the presence of the super-short mode in the fission of the present ^{257}Md nucleus. The above observation suggests that the onset of the super-short mode of fission can be considered to be from ^{257}Md [6].

Shell Effect at High Excitation Energy: Role of Multi-chance Fission

The shells of the fission fragment nuclei are known to play an important role in deciding the number of nucleons in the fragments leading to an asymmetric mass distribution [7]. However, this shell effect on the fission mechanism is expected to wash out at higher excitation energies (E*) of the compound nuclei [8]. To search for the limit on E* beyond which the shell effect do not play any role, fission fragment mass distributions have been measured in the ^{11}B+^{238}U reaction system populating the compound nucleus at E* in the range of ~37-70 MeV. The mass-TKE correlation plots obtained for different beam energies (E_{beam}=53-87.4 MeV) are shown in Fig.2 (a-j). The corresponding mass distributions, i.e., projections of Fig.2 (a-j) on X axis, shown as open circles in Fig.2 (a′-j′) are not perfect Gaussians. At low beam energies, the distributions are either double peaked or having flat tops. One of the peaks observed around A ~140 confirms the presence of a known asymmetric mode which is in strong competition with the symmetric mode described by the Liquid drop model. In order to find out the contribution from each modes, the measured distributions have been fitted using three Gaussian functions corresponding to one symmetric component (grey filled area) and two asymmetric components (cyan filled areas) as shown in Fig.2 (a′-j′). Interestingly, the asymmetric component is nonzero even at the highest excitation energy E*=70 MeV corresponding to E_{beam}=87.4 MeV. From different theoretical model calculations, the shell effect is predicted to wash out at an excitation energy 40 MeV, thus the presence of asymmetric mode observed at such high energies may actually be due to the reduced

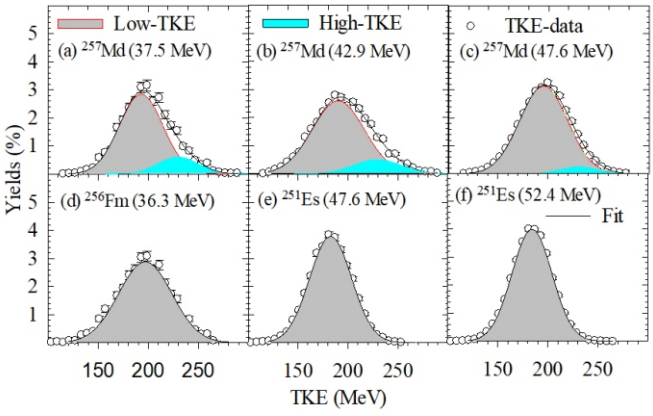

Fig.1: Measured total kinetic energy (TKE) distributions corresponding to ^{257}Md, ^{256}Fm and ^{251}Es at different excitation energies are shown by hollow circles. Contributions from low-TKE and high-TKE are represented by grey and cyan colours respectively. Solid lines represent sum of both the contributions.

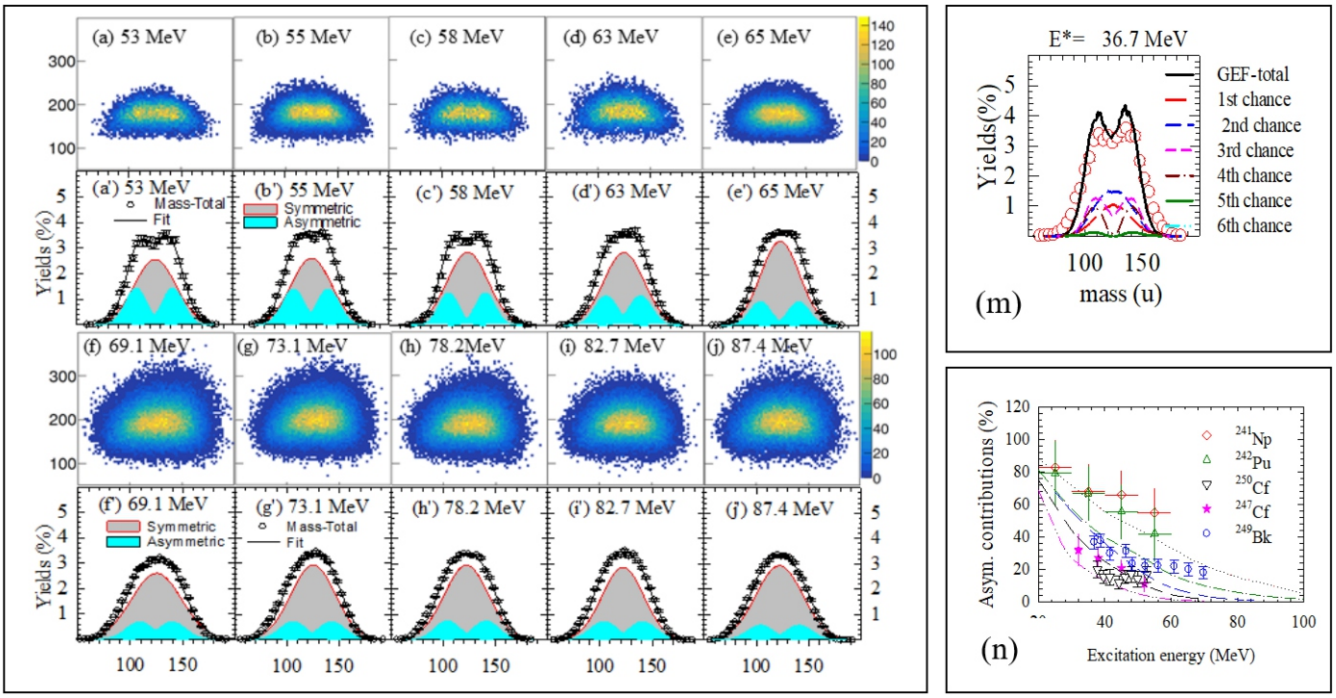

Fig.2: (a'-j') Mass-TKE correlation and (a'-j') fission fragment mass distributions (FFMD) for ^{249}Bk nuclei at different beam energies (E_{beam}=53-87.4 MeV), (m) FFMD for different chance fission for a typical beam energy E_{beam}=53 MeV (E=36.7 MeV) and (n) a systematic of asymmetric contributions as a function of excitation energy E* for different fissioning nuclei.*

effective excitation energies (E^*_{eff}) of the fissioning nuclei. This could be understood in terms of multi-chance fission (MCF) where neutrons successively get evaporated from the compound nucleus thereby reducing E^*_{eff} of the residual composite nuclei.

The semi empirical model code GEF has been used to calculate the mass distributions for different chance fission. For a typical initial compound nucleus excitation energy of E*=36.7 MeV, the contributions for different chance fissions are shown by different lines in Fig.2(m). It was observed that for all energies the calculated mass distributions corresponding to the first chance-fission are symmetric and cannot explain the experimental mass distributions. However, the presence of MCF up to 6th chance with varying probabilities with reduced *E** has introduced the asymmetric components. The sum total of mass distributions weighted over different chance fission, shown by the black solid lines in Fig.2(m), provides a reasonable agreement with the overall behavior of the measured mass distributions. The GEF calculations have been extended further for a wide range of excitation energies (25-85 MeV) to not only compare with the measured data at remaining energies but also estimate the highest value of *E** where shell effect washes out after incorporating the effect of multi-chance fission. We find that the shell effect that leads to asymmetric modes of fission in ^{11}B + ^{238}U start to disappear when the initial CN excitation energy E*~ 70 MeV, which is much higher than the results reported earlier. The systematic study made using the literature data and GEF predictions, as shown in Fig.2(n), suggest that shell effect washes out for initial *E**> 70 MeV for all the systems considered [9].

Shell Effect in Slow Quasi-fission Process

In order to search for shell effect in quasi-fission process, the Fission fragments have been measured for the ^{19}F + ^{238}U reaction at energies ranging from 99.7 to 142.1 MeV. The derived mass distributions are normalized to 200 % as shown in Fig.3(e-h) (left panel) by black circles. Data from our previous measurement on the same reaction at lower energies are shown in Fig.3 (b-d) (left panel) by green circles. The measured distributions were compared with the calculations (red solid lines in Fig.3 (left panel)) using a semi-empirical model code GEF (a model well validated for light particle induced fission) based on compound nuclear fission and found to be wider, especially at lower beam energies. To rule out the fact that the broadening of the measured data is due to the limited mass resolution of the experimental setup, the calculated distributions have been broadened incorporating the mass resolution of the experimental setup, sigma ~6 u, as shown by blue dashed lines in Fig.3 (left panel). But, they failed to explain the much wider measured data and hint at possibilities of having admixture of quasi fission along with the compound nuclear fission. Now the contribution from slow quasi-fission have been segregated by subtracting the GEF results (normalized at the peak position) from experimental data at all the measured energies (Fig.3 (a-d) (right panel)), which shows doubly peaked distributions, suggesting the role of shell effect in SQF process.

Similar analyses have been performed for the mass distribution data of other reaction systems involving heavy projectiles and heavy targets available in the literature. The mass distributions corresponding to QF process have been

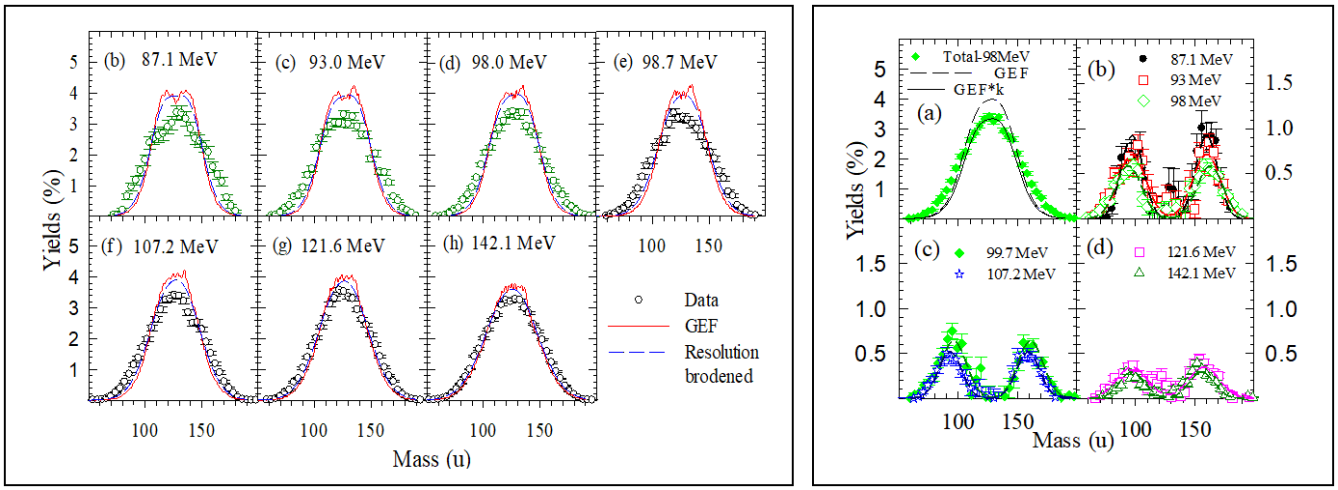

Fig.3: (left) Comparison of measured FFMD (hollow circles) with the compound nuclear fission model (lines); (right) segregating quasi-fission part by subtracting GEF results (normalized at the peak position) from the experimental mass distributions.

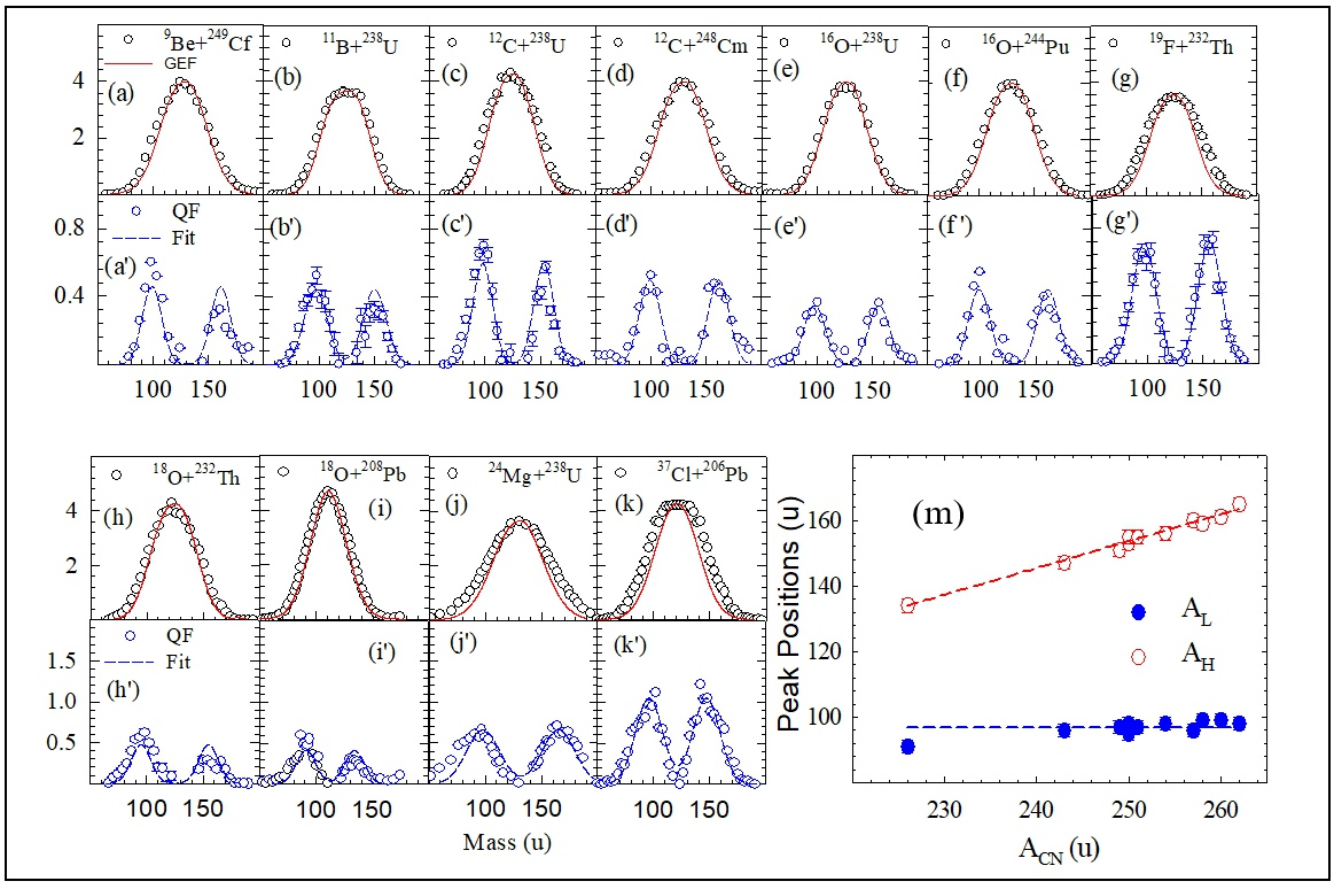

Fig.4: (a-k) & (a'-k') Segregation of QF modes from the data available in literature for eleven systems; (m) Comparison of the peak positions for both low and high masses of the quasi-fission mass distributions as a function of the masses of the fissioning nuclei A_{CN}, showing linear behaviour with mass of the lower peak A_L remaining constant and that of higher peak A_H increasing with A_{CN}.

obtained for different reaction systems at different excitation energies. The experimental FF mass distributions and the GEF calculations at excitation energies around 50 MeV have been shown for the reaction systems $^{9}Be+^{249}Cf$, $^{11}B+^{238}U$, $^{12}C+^{238}U$, $^{12}C+^{248}Cm$, $^{16}O+^{238}U$, $^{16}O+^{244}Pu$, $^{18}O+^{232}Th$, $^{18}O+^{208}Pb$, $^{24}Mg+^{238}U$ and $^{37}Cl+^{206}Pb$ in Fig.4(a-k). The corresponding QF modes for each system derived using the same method have been shown just below the respective mass distribution plots in Fig.4(a'-k'). It can be observed that the QF mass distributions are clearly doubly peaked for all the systems.

The QF mass distributions for all the above systems have been fitted with double Gaussian functions and the peak positions of the light and heavy fragments are plotted as a function of compound nuclear mass A_{CN} in Fig.4(m). It is interesting to note that the peak position corresponding to the light fragment is more or less constant around A=96, whereas the mass of the heavy fragment increases with the mass of the fissioning nuclei. This observation is very analogous to the one for asymmetric fission in actinides where the mass of the heavy fragment does not change with the mass of the fissioning nuclei, but the light fragment does. The fixed position of the peak of the heavier fragments in the asymmetric fission of actinides confirms the role of deformed shell closed nuclei with Z_H ~52 - 56. Similarly, the fixed peak position of the lighter fragments in the asymmetric fission of sub-Lead nuclei suggests the role of shell closed nuclei with Z_L ~34 - 38. Using the same analogy, the present observation of the fixed position of the lighter mass peak in the SQF mass distribution can be treated as a clear evidence of the shell effect in slow-quasi-fission process. Here, the lighter fragments are most probably the nuclei around the magic nuclei ^{96}Zr or ^{94}Sr [10].

Summary

Three interesting topics on fission manifesting different exotic modes have been discussed. The first of these is on the observation of a fission mode with very short elongation for the neutron-rich ^{257}Md nucleus at high excitation energy. To arrive at this conclusion we measured the mass and TKE distributions for three different reactions ^{19}F+^{238}u, ^{19}F+^{232}Th and ^{18}O+^{238}U producing ^{257}Md, ^{251}Es and ^{256}Fm respectively using the same experimental setup. The comparison shows clear observation of exotic supershort mode of fission in ^{257}Md for the first time.

The second interesting result was on finding the upper limit on the compound nuclear excitation energy up to which the effect of nuclear shell on fission fragment mass distribution persists. This limit was found to be 70 MeV, much higher than the existing limit of around 40 MeV based on available experimental data and theoretical understanding.

The third and the last topic was on the observation of shell effect on slow quasi-fission. A systematic analysis of the available data for about a dozen reaction systems in the literature along with a newly measured data on ^{19}F+^{238}U shows that the mass distributions of the quasi fission components are asymmetric in nature. The most importantly, the peak position of the low mass fragments is found to remain constant for different compound nuclear mass. This behavior, observed for the first time, is a clear indication of the shell effect on the mass distribution of quasi-fission.

References

[[1] E. K. Hulet et al., Phys. Rev. Lett. 56, 313 (1986)

[2] E. K. Hulet et al., Phys. Rev. C 40, 770 (1989).

[3] S. N. Dmitriev, et al., Mendeleev Commun. 15, 1 (2005).

[4] Y. Ts. Oganessian et al., J. Phys. G 34, R165 (2007).

[5] I. M. Itkis et al., Phys. Rev. C 83, 064613 (2011).

[6] A. Pal, S. Santra et al., Phys. Rev. C (Lett.) 104, L031602 (2021).

[7] Maria G. Mayer, Phys. Rev. 74, 235 (1948).

[8] R. Vandenbosch and J. R. Huizenga, Nuclear Fission (Academic, New York, 1973).

[9] S. Santra, A. Pal et al., Phys. Rev. C (Lett.) 107, L061601 (2023).

[10] A. Pal, S. Santra et al., Phys Rev. C 110, 034601 (2024).

भारी-आयन प्रेरित नाभिकीय विखंडन

11

आवेशित कण का उपयोग करके भारी-आयन प्रेरित विखंडन में उत्कृष्ट विशेषताएं

वाई.के. गुप्ता[1,2,*], जी.के. प्रजापति[1], बी.एन. जोशी[1,2], पवन सिंह[1,2], एन. सिरस्वाल[1], डी.सी. बिस्वास[1], बी.वी. जॉन[1], बी.के. नायक[1,2] और आर.के. चौधरी[1]

[1]नाभिकीय भौतिकी प्रभाग, भाभा परमाणु अनुसंधान केंद्र (भापअ केंद्र), ट्रांबे, मुंबई – 400085, भारत

[2]होमी भाभा राष्ट्रीय संस्थान, अणुशक्तिनगर, मुंबई – 400094, भारत

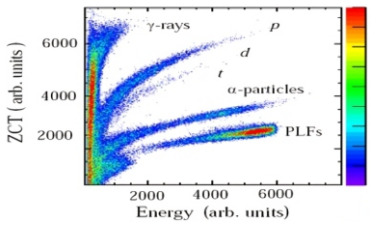

सीएसआई(टीएल) संसूचक में कण पहचान

सारांश

त्वरक और यंत्रीकरण प्रौद्योगिकियों में प्रगति के साथ, नाभिकीय भौतिकी अनुसंधान मानव जिज्ञासा को शांत करने के लिए भौतिक विज्ञान क्षेत्र के हॉटस्पॉट क्षेत्रों में से एक बना हुआ है। नाभिकीय चार्ट के विभिन्न क्षेत्रों की खोज समकालीन नाभिकीय भौतिकी अनुसंधान के प्राथमिक केंद्रों में से एक है। अतिभारी तत्वों संश्लेषण और बाहरी नाभिक के ज़मीनी अवस्था गुणधर्मों का अध्ययन समकालीन दौर में प्रमुख रूप से अग्रणी हैं। हम मुंबई में भापअ केंद्र-टीआईएफआर त्वरक सुविधा से स्थिर किरणपुंजों का उपयोग करके प्रयोगात्मक नाभिकीय भौतिकी कार्यक्रमों को आगे बढ़ाते हैं। विखंडन और विखंडन जैसी प्रक्रियाओं की अनुसंधान के साथ सीधी प्रासंगिकता है। अनुसंधान के अलावा, विखंडन प्रक्रिया सीमित नाभिकीय पदार्थ; नाभिकीय श्यानता के मौलिक गुण के बारे में अध्ययन की सुविधा भी प्रदान करती है। नाभिकीय श्यानता के बारे में कई सवाल अभी भी अनुत्तरित हैं। विखंडन प्रक्रिया के दौरान कण उत्सर्जन एक संभावित जांच प्रस्तुत करता है जो नाभिकीय श्यानता और पूरी विखंडन प्रक्रिया के प्रति भी संवेदनशील है। भापअ केंद्र-टीआईएफआर पेलेट्रॉन सुविधा में चल रहे हमारे कार्यक्रम से नाभिकीय विखंडन के बारे में कुछ नए पहलुओं पर हाल के प्रेक्षण यहां प्रस्तुत किए गए हैं।

Heavy-Ion Induced Nuclear Fission

11

Novel Features in Heavy-ion Induced Fission using Charged Particle Emissions

Y. K. Gupta[1,2,*], G. K. Prajapati[1], B. N. Joshi[1,2], Pawan Singh[1,2], N. Sirswal[1], D. C. Biswas[1], B. V. John[1], B. K. Nayak[1,2] and R. K. Choudhury[1]

[1]Nuclear Physics Division, Bhabha Atomic Research Centre (BARC), Trombay, Mumbai-400085, INDIA

[2]Homi Bhabha National Institute, Anushakti Nagar, Mumbai-400094, INDIA

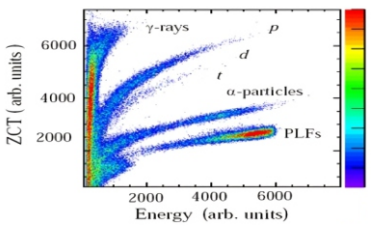

Particle identification in CsI(Tl) detectors.

ABSTRACT

With advancements in instrumentation & computation technologies, nuclear physics research continues to be one of the hotspot fields in physical science domain to quench the human curiosity. Exploring different regions of nuclear chart is one of the primary foci of contemporary nuclear physics research. We pursue experimental nuclear physics research using BARC-TIFR Pelletron Linac Facility (PLF) at Mumbai. Fission and fission like processes have direct relevance to research pertaining to super heavy elements synthesis. Fission process also facilitates study about a fundamental property of finite nuclear matter; nuclear viscosity. Several questions about the nuclear viscosity are still unanswered. Particle emission during the fission process presents a potential probe to study entire fission process and nuclear viscosity. Recent observations on some novel aspects about nuclear scission from our ongoing program at PLF are presented here.

KEYWORDS: *Nuclear physics research, Super Heavy Elements, Fission, Viscosity, Scission.*

**Author for Correspondence: Y. K. Gupta*
E-mail: ykgupta@barc.gov.in

Introduction

Despite the substantial advances in the field of nuclear physics, certain subtle aspects still remain unresolved. The neck rupture process during the nuclear fission is one of them. It is a fascinating example of a delicate interplay of nuclear and Coulomb forces. Particle emission near the scission stage can provide valuable insights about the neck rupture process. Fission Physics Section (FPS) of NPD is pursuing research activities at PLF to understand the finer details of the heavy-ion induced fission process using charged particle emissions during the fission.

Fission of an atomic nucleus provides an opportunity to learn about the properties of nuclear viscosity. Understanding about the precise nature of the nuclear viscosity (one-versus two-body) and its dependence on temperature and coordinate space (deformation) is still quite unclear [1, 2]. During fission, the finite nuclear matter undergoes through a steep potential gradient. As debated earlier in the literature, the energy dissipation at the scission stage might be quite different than just before it [3, 4]. The rapidly moving potential walls might justify suitability of one-over two-body viscosity near to the scission point [1, 2]. A clear understanding about the nuclear viscosity at such a nascent stage is of fundamental importance, in particular with varying temperature.

The overall study of fission dynamics can be divided in the two energy regimes; (a) Low energy fission (spontaneous-, thermal-neutron induced, photo-fission) and (b) heavy-ion induced fission which populate compound nucleus at an elevated temperature.

In the low energy fission, it is widely accepted that the neck rupture is quite sudden [5, 6]. Yield of various Light Charged Particles (LCPs) has been measured in the low energy fission [5,6]. It is seen that among various LCPs, α-particle emission near the scission stage is the dominant one. Historically, in the low-energy fission these α-particles are also known as Long Range α particles (LRAs) [7].

The LRAs are preferentially emitted perpendicular to the fission axis, also known as “Equatorial Emission (EE)” [8]. In the low energy fission, a very small fraction is also emitted along the fission axis, referred as the “Polar Emission (PE)” [8-11]. For Z=1 particles, total yield for each is much lesser than α particles, however, their relative intensities are greater in PE than EE [8, 9]. The difference is striking for the case of protons, where PE component is observed to be around twenty times of that of EE component [9]. On the other hand, in heavy-ion induced fission, except for α particles, none of the other near-scission emissions has been observed so far.

Disentangling of Near Scission Emission (NSE) particles in heavy-ion induced fission is quite challenging task due to presence of emissions from different stages. In heavy-ion induced fusion-fission, particle emission takes place continuously; from the onset of the fusion process to the stage where produced fission fragments have attained their asymptotic velocities. Other than the near scission emission, the rest could be categorized into two major groups, namely emissions from the fully equilibrated compound system (pre-scission) and from the fully accelerated fission fragments (post-scission) [12-16]. A systematic study of different particle emissions from different stages can provide valuable insight about the fission dynamics.

Heavy-ion induced fusion-fission plays a crucial role in reaching to the island of stability in the super-heavy mass region [17, 18]. Unravelling the very presence of non-equilibrium with respect to several degrees of freedom pertaining to heavy-ion induced fission is utmost important. Mass distributions, angular distribution, mass-angle correlation, and kinetic energy distributions of fission fragments (FFs), often deviate from the expected decay of an equilibrated compound nucleus in heavy-ion fusion reactions [19]. These deviations indicate about the presence of Non-Equilibrium (NEQ) fission. Over the years, “quasi fission” [20-22], pre equilibrium fission [23-26]”, and slow quasi fission [27,28]” have been associated with NEQ fission. But, it is not well established whether the underlying mechanisms are different or they originate from a common dynamic source. Charged particle multiplicities in heavy-ion induced fission could be instrumental in inferring the subtle presence of a NEQ. In this newsletter, we present results on various aspects of fission dynamics obtained from measurements of charged particle energy spectra in coincidence with fission fragments at different relative angles.

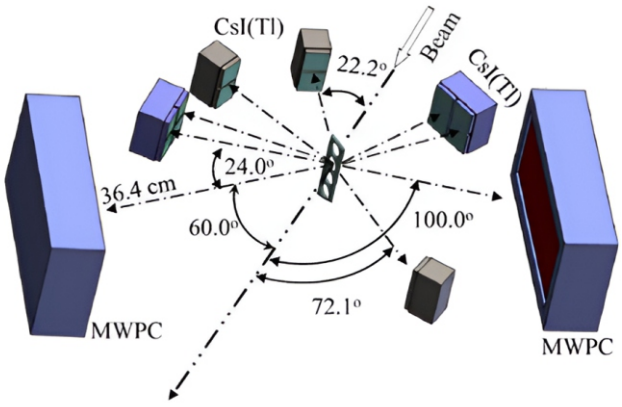

Fig.1: A schematic diagram of the experimental setup, consisting of a target ladder, two MWPCs, and a large number of CsI(Tl) detectors.

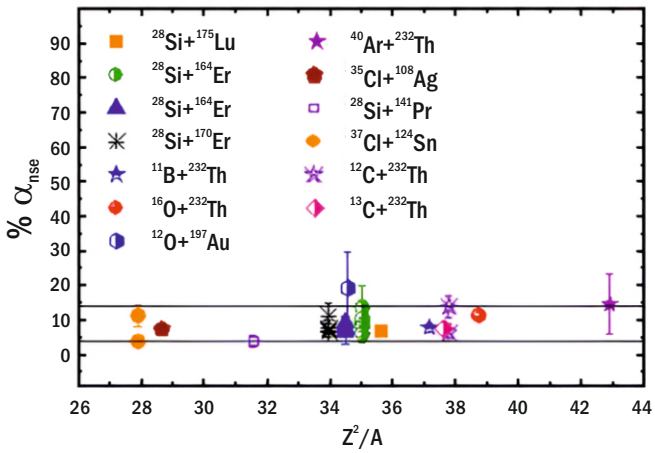

Fig.2: Fraction of near scission multiplicity of alpha particles as a function of fissility parameter.

Experimental Techniques

Experiments have been performed using the heavy-ion beams from Pelletron-Linac Facility (PLF). A schematic diagram of the typical experimental setup is shown in the Fig.1. Gas based detectors such as the Multi-Wire Proportional Counters, or ionization chambers have been used for detecting the fission fragments. CsI(Tl) detectors placed at different angles with respect to beam direction have been used for measuring the energy spectra of charged particles. In order to ensure a coincidence, time correlations are recorded between charged particles and fission fragments. CsI(Tl) detectors are energy calibrated periodically throughout the experiments using ^{229}Th source. The energy calibration in the full energy regime for protons as well as α particles is achieved using the techniques as outlined in the Refs. [29,30].

Particle identification is achieved using a pulse shape discrimination (zero crossover) technique. The gamma rays, light charged particles (p, d, t, and α), and PLFs are well separated in the two-dimensional plot of zero crossover versus pulse height [13, 29-31]. The time correlation between light particles and FFs is recorded through a time-to-amplitude converter (TAC). The event trigger for data collection is generated with the fission events from the gas detector.

Data Analysis & Results

Charged particle multiplicity spectra are obtained at different relative angles with respect to beam direction and the scission axis by dividing the energy spectra with fission-singles events. Typically, one billion fission singles events are collected for each measurement. Depending on relative angles, each spectrum includes different contribution for different particle emission stages. A Moving Source Disentangling Analysis (MSDA) is employed to determine contributions from different emission stages. Measurements have been performed for several reactions, major highlights of the results are as follows;

Changeover in neck-rupture process with energy

In low energy fission, a large fraction of particle emission take place near the scission stage (NSE) [6]. From different observations of NSE, it is widely accepted that the neck rupture is quite sudden in low energy fission [5, 6]. On the other hand, at elevated temperatures from heavy-ion induced fission the absolute near scission multiplicity does not show any systematic trend. However, fraction of near-scission multiplicity is observed to be nearly the same at around 10% of the total pre-scission multiplicity for various systems over a wide range of Z^2/A and excitation energy [13, 15, 29, 32-36] as shown in the Fig.2. It is well established that pre-scission emission is statistical in nature. The constant fraction of near scission multiplicity irrespective of fissioning system and excitation energy clearly suggest that at higher excitation energies, the near scission emission is a statistical process [13]. Whereas it is a dynamical process in low energy fission. It is conjectured from here the neck rupture becomes slower in going from low energy fission to heavy-ion induced fission (high excitation energy); nuclear viscosity at the scission stage undergoes a changeover from very low to a high value in going from low to high temperatures. This conjecture appeared true for near-scission proton emission too [30]. Specific investigations to look for the point around which the transition from dynamical to statistical occurs, are of fundamental importance to pursue in future.

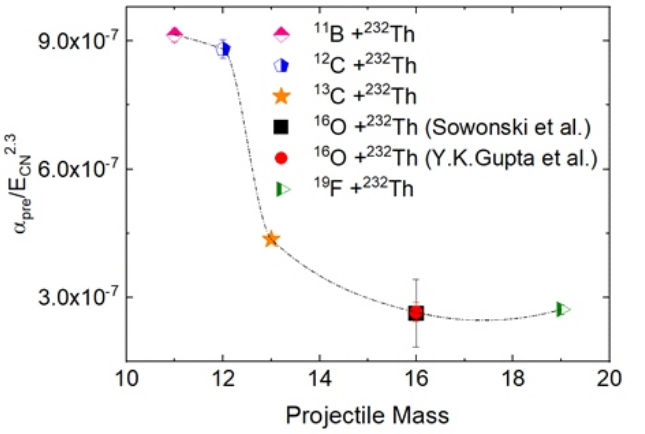

Fig.3: Normalized pre-scission alpha particle multiplicity as a function of projectile mass.

Signature of non-equilibrium fission

Using α_{pre} data of ^{11}B, ^{12,13}C, ^{16}O, and ^{19}F induced fission of ^{232}Th, a systematic study is carried out [13, 29, 31]. It is seen (Fig.3) that the α_{pre} makes a changeover from high to a very low value in going from asymmetric (^{11}B) to more symmetric (^{19}F) entrance channel [29]. The discontinuous behaviour in α_{pre} is similar to what has been observed earlier in angular anisotropy data [23], which was attributed to "pre-equilibrium fission". Using particle emission as a probe to understand the fission dynamics, a clear signature of non-equilibrium fission has been observed for the first time from α_{pre} [29]. However, such a discontinuous behaviour has not been observed for the pre-scission neutron multiplicity (ν_{pre}) data [37]. It is shown earlier that the vpre after normalizing with E_{CN} remains almost the same over a wide fissility range. Insensitivity of the ν_{pre} with respect to non-equilibrium fission has been observed in another work also. A transition to quasifission is clearly

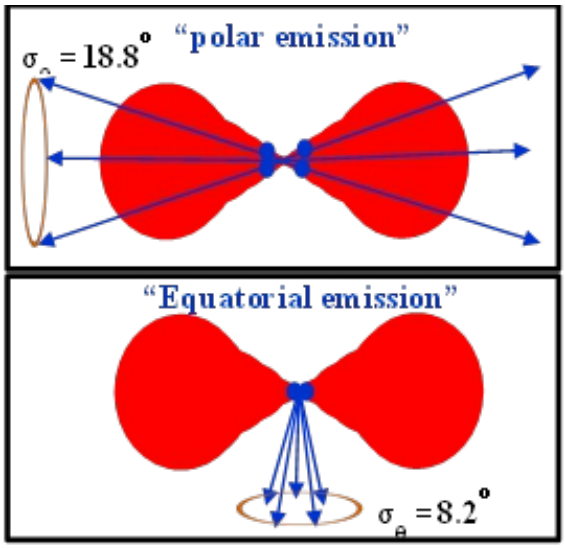

Fig.4: A schematic diagram of "polar" and "equatorial" emissions.

observed in ^{16}O + ^{238}U fission at beam energies just below the Coulomb barrier from fission fragment mass and angular distributions, however, the ν_{pre} does not show any discontinuity with decreasing beam energy. Present results demonstrate that α_{pre} could be a potential probe to gain further insight about the non-equilibrium fission. It would be of further interest to carry out measurements on α_{pre} using projectiles heavier than the ^{19}F bombarding on ^{232}Th in the similar excitation energy bracket as of the present work. Also, investigations are being made for ^{209}Bi target and varying projectiles.

Observation of near-scission "polar" and "equatorial" proton emission in heavy-ion induced fission

The proton multiplicity spectra were measured in coincidence with fission fragments at different relative angles in ^{16}O (96 MeV) + ^{232}Th reaction [30]. The multiplicity spectra were analysed within the framework of a Moving Source Disentangling Analysis (MSDA) to determine contributions from different emission stages. The MSDA conclusively shows "near-scission proton emission" as an essential ingredient in the proton multiplicity spectra. These near-scission proton emissions are observed to be focused parallel ("polar") and perpendicular ("equatorial") to the fission axis with similar intensities as depicted in the Fig.4. It is the first time that "near-scission proton emission" has been disentangled from other emission stages in a heavy-ion induced fusion-fission inevitable presence of "polar emission" in a heavy-ion reaction has been observed for the first time [30]. It is also observed that the pre-scission multiplicity for protons is one order of magnitude lesser than those of α particles. However, the near scission fraction of the proton yield is almost four times larger than the same fraction for α particles which is attributed to deformation effects of the fissioning nucleus. These results open up a new avenue for simultaneous investigation of different particle emissions in heavy-ion induced fission reactions with varying degrees of freedom.

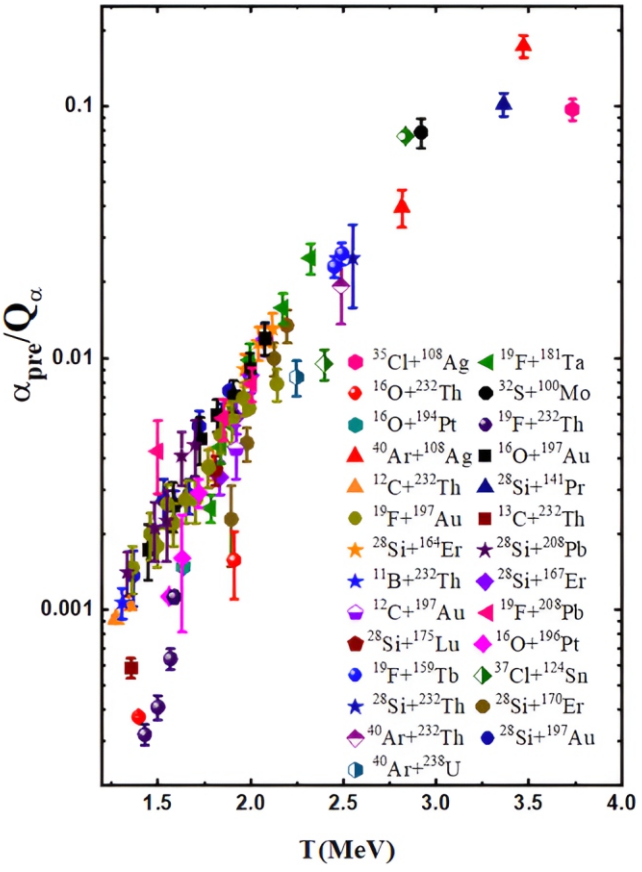

Fig.5: Normalized pre-scission alpha particle multiplicity as a function of compound nucleus temperature.

Presence of direct reaction as a source of α-particle emission during fusion-fission process

We have measured the α-particle energy spectra in coincidence with FFs in the ^{12}C(69 MeV)+^{232}Th reaction at different relative angles with respect to FF direction [31]. The α-particle multiplicity spectra are fitted with the moving-source model to determine prefission and postfission components of α-particle emission. In this analysis, the near scission multiplicity is observed to be anomalously enhanced in comparison to the established heavy-ion systematics, indicating the presence of another source of α-particle emission in the ^{12}C+^{232}Th reaction in addition to pre-scission, post-scission and near-scission emission stages. In the two-dimensional particle identification plot, a high-energy component corresponding to the summed energy of two α particles is observed [31]. The observation of these 2α events suggests that, due to the α-cluster structure of ^{12}C, there is a significant component of ^{8}Be breakup followed by α-transfer-induced fission events. Since the α-transfer grazing angle for the ^{12}C(69 MeV) +^{232}Th system is at ~120°, the intensity of these 2α events dominates at the backward angles with respect to the beam direction. The analysis of 8Be breakup explains very well the 2α-particle multiplicity spectra at different laboratory angles. For the first time, a new component corresponding to the transfer-breakup process has been considered in the moving-source model to disentangle the different contributions to the inclusive α-particle multiplicity. Reanalysis of the α-particle multiplicity spectra including five sources in the moving-source model- the compound nucleus, both fission fragments, the NSE, and 8Be breakup, has been carried out.

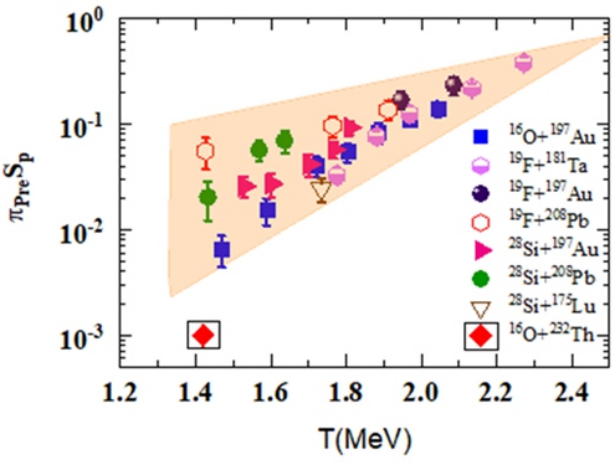

Fig.6: Normalized pre-scission proton multiplicity as a function of compound nucleus temperature.

The results obtained for pre-scission and near-scission multiplicities follow the recently developed heavy-ion systematics very well. The present results clearly indicate a possible extra source of α-particle emission in the α-cluster-projectile-induced fusion-fission reactions. The very presence of this transfer breakup source has been further verified by performing measurements at different beam energies and also using the ^{13}C projectile where α transfer results in ^{9}Be having a high threshold for breakup.

Global Systematics for pre-scission particle emissions

Pre-scission proton and α-particle multiplicity data have been compiled for a wide range of reactions. At first, the α_{pre} data were plotted as a function of compound nucleus temperature, T. The data show an overall increasing trend with increasing T. The α_{pre} at a given temperature deviate from single value and shows large spread. This spread reduces significantly if α_{pre} is normalized by α-particle emission Q-value (Q_α) as shown in the Fig.5. After normalizing α_{pre} with Q_α , one can note from the Fig.5 that cluttering of the data reduces quite significantly and increasing trend with increasing T becomes more robust. It shows that while looking at α_{pre} data globally encompassing a wide range of compound nuclear systems, the Q_α becomes important. In addition to increasing excitation energy and hence the nuclear level density of the residual nucleus, the larger Q_α also indicates about more pre-formation probability of the α-particle. One can note from the Fig.5 that even after correcting for the effects of Q_α, a certain spread in the normalized α_{pre} values at lower temperatures around 1.5 MeV remains. This spread is related to non-equilibrium fission as discussed earlier. Unlike to neutron and α--particle emission, the studies for other particles have been quite limited, primarily owing to their lower multiplicities. Proton-emission is the next candidate (charged particle) after α-particle emission which has been studied to some extent in heavy-ion induced fusion-fission. However, in the case of proton emission the background contribution to the energy spectra is significantly larger than the α-particle and neutron. The primary source of the background protons stems from direct reactions with hydrocarbon impurities deposited on the target during the experiments. Also enhanced random coincidences due to lower multiplicities contribute to the background. Amidst these difficulties, pre-scission proton multiplicity (π_{pre}) data have been reported only for a few number of heavy-ion induced fission reactions as shown in the Fig. 6.

Similar to pre-scission α -particle multiplicity data, the proton multiplicity (π_{pre}) data also exhibit a descent systematic behaviour after normalizing with proton separation energy (Sp) as shown in the Fig. 6. One can note from Fig. 6 that for a given temperature around 1.4 MeV, the π_{pre} value is noticeably smaller than the systematic trend in the case of ^{16}O + ^{232}Th reaction. It again reinforces the presence of pre-equilibrium fission as inferred from α_{pre} data [29].

Summary & Future Outlook

A program to study the fission dynamics using particle emission as a probe is being pursued at BARC-TIFR Pelletron Linac Facility (PLF). Experimental and data analysis techniques are briefly discussed. Recent observations on novel features of fission dynamics and nuclear viscosity are outlined. Further measurements to understand the fission dynamics from different perspectives will be performed at PLF. Specifically, measurements will be performed for different systems to establish the "polar" proton emission in heavy-ion induced fission. Experiments where event rates are quite small such as the measurement of mass gated particle and gamma multiplicities are envisaged. A Versatile Detector Array (VDA) is being developed at PLF to carry out above mentioned experiments.

References

[1] J. Blocki, Y. Boneh, J. R. Nix, J. Randrup, M. Robel, A. J. Sierk, W. J. Swiatecki, Ann. Phys. 113 (1978) 330 .

[2] K. T. R. Davies, A. J. Sierk, J. R. Nix, Phys. Rev. C 13 (1976) 2385.

[3] C. Simenel, A. S. Umar, Phys. Rev. C 89 (2014) 031601

[4] M. Rizea, N. Carjan, Nucl. Phys. A 909 (2013) 50.

[5] A. K. Sinha, D. M. Nadkarni, G. K. Mehta, Pramana J. Phys. 33 (1989) 85.

[6] I. Halpern, Annu. Rev. Nucl. Sci. 21 (1971) 245.

[7] E. Rutherford, A. Wood, Philos. Mag. J. Sci. 31 (1916) 379.

[8] E. Piasecki, L. Nowicki, in: Proc. Symposium, "Physics and Chemistry of Fission", Jülich, 14-18 May 1979, IAEA, Vienna, vol. II, 1980, p. 193.

[9] L. Nowicki, E. Piasecki, J. Sobolewski, A. Kordyasz, M. Kisieliński, W. Czarnacki, H. Karwowski, P. Koczoń, Nucl. Phys. A 375 (1982) 187.

[10] E. Piasecki, M. Dakowski, T. Krogulski, J. Tys, J. Chwaszczewska, Phys. Lett. B 33 (1970) 568.

[11] E. Piasecki, M. Sowiński, L. Nowicki, A. Kordyasz, E. Cieślak, W. Czarnacki, Nucl. Phys. A 255 (1975) 387.

[12] D. Hilscher, D. Rossner, Ann. Phys. Fr. 17 (1992) 471.

[13] Y. K. Gupta, D. C. Biswas, R. K. Choudhury, A. Saxena, B. K. Nayak, B. John, K. Ramachandran, R. G. Thomas, L. S. Danu, B. N. Joshi, K. Mahata, S. K. Pandit, A. Chat-terjee, Phys. Rev. C 84 (2011) 031603.

[14] D. J. Hinde, H. Ogata, M. Tanaka, T. Shimoda, N. Takahashi, A. Shinohara, S. Waka-matsu, K. Katori, H. Okamura, Phys. Rev. C 39 (1989) 2268.

[15] J. P. Lestone, J. R. Leigh, J. O. Newton, D. J. Hinde, J. X. Wei, J. X. Chen, S. Elfström, M. Zielinska-Pfabé, Nucl. Phys. A 559 (1993) 277.

[16] A. Di Nitto, E. Vardaci, G. La Rana, P. N. Nadtochy, G. Prete, Nucl. Phys. A 971 (2018) 21.

[17] S. A. Giuliani, Z. Matheson, W. Nazarewicz, E. Olsen, P. G. Reinhard, J. Sad-hukhan, B. Schuetrumpf, N. Schunck, P. Schwerdtfeger, Rev. Mod. Phys. 91 (2019) 011001.

[18] P. Möller, A. Sierk, Nature 422 (2003) 485.

[19] A. N. Andreyev, K. Nishio, K-H. Schmidt, Rep. Prog. Phys. 81 (2018) 016301.

[20] B. B. Back, H. Esbensen, C. L. Jiang, K. E. Rehm, Rev. Mod. Phys. 86 (2014) 317.

[21] W. J. Swiatecki, Phys. Scr. 24 (1981) 113.

[22] J. Töke, R. Bock, G. X. Dai, A. Gobbi, S. Gralla, K. D. Hildenbrand, J. Kuzminski, W. F. J. Müller, A. Olmi, H. Stelzer, Nucl. Phys. A 440 (1985) 327.

[23] V. S. Ramamurthy, S. S. Kapoor, R. K. Choudhury, A. Saxena, D.M. Nadkarni, A. K. Mohanty, B. K. Nayak, S. V. Sastry, S. Kailas, A. Chatterjee, P. Singh, A. Navin, Phys. Rev. Lett. 65 (1990) 25.

[24] S. Kailas, Phys. Rep. 284 (1997) 381.

[25] R. G. Thomas, R. K. Choudhury, A. K. Mohanty, A. Saxena, S. S. Kapoor, Phys. Rev. C 67 (2003) 041601.

[26] B. P. Ajitkumar, K. M. Varier, B. V. John, A. Saxena, B. K. Nayak, D. C. Biswas, R. G. Thomas, S. Kailas, Phys. Rev. C 77 (2008) 021601.

[27] T. Banerjee, D. J. Hinde, D. Y. Jeung, K. Banerjee, M. Dasgupta, A. C. Berriman, L. T. Bezzina, H. M. Albers, Ch. E. Düllmann, J. Khuyagbaatar, B. Kindler, B. Lommel, E. C. Simpson, C. Sengupta, B. M. A. Swinton-Bland, T. Tanaka, A. Yakushev, K. Eberhardt, C. Mokry, J. Runke, P. Thörle-Pospiech, N. Trautmann, Phys. Rev. C 102 (2020) 024603.

[28] J. Khuyagbaatar, D. J. Hinde, I. P. Carter, M. Dasgupta, Ch. E. Düllmann, M. Evers, D. H. Luong, R. du Rietz, A. Wakhle, E. Williams, A. Yakushev, Phys. Rev. C 91 (2015) 054608.

[29] Y. K. Gupta, G. K. Prajapati, B. V. John, B. N. Joshi, L. S. Danu, S. Dubey, S. Mukhopadhyay, N. Kumar, K. Mahata, K. Ramachandran, A. Jhingan, M. Kumar, N. Deshmukh, A. S. Pradeep, B. K. Nayak, D. C. Biswas, Phys. Lett. B 834 (2022) 137452.

[30] Pawan Singh, Y. K. Gupta, G. K. Prajapati, B. N. Joshi, V. G. Prajapati, N. Sirswal, K. Ramachandran, A. S. Pradeep, V. S. Dagre, M. Kumar, A. Jhingan, N. Deshmukh, B. V. John, B. K. Nayak, D. C. Biswas, R. K. Choudhury Phys. Lett. B 858 (2024) 139014.

[31] Y. K. Gupta, D. C. Biswas, B. John, B. K. Nayak, A. Chatterjee, R. K. Choudhury, Phys. Rev. C 86 (2012) 014615.

[32] K. Ramachandran, A. Chatterjee, A. Navin, K. Mahata, A. Shrivastava, V. Tripathi, S. Kailas, V. Nanal, R. G. Pillay, A. Saxena, R. G. Thomas, S. Kumar, P. K. Sahu, Phys. Rev. C 73 (2006) 064609.

[33] M. Sowiński, M. Lewitowicz, R. Kupczak, A. Jankowski, N. K. Skobelev, S. Chojnacki, Z. Phys. A - At. Nucl. 324 (1986) 87.

[34] L. Schad, H. Ho, G.-Y. Fan, B. Lindl, A. Pfoh, R. Wolski, J. P. Wurm, Z. Phys. A- At. Nucl. 318 (1984) 179.

[35] K. Siwek-Wilczynska, J. Wilczynski, H. K. W. Leegte, R. H. Siemssen, H. W. Wilschut, K. Grotowski, A. Panasiewicz, Z. Sosin, A. Wieloch, Phys. Rev. C 48 (1993) 228.

[36] B. Lindl, A. Brucker, M. Bantel, H. Ho, R. Muffler, L. Schad, M. G. Trauth, J. P. Wurm, Z. Phys. A - At. Nucl. 328 (1987) 85.

[37] A. Saxena, A. Chatterjee, R. K. Choudhury, S. S. Kapoor, D. M. Nadkarni, Phys. Rev. C 49 (1994) 932.

एकल-कण एवं सामूहिक तरीके

12

^{90}Zr के पास नाभिकीय संरचना के रोचक पहलू

आर. पालित
नाभिकीय एवं परमाणु भौतिकी विभाग, टाटा मूलभूत अनुसंधान संस्थान, मुंबई-400005, भारत

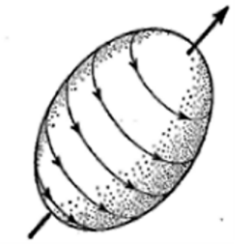

^{89}Zr में सबसे लंबा अक्ष परिभ्रमण

सारांश

एकल कण एवं सामूहिक उत्तेजना विधियों की प्रतिस्पर्धा का अध्ययन करने के लिए A~90 क्षेत्र के आसपास ^{88}Sr, ^{88,89,90,91}Zr, ^{89,90,91,92,93}Nb और ^{92}Mo आइसोटोप की उत्तेजित अवस्थाओं की भारी आयन संलयन प्रतिक्रियाओं का उपयोग करके अन्वेषण किया गया। हमारे माप इन नाभिकों में उच्च स्पिन तक एकल कण उत्तेजनाओं के प्रभुत्व का संकेत देते हैं, जो इस आइसोटोप में निम्न चतुर्ध्रुव सामूहिकता का सुझाव देते हैं। ^{91}Zr में जीवनकाल माप ^{90}Zr कोर की अष्टध्रुव सामूहिक स्थिति के साथ एक कण के युग्मन को मापने के लिए एक त्वरित-समय तकनीक का उपयोग करके किया गया है। ये परिणाम विभिन्न आधुनिक नाभिकीय संरचना मॉडलों के परीक्षण के लिए महत्वपूर्ण हैं। उच्च स्पिन पर ^{89}Zr में एक द्विध्रुवीय पट्टी को सबसे लंबे अक्ष के बारे में नाभिक के परंपरागत रूप से प्रतिकूल घूर्णन के रूप में चिह्नित किया गया है।

Single-particle and Collective Modes

12

Intriguing Aspects of the Nuclear Structure Near ^{90}Zr

R. Palit
Department of Nuclear and Atomic Physics, Tata Institute of Fundamental Research, Mumbai-400005, INDIA

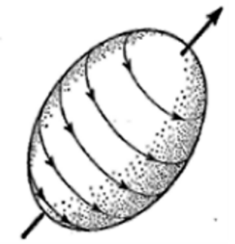

Longest axis rotation in ^{89}Zr

ABSTRACT

Excited states of ^{88}Sr, ^{88,89,90,91}Zr, ^{89,90,91,92,93}Nb and ^{92}Mo isotopes around A ~ 90 region have been investigated using heavy ion fusion reactions to study the competition of single particle and collective excitation modes. Our measurements indicate the dominance of single particle excitations up to high spin in these nuclei, suggesting lower quadrupole collectivity in this isotope. The lifetime measurement in ^{91}Zr has been carried out using a fast-timing technique to measure the coupling of a particle with the octupole collective state of the ^{90}Zr core. These results are crucial for testing various modern nuclear structure models. A dipole band in ^{89}Zr at high spin has been identified as the classically unfavoured rotation of the nucleus about the longest axis.

KEYWORDS: *High spin states, Shell model and Cranked Nilsson-Strutinsky model*

**Author for Correspondence: R. Palit*
E-mail: rpalit@tifr.res.in

Introduction

Nuclear shape is a fundamental property of atomic nuclei that determines the various excitation modes of atomic nuclei. These excitation modes are understood dominantly by single particle and collective motion of nucleons in the nuclei. The competition between these two modes and their coupling generates a wide variety of spectra in nuclei and continues to provide new insights about the atomic nuclei. As described by Bohr and Mottelson [1,2], "The problem of reconciling the simultaneous occurrence of single particle and collective degrees of freedom and exploring the variety of phenomena that arise from their interplay" remains a central theme of nuclear physics. The high-resolution gamma-ray spectroscopy using a large array of High-Purity Germanium (HPGe) detectors at a heavy-ion accelerator continues to play a pivotal role in the study of excited states of nuclei, which unravel a variety of phenomena related to novel shapes and modes of excitation in nuclei. In this context, a 24 Clover HPGe detector array with a total photo-peak detection efficiency of ~5%, named as Indian National Gamma Array (INGA), was conceived, designed and assembled within the country. This facility rotates between the three accelerator centres at TIFR (Mumbai), IUAC (New Delhi) and VECC (Kolkata). INGA is a powerful "femtoscope" for the study of the structure of atomic nuclei at high spins [3,4].

Several experiments have been performed to study the excited states of ^{88}Sr [5], ^{88,89,90,91}Zr [6,7,8,9], ^{89,90,91}Nb [10,11,12] and ^{92}Mo [13] isotopes around the A ~ 90 region at the BARC-TIFR Pelletron Linac Facility (PLF) at TIFR, Mumbai [3]. Some exciting physics results related to single particle and collective excitation around ^{90}Zr from the experimental campaigns are highlighted here. This spectrometer can measure lifetime ranges from hundreds of picoseconds (ps) to microseconds (μs) using fast timing method and Doppler shift attenuation method (DSAM) is used for measuring lifetimes in the sub-ps range. Recently, the INGA has been augmented with a Si-CD detector to study the low-lying octupole collectivity in this region through coulex.

The spin-parity of the gamma transitions are measured using Directional correlation of Oriented states ratio (R_{DCO}) or Angular Distribution of oriented states ratio (R_θ) and polarization methods. The typical values for stretched E1, M,1 and E2 and non-stretched M1, E2 are shown in Fig.1.

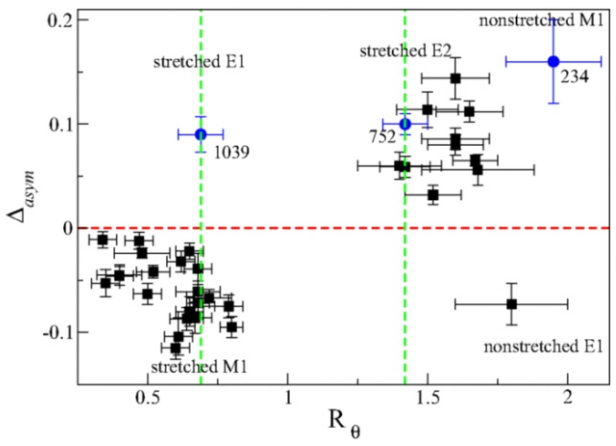

Fig.1: Experimental polarization asymmetry parameter (Δ_{asym}) plotted against R_θ for the trasitions belonging to ^{89}Nb [10].

Selected Results

Many attempts to study the structural features of closed-shell nuclei in different mass regions have been made over the past few decades in recent time. The A ~ 90 region (with Z ~ 40 and N ~ 50) remains one of the cornerstones to study the underlying mechanisms of excitation in atomic nuclei. The excitation of protons and neutrons across their respective shell gaps enables more active orbitals to generate high spin states. Extending SM calculations to higher excitation that incurs a larger model space and increased valence nucleons is now computationally feasible.

A comparison of the experimental excitation energies of the positive-parity states of ^{90}Zr [8] with those from shell-model calculations using the GWBXG effective interaction is shown in Fig.2. The shell-model calculations, with the extended model space including neutron excitations across the N = 50 shell gap, give a good description of both the positive- as well as the negative- parity states up to highest observed excitation energy and spin. This indicates the dominance of single-particle excitations in this nucleus.

The stability of a particular nucleus increases compared to the neighbouring nuclei when the outermost orbital is fully occupied and consequently, the concept of magic numbers emerged in closed-shell nuclei. Spectroscopy of nuclei near closed shells provides essential insight into the competition of these two modes as a function of excitation energy and angular momentum. Another aspect is the coupling of single particle motion with various collective degrees of freedom. In this connection, the lifetime of $11/2^-$ was measured with fast timing method. This results in a B(E3; $11/2^- \rightarrow 5/2^+$) = 18.51 ± 1.23 W.u indicating collective nature of $11/2^-$ state [9].

Investigation of nuclear excitation continues to provide new insight into the evolution of shell structure and its impact on nuclear shapes across the nuclear landscape. Different types of nuclear shapes can be seen depending on the number of valence particles in the active orbitals. In this context, the level scheme of ^{89}Zr has been extended up to spin I=49/2 with the observation of a new dipole band (Fig.3). Line shapes of several transitions have been analyzed to determine lifetimes of the levels. Possible configurations of the band have been discussed using the cranked Nilsson-Strutinsky model (CNS). The calculations suggest a triaxial shape of the nucleus at high spins, and the band may represent the rotation of the nucleus about the longest axis [14].

Another interesting aspect of the high-spin region of the nuclei in mass 90 region is the investigation of the tensor component of nucleon-nucleon (NN) interaction between valence proton(s) in the $1g_{9/2}$ orbital and the excited neutron in the orbitals above the N = 50 shell gap. For describing the generation of the states in band II in ^{91}Nb [12], configurations can be compared to those of band II and band III in ^{90}Zr [8]. In these two N = 50 isotones, one neutron in $1g_{9/2}$ gets excited across this neutron major shell gap. However, the applied truncation conditions are different for these two nuclei. In the calculation reported in Ref. [8], a maximum of one neutron

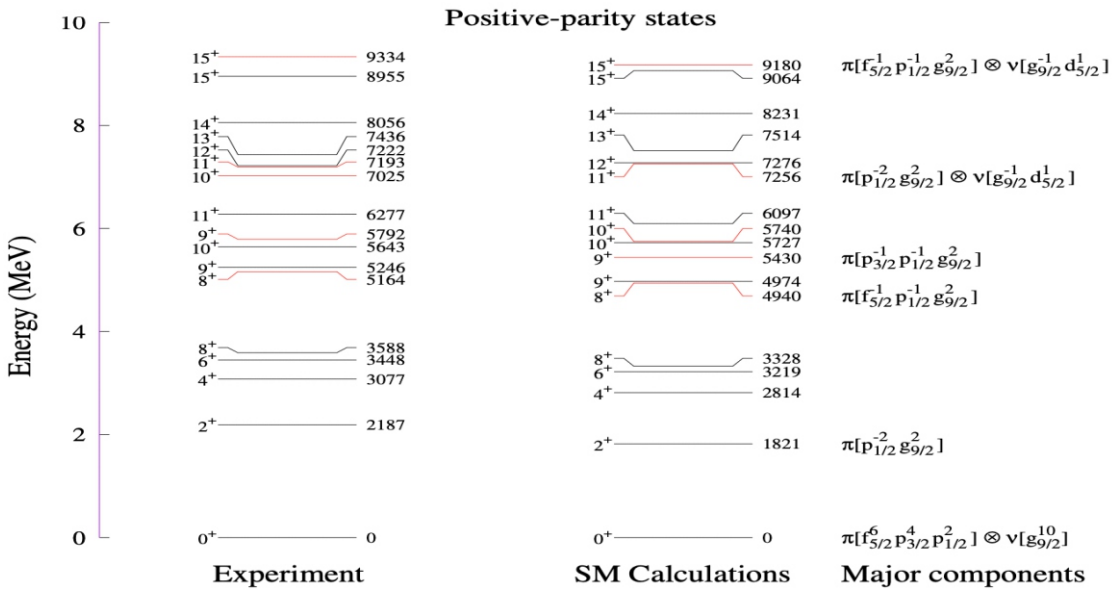

Fig.3: Comparison of experimental levels and shell model calculated levels using GWBXG interaction for positive parity states in ^{90}Zr [8].

excitation each in $2d_{5/2}$ and $3s_{1/2}$ is allowed. The calculations provide a reasonable description for the experimentally observed levels, and the average energy difference between them is ≈200 keV for neutron-core excited states [12]. If the neutron $1g_{7/2}$ orbital is made available for the excited neutron to occupy, as mentioned here, the average energy difference increases to ≈300 keV. This indicates the previous calculations [8] involving excitation in the $\nu[2d_{5/2}]$ orbital work better with no significant contribution from them $\nu[1g_{7/2}]$ orbital, as its role is not crucial for generating states up to the highest observed spin-parity in ^{90}Zr. On the other hand, for ^{91}Nb [12], including the neutron $1g_{7/2}$ orbital improves the agreement between experimentally observed and theoretically calculated energy states. One possible reason for the change in high-spin configurations moving from ^{90}Zr to ^{91}Nb could be the presence of one valence proton in the $\pi[1g_{9/2}]$ orbital [12]. This suggests the possible manifestation of the tensor force between the proton in $1g_{9/2}$ and neutron in $1g_{7/2}$ orbitals, which has an attractive interaction between them. This attractive nature would eventually lower the energy of the neutron-core excited levels. This effect can further be studied by probing the high-spin structures in the heavier N = 50 isotones with increasing number of protons in the $1g_{9/2}$ orbital.

The level scheme of ^{90}Nb and ^{92}Mo was investigated with ^{30}Si + ^{65}Cu fusion-evaporation reaction [11,13]. A comparison of the shell-model predicted levels with experimental data suggests that high-spin states in ^{90}Nb do not involve neutron excitation across the N = 50 shell gap [11]. At high spin, the shell model (SM) calculations fail to reproduce the correct

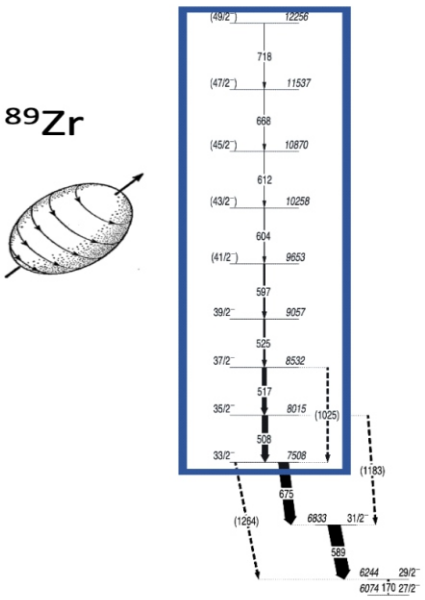

Fig.4: Partial level scheme of ^{89}Zr showing a regular structure of M1 transitions above $I^{\pi} = 29/2^-$ [13].

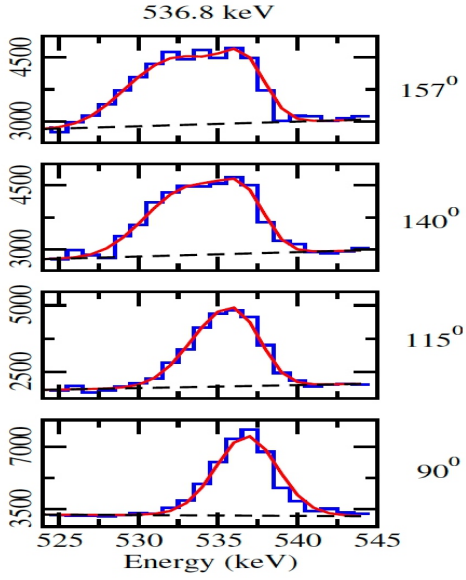

Fig.4: Spectra generated using a gate on 244.0 keV transition along with the simulated lineshape in different angles for few ΔI = 1 transitions in ^{92}Mo [13].

energies of the experimental levels for ^{90}Nb. In contrast, for odd-even nucleus, ^{91}Nb, a good agreement is observed between SM and experimental levels [12], describing the structure of odd-odd nuclei remains particularly challenging. A new transition E3 transition, decaying from 11^- to 8^+ was found out. The B(E3) value of this transition was determined to be 0.020(4) W.u., indicating the suppression of collective motion in ^{90}Nb [11]. In the case of ^{92}Mo, the high-spin states primarily originate from the coupling of proton and neutron-core structures in an almost stretched manner. Other fusion-evaporation reaction, ^{18}O + ^{80}Se was used for measuring the lifetimes of ΔI = 1 sequence in ^{92}Mo. The lifetime of few states of high-spin ΔI = 1 sequence was measured using DSAM (Fig.4) [13]. A relatively large B(E1) of 1075.1 keV transition was interpretated as the mutual enhancement of proton and neutron excitation [13].

Another interesting aspect in 90 mass region is the observation of decreasing transition energy with increasing spin in a ΔI = 1 band of ^{88}Sr. The extracted transition strengths from the measured lifetimes initially increase with spin and then decrease beyond $I^{\pi} = 10^-$. The observed gamma- ray energy behaviour and that of transition rates were explained using a novel stretched coupling scheme. In this geometrical model, an interplay between a particle-particle attractive shears and two particle-hole repulsive shears has been invoked to explain the observed behaviour. This confirms the existence of an attractive shears between two particle blades for the first time in any nuclei [5].

In these aforementioned studies, a number of heavy-ion induced fusion reactions are used. Most of the cases, the nucleus does not develop a well-deformed band structure even at high excitation energy. It is also rather surprising that, although the expected angular momentum imparted classically in the heavy-ion fusion evaporation reactions [5,6,7,8,10] used in TIFR recently being ~ 40 - 60 ħ, we were not able to observe any further excited states. This could possibly indicate a large change in structure of this nucleus at high-spin which may involve a highly fragmented decay path consisting of several weak high-energy gamma rays. This suggests a complex fragmentation of the level scheme at high spin and poses experimental challenge for the identification of exotic shapes at high spin.

Conclusion and future scope

Selected results from the gamma-ray spectroscopy carried out at PLF have been discussed. High spin spectroscopy studies were carried out to develop the level schemes of ^{88}Sr, ^{88,89,90,91}Zr, ^{89,90,91,92,93}Nb and ^{92}Mo isotopes around A ~ 90 region. The lifetime of 11/2- in ^{91}Zr was measured using a fast timing method. The measured B(E3) strength for $11/2^- \rightarrow 5/2^+$ transition established octupole collectivity in ^{91}Zr. In ^{92}Mo lifetime of few high-spin ΔI = 1 transitions are measurement using DSAM. The lifetime measurements are the stingiest test to the theoretical models. The deviations of the shell model predictions from the experimental data suggest the scope for improving the shell model calculations. The involvement of neutron particle in $1g_{7/2}$ orbital hints towards the tensor force between $\pi[g^{9/2}]$ and $\nu[1g_{7/2}]$. A systematic study in N = 50 isotones is required to understand this observation. A comparison of the experimental energy levels of the dipole band consisting of ΔI = 1 M1 transitions with CNS calculation suggests a triaxial shape of ^{89}Zr and represents the nuclear rotation along the long axis. The enhancement of M1 transition rates may be due to tilted-axis rotation. The level schemes of nuclei in 90 mass regions populated using fusion-evaporation are extended up to spin 20 - 25 ħ; however, classically, it should be more. The CNS calculation for ^{90}Zr suggests shape evolution towards the Jacobi shape transition above I = 30 ħ. These studies will be possible with a ^{50}Ti beam at 200 MeV from the upgraded PLF. Such heavy beams will be also useful for coulomb excitation studies to probe the low-lying collectivity in nuclei near ^{90}Zr.

Acknowledgements

The author would like to acknowledge the INGA collaborators for the success of the experiments. The author acknowledges the contributions of Dr. S. Saha, Dr. P. Singh, Dr. P. Dey, Dr. B. Das, and Mr. Vishal Malik are acknowledged. The author thanks Prof. P. C. Srivastava, Prof. E. Ideguchi, Prof. T. Inakura, and Prof. S. Nag for the theoretical calculations. This work was partially funded by the Department of Atomic Energy, Government of India (Project Identification No. RTI 4002) and the Department of Science and Technology, Government of India (No. IR/S2/PF-03/2003-II). The author also thanks the Pelletron LINAC Facility staff for providing excellent beams during all experimental campaigns.

References

[1] A. Bohr and B. R. Mottleson, Nuclear Structure Vol 2 (Bejamin, New York 1975).

[2] T. Ostuka *et al*., Web of Conf. 178, 02003 (2018).

[3] R. Palit *et al*. The EPJ A 61 (4), 1-36 (2025).

[4] R. Palit *et al*., Nucl. Instr. Meth. Phys. Res. A 680, 90 (2012).

[5] B. Das *et al*., Phys. Lett. B 862, 139324 (2025).

[6] S. Saha *et al*., Phys. Rev. C 89,044315 (2014).

[7] S. Saha *et al*., Phys. Rev. C 86,034315 (2012).

[8] P. Dey *et al*., Phys. Rev. C 105, 044307 (2022).

[9] P. Dey *et al*., Nucl.Phys.A,1057, 123035 (2025).

[10] P. Singh *et al*., Phys. Rev. C 90, 014306 (2014).

[11] Vishal Malik *et al*., Phys. Rev. C. 111, 024323 (2025).

[12] P. Dey *et al*. Phys. Rev. C. 109, 034313 (2024).

[13] Vishal Malik *et al*., Journal of Physics G: Nuclear and Particle Physics, 52 025101 (2025).

[14] S. Saha *et al*., Phys. Rev. C 99, 054301 (2019).

पीएलएफ में हाइब्रिड आईएनजीए के साथ नाभिकीय समावयवी

13

नाभिकीय समावयवी और अनुप्रयोग

आर. पालित
नाभिकीय एवं परमाणु भौतिकी विभाग, टाटा मूलभूत अनुसंधान संस्थान, मुंबई-400005, भारत

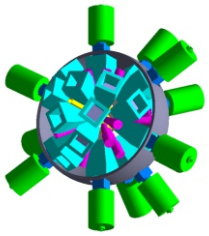

समावयवी स्पेक्ट्रमिकी के लिए हाइब्रिड आईएनजीए

सारांश

भापअ केंद्र-टीआईएफआर पेलेट्रॉन लीनॉक सुविधा (पीएलएफ) में नाभिकीय समावयवी के हाल के अन्वेषण का एक प्रेक्षण यहां प्रस्तुत किया गया है। नाभिकीय संरचना मॉडल की पूर्वानुमान शक्तियों के परीक्षण के लिए सममितीय अवस्थाओं के स्तर जीवनकाल और विद्युत चुम्बकीय क्षणों का माप महत्वपूर्ण है। $N = 82$ कवच अंतराल के पास समावयवी स्पेक्ट्रोमिकी के माप से चयनित परिणाम प्रस्तुत किए जाते हैं। इसके अलावा, ^{108}Ag में एक दीर्घकाल रहने वाले समावयवी के आसपास निम्न स्तर की स्थितियों के स्पेक्ट्रोमिकी माप के परिणामों की चर्चा निम्न स्तर की स्थितियों के माध्यम से प्रेरित समावयवी की कमी के संदर्भ में की जाती है। त्वरकों का उपयोग करके समावयवी स्पेक्ट्रमिकी में अनुसंधान के भविष्य की दिशा पर चर्चा की जाएगी।

Nuclear Isomers with Hybrid INGA at PLF

13

Nuclear Isomers and Applications

R. Palit
Department of Nuclear and Atomic Physics, Tata Institute of Fundamental Research, Mumbai-400005, INDIA

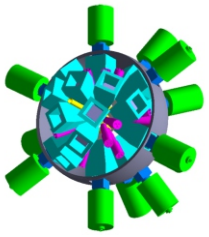

Hybrid INGA for Isomer Spectroscopy

ABSTRACT

An overview of the recent investigations of nuclear isomers at the BARC-TIFR Pelletron Linac Facility (PLF) is presented here. The measurements of level lifetimes and electromagnetic moments of the isomeric states are crucial for testing the predictive powers of nuclear structure models. Selected results from measurement of isomer spectroscopy near N=82 shell gap are presented. In addition, the results of spectroscopic measurements of low-lying states around a long-lived isomer in ^{108}Ag are discussed in the context of induced isomer depletion through the low-lying states. The future direction of research in isomer spectroscopy using the accelerators will be discussed.

KEYWORDS: *Nuclear Isomers, Lifetime measurements and electromagnetic moments*

**Author for Correspondence: R. Palit*
E-mail: rpalit@tifr.res.in

Introduction

Nuclear isomers were discovered by German Chemist Otto Hahn in 1921. The discovery of nuclear isomers by Hahn marked the birth of the field of nuclear structure. Isomers have fundamental importance in nuclear structure physics [1]. An isomer is a metastable state of a nucleus with a lifetime greater than 1 ns, caused by the hindrance of the decay process back to lower excited states. There are three main reasons for this hindrance. The first is the difference in the structural wave functions between the initial and final states. The other two reasons are the small decay energy and the significant change in angular momentum. Isomers can be classified based on the hindrance mechanisms affecting their decays. In spherical regions, they are categorized as spin and seniority isomers. In deformed regions, they are classified as shape, K, and fission isomers [1,2]. Nuclear isomers are produced within the same nucleus (N, Z) due to the different arrangement of nucleons. Isomers are crucial in basic nuclear structure studies, nuclear astrophysics, and energy storage in isomeric states. These isomeric states play an important role in testing the predictions of shell and collective models for nuclear structure. Using discrete gamma-ray spectroscopy, the excited levels of nuclei can be studied through different nuclear reactions. Nuclear moments are very sensitive probes that help us understand the detailed composition of the nuclear wave function.

This article will discuss the available experimental facilities for studying nuclear isomers at PLF and the selected results from isomer spectroscopy. We will also describe the scope of future research on this topic at PLF.

Experimental Facilities for Studying Isomers

Two experimental setups are used to investigate nuclear isomers. The first is for gamma-ray spectroscopy using a hybrid array of Compton-suppressed clover HPGe detectors coupled with $LaBr_3$(Ce) scintillator detectors. The other is for the time differential perturbed angular distribution (TDPAD) measurement. Brief descriptions of the setups and experimental results are given below.

Hybrid INGA for isomer spectroscopy

The gamma detector array at BARC-TIFR, PLF in TIFR can accommodate 24 Compton-suppressed HPGe clover detectors and 18 $LaBr_3$(Ce)/$CeBr_3$(Ce) detectors for fast timing measurements [3,4]. The Digital Data Acquisition system has been upgraded recently to a root-based multi-threaded software named TIFR Digital Data Acquisition Software for Nuclear Structure Studies (TIDES)" developed at TIFR to control and acquire data from PIXIE16 DGF from XIA for the hybrid configuration of 100 MHz for clovers coupled with 250 MHz or 500 MHz digitizers for different type of ancillary detectors with slow and fast signals. This hybrid spectrometer can perform lifetime measurements of excited nuclear states in the 50 ps to 2 microsec range to extract information on nuclear structure and isomers.

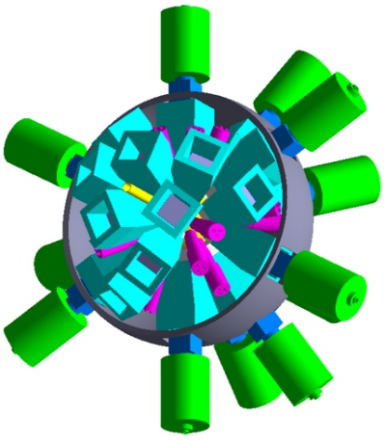

Fig.1: Schematic diagram of the hybrid INGA at PLF.

TDPAD setup at PLF and g-factor measurements

The g-factors of isomeric states were measured using the TDPAD method at the PLF facility. A split-coil superconducting magnet from American Magnetics, Inc. (AMI), capable of generating up to 7 T magnetic fields with 0.1% stability and 0.5% uniformity over a 1 cm diameter spherical volume, was used for magnetic moment measurements. The experiment employed a pulsed beam with 1 ns pulse width and 800 ns separation between pulses. Delayed γ-rays from the isomers were detected by four HPGe detectors positioned at $\pm 45^{0}$ and $\pm 135^{0}$ relative to the beam, 11 cm from the target. The detectors had a time resolution of ~5 ns (FWHM) for the 1173- and 1332-keV γ-rays from a ^{60}Co source. A time-to-amplitude converter (TAC) was started by the HPGe detector's time signal and stopped by the RF signal. Data were collected in LIST mode for energy and time signals from the four detectors, and two-dimensional energy vs. time spectra were constructed. Time difference spectra for γ-rays decaying from isomeric states were generated, and normalized counts N(θ, t) were used to create spin rotation spectra.

Selected Results

Several experiments have been conducted to study isomer spectroscopy across the nuclear landscape. This article highlights some physics results from these experiments related to testing nuclear shell model predictions and the depletion of long-lived isomers.

Our research focuses on nuclei near the N = 82 shell gap, gaining significant experimental and theoretical attention. In the Z > 50 transitional nuclei around A ≈ 135, for N < 82, a rich

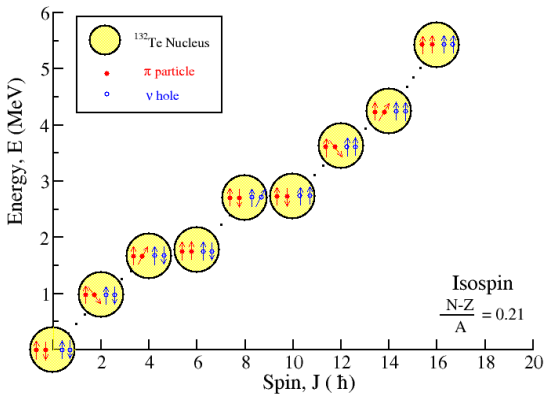

Fig.2: A schematic picture showing the alignment of the two proton particles in $g_{7/2}$ orbital and two neutron holes in $h_{11/2}$ orbital as a function of Spin(J) and Energy(E) in ^{132}Te (see Ref. [5]).

and complex level structure emerges due to the interplay of single-particle and collective excitation modes.

One crucial question is: How do we understand the competition of neutrons and protons in forming the high-spin states near the doubly magic ^{132}Sn? With the two proton particles and two neutron holes, the ^{132}Te is an interesting isotope near the doubly magic nucleus ^{132}Sn for studying the competition of protons and neutrons in forming sequences of high-spin states. Our experimental study provides new information on the *nn, pp* and *pn* interactions used in the shell model calculations to describe the level scheme of ^{132}Te. The states till 6^+ arise mainly due to the alignment of proton particles in the $g_{7/2}$ orbital, and the 8^+ and 10^+ states are due to the alignment of neutron holes in the $h_{11/2}$ orbital. In the present work, higher spin states above the 10^+ isomer have been observed, and these states arise because of the simultaneous alignment of protons and neutrons. The prompt-delayed coincident data from INGA complements the fragment-gated gamma spectroscopy data from EXOGAM-VAMOS++ and makes a firm assignment of the placement of various transitions in the level scheme of ^{132}Te with long-lived isomers [5]. Large-scale shell model calculations using the existing jj55pna interaction can predict the low-spin states, but deficiencies remain in the high-spin states. A similar study has been conducted for ^{66}Cu using a multi-nucleon transfer reaction [6].

The study of isomers in transitional nuclei around the A ≈ 135 region, which can be studied using low-energy stable beam accelerators, is particularly interesting due to the nuclear structure's evolution from spherical to deformed shapes as it moves away from the shell gap. These transitional nuclei between spherical and deformed regions present a significant challenge to nuclear models, particularly in studying high-spin structures. Experimental studies of nuclei near closed shells are ideal for testing evolving shell model predictions based on effective interactions, as well as projected shell model calculations. With recent advances in large-scale shell model (LSSM) calculations near A ≈ 130, it is now possible to study both transitional and closed-shell nuclei using the same effective interactions. The occupation of high-j orbitals by protons and neutrons leads to various structural phenomena, such as magnetic and chiral rotations, wobbling motion, and high-spin isomers. Many high-spin isomers with simple multi-quasiparticle configurations have been reported in this region, especially in nuclei near the N = 82 shell closure.

Lanthanum isotopes contain numerous low- and high-spin isomers, offering insights into nuclear structure changes as they approach the N = 82 shell gap. Experiments at the Pelletron Linac Facility (PLF) at TIFR, Mumbai, have investigated these isomers, while RCNP, Osaka University, has studied ^{135}La and ^{136}La using a Nitrogen-17 radioactive beam. The Z = 57 lanthanum isotopes are enriched with many low- and high-spin isomers. These isomers provide useful insight into the evolution of the nuclear structure of the lanthanum isotopes as we move toward the N = 82 shell closure. Recently, a longitudinal wobbling band has been found in ^{133}La, feeding the $11/2^-$ isomeric state in ^{133}La [9, 18]. The measurement of the nuclear moment of the $11/2^-$ isomeric state is needed to understand the structure of ^{133}La. The $11/2^-$ isomeric state at 535 keV in ^{133}La was studied using the reaction ^{126}Te(^{11}B, 4n)^{133}La at 52 MeV, with results reported by Laskar *et al*. The ^{126}Te target created a non-zero electric field gradient (EFG), causing the ^{133}La nuclei to experience both magnetic dipole and electric quadrupole interactions. The lifetime of the $11/2^-$ isomer was measured as 68.01 ± 0.41 ns, consistent with previous values. The spin-rotation spectrum indicated a strong damping due to perturbations, with extracted values of ω_L = 111.4 ± 6.7 Mrad/s and ω_Q = 8.0 ± 1.0 Mrad/s. For these, the g-factor was determined to be 1.16 ± 0.07, close to the value estimated for pure magnetic interaction (1.19 ± 0.06). The spectroscopic quadrupole moment was found to be 1.71 ± 0.34 b.

The level energy of the $11/2^-$ isomers in odd mass La nuclei increases, and the half lifetime decreases monotonically from ^{125}La to ^{139}La. The $11/2^-$ level is largely $h_{11/2}$ proton-dependent configuration. The results from LSSM calculations for the spectroscopic quadrupole moments and g-factors of these states in odd-A La isotopes are presented in Table 2 of Ref [6]. The quadrupole moment of ^{139}La (N = 82) was found to be relatively small. However, the quadrupole moment increases gradually as the neutron number decreases, indicating increased quadrupole collectivity. The LSSM quadrupole moment of ^{133}La was obtained as 1.25 b compared to the experimental value of 1.71 ± 0.34 b. On the other hand,

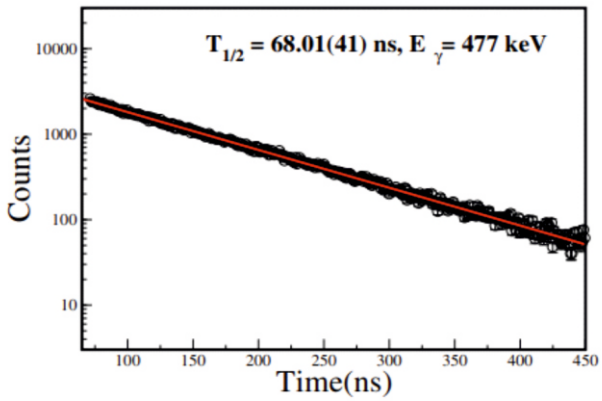

Fig.3: Decay curve for the 477 keV gamma-ray emitted from $11/2^-$ isomer in ^{133}La (adopted from Ref.[7]).

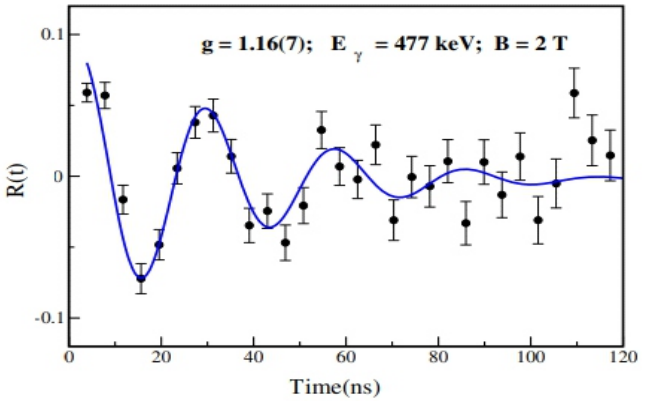

Fig.4: Spin rotation spectrum at B_{ext} = 2 T for the $11/2^-$ isomeric state of ^{133}La (Ref 7).

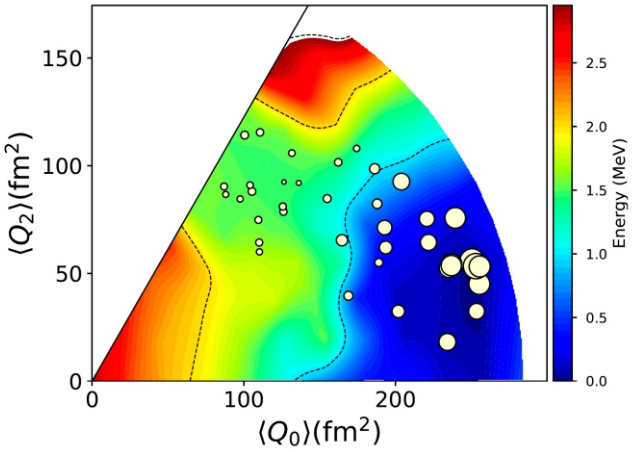

Fig.5: The T-plot for the 11/2⁻ state in ^{133}La. The locations of the circles indicate the intrinsic shape of the MCSM basis states. (Ref 7].

the g-factors of the isotopes instead show a constancy indicative of a proton $h_{11/2}$ configuration-based structure. To discuss the intrinsic shape of the 11/2⁻ state of ^{133}La in terms of the shell-model framework, Laskar *et al.* [7] presented the energy surface and the T-plot of the Monte Carlo shell model (MCSM) calculations. The published figure is reproduced in Fig.5. The contour lines represent the energy surface obtained by the quadrupole-constrained Hartree-Fock method utilizing the same shell-model Hamiltonian. The prolate minimum with modest triaxiality at Q_0 = 260 fm^2 is retrieved from the potential energy surfaces, corresponding to the deformation parameter β = 0.16. The LSSM provides the β value of 0.19, assuming K = 1/2. In another study, the *g* factor of an isomeric state at 2738 keV in ^{135}La was measured using the TDPAD technique. The measured g-factor of the high spin isomer, along with the LSSM calculations, was used to assign the configuration of the isomer in particular and then describe the level scheme of ^{135}La [8].

The nuclear isomers have the potential to provide material with the highest energy storage capacity with controlled release of its energy on demand. Spectroscopic measurement of the excited states around these isomers has become a topic of immense importance due to its crucial role in estimating the depletion pathway of the isomer and the concerned rate. The ^{108}Ag nucleus has been a subject of investigation for the study of isomer depletion due to the presence of a long-lived isomer with $T_{1/2}$ = 438 years at low spin and high production of this isomer through (n, gamma) cross-section using stable ^{107}Ag isotope. We have recently identified three possible transitions at energies below 500 keV from the isomer to the higher excited levels, whose subsequent decay can branch to the ground state in ^{108}Ag [9]. Our measurement will help improve the cross-section estimation for induced isomer depletion via these states. Recent developments on isomer depletion related to energy storage are described in Ref. [11].

Conclusion and Future Scope

Selected results from isomer spectroscopy carried out at PLF have been discussed. Prompt-delayed spectroscopy was carried out to develop the level schemes of neutron-rich ^{66}Cu and ^{132}Te isotopes. In the case of odd-A La isotopes, the g-factor of the isomeric states is discussed. These experimental results provide an excellent testing ground for the predictions of the modern shell model calculations. The deviations of the shell model predictions from the experimental data suggest the scope for improving the shell model calculations. A new configuration of high-efficiency gamma-ray detectors coupled with different ancillary systems, namely $LaBr_3$(Ce)/$CeBr_3$(Ce) detectors, active BGO collimators and CsI(Tl)/Si detectors, is proposed at PLF [10]. It aims to exploit the broad types of accelerated ions and beam pulsing systems available at the accelerator facility. Our main objectives are to investigate the coupling of single particles with collective vibrational modes, exotic modes of nuclei, rare decay modes of nuclei, nuclear isomers, reaction dynamics and applications of isomers in applied research.

Acknowledgements

The author would like to acknowledge the INGA collaborators for the success of the experiments. The author acknowledges the contributions of Dr Md. S. R. Laskar, Dr. S. Biswas, Dr J. Sethi, Dr. P. Singh and Prof. S.N. Mishra are acknowledged. The author thanks Prof. N Simuzu and Prof. Y. Utsuno for the calculations on the La isotopes. This work was partially funded by the Department of Atomic Energy, Government of India (Project Identification No. RTI 4002) and the Department of Science and Technology, Government of India (No. IR/S2/PF-03/2003-II). The author also thanks the Pelletron LINAC Facility staff for providing excellent beams during all experimental campaigns.

References

[1] P.M. Walker, G. Dracoulis, Nature 399, 6731 (1999).

[2] R. Palit et al., EPJST 233, 933 (2024).

[3] R. Palit et al., Nucl. Instr. Meth. Phys. Res. A 680, 90 (2012).

[4] Md S R Laskar et al., Phys.Rev. C 104, L011301 (2021).

[5] S. Biswas et al., Phys.Rev. C 93, 034324 (2016).

[6] P. Singh et al., Eur. Phys. J. A 53, 69 (2017).

[7] Md S R Laskar et al., Phys. Rev. C 101, 034315 (2020).

[8] Md S R Laskar et al., Phys. Rev. C 99, 014308 (2019).

[9] J. Sethi et al. J.Phys.(London) G43, 015103 (2016).

[10] B. Das et al., Nucl. Instr. Meth. Phys. Res. A 1060, 169030 (2024).

[11] J.J. Carroll et al., EPJST 233, 1151 (2024).

उच्च आवेशित आयन किरणपुंजों का उपयोग करते हुए आयन-परमाणु टकराव

14

N_2O के आयनीकरण प्रेरित विघटन गतिकी

एच. सिंह, जे. मुखर्जी, के. कुमार, मो. ए.के.ए. सिद्दीकी, एम. दास, और. डी. मिश्रा
टाटा मूलभूत अनुसंधान संस्थान, होमी भाभा रोड, मुंबई-400005, भारत

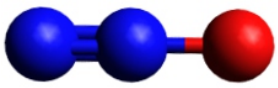

की आण्विक संरचना।

सारांश

उच्च वेग व्यवस्था ($v > 1$ a.u.) में N_2O के आयनीकरण प्रेरित क्षय गतिकी का अध्ययन करने के लिए एक नया COLTRIMS (कोल्ड टारगेट रिकॉइल आयन मोमेंटम स्पेक्ट्रोमीटर) विकसित किया गया। यह प्रयोग 30 MeV पर F^{9+} आयन किरण का उपयोग करके किया गया। N_2O परा-ध्वनिक गैस जेट के साथ अंतःक्रिया पर, ZN_2O का बहु-गुना आयनीकरण होता है। यह कुलम्ब विस्फोट के कारण अणु के वियोजन की ओर ले जाता है। वियोजन चैनल $N_2O^{3+} N^+ + N^+ O^+$ विश्लेषण किया और गतिज ऊर्जा निस्सरण (KER) वितरण की गणना की गई। खंडों के बीच गति संबंध का भी अध्ययन किया गया है। तब गतिशीलता की तुलना कम वेग ($v < 1$ a.u.) पर पहले से मौजूद डेटा ईसीआरआईए (इलेक्ट्रॉन साइक्लोट्रॉन अनुनाद आयन त्वरक) से की गई और यह समझने की कोशिश की गई कि अणुओं के वियोजन गतिकी में प्रक्षेप्य के वेग की भूमिका क्या रहती है। एक प्रतिक्रिया सूक्ष्मदर्शी भी अभिकल्पित की गई।

Ion–Atom Collisions Using Highly Charged Ion Beams

14

Ionization Induced Dissociation Dynamics of N_2O

H. Singh*, J. Mukherjee*, K. Kumar , Md. A.K.A. Siddiki, M. Das, and D. Misra*
Tata Institute of Fundamental Research, Homi Bhabha Road, Mumbai-400005, INDIA

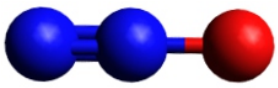

Molecular Structure of N_2O

ABSTRACT

We have developed a new COLTRIMS (Cold Target Recoil Ion Momentum Spectrometer) to study the ionization induced decay dynamics of N_2O in the high velocity regime ($v > 1$ a.u.). The experiment was performed using F^{9+} ion beam at 30 MeV. On interaction with the N_2O supersonic gas jet, multi-fold ionization of N_2O takes place. This leads to the dissociation of the molecule due to the coulomb explosion. We have analysed the dissociation channel $N_2O^{3+} \rightarrow N^+ + N^+ + O^+$ and calculated the Kinetic Energy Release (KER) distribution. Momentum correlation between the fragments has also been studied. We have then compared the dynamics with the already existing data at low velocity ($v < 1$ au.) from the ECRIA (Electron Cyclotron Resonance Ion Accelerator) and tried to understand how velocity of projectile plays a role in the dissociation dynamics of molecules. We have also designed a reaction microscope.

KEYWORDS: *COLTRIMS, Ion beam, Coulomb ionization, Kinetic energy release, Dissociation dynamics*

**Authors for Correspondence: H. Singh, J. Mukherjee, and D. Misra*
E-mail: harpreet.singh@tifr.res.in, jibak.mukherjee@tifr.res.in, and dmisra@tifr.res.in

Introduction

The ionization of atoms or molecules using Highly charged ions (HCI) is of importance for fundamental research as well as their applications in molecular physics and biology to study radiation-induced damage. In molecules, the complexity increases being a many-body system. On interaction with the highly charged projectile, elastic and inelastic processes can take place such as electron capture, transfer excitation, ionization, etc. In the high-velocity regime (v > 1 a.u.) Ionization dominates compared to other processes [1]. In atoms, interaction with HCI may lead to excitation or electron removal from outer shells or core shells. In the case of core-shell excitation or ionization, the atom relaxes either by radiative decay or auger decay. In the case of molecules, the ionization usually leads to dissociation due to Coulomb repulsion.

However, in the case of polyatomic molecules, after interaction we may get multiply ionized molecular ions which are rather unstable and tend to dissociate into constituent ions due to the Coulomb force coming into action (Coulomb Explosion). There can be many dissociation pathways such as two-body, three body etc. All the bonds can break simultaneously (concerted decay) or they can break sequentially (Sequential Decay). The interaction time scale is of the order of a hundred attoseconds which is small compared to the rotational and vibrational timescale due to which the nuclear motion freezes during the interaction. This leads to the excitation of the molecule in the Frank Cordon region. Also, since the axial-recoil approximation is valid, one can obtain the angular distributions of the fragment ions.

Experimental Setup

The experiment employed a novel momentum imaging technique known as COLTRIMS (Cold Target Recoil Ion Momentum Spectroscopy) [2]. F^{9+} ion projectile beam was provided by the PELLETRON-LINAC FACILITY at 30 MeV energy (v = 7.98 a.u.) The projectile beam was made to interact orthogonally with the supersonically cooled target jet of N_2O gas. The jet was produced by the isentropic expansion of gas through a 30 µm into the source chamber. The center portion of the jet is extracted with the help of a 400 µm skimmer in the skimmer chamber and further collimated with a 500 µm skimmer. The pressure in the main chamber at the time of the experiment was of the order of 10^{-7} mbar. After the interaction the ionized molecular ion fragments and the recoil ions are detected with the help of two-stage Wiley-McLaren type spectrometer [3]. The schematic of COLTRIMS is shown in Fig.1(a) and the actual image of the setup is shown in Fig. 1(b). The length of the extraction, acceleration and drift region are 15mm, 90mm and 520mm respectively. The field in the extraction and acceleration region was set to 173.33 and 250.67 V/cm, respectively which ensures 4π sr collection efficiency for singly charged ion with energy up to 13 eV. After the drift region the recoil ions are detected with the help of a position sensitive MCP (Micro Channel Plate-DLD (Delay Line Anode) detector.

The electron produced from the ionization of the molecules is detected with the help a CEM (Channel Electron Multiplier) which gives the start signal and the last recoil ion coming from the fragmentation gives the stop signal to complete the detection of all ions produced in a single event. Despite that, ions from other events may also come. To filter that out we have a momentum sum gate of about 15 a.u. as all the ions produced in a single event will follow momentum conservation. The momentum for the recoil ions can be calculated from the hit position x, y and the time of flight T. CoboldPC Software was used for the data acquisition and each event information is stored in a lmf (list mode file) format which can be later used for offline analysis.

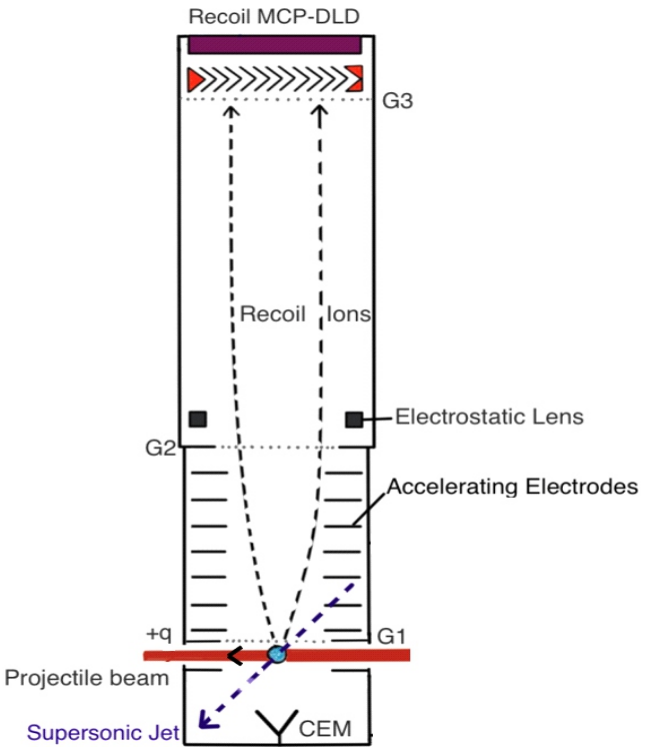

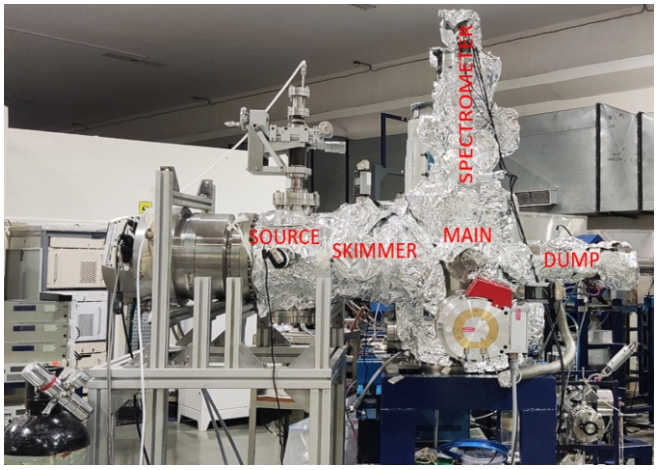

Fig.1: COLTRIMS (Cold Target recoil ion momentum spectrometer) (a) Schematic (b) Actual image of the Setup.

Results

TOF (Time of Flight) Spectrum

Time of flight spectrum in Fig.2 shows the various recoil ions recorded by the detector. This TOF corresponds to the first ion in the event recorded. We can see some prominent peaks such as N_2O^+, N^+_2, N^+, O^+ and, NO^+ which are characteristic of the target N_2O. Except for N_2O^+ all other ions are coming due to the Coulomb explosion of the parent ion. The time of flight separates each ion on the basis of the m/q ratio. There can be many possible channels of dissociation for two-body or three body dissociation depending on the charge state of the molecular ion. To filter out a particular channel of interest we plot the TOF coincidence maps which are Time of flight of first ion vs second ion and Time of flight of second ion vs third ion. We then select the region corresponding to channel of our interest which filters the ions coming from the single event.

KER (Kinetic Energy Release)

From the momentum we can calculate the KER which is the sum of the Kinetic energies of all the fragments. We have compared the KER for the two different projectile: F^{9+} at v = 7.98 a.u from the PLF and Ar^{8+} at v = 0.44 a.u from ECRIA. The KER peaks at 23 and 24 eV for F^{9+} and Ar^{8+}, respectively which is similar. From the KER we also get an idea about the states being populated as it is difference between the frank-cordon excitation point and the dissociation limit. High velocity projectile on interaction may lead to more population in the higher excited states thereby giving more intensity for higher KER values. This is slightly visible in KER range (30-40 eV) in Fig.2.

Comparison

We have done the analysis for Ar^{8+} at v = 0.44 a.u from ECRIA with the same target gas N_2O and tried to compare the two results. The results only differ in the statistics as the effective data obtained in case of Pelletron experiment was less, but in terms of the dynamics it is mostly similar. We have already seen the KER comparison and the peak value is about same though we expected the counts for higher KER values to increase. Similarly, the branching ratio for the sequential and concerted we got in case of Ar^{8+} was 15.2:84.8. Again, we expected the ratio to be less in case of F^{9+} as the higher excited states are mostly repulsive leading to a concerted breakup.

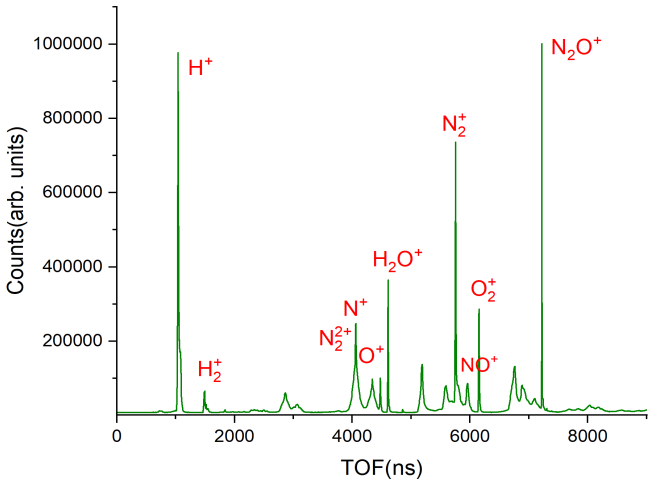

Fig.2: Time of Flight (TOF) Spectrum for first ion in event.

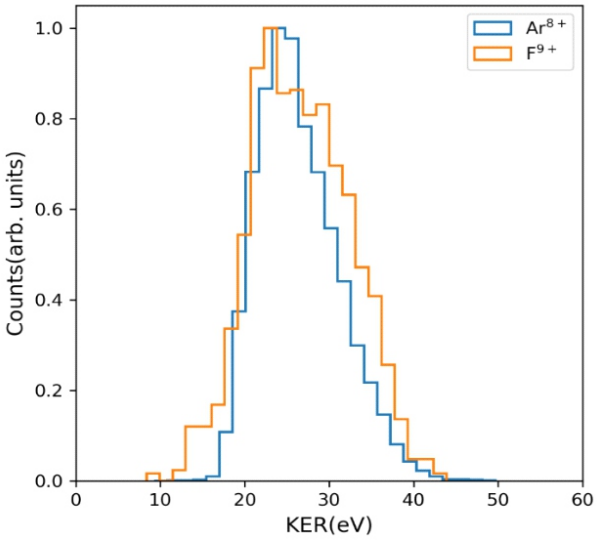

Fig.3: KER (Kinetic Energy Release) distribution.

Future Plan

Development of new COLTRIMS reaction microscope setup for kinematically complete ion atom/molecule collision studies

We have designed a new COLTRIMS reaction microscope [5] which is capable of measuring momentum vector of individual reaction products, the recoil ion and the electron, with subatomic scale precision. This will enable us to perform kinematically complete experiments involving ion atom collision. Once we measure the momentum vector of individual ions we can deduce quantities like kinetic energy, electron emission angle, orientation of molecule before fragmentation, etc.

Design of the spectrometer

The spectrometer consists of three regions. The extraction region for extraction of reaction products, the recoil ion and electrons. The field free drift region of the recoil ion to separate time of flight in m/q. The deceleration region for electron to achieve time focusing. The region between drift tube and extraction region will act as electrostatic lens for time and space focusing of the recoil ion. The extraction region has length 99 mm. The drift tube part has length 221 mm. The deceleration region of electron has length 60 mm. For confinement of electron within 80 mm diameter helical path, an external uniform magnetic field will be applied by a pair of Helmholtz coils.

Cold target: Cold target will be prepared by supersonic expansion through micro meter size nozzle. A geometrically cooled supersonic molecular jet will be formed by passing the beam through two skimmers.

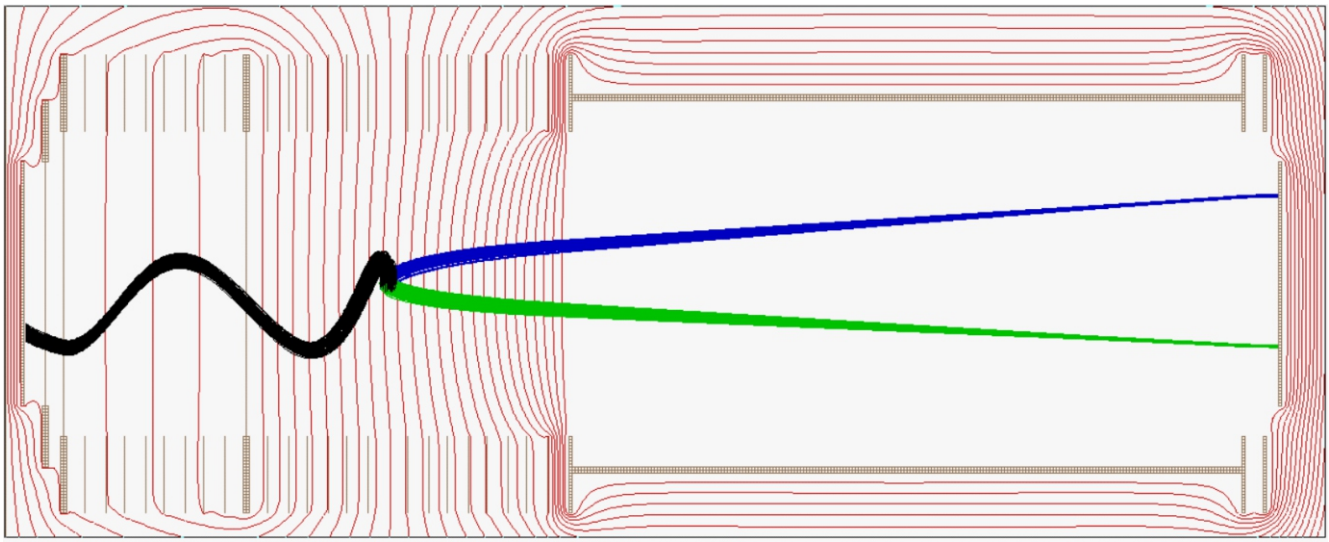

Fig.4: Design of the COLTRIMS reaction microscope. The equipotential surfaces are shown in red curves. Recoil on trajectories are shown in blue and green color. Electron trajectory is shown in black colour. The left most region is the deceleration region for electron, the middle part is extraction region for recoil ion and electron, the rightmost part is the field free drift region for recoil ion. Magnetic field lines are not show in this figure.

Simion simulation for momentum component of the recoil ion and the electron: We will record hit coordinates in the respective recoil ion and electron detectors and time of hitting as raw data for every event. From the hit position and time of flight we will calculate the momentum components.

The transverse momentum component of the recoil ion follows linear relationship with hit radius and the parallel component follows linear relationship with time of flight if kinetic energy gain during electrostatic extraction if much higher than initial energy of the recoil ion. The transverse component of the electron follows $p_{e\perp} = r_0 \sin(\omega t/2)$, where $\omega = B/m_e$ is the angular velocity in applied magnetic field. Since electron initial energy will be comparable to energy gain during extraction, parallel momentum component will follow a nonlinear relationship with time of flight.

Some possible Experiments with the Reaction Microscope

Fully differential cross section measurement of ionization followed by fragmentation of diatomic molecules

In earlier studies people have observed double slit interference pattern in electron emission from H_2 [6], N_2 [7], O_2 [8] upon heavy ion collision. They have measured double differential cross section (DDCS) of electron. But in those studies, information about fragmentation of parent diatomic molecules are missing. With the reaction microscope by measuring all reaction products momentum vectors we can study the orientational effect during collision. Measurement of Kinetic Energy Release (KER) spectrum and orientation during fragmentation will reveal complete information about ionization processes.

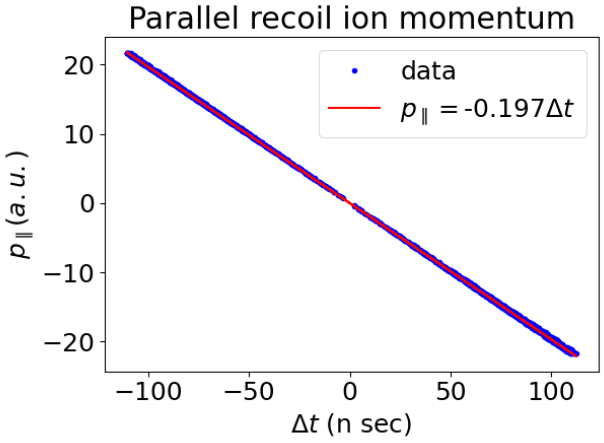

Fig.5: The recoil ion momentum parallel to spectrometer axis mapping function with time of flight. Here $\Delta t = t - t_0$, where t_0 is time of flight for zero momentum component.

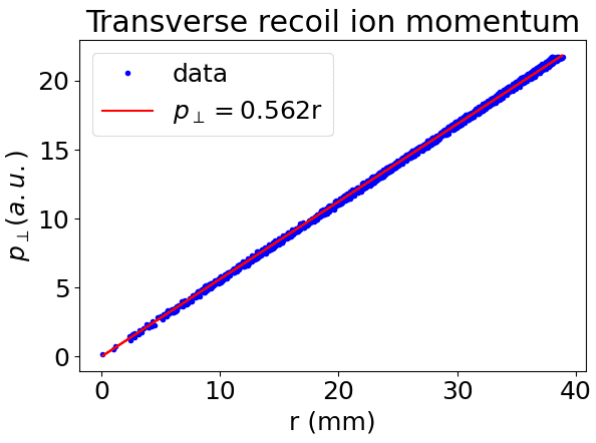

Fig.6: The recoil ion momentum component transverse to spectrometer axis mapping function with hit radius in the recoil ion detector.

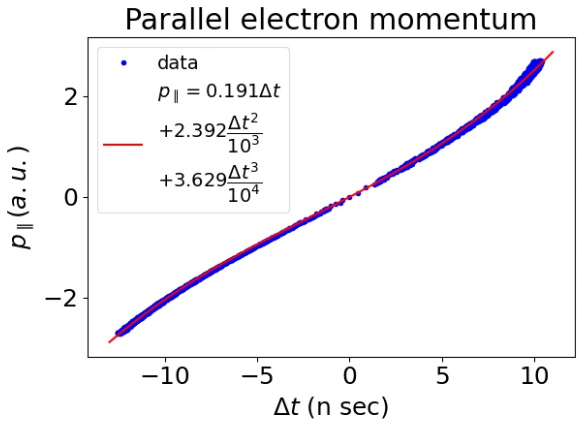

Fig.7: The electron momentum component parallel to the spectrometer axis mapping function with time of flight of the electron. Here $\Delta t = t - t_0$, where t_0 is time of flight for zero momentum component.

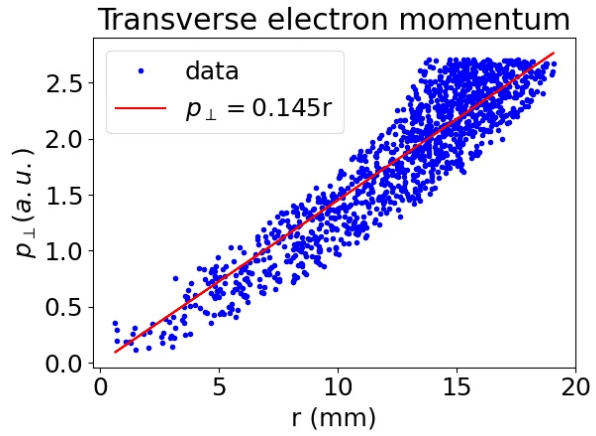

Fig.8: The electron momentum component transverse to spectrometer axis mapping function with hit radius at the electron detector.

Fragmentation dynamics of dimer

Measuring all momentum vectors of the fragmented dimer atoms or molecules we can measure kinetic energy release (KER) and the orientation during collision. Also measuring momentum vector of ejected electrons, we can distinguish between different phenomenon like Coulombic explosion (CE), radiative charge transfer (RCT), inter molecular Coulombic decay (ICD). As we know, charge transfer occurs differently in weakly bound system than molecules with strong bonding [5], [6], [7]. It is important to know role of the neighbor atom/molecule in energy transfer, electron emission. This helps us in understanding fundamental laws of nature as well as help in modelling radiation damage. Thus, it is important to study interaction of this kind of system.

Conclusion

We have developed a new COLTRIMS Setup to study ionization induced dissociation dynamics of N_2O on interaction with F^{9+} in the Pelletron LINAC Facility. We have studied the KER distribution coming the breakup of the ionized molecule. Using momentum Correlation plots we have tried to understand the different types of decay and found the concerted mechanism to be the dominant one. Finally, we have compared these dynamics at high velocity to a low velocity projectile. We have found the dynamics mostly remains the same. We have designed a new reaction microscope for complete kinematic study of molecular fragmentation. The simulation has been done and will be tested in the future.

Acknowledgement

We would like to thank the Pelletron staff for beam related assistance and also the ECR LAB staff for their support during the experiment.

References

[1] D. Vernhet, J.P. Rozet, K. Wohrer, L. Adoui, C. Stphan, A. Cassimi, and J.M. Ramillon. Nuclear .Instruments and Methods in Physics Research Section B: Beam Interactions with Materials and Atoms, 107(14):71{78, 1996

[2] R. Dorner, V. Mergel, O. Jagutzki, L. Spielberger, J. Ullrich, R. Moshammer, and H. Schmidt-Bocking. Cold target recoil ion momentum spectroscopy: a 'momentum microscope' to view atomic collision dynamics. Phys. Rep., 330(23):95{192, 2000.

[3] W. C. Wiley and I. H. McLaren. Time-of-flight mass spectrometer with improved resolution. Rev. Sci. Instrum., 26(12):1150, 1955.

[4] R.H. Dalitz. Lond. Edinb. Dubl. Phil. Mag, 44(357):1068{1080, 1953

[5] J Ullrich, R Moshammer, A Dorn ,R Dörner, L Ph H Schmidt and H Schmidt-Böcking Rep. Prog. Phys. 66 1463 (2003). DOI 10.1088/0034-4885/66/9/203.

[6] Deepankar Misra, U. Kadhane, Y. P. Singh, L. C. Tribedi, P. D. Fainstein, and P. Richard, Phys. Rev. Lett. 92, 153201 (2004). https://doi.org/10.1103/PhysRevLett.102.153201

[7] Saikat Nandi, Shubhadeep Biswas, Carmen A. Tachino, Roberto D. Rivarola, and Lokesh C. Tribedi, Eur. Phys. J. D 69: 192 (2015). http://dx.doi.org/10.1140/epjd/e2015-60102-0

[8] Saikat Nandi, A N Agnihotri, C A Tachino, R D Rivarola, F Martín and Lokesh C Tribedi, J. Phys. B: At. Mol. Opt. Phys. 45 215207 (2012). http://dx.doi.org/10.1088/0953-4075/45/21/215207

[9] J. Matsumoto, A. Leredde, X. Flechard, K. Hayakawa, H. Shiromaru, J. Rangama, C. L. Zhou, S. Guillous, D. Hennecart, T. Muranaka, A. Mery, B. Gervais, and A. Cassimi, Phys. Rev. Lett. 105, 263202 (2010) https://doi.org/10.1103/PhysRevLett.105.263202.

[10] A. Méry, A. N. Agnihotri, J. Douady, X. Fléchard, B. Gervais, S. Guillous, W. Iskandar, E. Jacquet, J. Matsumoto, J. Rangama, F. Ropars, C. P. Safvan, H. Shiromaru, D. Zanuttini, and A. Cassimi, Phys. Rev. Lett. 118, 233402 (2017) https://doi.org/10.1103/PhysRevLett.118.233402

[11] Xitao Yu, Xinyu Zhang, Xiaoqing Hu, Xinning Zhao, Dianxiang Ren, Xiaokai Li, Pan Ma, Chuncheng Wang, Yong Wu, Sizuo Luo, and Dajun Ding, Phys. Rev. Lett. 129, 023001 (2022).

आगामी सुविधा

15

भापअ केंद्र में ईसीआरआईएस सुविधा और इसके उपयोग के लिए अनुसंधान कार्यक्रम

ए. कुमार[1,*], आर. जी. थॉमस[1,2,*], जी. मिश्रा[1], एस. डे[1,2], जी. मोहंतो[1,2], एस. गोयल[1], आर. आर. साहू[1], एन.के. मिश्रा[1], ए. के. गुप्ता[1,2]

[1]नाभिकीय भौतिकी प्रभाग, भाभा परमाणु अनुसंधान केंद्र (भापअ केंद्र), ट्रांबे, मुंबई-400085, भारत

[2]होमी भाभा राष्ट्रीय संस्थान, अणुशक्तिनगर, मुंबई-400094, भारत

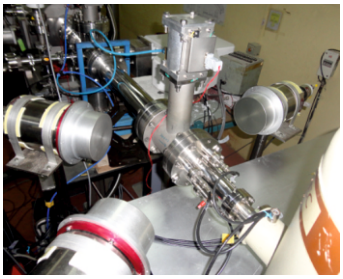

D+D संलयन के लिए स्थापित प्रयोग की तस्वीर।

सारांश

वीडीजी भवन, भापअ केंद्र, मुंबई में एक उच्च धारा अतिचालित इलेक्ट्रॉन साइक्लोट्रॉन अनुनाद आयन स्रोत (ईसीआरआईएस) संस्थापित किया गया है। इस आयन स्रोत का उपयोग करके निम्न ऊर्जा वाले नाभिकीय भौतिकी प्रयोग और बहु-विषयक अनुसंधान कार्यक्रम किए गए हैं। भापअ केंद्र-वैज़ाग में 'ईसीआर आधारित भारी आयन त्वरक' की दिशा में पूर्व-परियोजना अनुसंधान और विकास के लिए इस ईसीआरआईएस को हॉल-9, भापअ केंद्र में स्थानांतरित करने और इसके उपयोग को बढ़ाने की योजना है। पूर्व-परियोजना अनुसंधान और विकास के लिए, यह ईसीआरआईएस भारी आयन रेडियो आवृत्ति चतुर्ध्रुव के बाद अतिचालक रेडियो आवृत्ति नायोबियम गुहिकाओं के लिए एक अंतःक्षेपक होगा। मूलभूत एवं अनुप्रयुक्त अनुसंधान कार्यक्रमों के लिए एकल ईसीआरआईएस का उपयोग करने की भी योजना है। ईसीआरआईएस प्रणाली की संस्थापना के संबंध में, हाल ही में एक आरसीसी हॉल का निर्माण किया गया है और वर्तमान में हॉल-9 में संबद्ध सेवाओं के लिए स्थल की तैयारी का काम चल रहा है। इस लेख में, हॉल-9 में एकल ईसीआरआईएस का उपयोग करके त्वरक आधारित निम्न ऊर्जा नाभिकीय भौतिकी और बहु-विषयक अनुसंधान कार्यक्रमों के लिए अनुसंधान योजनाओं को रेखांकित किया गया है।

Nuclear Physics

15

The ECRIS Facility at BARC and Research Programs for its Utilization

A. Kumar[1,*], R. G. Thomas[1,2,*], G. Mishra[1], Sukanya De[1,2], G. Mohanto[1,2], S. Goel[1], R. R. Sahu[1], N. K. Mishra[1], and A. K. Gupta[1,2]

[1]Nuclear Physics Division, Physics Group, Bhabha Atomic Research Centre (BARC), Trombay, Mumbai-400085, INDIA

[2]Homi Bhabha National Institute, Anushakti Nagar, Mumbai-400094, INDIA

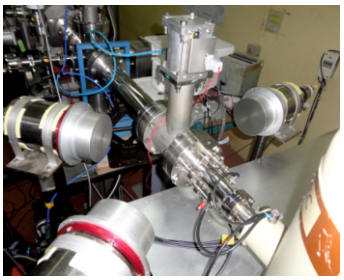

Photograph of experiment setup for D+D fusion

ABSTRACT

A high current superconducting Electron Cyclotron Resonance Ion Source (ECRIS) has been installed at the VDG building, BARC, Mumbai. Low energy nuclear physics experiments and multidisciplinary research programs have been carried out using this ion source. It is planned to relocate this ECRIS to Hall-9, BARC for pre-project R&D towards the 'ECR based Heavy Ion Accelerator at BARC-Vizag' and also to enhance its utilization. For the pre-project R&D, this ECRIS will be an injector for heavy ion Radio Frequency Quadrupole followed by superconducting Radio Frequency niobium cavities. It is also planned to utilize the stand-alone ECRIS for basic- and applied-research programs. With respect to setting up of the ECRIS system, a RCC hall has recently been constructed and site preparation works for associated services are currently underway at Hall-9. In this article, the research plans for accelerator based low energy nuclear physics and multidisciplinary research programs to be carried out using the stand-alone ECRIS at Hall-9 are outlined.

KEYWORDS: *Electron Cyclotron Resonance Ion Source (ECRIS), Low-energy Nuclear Physics.*

**Authors for Correspondence: A. Kumar, and R. G. Thomas*
E-mail: harpreet.singh@tifr.res.in, and jibak.mukherjee@tifr.res.in

Introduction

A high current superconducting Electron Cyclotron Resonance Ion Source (ECRIS) [1] capable of providing a wide range of ion species has been installed at the VDG building, BARC, Mumbai. This 18.0 GHz superconducting ECRIS has a maximum RF power rating ~1.7 kW and is capable of delivering a wide range of ion beams with typical species including p, $^{4}He^{2+}$, $^{16}O^{7+}$, $^{181}Ta^{32+}$, $^{209}Bi^{33+}$ etc. produced with eμA - to - emA currents. It operates at maximum 30 kV extraction voltage on the maximum 300 kV platform, providing a maximum kinetic energy of 330 keV per charge state of the ion [1]. The schematics of the ECR ion source system is depicted in Fig.1. Accelerator based low energy nuclear physics [2], x-rays emission from ion-atom collisions, and multidisciplinary research programs have been initiated with this ECRIS.

It is planned to relocate the ECRIS to Hall-9, BARC for pre-project R&D towards green field 'ECR based Heavy Ion Accelerator at BARC-Vizag' and also to enhance its utilization as a stand-alone ion source. For the pre-project R&D activities, installation of the superconducting ECRIS system and a room temperature heavy ion RFQ (Radio Frequency Quadrupole) followed by SRF (superconducting Radio Frequency) niobium cavities are being carried out at Hall-9, BARC. This ECRIS will be an injector element for the heavy ion RFQ. With respect to the setting up of ECRIS system, a RCC hall has already been constructed (Fig.2) and site preparation works for associated services are currently underway at Hall-9, BARC.

In this article, some of the low energy nuclear physics and multidisciplinary research programs to be carried out using the stand-alone ECRIS are outlined.

Research Programs using the ECRIS

Low-energy nuclear physics: Lattice assisted fusion studies

Nuclear fusion reactions, viz. D+D and D+T are of interest for both basic and applied nuclear physics. These reactions are important for the development of neutron sources, fusion-fission hybrid systems and advancement of nuclear technologies for controlled fusion [3].

In a recent work using the stand-alone ECRIS at the VDG building, we have carried out experiments to investigate the neutron production in D+D fusion during deuterium implantation in palladium at low temperatures [2].

In this experiment, 100 keV accelerated D^{+} ions from the ECRIS impinged on a cooled (-76^{0} C) palladium target (Fig.3) and the neutron emission rate was measured as a function of the number of implanted D^{+} ions. It is observed that the excess of neutrons in a certain region is significantly large (Fig.4) which might be ascribed to the strong matrix effect of the host material at large D/Pd ratios [2]. The phenomenon of neutron production in D+D fusion at low-energies using various host materials in different experimental conditions need to be investigated and further experiments are planned to examine the role of the host matrix in neutron production.

Characteristic and continuous x-rays studies

The experimental studies of the characteristic X-ray production yield is of interest for understanding basic ion-atom collision processes involving tightly bound electrons [4], and for different applications including elemental composition analysis. Therefore, to test the validity of theoretical models in the low-velocity region, the K/L/M X-rays production cross sections and X-rays relative intensities for different projectile-target combinations will be measured using ion beams from the ECRIS.

In another research program, the X-rays bremsstrahlung spectrum emitted by the electrons inside the ECR plasma source [5] will be measured for the temperature of the high energy electrons inside the plasma. A systematic study of the X-ray bremsstrahlung spectrum, thus, can bring out the dependence of electron temperature on different operating parameters (e.g. RF power, gas pressure, different gas mixing) that would help in the efficient operation of the ECR ion source at optimum conditions.

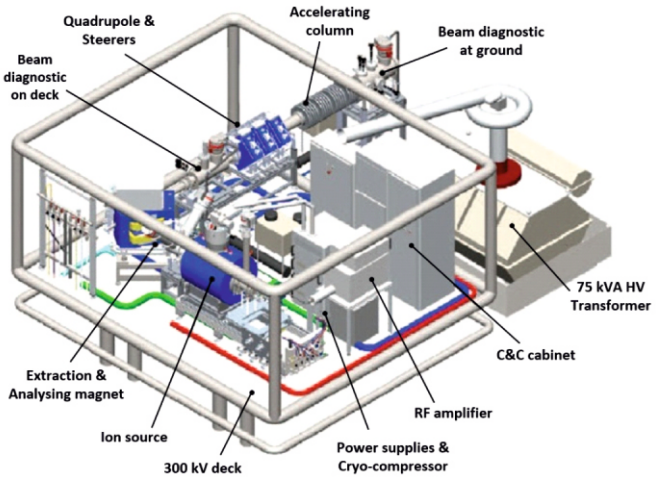

Fig.1: Schematic of the Electron Cyclotron Resonance Ion Source (ECRIS) system.

Fig.2: Newly built hall exclusively for the ECRIS at Hall-9, BARC.

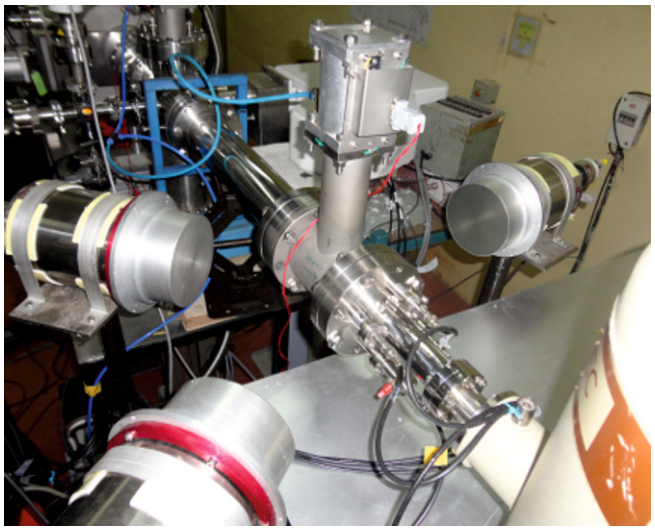

Fig.3: Photograph of the experimental setup used.

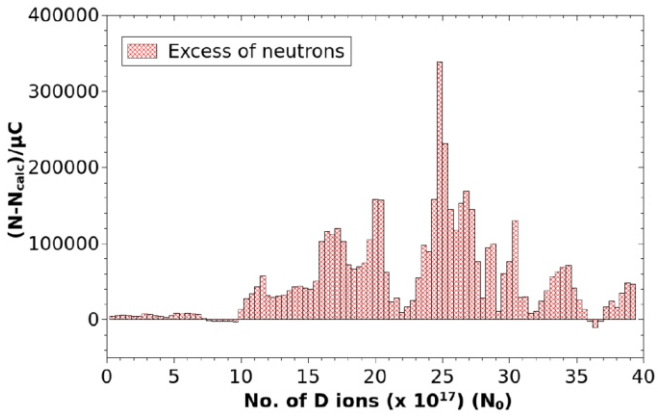

Fig.4: The excess of neutrons with respect to the simulated value as a function of the number of implanted ions (N_o).

Multidisciplinary research programs

In addition to aforementioned research programs, different experiments has been performed using the ECRIS at VDG building, for example, (1) assessment of long term radiation stability of nuclear waste glasses, borosilicate and iron phosphate glasses, due to irradiated by 2 MeV Xe ions and (2) testing of a high-resolution x-ray crystal spectrometer. Apart from NPD's research programs mentioned in previous sub-sections, various researchers from DAE have proposed research plans for utilization of the ECRIS after its relocation to Hall-9, namely (a) understanding of radiation induced changes in matrices proposed for immobilization of nuclear waste (b) alpha decay induced recoil of trapped radionuclides in crystalline matrices (c) radiation damage study in reactor pressure vessel steel and Zr-Nb pressure tube material and (d) measurement of cross sections and astrophysical S-factors for reactions at astrophysically relevant energies.

Summary

A high current superconducting Electron Cyclotron Resonance Ion Source has been successfully installed at the VDG building BARC. A number of experiments related to low energy nuclear physics and multidisciplinary research have been performed using this ECRIS. It is planned to relocate the ECRIS to Hall-9, BARC for pre-project R&D towards green field 'ECR based Heavy Ion Accelerator at BARC-Vizag' and also to enhance its utilization as a stand-alone ion source. For setting up of the ECRIS system, a RCC hall has been constructed and site preparation works for associated services are underway at Hall-9. The research plans for low energy nuclear physics and multidisciplinary research programs to be carried out using the stand-alone ECRIS at Hall-9 have been described.

References

[1] G. Gaubert, C. Bieth, W. Bougy, N. Brionne, X. Donzel, R. Leroy, A. Sineau, C. Vallerand, A. C. C. Villari, T. Thuillier, Pantechnik new superconducting ion source: PantechniK Indian Superconducting Ion Source, Rev. Sci. Instrum. 83 (2012) 02A344. https://doi.org/10.1063/1.3673635.

[2] R. K. Choudhury, Ajay Kumar, R. G. Thomas, G. Mishra, A. Mitra, B. K. Nayak, A. Saxena, Anomalous oscillatory features in neutron emission from D + D fusion in palladium at 100 keV implantation energy, Europhysics Letters 126 (2019) 12002, doi: 10.1209/0295-5075/126/12002.

[3] P. R. Goncharov, Differential and total cross sections and astrophysical S-factors for ^{2}H(d,n)^{3}He and ^{2}H(d,p)^{3}H reactions in a wide energy range, At. Data Nucl. Data Tables 120 (2018) 121-151. https://doi.org/10.1016/j.adt.2017.05.006.

[4] Shehla, Ajay Kumar, Anil Kumar, Deepak Swami, Sanjiv Puri, Low energy carbon ion induced M X-ray relative intensities for $_{70}$Yb, $_{82}$Pb and $_{83}$Bi, Nuclear Instrum. and Methods B 458 (2019) 130-135. https://doi.org/10.1016/j.nimb.2019.08.005.

[5] R. Geller, Electron Cyclotron Resonance Ion Sources and ECR Plasmas (Institute of Physics Publishing, 1996). https://doi.org/10.1201/9780203758663.

प्रस्तावित सुविधा

16

नाभिकीय खगोल भौतिकी हेतु भूमिगत सुविधा

एस. संत्रा
नाभिकीय खगोल भौतिकी अनुभाग, भाभा परमाणु अनुसंधान केंद्र (भापअ केंद्र), ट्रांबे, मुंबई – 400085, भारत
होमी भाभा राष्ट्रीय संस्थान, अणुशक्तिनगर, मुंबई – 400094, भारत

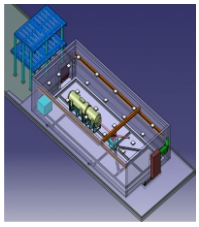

प्रस्तावित 5 MV डीसी त्वरक प्रयोगशाला की योजना

सारांश

एक भूमिगत नाभिकीय खगोल भौतिकी सुविधा का निर्माण 10 वर्षों की समय सीमा के भीतर प्रस्तावित है, जिसका कम से कम 1.5 किलोमीटर हिस्सा चट्टान के भीतर होगा। यह नाभिकीय खगोल भौतिकी की अपेक्षा के अनुरूप निम्न अनुप्रस्थ काट नाभिकीय अभिक्रियाओं के मापन हेतु आवश्यक स्तर तक ब्रह्मांडीय पृष्ठभूमि को कम करने में सहायक होगा। रु. 300 करोड़ की लागत से प्रथम 7 वर्षों के दौरान एक ईसीआईआर आधारित 5 MV डीसी त्वरक का निर्माण करने का प्रस्ताव है, जिसके बाद अगले 3 वर्षों के भीतर प्रायोगिक सुविधाओं का विकास किया जाएगा। यह सुविधा हीलियम और कार्बन दहन अभिक्रियाओं के लिए समर्पित होगी जिसका तापमान हाइड्रोजन दहन के दौरान होने वाली अभिक्रियाओं की तुलना में उच्च होती है।

Proposed Facility

16

An Underground Facility for Nuclear Astrophysics

S. Santra
Nuclear Astrophysics Section, Bhabha Atomic Research Centre (BARC), Trombay, Mumbai-400085, INDIA
Homi Bhabha National Institute, Anushakti Nagar, Mumbai-400094, INDIA

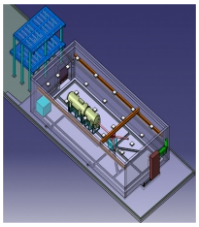

Schematic of the proposed 5 MV DC accelerator laboratory

ABSTRACT

An underground nuclear astrophysics facility has been proposed to be built in a time frame of 10 years, with a rock overburden of at least 1.5 km. This will help reduce the cosmic background to a level essential for the measurement of low cross section nuclear reactions of nuclear astrophysics interest. An ECIR based single ended 5 MV DC accelerator is proposed to be built in first 7 years, followed by the development of experimental facilities within next 3 years, with an outlay of Rs. 300 crore. This facility will be devoted to Helium and Carbon burning reactions that take place at higher temperatures than those occurring during the hydrogen-burning processes.

KEYWORDS: *ECR, Cosmic, Carbon burning, Hydrogen-burning.*

**Author for Correspondence: Satyaranjan Santra*
E-mail: ssantra@barc.gov.in

Background

For more than two decades LUNA (Laboratory for Underground Nuclear Astrophysics) in Gran Sasso, Italy [1-3] has been the only underground laboratory in the world. Over the years many plans have been discussed on different continents for additional laboratories dedicated to the study of nuclear reactions of astrophysical interest at very low energies under almost background free conditions. Only now some of these projects (like Jinping Underground facility for nuclear astrophysics (JUNA) in China [4], Compact Accelerator System for Performing Astrophysical Research (CASPAR) in USA [5] and Felsenkeller shallow underground facility at Germany [6] became or will soon become reality. To keep pace with the international communities, we propose a low energy underground accelerator for nuclear astrophysics, the first of its kind in India.

Motivation

Accurate knowledge of thermonuclear reaction rates is a key issue in nuclear astrophysics since it is important for understanding the energy generation, neutrino production and the synthesis of the elements in stars. Cross-section measurements are mainly hampered by the very low counting rate and cosmic background. An underground location is extremely advantageous for such studies, as demonstrated by the experiments in LUNA and recently in JUNA. It has been found that the rock overburden of about 1400 m (3800 m water equivalent) reduces the muon component of the cosmic background by a factor of 106; the neutron component by a factor of 103; and the gamma component by a factor of 10 with respect to a laboratory on the Earth's surface. As a result, the gamma background above 3 MeV in an HPGe detector placed underground is reduced by a factor of ~2500 with respect to the same detector placed over-ground. In addition, going underground enhances the effect of passive shielding particularly for lower energy gammas where the background is dominated by environmental radioactivity.

The proposal

We propose an underground nuclear astrophysics facility to be built in 10 years, with a rock overburden of at least 1.5 km. An ECR based single ended 5 MV DC accelerator is proposed to be built in first 7 years, followed by the development of experimental facilities within next 3 years, with a cost of Rs 300 Cr (excluding the tunnel cost).

Physics interest

The experimental programs using this facility are planned to be mainly devoted to Helium and Carbon burning reactions that take place at higher temperatures (i.e. higher energies) than those occurring during the hydrogen-burning processes. In particular, the 12C(α, γ)16O, 12C+12C and the (α, n) reactions on 13C and 22Ne are very important.

These key reactions of helium and carbon burning are responsible for the evolution of massive stars towards their final fate and the nucleosynthesis of most of the elements in the Universe. In particular, the 12C(α, γ)16O and 12C+12C reactions are the most ambitious goals of this project. During the He burning, the reaction 12C+α⟶ 16O+γ competes with the reaction 3α⟶ 12C+γ. These reaction rates will help determine the timescale of helium burning and the C/O ratio left at the end of the He burning. It also affects the white dwarf cooling timescale and the outcomes of both type Ia and core-collapse supernovae where 12C+12C is the trigger of C burning. The temperature at which C burning takes place depends on its rate: the larger the rate, the lower the C-burning temperature. Since the temperature controls the nucleosynthesis processes, reliable estimations of all the yields produced by C burning, for example the weak component of the s process which produces the elements between Fe and Sr, require precise knowledge of the 12C+12C rate. The 12C+12C rate also determines the lower stellar mass limit for C ignition. This limit separates the progenitors of white dwarfs, nova and type Ia supernovae, from those of core-collapse supernovae, neutron stars, and stellar mass black holes. This mass limit also controls the estimations of the expected numbers of these objects in a given stellar population, which are required to answer crucial questions such as: how many neutron stars are there in the Milky Way? How many double neutron stars are there in close binaries? And what is the expected merging rate?

Among the key processes for stellar nucleosynthesis, the sources of neutrons represent a longstanding and debated open problem [7,8]. Neutron-captures (the s or r processes) are known to be the most important mechanisms to produce the elements heavier than iron. The 13C(α,n)16O and 22Ne(α,n)25Mg reactions represent the most promising neutron sources as they operate from relatively low temperatures typical of He burning (100-300MK) and because 13C and 22Ne are relatively abundant nuclei in stellar interiors. The 13C(α,n)16O reaction operates in the He-burning

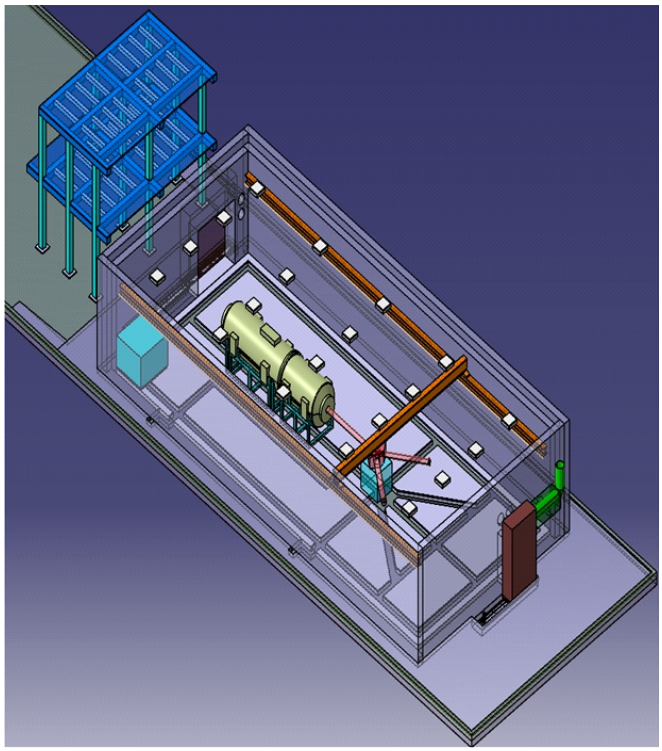

Fig.1: Schematic of the 5 MV accelerator laboratory.

shell of low-mass (less than 4 solar masses) AGB stars and it is the neutron source reaction that allows the creation of the bulk of the s-process elements such as Sr, Zr and the light rare earth elements in the Universe. The 22Ne(α,n)25Mg reaction operates in the He-burning shell of high-mass (more than 4 solar masses) AGB stars and during the core-He burning and the shell-C burning of massive stars (more than 10 solar masses). Experiments with the proposed underground accelerator facility will allow us to gain a full understanding of not only these two reactions but also many other important reactions through the direct measurement of their cross sections in the energy range of astrophysical interest.

Plans

Fig.1 shows the schematic of the 5 MV accelerator laboratory. It requires a minimum underground space of about 80 m x 10 m. However, in addition to the facility for nuclear astrophysics, several other underground experimental facilities (e.g., dark matter searches, neutrino observatory, etc.) have also been proposed to be built within the same underground laboratory. So, a total space of about 150 m x 500 m that can accommodate all these facilities has been proposed.

Where do we stand today?

The research in the area of experimental Nuclear Astrophysics in our country is very nascent. With the commissioning of a 3 MV tandem accelerator FRENA (Facility for Research in Nuclear Astrophysics) at Saha Institute of Nuclear Physics, the planning of a few experiments has just begun. However, the number of experiments that can be pursued using FRENA is limited due to following reasons: 1) Cosmic background is too high as the accelerator is kept over-ground 2) Non-availability of inert beam 3) minimum energy is too high with respect to Gamow peaks of many reactions and 4) maximum energy is too low for inverse kinematics. To overcome some of these problems, a new single ended 5 MV over-ground accelerator with ECR based positive ion source has been proposed at Cotton University, Guwahati. But to solve the background problem an underground facility is essential. Already, the search for a suitable site for an underground laboratory in India has been initiated for Indian Neutrino Observatory, Dark Matter search, etc., and hence this facility can also be placed in the same underground laboratory.

Plan of execution/Timeline

Years	Implementation/Delivery
Phase-I	150 MHz
1st – 3rd	Building of tunnels and caverns; design of laboratories, beam lines & experiments.
4th to 7th	Procurement and commissioning of a 5 MV machine.
Phase-II	
7th – 10th	Setting up of experimental facilities including beam lines, detector array, target assembly and data acquisition system including a few challenging experiments will be completed.

Summary

An underground accelerator facility for nuclear astrophysics studies has been proposed, with an estimated cost Rs 300 Cr, to be built within 10 years after the project is sanctioned. The depth of the underground lab will be a minimum of 1.5 km. The space required just for the nuclear astrophysics lab may be about 80 m x 10 m, however, an area of about 500 m x 150 m will be necessary to include all other underground labs in the same place. Some of the important reactions relevant to nuclear astrophysics that are planned to be measured using the proposed accelerator facility are 12C(α, γ)16O, 12C+12C, 13C(α,n)16O and 22Ne(α,n)25Mg.

References

[1] U. Greife, C. Arpesella, C. A. Barnes, F. Bartolucci, E. Bellotti, C. Broggini, P. Corvisiero, G. Fiorentini, A. Fubini, G. Gervino, et al., Nuclear Instruments and Methods in Physics Research A 350, 327 (1994).

[2] A. Formicola, G. Imbriani, M. Junker, D. Bemmerer, R. Bonetti, C. Broggini, C. Casella, P. Corvisiero, H. Costantini, G. Gervino, et al., Nuclear Instruments and Methods in Physics Research A 507, 609 (2003).

[3] Paolo Prati and on behalf of the LUNA Collaboration, Journal of Physics: Conference Series 1342, 012088 (2020).

[4] W. P. Liu et al., Few-Body Syst (2022) 63:43, https://doi.org/10.1007/s00601-022-01735-3

[5] https://caspar.nd.edu/

[6] D. Bemerer, Proc. Of Science, Vol-204, XIII Nuclei in the Cosmos (NIC-XIII) – Nuclear Reactions at Low Energies, 2015

[7] E. M. Burbidge, G. R. Burbidge, W. A. Fowler, and F. Hoyle, Reviews of Modern Physics 29, 547 (1957).

[8] A. G. W. Cameron, Publications of the Astronomical Society of the Pacific 69, 201 (1957).8] E. Piasecki, L. Nowicki, in: Proc. Symposium, "Physics and Chemistry of Fission", Jülich, 14-18 May 1979, IAEA, Vienna, vol. II, 1980, p. 193.

प्रस्तावित सुविधा

17

वैज़ाग में भारी आयन अन्वेषण हेतु स्थायी एवं अस्थायी समस्थानिक कणपुंज (सुभीर) सुविधा

ए. श्रीवास्तव[1,2,*], के. रामचंद्रन[1], एवं के. माहात[1,2]
[1]नाभिकीय भौतिकी प्रभाग, भाभा परमाणु अनुसंधान केंद्र (भापअ केंद्र), ट्रांबे, मुंबई – 400085, भारत
[2]होमी भाभा राष्ट्रीय संस्थान, अणुशक्तिनगर, मुंबई – 400094, भारत

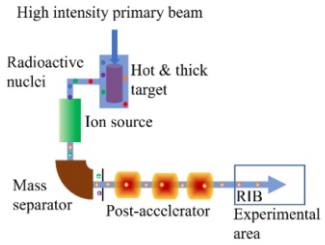

रेडियोसक्रिय आयन कणपुंज (आरआईबी) उत्पादन की ऑनलाइन रेडियोसक्रिय (आईएसओएल) विधि का योजनाबद्ध प्रदर्शन।

सारांश

मौलिक अनुसंधान एवं अनुप्रयोगों के लिए 10MeV/u तक ऊर्जा के स्थिर और अस्थिर आयनों के किरणों को तीव्र करने हेतु वैज़ाग के त्वरक परिसर में एक बहुउद्देश्यीय भारी आयन त्वरक सुविधा का निर्माण प्रस्तावित है। 30 MeV इलेक्ट्रॉन और 40 MeV प्रोटॉन त्वरक का उपयोग करके रेडियसक्रिय आयनों को चालक त्वरक के रूप में उत्पादित किया जाएगा। भारी आयन त्वरक में, दो अलग-अलग ईसीआर आयन स्रोतों को स्थिर और अस्थिर आयनों से अंतःक्षेपित करने का प्रस्ताव है, जो स्थिर भारी आयन (1 से 92 की सीमा के भीतर Z) और रेडियोधर्मी आयनों (~Z = 38 से 60, A = 90 से 170) दोनों की आपूर्ति में सक्षम हैं। यह सुविधा, न्यूट्रॉन, गामा किरणों और आवेशित कणों के मापन का पता लगाने की व्यवस्था के साथ अत्याधुनिक प्रयोगात्मक क्षेत्र हेतु अग्रणी अनुसंधान का कार्य करेगा।

Proposed Facility

17

Facility for Stable and Unstable isotopic Beam for Heavy Ion Research (SUBHIR) at Vizag

A. Shrivastava[1,2,*] , K. Ramachandran[1] and K. Mahata[1,2]
[1]Nuclear Physics Division, Bhabha Atomic Research Centre (BARC), Trombay, Mumbai-400085, INDIA
[2]Homi Bhabha National Institute, Anushakti Nagar, Mumbai-400094, INDIA

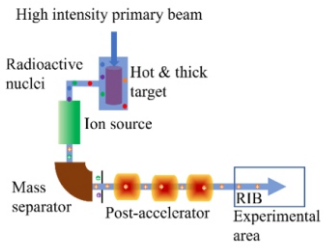

Schematic representation of isotopes online (ISOL) method of Radioactive Ion Beam (RIB) Production.

ABSTRACT

It is proposed to construct a versatile heavy ion accelerator facility at the accelerator complex at Vizag for accelerating beams of stable and unstable ions of energy up to 10MeV/u for basic research and applications. The radioactive ions will be generated using the proposed 30 MeV electron and 40 MeV proton accelerator as driver accelerators. Two separate ECR ion sources are proposed to inject stable and unstable ions to the heavy ion accelerator, capable of delivering both stable heavy ion (Z within the range of 1 to 92) and radioactive ions (~ Z=38 to 60, A= 90 to 170). The facility will have state-of-of the art experimental area with detection setup for measurement of neutrons, gamma rays and charged particles to perform frontline research.

KEYWORDS: *Stable and radioactive ion beams, Electron accelerator, Proton accelerator, Heavy ion accelerator.*

**Author for Correspondence: A. Shrivastava*
E-mail: aradhana@barc.gov.in

Introduction

Ion accelerators are one of the primary tools for nuclear physics research which involves the transmutation of elements through fusion, fission, transfer, breakup, spallation and fragmentation reactions. Studies of static and dynamic properties of nuclei require accurate knowledge of nuclear structure and reaction mechanism. By accelerating and colliding ion beam with target nuclei, and observing the collision products, properties of the interacting nuclei and atoms can be studied. These studies can be performed at various energy regions starting from very low energies like few keV/nucleon (A) to GeV/A. The medium and high energy regions deal with nucleons and its internal structure. The low energy nuclear physics focuses on the fundamental issues related to the nature of strongly interacting matter in the universe, starting from its creation and more specifically the interaction between nucleons. Nuclear physics research has led to the basic understanding of the energy generation in sun and other stars, energy generation using nuclear fission and fusion reactions, nuclear medicine, etc. [1]. Most of the current knowledge on nuclear properties has been gained by performing experiments using stable ion beams or long lived naturally occurring isotopes from accelerator facilities that are restricted to about 300 nuclei mostly on stable elements or long lived naturally occurring isotopes as target.

The fusion reaction between two stable nuclei leads to the production of nuclei in the neutron deficient side of the nuclear chart while, the fission and fragmentation reactions in general produce nuclei in the neutron rich side. The nuclear collision between stable ion beam with stable target can produce only a limited number of unstable nuclei which have been thoroughly studied. By colliding stable ion beam on target made of stable isotopes one cannot reach a large fraction of nuclei which are among the around 7000 nuclei that are estimated to be lying between the proton and neutron drip-lines [2,3]. To produce most of the unstable nuclei away from the line of stability on the nuclear chart, radioactive ion beams and/or radioactive targets are required. To produce unstable/radioactive ion beam (RIB), stable ions need to be transmuted through nuclear reaction in reactors or accelerator facilities. Using accelerators, the unstable ion beam produced by bombarding high intensity stable ion beams on suitable target can either be directly used for experiments after purification if it has enough energy or after reacceleration for secondary reaction studies. Owing the nature of production of secondary radioactive ion beam, the beam current is typically very low compared to the stable ion beam. However, developments over the last few decades have resulted in mature techniques that allow to explore the properties of isotopes that have a neutron-to-proton ratio very different from the stable isotopes in an unprecedented way [3-8]. The present proposal is to build a world class National Radioactive Ion Beam (RIB) facility with moderate to low beam current at Vizag, to perform 'forefront research' in nuclear physics, and other branches of physics with capability to provide stable heavy ion beam across the periodic table at high intensities. Specifically, this facility will focus on the production of neutron rich nuclei which are less synthesized and studied.

Physics Interest

Radioactive ion beam facilities are transforming nuclear science by making beams of exotic nuclei with various properties, available for experiments. The study of novel nuclear structures and the decay modes associated with weak nucleon binding and isospin can be explored using the RIB. At present, the main excitement and thrust of work with unstable beams are given below.

Role of exotic shape, size and weak binding on reaction dynamics, and decay modes

Nuclei come in a variety of sizes and shapes, from spherical to deformed shapes, which can be prolate or oblate or triaxial. Experiments using RIB can produce and investigate static properties, structure and reaction dynamics of nuclei having exotic shape and structure like halo nuclei, Borromean nuclei, Bubble nuclei, nuclei with neutron skin, etc. For example, nuclei like ^{11}Li, which has only 11 nucleons (neutrons and protons) has a matter radius as big as a lead nucleus with 208 nucleons and hence higher reaction cross-section. These exotic nuclei near drip line have also demonstrated exotic decay modes like proton radioactivity which is not observed in nuclei close to the line of stability. Some of the exotic nuclei have also shown soft dipole resonance seen as the collective oscillation of tightly bound core against the loosely bound valency nucleons. Nuclear reaction and structure studies using exotic beams will be one of the main focuses of this facility. The high quality of the beam produced from Isotope Separation OnLine (ISOL) facility, with proton-to neutron numbers varying over a wide range, allows high-precision measurements of beta decay, particle correlations and atomic masses. These kinds of measurements will be a good testing ground for fundamental symmetries like isospin. Most of the nuclear models developed to describe the properties of stable nuclei fail to describe the nuclei at the extremes of neutron to proton ratio. The three body forces required to explain the halo nuclei and the new magic number are few of the examples. With further studies in the unexplored region, the surprises could be plenty.

Production of super heavy elements (SHE)

Like atoms, nuclei having 2, 8, 20, 28, 50, 82 protons and/or 2, 8, 20, 28, 50, 82, 128 neutrons show more stability compared to nearby mid shell nuclei. Beyond Z=83 and N=128 (^{209}Bi nuclei), no stable nuclei have been found even though the long living isotopes of thorium and uranium are found in nature. These heavy nuclei are unstable mostly against fission or alpha decay. However, the major shell closure beyond Z=82 and N=126 can stabilize nuclei and increase their half-life. There are predictions for stability of super heavy elements with N=184 and Z between 110 or 114 or 126 [10].

In addition, the stability can also be brought in by deformed shell closure. Recent calculations indicate that ^{270}Hs is a doubly magic deformed nucleus, with deformed magic numbers Z = 108 and N = 162 [11]. Apart from the production and identification of nuclei in super heavy island, studies using them are very important. On the other hand, recent calculation indicates the smearing of the electronic and nuclear shell structure of SHE due to the relativistic effects and other phenomena leading to no major distinction between the shells

[12]. The RIB facility with neutron rich isotopic beam will be required to study properties of such nuclei and atoms.

Nuclear astrophysics

Unlike the earth's composition where most of the elements are stable, stellar environment specifically during stellar explosion is expected to generate a lot of heavy radioactive nuclei. The nuclear reactions happening in this environment has led to the formation the elements from iron to uranium. Nuclear reactions occurring in such explosive stellar environments, such as novae, supernovae and X-ray bursters, are believed to play an important role in the synthesis of these heavier elements. The pathways of the reactions leading to them involve short-lived radioactive exotic nuclei, which can be studied using RIB.

Atomic and condensed matter physics

Collinear laser spectroscopy with radioactive ions can be performed to obtain information on hyperfine structure and isotope shift. Beta NMR spectroscopy which can be used to study the magnetic and electronic properties of ultrathin films, nanostructures and interfaces is possible only with radioactive ion beams. By implanting radioactive species inside the material, the surface and bulk properties of the solid and diffusion properties can be studied. Perturbed angular correlation to study the electric field gradient and magnetic field at implant site, emission channeling which uses the emitted radiation to measure the lattice position of the implanted ion in a crystalline host material, tracer diffusion studies and Mossbauer spectroscopy can be used to study various properties of the condensed matter.

Nuclear medicine

Radioisotopes can be used for medical diagnosis and treatment. Photofission and proton induced fission provides wide range of radioisotopes among them many of the isotopes can be of use for medical applications. One of the main advantages of RIB facility for production of radioisotopes for medical isotopes is due to the beam purification using high resolution mass spectrometers.

In addition, the high current stable heavy ion beam from the proposed accelerator will have uses in nuclear physics studies with many more projectile-target combinations at much larger beam energy and intensity allowing us to measure ultra-low cross-sections, SHE production, etc. It has uses in genetic modification of food grains, radiotracers, material surface corrosion studies, atomic physics, condensed matter physics studies, etc.

RIB Production Methods and Current Status

RIB can be produced majorly using two methods namely projectile fragmentation (PF) method and ISOL method [5]. In the projectile fragmentation method, the primary beam which is made up of very high energy heavy ions, on hitting a thin stable target, breaks into fragments through fragmentation, spallation and fission reactions. These fragments are forward focused and have high energy. Typically, mass separators are used to separate the species of interest from the rest of the beam and decelerated if required to reach suitable energy, focused and used as secondary radioactive ion beam for experiments. Even though this method is good for accessing short lived isotopes, the purity and quality of the beam is of a major concern. In ISOL method, the primary beam which can be neutrons or electrons or protons or heavy ions (having very low energy to very high energy of the order of GeV) can be used to produce radioactive ions through various reaction processes like neutron/ proton/ deuteron/ heavy ion induced fission or photofission or spallation or nuclear fusion or transfer or breakup. The radioactive ions thus produced are stopped, extracted, separated and accelerated to form secondary radioactive ion beam. The beam quality of ISOL generated RIB is much better than the fragmentation method. However due to the delay in stopping, extraction and reacceleration, the short half-life radioactive nuclei decay before reaching the secondary target station limiting its usefulness for short lived isotope acceleration.

The ISOL facilities presently operating are ISOLDE, CERN at Switzerland, SPIRAL- GANIL at France, and upcoming facilities are SPES, LNL at Italy, TRIUMF at Canada, ITHEMBA at South Africa and RAON at South Korea. Apart from the ISOL facilities listed above, FRIB at USA, Super-FRS, FAIR, GSI at Germany, RARF, RIKEN at Japan and FLNR, JINR at Russia are few of the important operating RIB facilities worldwide.

Currently India has only a few heavy ion accelerator facilities namely BARC-TIFR Pelletron-LINAC accelerator facility at Mumbai, IUAC Pelletron-LINAC accelerator Facility at Delhi, Variable energy cyclotron and Super Conducting Cyclotron (SCC) at VECC, Kolkata. Other than the recently commissioned K=500 cyclotron, other accelerator facilities do not have enough energy to cross the Coulomb barrier for most of the heavy projectile target combinations. VECC and SCC produce only a few species of beams. At VECC, ANURIB phase-I with very low energy and low current RIB using driver beam from VEC is operational.

Proposed Stable and Unstable isotopic Beam for Heavy Ion Research (SUBHIR) Facility at Vizag

This facility is proposed to deliver radioactive ion beam as well as intense stable ion beam across the periodic table from Hydrogen to Uranium at energies exceeding the Coulomb barrier. Thus, it will significantly surpass those achievable with the existing BARC-TIFR Pelletron-LINAC facility, which is the current workhorse for the nuclear physics community at Trombay. The short-lived nuclear reaction products mainly the unstable fission fragments, produced in proton induced fission and photo fission of actinide targets, will be the source of radioactive ions. The schematic layout of the proposed SUBHIR facility at Vizag is shown in Fig.1. The 40 MeV high intensity (2mA average beam current) proton beam extracted from the first stage of the MEHIPA (Medium Energy Heavy Ion Proton Accelerator), the 30 MeV 0.6mA (average) electron beam from the room temperature (RT) electron LINAC and in future the 50 MeV 2mA (ave) electron beam from the superconducting eLINAC proposed at the same accelerator complex will be used for producing unstable nuclei. The proton beam is expected to directly collide with the actinide target to produce radioactive ion (RI) inside a vacuum chamber. The electron beam from the eLINAC is expected to fall on a conversion target made of high atomic number, high melting point metal like tungsten to

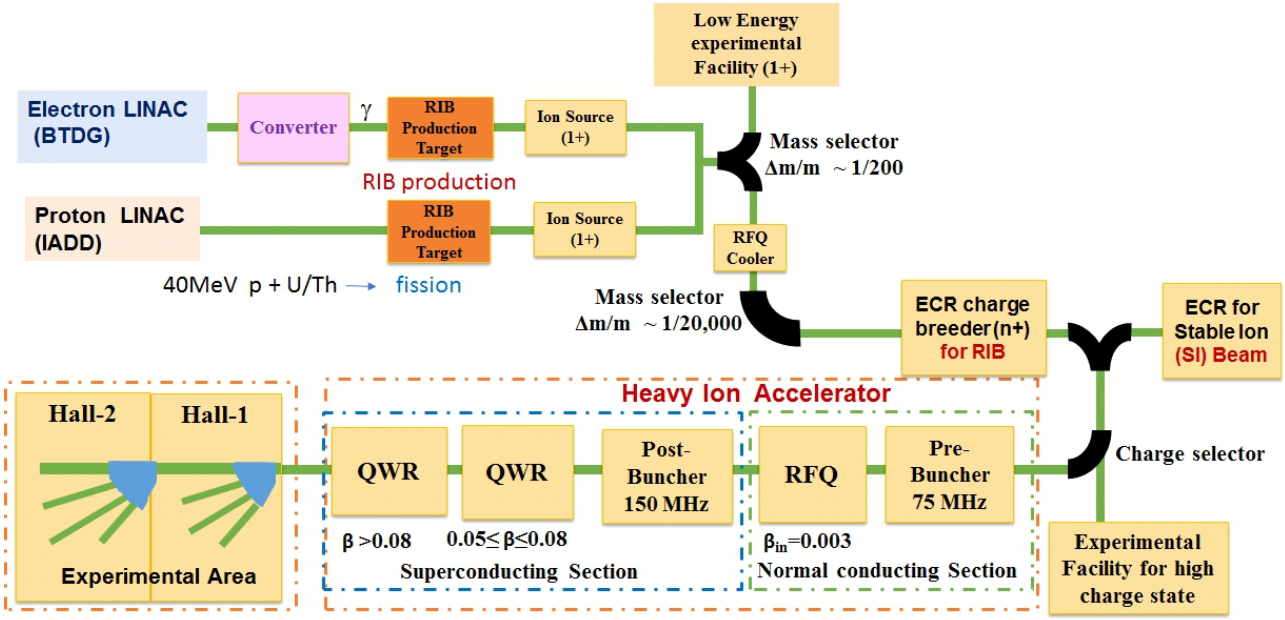

Fig.1: Schematic Layout of SUBHIR at Vizag.

produce forward focused bremsstrahlung photons which in turn upon interaction with actinide target (^{238}U or ^{232}Th) inside a vacuum chamber will produce fission fragments. Proton induced fission can provide neutron rich (via fission) as well as proton rich RIB (using (p,xn) reactions), while electron driver can provide neutron rich RIB (via photo fission). In case of electron driver, photo-fission involves low excitation energy and hence less neutron emission from fission fragments, yielding more neutron rich RIB relative to proton-induced fission. This facility is proposed to be constructed at the accelerator complex at BARC, Vizag.

The Phase-wise development of the proposed proton accelerator has already started for the 1GeV Accelerator Driven Subcritical Reactor System (ADSS) project that will be constructed at Vizag by Ion Accelerator Development Division (IADD), Multidisciplinary Research Group (MRG). IADD has already achieved acceleration of proton beam upto 20 MeV energy at Low Energy High Intensity Proton Accelerator (LEHIPA) facility, BARC, Trombay. The proton accelerator for ADSS at Vizag is planned to be used as the driver accelerator for RIB, when it reaches ~ 40 MeV of proton energy. Beam Technology Development Group (BTDG) has already obtained the financial approval for the development of a 30 MeV RT electron accelerator in the same accelerator complex for producing RIB via photo-fission. Two highly shielded RIB production caves, one each for electron and proton accelerator, will be used to produce, extract and transport radioactive ions. The RIB production targets technology is one of the most challenging parts of this project. It should be able to handle high beam power in small volume. It should be porous enough to release unstable ions produced inside. The production target R&D has already started at BARC. Efficient extraction of the radioactive ions produced is another crucial step. There are mainly two methods of radioactive ion (RI) extraction and transport from the production target namely diffusion-effusion method and gas jet method. Both the methods are proposed for the future RIB facility.

The extracted radioactive ions will be converted into singly charged ions for further transportation. An RFQ beam cooler will be used to reduce the emittance of RIB before sending it through high resolution mass selector for purification of the beam. After mass selection, the singly charged radioactive ions will be stripped of many electrons to form highly charged positive ions using charge breeding ion source. An Electron Cyclotron Resonance (ECR) ion source is proposed to be used for this purpose.

For further accelerating, it is proposed to construct a heavy ion accelerator facility comprising of room temperature Radio Frequency Quadrupole (RFQ), and superconducting Nb cavities to accelerate even the heavy ions like ^{238}U upto 10MeV/u. For lighter ions the accelerator should be able to accelerate the beam to even higher energies per nucleon. The focus of the RIB facility is to produce, extract and accelerate unstable neutron rich fission fragments with Z=38 to 60 and A= 90 to 170. A separate ECR ion source capable of delivering beams across the periodic table from ^{1}H – ^{238}U with high beam current (upto 100pnA) is proposed to inject beam into the heavy ion accelerator. Further, advanced experimental facilities are planned in experimental halls for research purposes. This facility requires 8700 m^2 of space at the accelerator complex BARC, Vizag.

This state-of-the-art facility involves advanced scientific and technical know-hows where some of the technologies do not exist in the country at this moment. The project is planned in a phased manner. Work has already started for the construction of the 30 MeV electron accelerator at Vizag. The first phase of the MEHIPA accelerator for energies upto 40MeV is expected to start soon. R&D on the RIB production target -ion source system, prototyping of RFQ and SRF cavities are also ongoing. During the phase-I, medium energy RIB facility will be built utilizing the technologies currently under development. In

phase-II, additional high beta SRF cavities along with enhanced user facilities are proposed to be developed.

Phase I: Construction, installation and commissioning of heavy ion accelerator at BARC-Vizag

- Civil construction of the accelerator hall and beam line caves, beam halls will be taken up during this phase. All the laboratories required for this facility will also be built during this phase.
- Commissioning of RIB Target Ion Source and getting very low energy RIB with electron and proton accelerators
- Utilization of very low energy RIB for research and applications
- Fabrication, installation and commissioning of stable ion ECR ion source
- Development of radiofrequency (RF) power supplies, power amplifiers, LLRF systems and accelerator control system by Accelerator Power Control Section and Advanced Electronics Application Section.
- Fabrication, installation and commissioning of RFQ
- Fabrication, installation and commissioning of cryogenic plant for liquid helium production for this facility by Cryo-Technology Development Division (CrTDD), MRG, BARC.
- Fabrication, installation and commissioning of low beta and medium beta niobium superconducting quarter wave resonating radiofrequency (SRF) cavities.
- Integration, testing, beam trials, commissioning and utilization of phase-1 heavy ion accelerator.

Phase II: Enhancement in beam energy, and user facilities

- Fabrication, installation and commissioning of RFQ beam cooler for RIB
- Fabrication, installation and commissioning of charge breeding ECR ion source for RIB
- Installation and commissioning of high-resolution mass separator
- Integration of charge breeder with HIA
- Fabrication, installation and commissioning of medium beta SRF cavities.
- Development of beam lines and experimental facilities.
- Commissioning and utilization of full scope SUBHIR facility.

Conclusion

During the last 30 years, a lot of leading research activities have been performed using the stable ions from BARC-TIFR Pelletron LINAC accelerator Facility (PLF), Mumbai and now it is time for us to take our scientific endeavor to the level of current international pursuits and build a green field facility. This facility can provide much larger species of stable ion beams with much higher energy, intensity. The unstable ion beam from this facility with moderate intensity and medium energy is going to be something very new in India.

References

[1] A C Hayes Rep. Prog. Phys. 80 (2017) 026301

[2] B R Fulton J. Phys.: Conf. Ser. 312 (2011) 052001

[3] M. Huyse, The Why and How of Radioactive-Beam Research, Lect. Notes Phys. 651, (2004) 1

[4] Y Blumenfeld, T Nilsson and P Van Duppen, Phys. Scr. T152 (2013) 014023

[5] M. Durante, A. Golubev, W.-Y. Park et al. / Physics Reports 800 (2019) 1

[6] SPIRAL2 facility at GANIL https://www.ganil-spiral2.eu/.

[7] http://www.gsi.de/fair/.

[8] G.Prete, A.Covello “Selective Production of Exotic Species” Technical Design Report INFN-LNL-223 (2008) http://spes.lnl.infn.it/~spes/TDR2008/tech_design08_index.htm.

[9] https://www.vecc.gov.in/projects/details/57/4

[10] Bemis, C. E.; Nix, J. R. "Superheavy elements – the quest in perspective" (PDF). Comments on Nuclear and Particle Physics. 7 (1977) (3): 65

[11] Meng, X.; Lu, B.-N.; Zhou, S.-G. "Ground state properties and potential energy surfaces of 270Hs from multidimensionally constrained relativistic mean field model". Science China Physics, Mechanics & Astronomy. 63 (2020) 1

[12] Paul Jerabek, Bastian Schuetrumpf, Peter Schwerdtfeger, and Witold Nazarewicz Phys. Rev. Lett. 120 (2018) 053001

[13] Bracco A. The nuPECC long range plan 2017: Perspectives in nuclear physics Nucl. Phys. News., 27 (2017), pp. 3-4, 10.1080/10619127.2017.1352311

[14] The 2015 long range plan for nuclear science, DOE/NSF (2015) https://science.energy.gov/np/nsac/

Dr. M. R. Srinivasan

A visionary engineer who steadfastly honed home-grown capabilities in nuclear energy

By SIRD Newsletter Editorial Team

Dr. M.R. Srinivasan addressing at the India Power Awards 2011 ceremony, in New Delhi on November 24, 2011.
Photo: Wikimedia Commons

Dr. Malur Ramasamy Srinivasan, one of the key architects of India's civil nuclear energy programme, passed away on May 20, 2025 in Udhagamandalam (Ooty), Tamil Nadu, at the age of 95. His passing away marks the end of a historic era spanning five decades of illustrious career in India's nuclear journey and leaves behind a towering legacy.

Born on January 5, 1930, in Bangalore, Dr. Srinivasan was educated at Intermediate College, Mysore (now Mysuru), and later at the College of Engineering, Bangalore (now University of Visvesvaraya College of Engineering), where he earned his B.Tech. in Mechanical Engineering. He pursued advanced education abroad, completed his Master's in 1952 and Ph.D. in 1954 in gas turbine technology at McGill University, Montreal, Canada.

Life and Career

Dr. Srinivasan joined the Department of Atomic Energy (DAE) in September 1955, at a time when India was taking its very first steps in nuclear research. He began his career under the mentorship of Dr. Homi J. Bhabha, where working alongside other prominent individuals helped build Apsara, India's first nuclear research reactor, which became operational in 1956. From the outset, he was entrusted with leadership in pivotal projects in DAE.

Under his leadership, 18 nuclear power reactors were developed (seven operational, seven under construction, and four at planning stage), laying the foundation of India's indigenous nuclear program.

Dr. Srinivasan's expertise in Pressurised Heavy Water Reactors (PHWRs) made them the backbone of India's nuclear reactor fleet, and he spearheaded projects at Tarapur, Kalpakkam, Rawatbhata, Narora, Kakrapar, and Kaiga, making India self-reliant in nuclear power technology despite global headwinds.

Institution Builder

Beyond engineering marvels, Dr. Srinivasan was an extraordinary institution builder and policy advisor. His expertise and services were roped in by varied organizations both in India and abroad, including the IAEA and India's Planning Commission.

Personality and Legacy

Fondly remembered as a "walking encyclopedia" by colleagues, Dr. Srinivasan combined technical brilliance with humility, warmth, and a deep commitment to the nation. Whether addressing international conferences, mentoring young engineers, or defending the role of nuclear energy in public debates, he remained a steadfast advocate for science-driven development. As his contemporaries noted during a condolence gathering held in BARC Trombay soon after his passing, he was "firm but gentle", possessing an extraordinary ability to build consensus, "inspire confidence", and uphold scientific excellence. He played a constructive role during the period 2003-2008 when India and the US were engaged in serious negotiations for building a new nuclear energy partnership.

Awards and Honors

For his lifetime of contributions, Dr. Srinivasan was honored with India's highest civilian decorations. Padma Shri in 1984, Padma Bhushan in 1990 and Padma Vibhushan in 2015.

Family

Dr. Srinivasan is survived by his wife, Geetha Srinivasan, daughter Sharada Srinivasan, and son Raghuvir Srinivasan- along with a vast community of colleagues, students, and admirers who view him as one of the towering visionaries of India's nuclear energy programme.

An everlasting legacy

Dr. M.R. Srinivasan's contributions are etched into the very framework of India's nuclear energy programme. He not only helped shape the country's energy security but also ensured it was achieved with indigenous capability and global vision. His life serves as a testament to the power of determination, scientific curiosity, and service to the nation. As India continues its nuclear journey, his legacy will endure as both foundation and inspiration for generations to come.

Key positions held in DAE

1959: Principal Project Engineer of India's first atomic power station at Tarapur, Maharashtra.

1967: Chief Project Engineer of the Madras Atomic Power Station (MAPS), a landmark project in India's journey toward nuclear self-reliance.

1974: Director of Power Projects Engineering Division, responsible for planning and implementation of nuclear power stations.

1984: Chairman of the Nuclear Power Board (NPB).

1987: Chairman of the Atomic Energy Commission (AEC) and Secretary, DAE, while also serving as the founding Chairman of the Nuclear Power Corporation of India Limited.

Key positions held outside DAE

Senior Adviser, International Atomic Energy Agency (IAEA), Vienna (1990–1992).

Member, Planning Commission (1996–98), handling the Energy and Science & Technology portfolios.

Member, National Security Advisory Board (2002–04; 2006–08).

Chairman, Karnataka Task Force on Higher Education (2002–04).

Founder-member of the World Association of Nuclear Operators (WANO).

Fellow of the Indian National Academy of Engineering (INAE).

NTD 2025 Inaugural Day program on May 11th 2025.

Advanced Nuclear Material Technologies' impetus to Aatmanirbhar Bharat

By SIRD Newsletter Editorial Team

The Bhabha Atomic Research Centre (BARC) hosted a three-day National Technology Day (NTD) celebration during May 11-13, 2025 with the theme **"Transition to Clean, Green Viksit Bharat: Advanced Materials & Nuclear Technology"** at the picturesque DAE Convention Centre." The event drew around 1000 students from Atomic Energy Central Schools situated in Anushakti Nagar besides those from several Mumbai-based schools, who constituted the core audience for the program, offering them a unique opportunity to explore and experience India's nuclear science and technology landscape, and understand the role of advanced materials and nuclear energy in building a developed India (Viksit Bharat).

Program Inaugural Session

The opening day set the tone for the 3-day technology fest with distinguished speakers highlighting the importance of nuclear science and technology in India's sustainable development journey and the role of disruptive technological innovations in India's transformation into the future.

Shri. K. N. Vyas, Distinguished Homi Bhabha Chair Professor and Former Chairman, AEC was the program Chief Guest. His keynote address provided insights into India's seven-decade atomic energy journey and the key role of material innovations in addressing complex technological challenges.

In his address, Dr. Ajit Kumar Mohanty, Chairman, AEC & Secretary, DAE inspired the young minds by outlining the vital role of students in realizing the vision of Viksit Bharat. DAE's recent milestones in global science and technology arena, including the 'Breakthrough Prize' in Fundamental Physics, and the launch of Brahmos Aerospace Integration and Testing Facility in defense industrial sector were the main points of his address.

Shri Vivek Bhasin, Director, BARC, underscored the need for carbon-free electricity to achieve sustainable development and highlighted the critical role of special materials in nuclear technology in his address.

Dr. Raghvendra Tewari, Director, Materials Group, gave a compelling insight into how materials science transforms lives, citing the Nobel Prize-winning innovation of the blue LED.

Dr. Alok Awasthi, Chairman of NTD-2025 offered the chief guest's introduction while Dr. Bikas Chandra Maji, Convenor of NTD-2025 proposed the 'Vote of Thanks' for the session.

Technology Exhibition

The inaugural session was soon followed by the opening of the technology exhibition pavilion by the Chief Guest, Shri K.N. Vyas, who was accompanied by other dignitaries on an in-depth tour of the various exhibits, amplifying the range of activities in BARC and other constituent units of DAE. Students, educators, science enthusiasts and family members of DAE units residing in Anushakti Nagar visited the exhibition and also appreciated the working models.

Student Engagements

One of the major draws of the program - Scientific Quizzes - took the centrestage with the enthusiastic participation of students. It was interspersed with a highly immersive edutainment skit , performed by a dedicated team of artists from BARC. To enhance the overall experience of the participants, feedback forms were created and distributed using Google Forms. This approach allowed attendees to easily provide their insights and suggestions in a convenient, accessible, and organized manner.

NTD 2025 Inaugural Day Program Chief Guest, Shri K.N. Vyas (Distinguished Homi Bhabha Chair Professor, DAE), inaugurated the exhibition gallery on BARC-DAE technologies.

Popular Lectures

To spark students' curiosity about the science and technology that shape our everyday lives, the program featured engaging lectures delivered by experienced scientists of DAE. On Day One, the lecture on 'The World of Men and Materials' by Dr. Raghvendra Tewari, Director (Materials Group, BARC) opened the doors to the fascinating realm of materials, captivating and inspiring the students.

The Day 2 engagement with students on the topic 'Advanced Materials and Technologies for Nuclear Waste Management' by Dr. G. Sugilal, Associate Director (Nuclear Recycle Group, BARC) showcased robust nuclear waste management practices in the department.

Finally, Dr. S.K. Satpati, Chairman & Managing Director, UCIL captivated students with his lecture on 'Uranium Technology in India: An Overview' on the final leg of the program.

Audio-Visual Screenings and Social Media Outreach

Engaging young minds through audio, video, and social media is crucial in today's digital era. A short film showcasing the remarkable contributions of materials science research to India's atomic energy expansion alongside lifetime contributions of noted scientists, was screened during the program. Materials Group and SIRD (Knowledge Management Group) have joined hands in making this resourceful video. Additionally, social media was leveraged to reach out to a broader audience.

Social media engagement was shaped by several key elements - Highlights of advanced technology development, vibrant multi-colored portraits reflecting the program's theme, and a poetic tribute underscoring the significance of commemorating National Technology Day and the milestone achievements of BARC Materials Group.

Program Leadership

The National Technology Day 2025 celebration was spearheaded by BARC Materials Group, under the distinguished leadership of Dr. Alok Awasthi, Outstanding Scientist, who served as Chairman of the Program. He was assisted in his efforts by Dr. Bikas Chandra Maji, Scientific Officer/H, Materials Group, who acted as the Program Convenor. The event's success was further enhanced through valuable collaborative efforts from various Groups of BARC.

Significance of the Event

The commemoration of National Technology Day served multiple important purposes, which include

- Honoring India's vibrant science and technology culture
- Highlighting the significance of nuclear energy in India's transformation towards becoming self-reliant (Aatmanirbhar Bharat) and developed nation (Viksit Bharat)
- Demonstrating how nuclear energy contributes to a clean, green, and sustainable future
- Emphasizing the role of advanced materials in successfully harnessing nuclear energy
- Inspiring the next generation of scientists and innovators who will steer India's scientific progress
- Fostering critical thinking and creativity among the citizenry

Additionally, the program saw unveiling of iGOT (Mission Karmanyogi) course content on atomic energy activities such as the Life and achievements of nuclear pioneer Dr. Homi J. Bhabha, Isotope applications in water resources management among others.

Finally, this immersive three-day program emphasized technology development and innovation, providing students with hands-on experiences in nuclear science and advanced materials to equip them for future scientific and technological breakthroughs.

Industry

BARC's Nuclear

By Technology Transfer & Collaboration Division and SIRD Newsletter Editorial Team

Technology Transfer

Technology Transfer Agreement was signed by BARC's Technology Transfer and Collaboration Division with Indore-based M/s. Pacetronix Pvt. Ltd. for the transfer of the technology of "ANUCHITRA Deep Brain Stimulator (DBS)" (Code: MD25ED). The DBS technology has vital applications in healthcare and is primarily deployed in treating Parkinson's disease, essential tremor, and dystonia. ANUCHITRA DBS technology was developed by BARC along with Shree Chitra Tirunal Institute for Medical Sciences and Technology (SCTIMST) Thiruvananthapuram, Kerala.

Hyderabad-situated DAE unit, ECIL, has picked up the technology of "Compact RF & DC electronics Unit for QMS". The DC supply along with the RF counterpart in Quadrupole Mass Spectrometer or QMS are used as quadrupole mass analyzer supply for analyzing ions coming out of the ion source of any type of mass spectrometer.

For waste water treatment and urban waste management, the technology of "Hybrid Granular SBR for Wastewater Treatment (Code: EV05WSCD)" was transferred to Indore-based Nilgiri Builders Pvt Ltd. and the technology for "Rapid Composting Technology for decomposition of dry leaves, kitchen waste and temple waste" (Code: AB25NABTD) was transferred to Mumbai-based M/s. Organica Biotech Pvt. Ltd and to Indore-located M/s. Neev Bioroots LLP., respectively.

In food and agri tech, the process for de-bittering Fenugreek (Methi) seed extracts and Shatavari root extracts (Combined Code: AB34FTD) was transferred to Hyderabad-based M/s. Waleria Healthtech Pvt. Ltd and the Biosensor Kit for detection of Organophosphate and Organocarbamate Pesticides (Code: AB37NABTD) was picked up by M/s. Green Collar Agritech Solutions Pvt. Ltd of Coimbatore, Tamil Nadu, respectively.

Inking of agreement with the industry partner for transfer of BARC's Deep Brain Stimulator technology.

Photograph of the BARC know-how based Emergency in-situ advanced leakage arresting devices technology for piping of varied configuration.

Additionally, technology transfer renewal agreement signed with M/s. C S Zircon Products Pvt.Ltd., Kala Amb (H.P.) for the seventh time for Zirconium Oxide & Zirconium Oxychloride Production.

Technology Commercialization

Some of the licensees of BARC technologies have integrated the technology know-how into their business operations and have begun supplying manufactured products to cater to domestic industry. Some of them are listed below:

- Mumbai-headquartered M/s. TEMA India Ltd., which obtained license to manufacture products based on BARC's High-Efficiency Distillation Columns for Separation of Fluid Mixtures technology, during July this year, shipped 56 units of the manufactured Distillation Columns to NPCIL for deployment in its nuclear reactor operations.
- By leveraging BARC's technology for Emergency in-situ advanced leakage arresting devices for piping, Mumbai-based M/s. Quality Manufacturing Company supplied devices made at its plant to meet the needs of Heavy Water Plant in Baroda during May.

beckons

Spin-off Technologies

BARC technologies witnessing good interest from participants at the 'Ente Keralam 2025' exhibition at Kochi.

- Mumbai-based firm, 6C NanoCarb Pvt. Ltd., started mass production of high quality, versatile MW-CNT powder with high surface area, superior properties for customized applications based on the technology know-how made available by BARC for large-scale synthesis of carbon nanotubes.

Advertising of New BARC Technologies

BARC-DAE technologies which have significant industrial applications are regularly featured on the official webpage (https://barc.gov.in/technologies/index.html) of BARC. Some of the newly introduced technologies that are ready for transfer to the industry are as follows.

- The technology of ANUCHITRA Deep Brain Stimulator (DBS) was listed with the code MD25ED.
- The technology of Economical, Eco-friendly Radiation Indicator Labels for 25 kGy radiation dose, intended to use in radiation sterilization of medical products was listed under the code EcoRIL25.
- OPACIMETER (Code: AI40L&PTD) with applications in determining the transmissivity of a medium and in estimation of smoke emitted from a chimney/stack of an industry.
- "LASCAN DIA-GAUGE (Code: AI39L&PTD) with important application in determining the transmissivity of a medium and in estimation of smoke emitted from a chimney/stack of an industry.

AKRUTI Programme Activities

Under the AKRUTI Program, select BARC-DAE technologies are identified which can aid entrenuership in the remotest parts of the country (villages); and these technologies are widely propagated through engagement with partners from the ranks of academic institutes, women self-help groups, individuals with proven capabilities among others. During the review-period, several agreements were inked for establishment of AKRUTI Kendras (Centres) across various parts of the country, which include:

- Shri Sanganabasava Mahaswamiji College of Pharmacy and Research Centre, Vijayapura, Karnataka.
- Punyshlok Ahilyadevi Holkar Solapur University (PAHSU) in Solapur, Maharashtra.

Besides, AKRUTI also spearheads transfer of BARC technologies' know-how among young entrepreneurs at grassroots. Some of the technologies for which licenses were offered during the review-period are as follows.

- A purely organic, seed dressing bio-fungicide formulation of an improved Trichoderma Virens Mutant Strain with Toxicological and Environment safety data technology as well as the technology based on a Process for Development of Zinc (Zn) Fertilizer Formulation from Biosludge (Code: AB27NABTD) technology were transferred to Organic India LLP, Pune.
- A Process for Development of Phosphorus (P) Fertilizer Formulation from Biosludge (Code: AB26NABTD) technology transferred to Organic India LLP, Pune
- A Rapid Composting Technology for decomposition of Dry leaves, Kitchen waste and Temple waste. (AB25NABTD)" was transferred to M/s. Tech Indra Organic, Tarapur (a business entity for AKRUTI Kendra-Tarapur)

Trainings and Outreach

TT&CD, BARC has arranged for training of resource persons engaged with the newly established AKRUTI Kendra at Uttar Banga Krushi Vishwavidyalaya in Cooch Behar faculties at BARC Trombay facilities. To disseminate the benefits of BARC technologies, a Food Technology Workshop was organized in coordination with AKRUTI Kendra Tarapur at Triveni Sangam Mahila Gram Sangh Dhakti in Dahanu and SDSM College in Palghar.

The AKRUTI Kendra at Mahatma Gandhi University at Kottayam in Kerala participated in the "Ente Keralam 2025" exhibition at Kochi. Demonstrations on BARC's Foldable Solar Dryer and Domestic water Purifier technologies were carried out at the exhibition for the benefit of participants.

Picture Illustration by SIRD

Chairperson of the BARC Women's Cell, Dr. B.K. Sapra, felicitated IAF Squadron Leader Bhawana Kanth during the event.

Indian Navy Surgeon Captain Vidhu Bhatnagar was felicitated by Shri M. L. Mascarenhas, Director, BTDG during the event.

BARC Celebrates Int'l Women's Day with the theme *'Women Warriors: Unlimiting Potential'*

By Dr. B.K. Sapra
Chairperson of BARC Women's Cell

The Women's Cell of Bhabha Atomic Research Centre (BARC) celebrated International Women's Day on April 25, 2025, with great enthusiasm based on the inspiring theme of "***Women Warriors: Unlimiting Potential.***" The event was held at the CC Auditorium and drew a large and engaged audience. Dr. B. K. Sapra, Chairperson of the Women's Cell, BARC delivered the welcome address, while Shri M. L. Mascarenhas, Director, BTDG presented the institutional address.

The celebration was graced by two eminent guest speakers whose lives exemplify courage, determination, and the ability to break through barriers. Squadron Leader Bhawana Kanth, one of India's first women fighter pilots to be inducted into the Indian Air Force in 2016, delivered a rousing talk on perseverance and breaking gender norms in male-preferred field of aviation. Her journey from engineering to flying supersonic jets deeply resonated with the audience.

The second guest speaker was Indian Navy Surgeon Captain Vidhu Bhatnagar, a distinguished neuro-anesthesiologist from Indian Navy Hospital Ship (INHS) Asvini and an author by passion. With extensive experience in this enigmatic field of medicine and use of impactful visuals, she kept the audience thoroughly engaged during her address that focused on resilience of women in high-pressure professions.

Adding an emotional dimension to the celebration was a powerful drama "***खामियों की कहानी***" performed by BARC employees. This production, which has already won multiple awards at the All India Civil Services Cultural Meet 2025, received a spontaneous ovation for its gripping script, and poignant portrayal of struggles and triumphs of individuals with disabilities.

The event concluded with a vote of thanks by Shri A.G. Tirpude, Convener of Women's Cell, BARC. More than just a celebration, the event highlighted the immense capabilities and potential of women, indeed "Women Warriors."

This page intentionally left blank

Edited & Published by
Scientific Information Resource Division
Bhabha Atomic Research Centre, Trombay, Mumbai-400 085, India
BARC Newsletter is also available at URL:https://www.barc.gov.in